Underdetermined DOA Estimation of Deterministic Signals Using High Order Statistics and Noncircularity

by

Yuexian Wang

B.E. (Electrical & Electronic),
Northwestern Polytechnical University, China, 2006.
M.Eng.Sc. (Electrical & Electronic),
The University of Adelaide, Australia, 2011.

Thesis submitted for the degree of

Doctor of Philosophy

in

School of Electrical and Electronic Engineering
The University of Adelaide, Australia

September 2015

THE UNIVERSITY *of* ADELAIDE

Typeset in LaTeX 2ε

Yuexian Wang

To my parents

Contents

Abstract

Sensor arrays play important roles in signal transmission/reception, estimation, and tracking, and have been successfully applied to many engineering fields such as radar, sonar, wireless communications to name a few. Practically, sensor array systems usually suffer from nonideal factors such as signal coherency, spatially coloured noise, and a limited number of sensors. In this thesis, problems of direction of arrival (DOA) estimation in the presence of nonideal factors are addressed, and new algorithms to tackle these problems are developed that achieve improved performance with a limited number of sensors.

Under multipath propagation, independent and coherent signals coexist, resulting in rank deficiency of the cumulant matrix. To tackle this problem, two methods for DOA estimation of mixed independent and coherent signals using fourth-order cumulants (FOC) are proposed, and both algorithms can make efficient use of the array degrees of freedom (DOFs). The first algorithm implements the estimation via two-stage processing by separating the independent and coherent signals. In this method, new matrix reconstruction techniques for independent signal cumulants and rank restoration are developed, and the DOAs of both the independent and coherent signals can be estimated by polynomial rooting without performing a spectral grid search. Its superiority over existing methods is demonstrated by simulation results.

The second algorithm considers the case when a large number of coherent signals, greater than the number of sensors, exist due to the propagation channel. Here, we exploit temporal correlation in the signals to form an array output matrix with pseudo snapshots, spanning the same signal subspace as the one using real snapshots. By incorporating this property, new augmented cumulant matrices are constructed and the corresponding method for coherent group separation is derived. Compared with the existing method, the proposed one achieves better performance in terms of estimation accuracy and robustness of the spatial signature, especially for weak signals.

Apart from signal with circular statistics discussed above, we study the noncircularity embedded in modern wireless communication signals to further extend the effective aperture, enhance DOFs, and improve the estimation performance. A new FOC-based direction finding method which can extend the array aperture as well as maximise the DOFs is proposed. By combining noncircularity with high order cumulants and optimsing geometric arrangement of the virtual array arising accordingly, the resultant identifiability of DOA estimation can be up to twice larger compared with the using the same order cumulants for circular signals. Simulation results validate that the proposed method offers better performance in terms of identifiability as well as accuracy.

Last, we revisit the case when uncorrelated and coherent signals coexist and utilise the noncircularity of signals in this scenario. To the best of our knowledge, there are no publications addressing the class of DOA estimation problem, and a novel two-stage second order statistics (SOS) estimator is introduced accordingly to further increase the DOFs. In this method, a more robust approach is presented to identify the true DOA estimates from the pseudo ones, the estimates of noncircular phases are derived in closed-form, and a novel spatial smoothing technique based on the eigenvectors is developed to restore the rank deficiency. Additionally, new deterministic Cramér-Rao lower bounds (CRLBs) are derived for the considered mixture model of noncircular signals. The theoretical analysis justifies that the number of identifiable signals is larger than the current algorithms. Extensive simulation results show that the proposed method offers sufficient DOFs as well as improving the estimation accuracy of both the uncorrelated and coherent signals.

Statement of Originality

This work contains no material that has been accepted for the award of any other degree or diploma in any university or other tertiary institution and, to the best of my knowledge and belief, contains no material previously published or written by another person, except where due reference has been made in the text.

I give consent to this copy of the thesis, when deposited in the University Library, being available for loan, photocopying and dissemination through the library digital thesis collection.

The author of this thesis acknowledges that copyright of published work contained within this thesis (as listed in the publications page) resides with the copyright holder(s) of that work.

Signed

Date

Acknowledgments

First and foremost, I must recognise my principal supervisor Dr. Brian W.-H. Ng for his continuous support and inspiration during the period of my Ph.D study. Since my first discussion with him, he has been assisting me to find and direct my own path, and is always there as to offer advise that I should conform to the main goals. I also thank him for his tireless work in reviewing journal manuscripts and this thesis. In addition, I have learnt a lot from his expertise in research management, his excellent personality and his good skill of language. Thanks for Brian's generosity and openness, I am now confident to continue on my own academic research.

I would also like to wholeheartedly thank my co-supervisor Mr. Matthew Trinkle for introducing me to the wonderful world of array signal processing. I was fortunate to work with him since Matthew gave me great freedom to develop new ideas and provides invaluable comments on my work. Matthew also gave me plenty of insight into hardware implementation issues, which has no doubt helped me to integrate theory with practice. His meticulous approach to learning and tolerance towards others will influence me for the rest of my life. Talking with him not only in professional areas but also discussing culture topics has always been enjoyable and beneficial.

Sincere thanks to my colleagues in the School of Electrical and Electronic Engineering for their unselfish help in extending my knowledge. They are Prof. Lang White, Prof. Doug Gray, Dr. Zhonghao Hu, Dr. Geng Tian, Dr. Yingbo Zhu, Mr. Zili Xu, and Mr. Paul Pincus.

I am indebted for the work done by the staff in the School of Electrical and Electronic Engineering, particularly, Dr. Cheng Chew Lim and Mrs Rose-Marie Descalzi who managed my scholarship and research funding issues. Of course thanks also to the four kind ladies in the school office.

Many thanks to my friends, specifically Ruiting Yang, Shaoming Zhu, Chow Yii Pui, and Vichet Duk in Adelaide for their constant support and encouragement during my Ph.D studies.

I am grateful to my parents who dedicate their unconditional love and encouragement to me. Since I first entered primary school, all through my educational journey of twenty years, their love has always accompanied me. Without them, I could not imagine how I could have accomplished this work.

Yuexian Wang (September 2015)

Conventions

Typesetting

This thesis is typeset using the LaTeX2e software.

The fonts used in this thesis are Times New Roman and Sans Serif.

Referencing

Referencing and citation style in this thesis are based on the Institute of Electrical and Electronics Engineers (IEEE) Transaction style [1].

For electronic references, the last accessed date is shown at the end of a reference.

Units

The units used in this thesis are based on the International System of Units (SI units) [2].

Spelling

The Australian English spelling is adopted in this thesis.

Publications

Journal

[1] Y. Wang, M. Trinkle, and B. W.-H. Ng, "DOA estimation under unknown mutual coupling and multipath with improved effective array aperture," *Sensors*, vol. 15, no. 12, pp. 30 856–30 869, Dec. 2015.

[2] Y. Wang, M. Trinkle, and B. W.-H. Ng, "Two-stage DOA estimation of independent and coherent signals in spatially coloured noise," *Signal Process.*, vol. 128, pp. 350–359, Nov. 2016.

[3] Y. Wang, M. Trinkle, and B. W.-H. Ng, "Efficient DOA estimation of noncircular signals in the presence of multipath propagation," *Signal Process.*, under review, 2016.

[4] Y. Wang, A. Hashemi-Sakhtsari, M. Trinkle, and B. W.-H. Ng, "Sparsity-aware DOA estimation of quasi-stationary signals using nested arrays," *Signal Process.*, under review, 2016.

[5] Y. Wang, M. Trinkle, and B. W.-H. Ng, "Direction finding and mutual coupling estimation for monostatic MIMO radar," *Signal Process.*, in preparation for submission, 2016.

Conference

[1] Y. Wang and M. Trinkle, "DOA estimation for coherent signals with symmetric virtual array," in *International Global Navigation Satellite Systems Symposium, IGNSS 2013*, Outrigger Gold Coast, Australia, Jul. 2013.

[2] Y. Wang and M. Trinkle, "Coherent signals DOA estimation in the presence of complex noise," in *International Global Navigation Satellite Systems Symposium, IGNSS 2013*, Outrigger Gold Coast, Australia, Jul. 2013.

Abbreviations

AIC	Akaike Information Criterion
AM	Amplitude Modulation
AP	Alternating Projection
AR	Autoregressive
ARMA	Autoregressive Moving Average
ASK	Amplitude Shift Keying
BPSK	Binary Phase Shift Keying
CB	Conventional Beamforming
CCI	Co-Channel Interferences
CRLB	Cramér-Rao Lower Bound
CW	Continuous Wave
DML	Deterministic Maximum Likelihood
DOA	Direction Of Arrival
DOFs	Degrees Of Freedom
EM	Expectation-Maximization
ESPRIT	Estimation of Signal Parameter by Rotation Invariance Techniques
FBSS	Forward/Backward Spatial Smoothing
FOC	Fourth Order Cumulants
GDE	Gerschgorin Disk Estimator

HOC	High Order Cumulants
HOS	High Order Statistics
LL	Log-Likelihood
MDL	Minimum Description Length
ML	Maximum Likelihood
MLE	Maximum Likelihood Estimator
MRAs	Minimum Redundancy Arrays
MSE	Mean Squared Error
MUSIC	MUltiple Signal Classification
MVDR	Minimum Variance Distortionless Response
NSF	Noise Subspace Fitting
OQPSK	Offset Quadrature Phase Shift Keying
PAM	Pulse Amplitude Modulation
PDF	Probability Density Function
RMSE	Root Mean Squared Error
SAGE	Space Alternating Generalized EM
SF	Subspace Fitting
SML	Stochastic Maximum Likelihood
SNR	Signal-to-Noise Ratio
SORTE	Second ORder sTatistic of Eigenvalues
SOS	Second Order Statistics
SS	Spatial Smoothing

SSF	Signal Subspace Fitting
SVD	Singular Value Decomposition
TAM	Toeplitz Approximation Method
ULA	Uniform Linear Array
VESPA	Virtual ESPRIT Algorithm
WSSF	Weighted Signal Subspace Fitting

Notations

λ	The wavelength of corresponding frequency
θ	Azimuth angle
c	The speed of light
d	The spacing between adjacent sensors
$\mathbf{x} \in \mathbb{R}^M$	A vector with dimension M in real domain
$\mathbf{x} \in \mathbb{C}^M$	A vector with dimension M in complex domain
$(\cdot)^T$	The transpose operation
$(\cdot)^*$	The conjugate operation
$(\cdot)^H$	The conjugate transpose operation
$(\cdot)^{-1}$	The inverse operation
$(\cdot)^+$	The pseudo-inverse operation
$\lceil \cdot \rceil$	The ceiling operation of a decimal number
$\lfloor \cdot \rfloor$	The flooring operation of a decimal number
$E_t[\cdot]$	Statistical expectation implemented by $\lim_{L\to\infty} \frac{1}{L} \sum_{t=1}^{L} [\cdot]$
$\frac{\partial f(\mathbf{x})}{\partial \mathbf{x}}$	The first derivative of the function $f(\mathbf{x})$ with respect to $\mathbf{x}$
$\frac{\partial^2 f(\mathbf{x})}{\partial \mathbf{x}^2}$	The second derivative of the function $f(\mathbf{x})$ with respect to $\mathbf{x}$
$\mathrm{Re}\{\cdot\}$	Real part of a complex number
$\mathrm{Im}\{\cdot\}$	Imaginary part of a complex number
$\mathrm{span}\{\cdot\}$	Linear span
$\dim\{\cdot\}$	Dimension of linear space
$\mathcal{R}(\cdot)$	Range (or signal space) of a matrix
$\mathcal{N}(\cdot)$	Null space of a matrix
$\mathcal{V}^\perp$	Subspace orthogonal to a linear space $\mathcal{V}$
$\mathbf{P}_{\mathbf{A}}^\perp$	Orthogonal projection to the range of $\mathbf{A}$
$\mathbf{E}_{\mathbf{A}\|\mathbf{B}}$	Oblique projection with the range $\mathcal{R}(\mathbf{A})$ and null space $\mathcal{N}(\mathbf{B})$
$\max\{a, b\}$	The maximum value between a and b
$\min_x f(x)$	Minimise the function f with respect to the variable x
$\|\cdot\|_2$	Euclidean (ℓ_2) norm

$\|\cdot\|_F$	Frobenius norm
$\det\{\cdot\}$	Matrix determinant
$\circ$	Khatri-Rao product
$\otimes$	Kronecker product
$\odot$	Schur-Hadamard product, i.e., element-wise product
$\mathrm{tr}\{\cdot\}$	Matrix trace
$\mathrm{rank}(\cdot)$	Matrix rank
$\mathrm{diag}\{z_1, z_2\}$	Diagonal matrix with diagonal entries z_1, z_2
$\mathrm{blkdiag}\{\mathbf{Z}_1, \mathbf{Z}_2\}$	Block diagonal matrix with diagonal entries $\mathbf{Z}_1, \mathbf{Z}_2$
$\mathbf{Z}(a:b, c:d)$	Submatrix by the entries from rows a to b and columns c to d of $\mathbf{Z}$
$\mathbf{Z}(a, b)$	Entry in the a-th row and b-th column of $\mathbf{Z}$
$\mathbf{I}$	Identity matrix
$\mathbf{J}$	Exchange matrix
$\mathbf{R}$	Covariance matrix
$\mathbf{U}_s$	Signal subspace
$\mathbf{U}_n$	Noise subspace
$\mathbf{a}(\theta)$	Steering vector
$\mathbf{A}(\theta)$	Array manifold

List of Figures

List of Tables

Chapter 1

Introduction and Motivation

OUR research journey on the exploration of sensor array processing begins right here. This chapter provides a basis for the remainder of this body of work, giving a definition of what this research is really about, details and motivation for all the work that follows. This introduction serves to explain the most fundamental meaning of sensor array processing, and explain the pathway that the research follows, and thus provide the reader with a road map for what lies ahead in this thesis.

1.1 Research Area and Motivation

Array signal processing involves manipulation of signals induced in various sensor elements, such as antennas, hydrophones, microphones, seismometers, etc, depending on the function of the array system. An array of sensors located at different points in space are used to receive signals that are reflected from the targets (objects) of interest. One traditional application is signal enhancement. If the same signal is received at multiple sensors and can be coherently added with the same delay at each sensor, then additive noise is averaged out by an array gain equal to a factor M, the number of sensors. The delay-and-sum operation is known as beamforming, since it can be regarded as forming a beam into the direction of the source. The delay-and-sum beamformer acts equivalently to a parabolic dish, as shown in Fig. 1.1, which physically inserts the correct delays to look in the desired direction. Additionally, an array's capability of steering nulls to reduce co-channel interferences (CCI) and pointing independent beams toward various mobile users, as well as its ability to estimate the direction of arrival (DOA) and associated parameters like powers of the signal and noise fields, make it prevalent in several application areas such as radar [3, 4], sonar [5, 6], wireless communications [7–9], navigation [10–12], acoustics [13, 14], seismology [15, 16] to name a few.

Early contributions to this field have been made mostly in the context of radar and sonar systems in the latter parts of the 20th century. With the onset of the 21st century, great advances in digital processing hardware has meant that array processing played an increasingly important role in numerous emerging developments and applications in wireless and mobile communications. The received data depends on the characteristics of the sources, the channels, the noise, and the measurement devices.

A sensor array has spatially separated sensors whose output are fed into a weighting network or a beamforming network as illustrated in Fig. 1.1. The sensors simultaneously measure a spatial field at different locations. Multiple plane waves either narrowband or wideband are incident from different directions on an array of sensors distributed in space. The DOA is specified by the radial directions (azimuth and elevation) of the incident plane waves using observations (snapshots) received by the

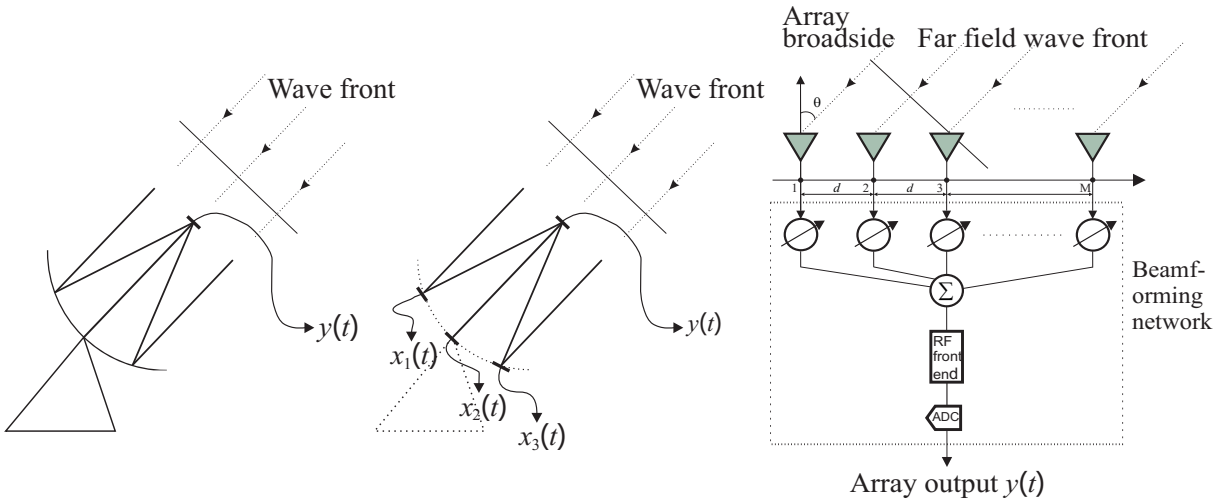

Figure 1.1. Coherent addition of signals.

array. Sensor data are processed to gain information about the sources. Due to the large number of applications involving different system models and signal processing objectives, array processing is a broad research field.

In this thesis, we mainly focus on the direction finding topic, which is of great interest and importance in array processing. Many DOA estimation techniques have been proposed under the assumption that signals undergo line-of-sight direct path propagation in isotropic media, and are statistically uncorrelated to each other. Also, an underlying assumption that the number of physical sensors is greater than that of signals is always required. Unfortunately, such assumptions are often far away from reality. In fact, sensor arrays in practical applications may suffer from various factors, especially for civilian usage, such as ubiquitous multipath propagation due to tall buildings and limited numbers of sensor due to cost and portability of the hardware. It is known that coherency between signals caused by reflections will render popular subspace-based estimators ineffective, and overlooking potential degrees of freedom (DOFs) hidden in the signal structure and array configuration may result in performance loss. However, conventional array processing techniques are incapable of handling such problems. Motivated by this fact, the problems of direction finding in the presence of multipath propagation and utilising additional information embedded in signals to improve DOFs are addressed and two classes of new methods are proposed in this thesis.

1.2 Original Contributions

This thesis makes the following original contributions to the research area:

1. DOA estimation utilising fourth order cumulants (FOC) in multipath: Second order statistics cannot identify the signal bearings contaminated by unknown coloured noise under multipath propagation. This issue can be effectively tackled by employing FOC since higher even order cumulants are blind to Gaussian distributions. FOC also inherently have more DOFs than second order statistics (SOS) at a cost of increased variance. We introduce a new algorithm for the case when independent and coherent signals coexist. This would happen in practice where some signals are affected by multipath. The existing accurate FOC algorithm to handle this scenario is based on a two-stage processing approach that first identifies and eliminates the independent signals and then resolves the coherent signals by rank restoration. We propose a new two-stage algorithm that is more accurate than the previous methods by employing a novel signal separation and rank restoration approach. Based on the DOA estimates of independent signals, we first reconstruct the cumulant matrix of independent signals and remove it from the original cumulant matrix to deal with the remaining coherent signals. By introducing a new matrix reconstruction approach and applying it to restore the deficient rank caused by signal coherency, the desired coherent signals can then be resolved by common subspace-based DOA estimators. This work is described in Section 5.4 of Chapter 5.

2. Space-time FOC for improving coherent group separation: In wireless communications, channel estimation needs to identify and estimate spatial signature (i.e., a linear combination of the steering vectors scaled by the fading coefficients) [17–19] of different users-of-interest at the receiver side. A large number of coherent signals will arise from multipath propagation, especially in urban areas, where the two-stage algorithms are no longer valid as they cannot handle more coherent signals than the number of sensors. So far the extended virtual ESPRIT algorithm (VESPA) can resolve the highest number of coherent signals. However, it is less accurate and robust than our two-stage method, especially in low SNR environments.

We propose a new blind separation strategy based on rotation invariance between augmented cumulant matrices to address the problem of robust DOA estimation of coherent signals belonging to different groups in spatial coloured noise (Chapter 5). Our algorithm is more accurate and robust than VESPA while still resolving the same number of coherent signals. We introduce temporal correlation to form an array output matrix with pseudo snapshots, spanning the same signal subspace as the one using real snapshots. Then the augmented cumulant matrices can be constructed in terms of the pseudo snapshots (Section 5.4). The separation of coherent groups is carried out by exploiting the rotation invariance between the augmented cumulant matrices, which gives rise to a more robust generlised steering vector estimation. This work is described in Section 5.5 of Chapter 5.

3. DOA estimation of noncircular signals utilising FOC: Exploiting noncircularity of modern wireless communication signals in direction finding has been drawing increasing attention over the past few years. Only limited solutions to this problem have been reported and most of them depend on SOS which can determine at most $2(M-1)$ noncircular sources where M is the number of sensors.

   A new subspace-based estimator, referred to as NC-2q method, was proposed by Liu et al. [20] to address DOA estimation of noncircular signals using high order statistics. This technique attracted our attention since it is found to have improved estimation capacity and can resolve up to $3(M-1)$ sources. However, the authors in [20] did not give clear physical interpretations of their idea. More significantly, a disadvantage of their method is that it does not fully exploit the maximum effective array aperture which can be obtained by virtual arrays arising from noncircular signals.

   The work in Chapter 6 provides an interpretation of the virtual array principles by using FOC coupled with noncircularity. Some links with previous work, which are left out by Liu et al. [20], are discussed. In addition, according to the explanation of the virtual array principles, the number of DOFs and array aperture are increased by up to an additional M elements, meanwhile the performance is also enhanced. Our algorithm can also be extended to even higher order cumulants in a similar fashion

to the NC-2q method, allowing up to $2q(M-1)$ sources to be identified. This work is described in Section 6.2 of Chapter 6.

4. DOA estimation of noncircular signals under multipath propagation: There are possibilities in improving estimation performance in the presence of multipath by using the noncircular statistics of signals. We revisit the scenario of the coexistence of uncorrelated signals with coherent ones, which has been discussed in Chapter 5 where circular statistics were assumed.

   To the best of our knowledge, there are no publications addressing the noncircular signal estimation problem for the case where uncorrelated and coherent signals coexist. A SOS estimator to this problem is investigated in Chapter 6, and a novel two-stage processing algorithm is introduced to further increase the DOFs. By exploiting the noncircularity, the DOA estimates of the uncorrelated sources are obtained first from an augmented signal subspace, then the covariance matrix of the uncorrelated signals is reconstructed and removed. Secondly, spatial smoothing on the eigenvectors of the coherent signal covariance matrix is performed to restore the rank deficiency. The theoretical analysis shows that the number of identifiable signals is larger than the current algorithms. Additionally, new deterministic Cramér-Rao lower bounds (CRLBs) are derived for the considered mixture model of noncircular signals. This work is described in Section 6.3 of Chapter 6.

1.3 Thesis Structure

The thesis can be divided into four parts. The first part provides the motivations, contributions and structure of this thesis. In addition, it also gives a literature review of array signal processing on nonideal models. This part includes Chapters 1 and Chapters 2. The second part is composed of Chapter 3 and Chapter 4 which introduce prerequisites of linear algebra, its application to sensor arrays, as well as the classical DOA estimation algorithms. The third part, including Chapter 5 and Chapter 6, mainly addresses the problem of enhancing the effective DOFs while preserving good DOA estimation performance, by exploiting FOC and noncircularity hidden in the signals. The last part is Chapter 7 describing conclusions of the work done in this thesis

and making recommendations of possible work to extend this research in the future. The content in each chapter is summarised as follows.

Chapter 1 provides a brief introduction to array signal processing. In addition, the research problems, the contributions to knowledge provided by the thesis, and the structure of the thesis are also discussed.

Brief background material into our research topics is provided in Chapter 2. This is followed by a comprehensive study of the contemporary literature on models for the nonideal factors in array processing, specifically the estimation of coherent signals, unknown noise, and noncircular signals, which are the main topics of the research done in this thesis. An exploration of the many ideas for these tough tasks is provided, commenting on various merits and problems, application areas, and advances in the theory related to sensor arrays.

Chapter 3 introduces the foundation of linear algebra which is utilised extensively in array processing. Definitions and properties that will be useful in the thesis are summarised.

Chapter 4 gives the basis of DOA estimation theory. Within this chapter, some fundamental ideas underlying direction finding are described and evaluated. A discussion of the development of the signal models, for uncorrelated and coherent signals respectively, is provided as well. The research topic of this thesis is also narrowed down into meeting some particular challenges, e.g., estimation in multipath with spatially coloured noise, in array processing.

To handle the multipath case, all the algorithms assume a mixture of independent and coherent signals. While to deal with coloured noise, FOC are applied. Chapter 5 describes two new DOA estimation algorithms for the multipath signal model using cumulants. While Chapter 6 discusses how to exploit the noncircularity of signals to improve the estimation performance, and also introduces two novel direction finding methods, one for uncorrelated signals combined with cumulants and the other for the mixture signal model under multipath propagation utilising SOS.

In Chapter 5, the basic signal model for circular statistics is introduced, including a detailed discussion on how the FOC are incorporated. Then an improved two-stage algorithm based on FOC is given. This algorithms follows the existing ideas of dealing with independent and coherent signals separately but can resolve more signals with better accuracy than the existing two-stage FOC method. Secondly, an improved single stage DOA estimation algorithm is described which is more accurate than VESPA by exploiting temporal correlation in the signals. The single-stage algorithm separates the coherent groups directly and can resolve many more signals than the two-stage method considered previously. For each algorithm, the simulation environment is described, and the performance improvement in terms of accuracy and robustness is validated by the simulation results.

In Chapter 6, we explore the additional benefits of exploiting noncircular statistics in DOA estimation. First of all, we discuss the additional degrees of freedom that can be obtained by the combination of noncircular statistics and FOC. The concept of virtual arrays interprets in a physical way how noncircular statistics and FOC can effectively increase the array DOFs and effective aperture. Using the tool of virtual arrays, we describe a new noncircular FOC-based algorithm which has a larger virtual array aperture and DOFs than existing methods. Simulation results demonstrate its better identifiability and accuracy of DOA estimates. The second part of Chapter 6 considers exploiting noncircular statistics for the case when uncorrelated and coherent signals coexist. This section builds on the existing SOS two-stage algorithms that assume circular statistics, and introduces a novel two-stage algorithm with improved DOFs and accuracy by exploiting noncircularity. A discussion of identifiability of DOA estimation and performance bounds are also provided, along with more simulation results demonstrating potential improvements in the algorithm performance.

Finally, Chapter 7 reviews and re-summarises the original contributions to knowledge in the thesis. In addition, some recommendations for future work are given before final conclusions are drawn.

Chapter 2

Background and A Review of Array Processing with Nonideal Models

HISTORICALLY, array processing is a well visited concept, though it can still hold tremendous potential for great progress. This chapter examines the recently published literature on array processing, discussing three main nonideal models to DOA estimation, specifically coherent signals, unknown noise, as well as noncircular signals, and existing state of the art. A variety of ideas are explored, looking at many aspects of array processing with a strong view to further developments. Additionally, the chapter provides a background of outlining the significance of current research in advancing the state of the art in array signal processing.

2.1 Introduction

Subspace-based estimation methods such as MUSIC and ESPRIT can provide precise DOA estimation and high resolution for resolving uncorrelated signals. In real environments, this assumption may not hold as components of the received signal from a target may undergo several reflections from various reflective surfaces (e.g., sea, buildings, hills, etc.) or multiple coherent signals may be deliberately transmitted in a military scenario. As a result, uncorrelated and coherent signals may coexist, which cause the spatial covariance matrix to be deficient in rank. The aforementioned prevalent methods, in the presence of multipath propagation, fail to effectively identify or estimate bearing due to an incorrect interpenetration of signal and noise subspaces of the coherent sources. Therefore, the estimation of coherent sources is always a thorny problem and remains a topic of intense interest in spatial spectrum estimation.

Another nonnegligible factor is the omnipresent noise. Ideally, sensor noise is presumed to be uniform, Gaussian and white. However, the assumption may be unrealistic in certain applications, where the noise environment is unknown or changes slowly with time. In such cases, the sensor noise should be considered as an unknown spatially coloured process. Additionally, when sparse arrays are utilised, the sensor noise can be simplified to a spatially nonuniform white process. Both these circumstances render the prevalent algorithms based on the ideal model ineffective.

Besides, recent research shows that exploitation of noncircularity within some modulated signals can improve DOA estimation accuracy and degrees of freedom. Consequently, it becomes significant to make the best use of the incident signal structure in practice.

This chapter seeks to provide a comprehensive background knowledge of the issues mentioned above in array signal processing and, hence, to serve as a precursor for this current research. In this chapter, we first review the solutions to rank deficiency due to signal coherency, then we address the unknown noise issues, including the spatially coloured and nonuniform white noise cases, and review some widely used algorithms which are robust to the nonideal noise. In addition, we review the recent research

work on DOA estimation of noncircular signals and discuss how to take advantage of the noncircularity to improve the performance of standard subspace-based algorithms.

2.2 Development of Coherent Signals Processing

The methods proposed so far to deal with coherent signals can be divided into two distinct camps, with one based on dimension reduction processing and the other full dimension processing. The two classes of methods present fundamentally different ideas, and both inspire a great deal of subsequent research from passive beamforming to active radar and sonar. The methods using dimension reduction processing are discussed in Section 2.2.1, with full dimension processing discussed in the sequel, Section 2.2.2.

2.2.1 Dimension Reduction Processing

Existing dimension reduction approaches can be further sub-divided into one-stage or two-stage approaches.

One-stage Procedure

Dimension reduction processing is the most popular class of decorrelation approaches, and it can be further categorised into spatial-smoothing- and matrix-reconstruction-based techniques. The former comprises (forward) spatial smoothing (SS) [21–23], forward/backward spatial smoothing (FBSS) [24], and modified spatial smoothing [25–27], while the latter mainly refers to matrix decomposition and eigenvector singular value decomposition. The two techniques differ markedly in the structures of the processed covariance matrix, i.e., the square matrix for the spatial-smoothing-based techniques while the rectangular matrix for the matrix-reconstruction-based techniques.

The SS technique doubtlessly plays the most significant part in combating signal coherency, which was first introduced by Evans et al [21] and further examined by Shan

et al [22,23]. This technique is based on a preprocessing scheme that partitions the original array into a series of overlapping subarrays, then averages the subarrays' covariance matrices to construct the spatially smoothed covariance matrix, and subsequently applies MUSIC or ESPRIT to the smoothed covariance matrix to obtain DOA estimates. The number of subarrays and the number of elements in each subarray are regarded as a pair of inter-constrained parameters, and are determined from the number of directional sources under consideration. For N sources, one needs a subarray size of $N+1$ and the number of subarrays K greater than or equal to N subject to $N+K \leq M$, where M is the number of array elements. Extensive studies and analysis show that the SS technique is able to at most decorrelate $\lfloor \frac{M}{2} \rfloor$ coherent signals where $\lfloor \cdot \rfloor$ is the flooring operator [22,23].

Under a mild restriction, an improved spatial smoothing scheme referred to as the FBSS was developed, allowing up to $\lfloor \frac{2M}{3} \rfloor$ sources to be estimated, upper bound for the FBSS technique [24]. The technique carries out averaging not only on covariance matrices obtained from the forward smoothing scheme described above, which divides the array along one direction of the linear array, but also on covariance matrices obtained from the backward smoothing scheme, which divides the array from the other direction of the linear array. Despite increasing the number of resolvable coherent signals when compared with SS, FBSS still suffers from poor utilisation of antenna elements, as approximately $\frac{M}{3}$ DOFs are lost.

The FBSS has been further developed in subsequent work [25–27], and the authors demonstrate improvements either in performance of angular resolution or computational efficiency. A method in [25] reduces sensor noise before applying spatial smoothing to make the covariance matrix more robust with respect to low SNR. Another method described in [26] squares the array covariance matrix before forming the smoothed array covariance matrix, which improves the DOA resolution. The work in [27] focuses on reducing computation complexity of direction finding methods incorporating forward-backward soothing. It shows that by applying a unitary transformation, both the covariance matrix and observation data can be converted from complex to real values, and then the forward-backward smoothing can be applied in the real number domain to obtain the DOA estimates.

Matrix reconstruction [28] is an alternative subarray technique to restore the loss of rank due to coherency among signals. It segments the whole array into subarrays, and then stacks the covariance matrices of forward subarrays rather than averaging them. As matrix reconstruction techniques are based on similar principles as SS and also have similar performance characteristics. Later on, the work by Cadzow et al [29] observed that eigenvectors corresponding to large eigenvalues may each be represented as linear combinations of the steering vectors, so the eigenvectors can be used to form a matrix whose rank can be restored accordingly, then singular value decomposition can be applied to find the directions. Simulation results show that the resolution of the DOA of the eigenvector singular value decomposition is slightly better than for the SS technique. Recently, a different idea is developed by Han et al [30], where a Toeplitz matrix reconstructed from the covariance matrix improves accuracy of DOA estimates irrespective of whether the sources are coherent or not, but at the cost of halving the effective array aperture.

The methods reviewed above are based just on second order statistics (SOS) of the received data. However, these SOS methods suffer from serious drawbacks. Firstly, they are not able to process more than $M-1$ uncorrelated sources from an array of M sensors and have a poor robustness both to modeling errors [31–33], which are always present in practical situations, and to the presence of a coloured Gaussian additive noise without *a priori* knowledge of its covariance matrix [34]. Secondly, their performance may suffer severe degradation from closely separated sources with a low SNR or a limited number of snapshots [35].

To overcome these limitations, many direction-finding methods [36–39] based on fourth order cumulants (FOC) have been developed for non-Gaussian sources. The MUSIC-like method proposed by Porat et al, as an extension of the MUSIC to FOC [36], is the most popular. Later on, a series of work by Mendel and his colleagues drew much attention to the virtual ESPRIT algorithm (VESPA) based on FOC. VESPA was developed firstly for DOA estimation of independent signals, where a virtual covariance matrix is constructed by substituting cumulants for the cross-correlations between actual and the so-called virtual array elements [37]. The virtual array (VA) concept allows both an improvement of resolution and the processing of more sources than sensors.

In [38, 39], VESPA was extended to the case of coherent signals. By constructing two different FOC matrices, the generalised steering vectors (i.e., a linear combination of the steering vectors scaled by the fading coefficients) can be estimated blindly using the rotation invariance property. Coherent groups (a group of coherent signals are generated by the multipath propagation of one far-field source) are separated accordingly, then the DOAs of coherent signals in each group can be estimated via FBSS. The benefits of the VESPA are: i) a larger capacity for processing coherent signals than the number of sensor; ii) a high robustness with respect to modeling errors (e.g., gain-phase errors and mutual coupling), and requiring only two calibrated array elements, which are very attractive and inspired further research. At about the same time, Yuen et al [40] presented a blind estimation technique based on FOC to "blindly" estimate the generalised steering vectors without having *a priori* knowledge of the array manifold. Then, they used a high-resolution spectral analysis technique to estimate the DOAs. However, compared with the VESPA, the blind algorithm is more complex, and there will be one or more extraneous DOAs when the SNR is low.

Two-stage Procedure

A common characteristic of the one-stage procedures discussed above is that all the uncorrelated, partially coherent or fully coherent signals, caused by multipath propagation or malicious jamming in wireless communication or electronic warfare, are resolved simultaneously. This implies that they cannot distinguish uncorrelated sources from coherent signals, and thus the number of their resolvable signals will be restricted in most algorithms except VESPA which can actually resolve more signals than the two-stage algorithms at the cost of estimation accuracy.

To deal with this problem a pre-processing step that estimates and removes the uncorrelated signals prior to decorrelation is typically applied [41–47]. The fundamental principle of this category of technique is that the DOAs of uncorrelated signals are estimated by conventional high-resolution methods first, then the information of uncorrelated signals are eliminated by a differencing or oblique projection operation, and the remaining coherent signals can be resolved using decorrelation approaches discussed earlier. Applying a separation process allows the combination of uncorrelated

and correlated signals resolved by these techniques to exceed the number of antenna elements. The existing algorithms differ in how they remove the uncorrelated signals from the covariance matrix and how the rank restoring step is applied.

One of the publications that initially introduced this two-stage technique utilised the idea of spatial differencing to estimate and remove the uncorrelated signals [41]. This work established a standard approach to the issue that was to be adopted by a number of subsequent researchers. In their paper, the authors utilised the property that the covariance matrix of uncorrelated sources has a Toeplitz structure for a uniform linear array (ULA), but their technique could only resolve two sources in each coherent group. Al-Ardi et al [48] proposed an algorithm that combines spatial differencing and iterative spatial smoothing to make DOA estimates. A key step in this algorithm is the construction of a covariance matrix of uncorrelated sources, but the paper provided scant details on this, which raises doubt over the algorithm's general applicability. This work was followed up by Qi et al [43] and Ye et al [46], where the problem of rank deficiency was considered and the restoring operation for the issue was introduced. In [43] and [46] spatial differencing is used to remove the uncorrelated signals, which gives rise to extra spurious sources resulting in fewer correlated signals being resolvable in the spatial smoothing step. Thus, extra processing is required to identify and alleviate pseudo-DOA estimates. Although the pseudo DOAs are removed eventually, the mathematical manipulations of the method by Qi et al are verified only by simulation and lack a theoretical proof, while the method by Ye et al is not robust as the number of coherent signals is increased. In order to complete the family of spatial differencing methods, an FOC-based approach [49] was proposed for non-Gaussian mixed signals corrupted with unknown coloured Gaussian noise. The method can be regarded as an FOC version of the work in [46]: the first step estimates the DOAs of independent signals with the cumulant matrix, and the second step resolves the coherent signals with the smoothed cumulant matrix whose rank has been restored by firstly squaring the difference cumulant matrix and then applying forward/backward smoothing. In [44] the spatial smoothing step in [43] is replaced by a matrix reconstruction technique which restores the number of resolvable correlated signals to the full number achievable without the spurious sources. The drawback of this technique is its high

complexity and loss in DOA accuracy. In [45] the uncorrelated signals are removed by subtracting their reconstructed covariance matrix, allowing the same number of coherent signals to be resolved as in [44] by using traditional FBSS. This improves the DOA estimation accuracy and reduces the complexity. A new technique in [47] only uses a single subarray in the forward smoothing step which improves the accuracy but only allows pairs of coherent signals to be resolved.

The methods in [41–47] cannot separate the signals from diverse coherent groups according to their coherence despite efficiently distinguishing between uncorrelated and coherent signals. Thus, a new method suggested in [50] uses rotation invariance property to inherently separate eigenvectors of uncorrelated and different coherent groups. However, the eigen-decomposition of the DOA estimation matrix in [50] gives rise to cross-term effects due to noise and the limitation of having a finite number of snapshots, which result in a high probability of failure of this method. Although an orthogonal projection technique to solve this problem was also presented in the same paper, it can only reduce but not completely eliminate the cross-term effects.

2.2.2 Full Dimension Processing

The Perspective of Matrix Structure

The other major research direction for dealing with coherency of incident signals has considered maintaining the full effective array aperture with no reduction in the degrees of freedom of an array [51–54]. The SS methods using subarray arrangements cannot achieve this requirement, and thus one needs a higher number of elements to process correlated arrivals than would otherwise be required. The schemes that do not reduce the effective size of the array include those that restore the structure of the array covariance matrix for a linear array to that when there is no correlation. These are referred to as Toeplitz approximation method (TAM). For a uniform linear array, the covariance matrix in the absence of coherent arrivals has a Toeplitz structure, that is, entries of the matrix along its diagonals are equal, but this structure will not hold if any degree of coherency exists between sources.

In [51], the Toeplitz array structure is restored by averaging the matrix obtained in the presence of correlated arrivals by simple averaging along the diagonals, while in [52], a weighted average is used. To further enhance the capabilities of the TAM method, a modification was made in [53], where averaging is carried out on the magnitude of entries of the matrix along its diagonals without altering the phase. In addition, an iterative algorithm, in the same paper, was applied to iteratively reconstruct both the Toeplitz matrix and the desired eigenstructure from the observed covariance matrix. A method using an array covariance matrix obtained by averaging along the diagonals for DOA estimation is discussed in [54] and appears to offer computational advantages over similar methods.

As we shall see, Toeplitz-approximation-based methods are different from the dimension reduction processing techniques in obtaining the decorrelation capability by changing the data structure of the covariance matrix rather than sacrificing degrees of freedom, so the array aperture is taken full advantage of. However, generally speaking, Toeplitz-approximation-based methods, particularly for small arrays, are likely to be inferior to have a larger deviation in bearing estimates than other averaging methods such as FBSS or matrix reconstruction techniques.

Optimisation

While the spectral-based methods presented in the previous section are computationally attractive, they do not always yield sufficient accuracy. In particular, for scenarios involving highly correlated (or even coherent) signals, the performance of spectral-based methods may be insufficient. Parametric array processing methods, as an alternative, tackle the problem of coherent signals from a different point of view, by exploiting the underlying data model rather than restoring the rank deficiency of the covariance matrix. These techniques are not affected by signal coherency which causes the spectral based methods to fail in the eigen-decomposition step. However, they generally have a much higher computation load as they require a nonlinear multidimensional optimisation.

In array processing literature, maximum likelihood (ML) is the most representative technique as well as the optimum estimator since in the absence of errors, it maximises the log-likelihood function to find the ML estimate of the direction. According to the data model of the incident signals, this methodology can be divided into two approaches: deterministic maximum likelihood (DML) and stochastic maximum likelihood (SML).

One observed data model assumes that the signal waveforms are deterministic and unknown whereas the noise is a zero-mean isotropic and temporally spatially white Gaussian random process, leading to so-called deterministic maximum likelihood. The likelihood function is the joint probability density function (PDF) of all snapshots given the DOAs and viewed as a function of the desired variables, including the DOAs θ, the signal waveforms and the noise power, for this case.

As is well-known [55–58], DML signal parameter estimates are obtained by solving the following minimisation problem:

$$\hat{\theta}_{DML} = \arg\min_{\theta} \left\{ \mathrm{tr} \left\{ \mathbf{P}_{\mathbf{A}}^{\perp} \hat{\mathbf{R}} \right\} \right\} \tag{2.1}$$

where the operators $\mathrm{tr}\{\cdot\}$ and $\mathbf{P}_{\mathbf{A}}^{\perp}$ denote the trace of the bracketed matrix and the orthogonal projector onto the null space of $\mathbf{A}$, the array manifold, respectively, and $\hat{\mathbf{R}}$ is the observation covariance matrix.

The interpretation of ML is that the measurements $\mathbf{x}(t)$ from array are projected onto a subspace which is orthogonal to the subspace spanned by all anticipated signal components, and a power measurement $\frac{1}{N}\sum_{t=1}^{N} \|\mathbf{P}_{\mathbf{A}}^{\perp}\mathbf{x}(t)\|_2^2 = \mathrm{tr}\{\mathbf{P}_{\mathbf{A}}^{\perp}\hat{\mathbf{R}}\}$ is evaluated. The energy is clearly at a minimum if the projector indeed nulls everything in the subspace spanned by all the incident signals, i.e., when $\hat{\theta} = \theta_0$. Since only a finite number of snapshots, each contaminated by noise, are available, $\hat{\theta}$ may deviate from θ_0 to some extent to make the power minimum. However, if the observation is wide-sense stationary, the error will converge to zero as the number of samples approaches infinity. This remains valid for correlated or even coherent signals, although the accuracy for finite samples is somewhat dependent upon signal correlations.

The other ML technique reported in the literature is termed the SML method as both the signal waveforms and noise are modeled as white Gaussian random processes. Similar to DML, SML searches for desired directions that maximise the log-likelihood function of a given set of snapshots. After some algebraic manipulation and simplification, the DOA estimates can be obtained by [58–61]

$$\hat{\theta}_{SML} = \arg\min_{\theta} \left\{ \ln \det \left\{ \mathbf{A}\hat{\mathbf{R}}_s \mathbf{A}^H + \hat{\sigma}^2_{SML}\mathbf{I} \right\} \right\} \tag{2.2}$$

where the operator $\det\{\cdot\}$ denotes the determinant of the bracketed matrix, $\hat{\mathbf{R}}_s = \mathbf{A}^+(\hat{\mathbf{R}} - \hat{\sigma}^2_{SML}\mathbf{I})(\mathbf{A}^+)^H$ where the operator $\{\cdot\}^+$ denotes pseudo-inverse, and $\hat{\sigma}^2_{SML}$ is the power of noise in the SML model.

As seen in (2.1) and (2.2), the criterion functions are both highly nonlinear optimisation problems of their argument θ. In the absence of a closed form solution, it requires iterative schemes for finding solutions. Given sufficiently accurate initial estimates, the well-known Gauss-Newton algorithm [62–64] updates the search direction at each iteration so as to converge rapidly to the global minimum, but at the cost of expensive computation. Other schemes, such as the alternating projection (AP) method [55, 65] and the expectation-maximization (EM) algorithm [58, 66, 67] have been proposed to decrease computation complexity while maintaining satisfactory performance. The more general space alternating generalized EM (SAGE) algorithm was applied to the direction finding problem in [68, 69], which has much shorter computation time than EM does. However, there are still two issues affecting these implementation schemes: one is the search step size, and the other is the initial DOA estimates. As known, a large step size will bring about faster convergence but may miss local minima, while a smaller step size will take a longer period of time to converge. It is crucial for most iterative algorithms to have good initial estimates. If the selection is improper, the search procedure may fall into a local minimum, and be unable to jump out of it to reach the desired global minimum.

Among all popular methods the ML approaches provide a superior asymptotic performance and remain stable in scenarios involving small numbers of snapshots, coherent signals and low signal-to-noise ratio (SNR). For Gaussian signals, the SML estimates attain the Cramér-Rao lower bound (CRLB) on the estimation error variance, derived

under the stochastic signal model, while the DML estimates do not attain the corresponding (deterministic) CRLB since all unknowns in the deterministic model cannot be estimated consistently.

In order to further reduce computation cost by incorporating the advantages of subspace, some subspace-based methods [57,70], which are so-called subspace fitting (SF), were derived as a large-sample realisation of the ML methods. These methods are computationally efficient, especially for the ULA case [3,71], but offer similar performance to the ML methods, resolving the coherent sources without reducing the array aperture.

The subspace-based methods rest on the fact that the signal subspace is a linear combination of a space spanned by the array manifold. When noise exists, this relationship does not hold exactly. One solution is to construct a fitting relationship to find out the desired angles which can get the two fitted the most closely in the least squares sense, i.e., the signal subspace fitting (SSF) estimate can be obtained by solving the following nonlinear optimisation problem

$$\hat{\theta}, \hat{\mathbf{T}} = \arg\min_{\theta, \mathbf{T}} \left\| \hat{\mathbf{U}}_s - \mathbf{A}\mathbf{T} \right\|_F^2 \tag{2.3}$$

where the columns of $\hat{\mathbf{U}}_s$ are the eigenvectors corresponding to large eigenvalues of $\hat{\mathbf{R}}$, and span the signal subspace, and $\mathbf{T}$ is a full rank matrix. Obviously the SSF estimate can be obtained by solving (2.3), a nonlinear optimisation problem. Extending (2.3) to a more generic case, we will naturally have a weighted subspace fitting problem as

$$\hat{\theta}, \hat{\mathbf{T}} = \arg\min_{\theta, \mathbf{T}} \left\| \hat{\mathbf{U}}_s \mathbf{W}^{\frac{1}{2}} - \mathbf{A}\mathbf{T} \right\|_F^2 \tag{2.4}$$

where $\mathbf{W}$ is a weighting matrix. Hence, the solution with regard to $\hat{\theta}$ can be obtained by

$$\hat{\theta} = \arg\min_{\theta} \left\{ \mathrm{tr} \left\{ \mathbf{P}_{\mathbf{A}}^{\perp} \hat{\mathbf{U}}_s \mathbf{W} \hat{\mathbf{U}}_s^H \right\} \right\}. \tag{2.5}$$

It should be specifically noted that when the weighting matrix satisfies following equation

$$\mathbf{W}_{sopt} = (\hat{\mathbf{\Sigma}}_s - \hat{\sigma}^2 \mathbf{I})^2 \hat{\mathbf{\Sigma}}_s^{-1} \tag{2.6}$$

where $\hat{\mathbf{\Sigma}}_s$ is a diagonal matrix consisting of large eigenvalues of $\hat{\mathbf{R}}$, and $\hat{\sigma}^2$ denotes a consistent estimate of the noise power, (2.5) is the so-called weighted signal subspace fitting (WSSF) method with optimum weights [72,73].

On the other hand, a relationship also exists between the noise subspace and the array manifold—the noise subspace is orthogonal to the subspace spanned by the array manifold. Based on this, we can obtain a fitting relationship, which is termed noise subspace fitting (NSF), as follows

$$\begin{aligned}\hat{\theta} &= \arg\min_{\theta} \left\| \hat{\mathbf{U}}_n^H \mathbf{A} \right\|_F^2 \\ &= \arg\min_{\theta} \left\{ \mathrm{tr} \left\{ \hat{\mathbf{U}}_n^H \mathbf{A}\mathbf{A}^H \hat{\mathbf{U}}_n \right\} \right\}\end{aligned} \tag{2.7}$$

where the columns of $\hat{\mathbf{U}}_n$ are the eigenvectors corresponding to small eigenvalues of $\hat{\mathbf{R}}$, and span the noise subspace.

Likewise, NSF represented in (2.7) can be further extended to a weighted expression, that is,

$$\begin{aligned}\hat{\theta} &= \arg\min_{\theta} \left\| \hat{\mathbf{U}}_n^H \mathbf{A}\mathbf{W}^{\frac{1}{2}} \right\|_F^2 \\ &= \arg\min_{\theta} \left\{ \mathrm{tr} \left\{ \hat{\mathbf{U}}_n^H \mathbf{A}\mathbf{W}\mathbf{A}^H \hat{\mathbf{U}}_n \right\} \right\} \\ &= \arg\min_{\theta} \left\{ \mathrm{tr} \left\{ \mathbf{W}\mathbf{A}^H \hat{\mathbf{U}}_n \hat{\mathbf{U}}_n^H \mathbf{A} \right\} \right\}.\end{aligned} \tag{2.8}$$

It is natural to ask a question—If there is an optimum weighting matrix in the weighted signal subspace, then does noise subspace have an optimum weighting matrix which makes the estimation optimal? The answer is "yes". Ottersten et al gave an expression of the optimum weighting matrix of the weighted noise subspace in [74] as

$$\mathbf{W}_{nopt} = \mathbf{A}^+(\theta_0) \hat{\mathbf{U}}_s \mathbf{W}_{sopt} \hat{\mathbf{U}}_s^H (\mathbf{A}^+(\theta_0))^H. \tag{2.9}$$

It should be noted that (2.7), (2.8), and (2.9) are all derived on the condition that orthogonality between the noise subspace and array manifold hold, which implies the signals should be uncorrelated in the NSF model. If the sources are coherent, the noise subspace is not orthogonal to the array manifold any more, and the conditions for the

NSF algorithm do not hold accordingly. This fully demonstrates that the drawback of NSF lies in its inability to resolve estimates for coherent signals.

Some other preprocessing schemes to decorrelate the coherent sources include frequency smoothing [75, 76], polarimetric angular smoothing [77, 78], phase mode excitation [79], virtual array transformation [80, 81], etc., but these categories are usually applicable to particular circumstances, such as wideband signals, polarisation sensitive arrays, circular arrays, nonuniform spaced arrays, etc.

2.3 Development of Unknown Noise Processing

Many proposed estimators, like MUSIC, ESPRIT, ML, WSF, etc., are established with the so-called uniform white noise assumption. Accordingly, sensor additive noises are modeled as spatially and temporally uncorrelated zero-mean Gaussian processes such that the noise covariance matrix is proportional to an identity matrix. Alternatively, if the noise is arbitrary but its covariance can be estimated from noise-only data, the noise model can be easily transformed to the uniform one by the prewhitening technique and any high-resolution direction finding algorithm can be straightforwardly applied to the transformed data [82, 83]. However, this assumption is not realistic in many practical applications [34, 84–90], where the noise fields are spatially coloured or nonuniform, and its covariance may change slowly with time or a signal-free environment is not always available. The question that then arises is how to solve the estimation problem without the prior knowledge of the noise environment. The spatial correlation or nonuniformity in the unknown noise may cause significant bias of the estimates assuming spatially white noise [91, 92]. In these applications, it is beneficial to take the spatial colour or nonuniformity of the noise into account to improve the resolution of the DOA estimation.

2.3.1 Parametric Model for Unknown Noise

To address the problem of DOA estimation in the presence of coloured or correlated unknown noise, a number of algorithms have been developed but with special parametric models imposed on the signals or noise. For instance, in [84, 87, 89], the noise field is assumed to satisfy standard autoregressive/autoregressive moving average (AR/ARMA) models. It can be readily verified that the noise is uniform and white under the condition of a zero order model, but it becomes coloured when the model order is larger than zero. In [82, 93], the noise covariance can be parameterised using a linear combination of known weighting matrices. The method in [86] requires the temporal correlation interval of the signals to be larger than that of the sensor noise. Differing from the prevailing perspective of noise parameterisation, the signals in [90] are required to be partially known as a linear combination of a set of basis functions. Clearly, such constraints on noise or signal may severely restrict the applications of the aforementioned techniques because these assumptions are built up only for certain cases, and are not generic in practice. The performances of these estimators will deteriorate if the required constraints do not match the real ones. Unlike previous work, a modified ML-based approach has been proposed in [94] where structural constraints of the signal or noise covariances are not required. Since an implicit approximation is adopted to estimate the noise covariance matrix, the practical performance of this approach can be substantially worse than that dictated by the corresponding CRLB [95]. Additionally, this method relies on a certain array structures, like a ULA, so is not applicable to an arbitrary geometry.

Owing to the superior statistical performance of ML techniques, most aforementioned methods attempt to apply ML criteria to handle coloured or correlated noise with unknown covariance. However, these approaches have to carry out multidimensional search with respect to all unknown variables, including the DOA angles, the signal powers, and the noise parameters, where the noise and signal variances are nuisance parameters. Compared with one unknown, i.e., the noise power, in the case of uniform white noise, the number of unknowns in the coloured noise model, without any prior knowledge, will rise with the square of the number of array elements, which

can be a considerable number, resulting in a huge computation burden. Even if these methods reduce the dimension of the parameter space and the associated computation of the ML functions by using partial prior knowledge or particular assumptions regarding the signals, noise, or array structures, it is still difficult to completely separate the DOA angles from other unknown parameters. As a result, the DOAs must be jointly estimated along with other nuisance parameters by solving nonlinear and multidimensional optimisation problems.

2.3.2 Sparse Model for Unknown Noise

To overcome the drawbacks of the aforementioned ML techniques, an alternative approach for reducing the number of noise parameters is to make the noise covariance matrix sparse by adopting a certain array geometry. In several real applications (for example, if a sparse array is used), the general coloured noise assumption can be simplified by assuming the sensor noise is spatially white [91, 92, 96]. In this case, the noise covariance matrix of the array can be represented by a diagonal matrix while its power in each channel is no longer identical. Such a noise model is reasonable in practice where the hardware in receiving channels or prevailing external noise (for example, reverberation noise in sonar or external seismic noise) received by the elements of sparse arrays are not homogenous [91].

Many algorithms have been proposed in the past decade for DOA estimation with nonuniform white noise. Pesavento and Gershman [91] first derived the deterministic and stochastic CRLBs for such a DOA estimation problem. In order to avoid the computational burden of the straightforward implementation of the ML estimator (MLE), a new deterministic MLE based on stepwise concentration was also proposed. Following this work and to bridge the gap for the stochastic MLE, Chen et al [92] extended a stochastic ML DOA estimator under the same noise model, and discussed the application of the algorithm to a ULA.

Undoubtedly, as mentioned in Section 2.2.2, the ML DOA estimator is too complex for a real-time system, though much work has been done in reducing the dimensionality of the search space. As a result, there is a demand for suboptimum solutions, and many

modified subspace-based estimators are subsequently proposed. In [96], a transform-based covariance differencing approach is introduced which not only improves the resolution of the bearing estimation in the case of uniform noise, but can also be used to eliminate the effects of (unknown) unequal noise power on the array eigenstructure. The price for the advantages in this approach is the halving of the number of sources which can be estimated. In another method [97], the noise covariance can be estimated from the array covariance directly, then the received data is prewhitened by the estimated noise covariance, but such a procedure has the drawback of shrinking the number of estimated signal by an even more aggressive factor of three. Liao et al [98] developed a modified algorithm based on the work in [97] to improve the performance of estimation while mitigating the effect of nonuniform noise. The idea is based on the fact that the array covariance is a Toeplitz Hermitian matrix in the noise-free situation. The estimated noise covariance matrix can be subtracted out from the array covariance, then the MUSIC algorithm can be applied directly. Unfortunately, compared with [97], this algorithm does not improve the number of sources which can be estimated, and it only works for a ULA.

Recently, a more generic sparse model of unknown noise was firstly proposed by Vorobyov et al [95], then developed by Li and Nehorai [99]. The model requires a sensor array comprised of multiple widely separated subarrays such that noise can be assumed uncorrelated between different subarrays. As a result, the array noise covariance matrix becomes block-diagonal. By virtue of sparsity of the matrix, the number of nuisance noise parameters is still much less than that for the completely coloured noise case, which results in better computational efficiency. In [95], a deterministic MLE was introduced for the case of multiple subarrays. Authors in [99] added a stochastic MLE, based on an Expectation-Maximization (EM) framework, in spatially coloured noise fields using sparse sensor arrays. Additionally, since previous work [100] showed that DOA estimates under spatially coloured noise can be separated using the non-zero-mean component without specific constraints on array geometry, signals or noise, both cases of zero-mean and non-zero-mean Gaussian signals are presented and extensively studied in [99].

Because of the attractive property of Gaussian processes that all cumulant spectra of order higher than two are identical to zero, high order cumulants (HOC), as a by-product, are effective against Gaussian noise whose spatial coherency may be unknown, though its main function is to gain more DOFs for non-Gaussian signals. The issue has been addressed by a number of papers, where corresponding estimators and performance analysis have been developed [101–104]. However, due to the constraint on statistical property of incident signals, i.e., non-Gaussian process, and the requirement of a large number of snapshots, HOC-based methods for estimation problems in the presence of unknown noise have faded into oblivion in the more recent literature.

2.4 Development of Noncircular Signal Processing

DOA estimation of narrowband planewave signals has been extensively studied in the past few decades, and many high-resolution algorithms have been developed for it. However, *a priori* knowledge such as the structure of incident signals has not been considered in these traditional algorithms.

In many modern wireless communication systems or satellite systems, some modulated signals are noncircular. Only recently has some work taken into account the extra information contained within these incident signals, where subspace-based methods are the most representative [105–109]. By exploiting second order noncircularity, the array aperture is virtually doubled, which results in a significantly reduced estimation error and the ability to resolve approximate twice as many sources. In the meantime, Delmas and Abeida derived the stochastic CRLB for DOA estimation of noncircular signals and analysed asymptotic properties of noncircular MUSIC-type algorithms [110, 111]. Roemer and Haardt comprehensively presented asymptotic performance analysis of noncircular ESPRIT-type algorithms and derived the deterministic CRLB [112, 113].

Although most of the research on direction finding of noncircular signals follows the same line of the existing work on the circular signals estimation, the improvement of estimation performance obtained by taking advantage of noncircularity can expand its

application field and reduce the complexity of hardware design, so investigation in this area is still essential and valuable.

2.4.1 Description

Definition of circularity of second order statistics is simple. Consider a signal $s(t)$ that is complex and zero-mean, but not necessarily Gaussian. The variable $s(t)$ is said to be noncircular, if the elliptic covariance $E_t[s^2(t)] \neq 0$ [114], otherwise $s(t)$ is defined to be circular. For the arbitrary signal $s(t)$, we have $E_t[s^2(t)] = \rho e^{j\phi} E_t[|s(t)|^2] = \rho e^{j\phi}\sigma_s^2$, where ϕ is the noncircularity phase which is deterministic and does not vary with time, and ρ is noncircularity rate which satisfies $0 \leq \rho \leq 1$ (from the Cauchy-Schwartz inequality). Obviously, the signals which satisfy $0 < \rho \leq 1$ are noncircular. The noncircularity rate ρ is determined by the modulation of the signal, e.g., $\rho = 1$ for standard BPSK signals. Note that the signal with $\rho = 1$ is the so-called strictly second-order noncircular signal or rectilinear signal [111]. In this case, let $s(t) = e^{j\psi}s_0(t)$, where ψ and $s_0(t)$ are the initial phase and real-valued symbol (i.e., amplitude) of $s(t)$, respectively. Since $E_t[s^2(t)] = e^{j2\psi}E_t[s_0^2(t)] = e^{j2\psi}\sigma_s^2 = e^{j\phi}\sigma_s^2$, it shows clearly that $\psi = \frac{\phi}{2}$ [20].

In real applications, common noncircular signals include amplitude modulation (AM), binary phase shift keying (BPSK), offset quadrature phase shift keying (OQPSK), amplitude shift keying (ASK), pulse amplitude modulation (PAM) signals [106,113]. These signals can be divided into two categories: one is inherently noncircular, like AM, BPSK, ASK, and PAM signals which can be obtained by shifting the phase of real signals and of rectilinearity (i.e., $\rho = 1$), while the other can have noncircularity with $\rho = 1$ by applying a preprocessing procedure, like OQPSK modulated signals.

2.4.2 Research Status of DOA Estimation of Noncircular Signal

The classical high-resolution direction finding algorithms only consider the covariance $E_t[s(t)s^*(t)]$, and do not exploit the information in $E_t[s^2(t)]$. New estimation approaches of noncircular signals make use of the elliptic covariance based on the classical subspace-based algorithms instead of changing the essence of the algorithm itself.

The main task of the research is to analyse the characteristics of noncircular signals, especially the difference in estimation performance, caused by noncircularity, from the classical subspace-based methods.

In 1998, Gounon et al [115] proposed the first MUSIC-type algorithm for noncircular signals, which is called NC-MUSIC, and Galy introduced NC-MUSIC in his Ph.D thesis [116] as well. Unfortunately, their work was published in French, which greatly reduced its influence among the international research community. The first English article that really introduced the idea of DOA estimation of noncircular signals in its true sense was that of Chargé et al [105]. This work introduced the concept of noncircular signals and established a standard approach to the area that was to be adopted by a number of subsequent researchers. In their paper, the authors utilised snapshots of the array output and their conjugates simultaneously to construct an augmented covariance matrix, then performed the eigen-decomposition on it to obtain the eigenvectors corresponding to the noise subspace, and subsequently constructed a spatial spectrum function, which is similar to that of the standard MUSIC algorithm, via the orthogonality between the steering vectors and noise subspace. To get the DOA estimates, polynomial rooting was adopted instead of a two dimensional search over all azimuth angles and noncircularity phases using the spatial spectrum function. As a result of this processing procedure, the DOA estimation becomes independent from the noncircularity phase estimation, and computation cost is reduced considerably. The proposed algorithm is restricted to a ULA, but has distinct advantages over the standard Root-MUSIC [117] algorithm since it expands the effective array aperture and shows improvements both in the estimation accuracy and resolution.

In 2004, Haardt and Roemer applied unitary ESPRIT to direction finding of rectilinear signals, which they called NC-UESPRIT [106]. The key processing step of NC-UESPRIT is a unitary transformation of the augmented covariance matrix from the complex to the real domain, which has the advantage of computational attractiveness. Additionally, the combination of the SS technique with NC-UESPRIT to separate more than two coherent wavefronts and extensions of NC unitary ESPRIT to the multidimensional case (e.g., uniform rectangular arrays) are given in the same paper as well.

Like noncircular Root-MUSIC, NC-UESPRIT allows resolution of more noncircular signals and improve the accuracy of direction finding.

Combining HOC and noncircularity, Liu et al proposed an extended $2q$-MUSIC algorithm for rectilinear signals, which is called NC-$2q$-MUSIC [20]. This algorithm is just an extension of standard $2q$-MUSIC [118] to noncircular applications. Three $2q$th order cumulant matrices, one of which has to contain the noncircular information, are required to construct an augmented matrix which is twice the size of the elemental matrices. In order to avoid a two dimensional search, this technique eliminates the noncircularity phase by taking the partial derivative of the spatial spectrum function with respect to it. Moreover, the authors explored the estimation capacity and computation complexity of NC-$2q$-MUSIC in the case of a ULA with M sensors, and found that the fourth order version can handle up to $3(M-1)$ signals, which is a big increase in estimation capacity especially when M is large.

The aforementioned methods all assume that the signals impinging on sensors are purely noncircular, but this assumption is not always valid in practice. DOA estimation under the coexistence of both circular and rectilinear sources was addressed in [114]. Based on the different characteristics of the augmented matrix when sources are circular or rectilinear, the noise and signal (circular or rectilinear) subspace are identified for each case, so the bearings of circular and rectilinear sources can be estimated respectively. In fact, the approach in [114] can be applied to a relaxed case when there are arbitrary sources with noncircularity rate $0 < \rho < 1$ besides circular and rectilinear sources. It is noteworthy that in this case each circular or noncircular ($0 < \rho < 1$) signal corresponds to two eigenvalues, while each rectilinear signal corresponds to only one eigenvalue.

Recently, Liu et al made use of sparse representation to tackle the problem of DOA estimation of noncircular signals [109]. The work has been reported on using the ℓ_p-norm-based ($0 \leq p \leq 1$) techniques to exploit the joint sparsity property of the covariance and elliptic covariance matrices for DOA estimation by reconstructing the array outputs on a directional overcomplete dictionary. The results in this paper show that,

the exploitation of spatial sparsity of the incident noncircular signals helps to significantly enhance the adaptation of the DOA estimators to much more demanding scenarios, such as low SNR and limited snapshots, and they are also much more immune to the lack of prior source number information. However, as the ℓ_p-norm-based techniques are based on separable penalties, they can hardly reduce the structural errors (biased global minimum) and the convergence errors (failure of achieving the global minimum) simultaneously [119], and those two kinds of errors are defined in [120]. Although some modified algorithms are available to reduce the estimation biases of the source bearings [121, 122], they can hardly modify the selected model which is valid only when the DOA estimates are located exactly on the sampling grid, otherwise significant performance deterioration of the estimator will occur.

A significant amount of research has focused on the performance analysis of noncircular signal estimation, including CRLB, asymptotic performance, and resolution. Delmas and Abeida investigated the stochastic CRLB [110] as well as it in the presence of unknown noise [123]. In [110], the noncircular signals are assumed to be a complex Gaussian random process, and the stochastic CRLB was derived by either computing the asymptotic covariance matrix of the MLE or an extended Slepian-Bangs formula. Similar to [110], an explicit closed-form expression of the stochastic CRLB was obtained directly from the Slepian-Bangs formula in the general case of arbitrary unknown Gaussian noise [123]. As a special case, the CRLB under the nonuniform white noise assumption was given as well. However, these bounds cannot be applied to the rectilinear signal case since the real and imaginary parts of noncircular signals were treated as different random variables in [110, 123], which only hold under the condition of $0 < \rho < 1$ but are not true when $\rho = 1$ due to the linear dependence [112]. As a result, Roemer and Haardt bridged this gap with a derivation of the deterministic CRLB, and through analysis of the result they found that in the case where two rectilinear sources approach the same direction, the CRLB reaches a finite value, compared with an infinite CRLB for arbitrary (i.e., not necessarily noncircular) sources in the same scenario. The cases where the rectilinear signals do not provide any gain over generic signals in terms of the CRLB are also stated.

When it comes to asymptotic performance, Abeida and Delmas extensively investigated MUSIC-type algorithms for an arbitrary array geometry by providing closed-form expressions of the covariance of the asymptotic distribution of different projection matrices [108]. Different robustness properties of the asymptotic covariance of the DOA estimate resolved by such algorithms were proved as well. As prevalent as MUSIC, the asymptotic performance of ESPRIT-type algorithms is analysed comprehensively by Steinwandt et al [113] more recently. Besides proposing R-dimensional NC standard ESPRIT and NC unitary ESPRIT algorithms, the authors presented an asymptotic performance analysis of both algorithms by performing the first order Taylor series expansion of the estimation error in terms of the explicit noise perturbation, and proved that the performance is identical for both algorithms with respect to high SNRs or a large number of snapshots. Mean squared error (MSE) expressions were also given in the same paper with common assumptions that the noise is zero mean and has finite SOS.

The work on resolution analysis has been done by Abeida and Delmas for an NC MUSIC-type algorithm to compare it against standard MUSIC [111]. The authors provided theoretical and approximate interpretable closed-form expressions of the threshold array SNR at which two closely separated sources can be distinguished, and proved that the thresholds of the standard MUSIC are independent of the distribution of the sources including their noncircularity, while the NC MUSIC-type algorithm relies on the noncircularity phase for the bearing separation.

2.4.3 Direction of Noncircular Signal Research

There is a considerable amount of research on noncircular signals in array processing besides the work outlined in the above sections. The research can be categorised into a number of different theoretical areas, including source enumeration, optimisation of spatial spectrum estimation and beamforming, spatial spectrum estimation and beamforming of special signals, for special array geometries, and in the presence of imperfections, and application of advanced signal processing to spatial spectrum estimation, which could all be investigated further.

Spatial spectrum estimation and its application for particular purposes will continue to form a large contingent of research. Source enumeration is of significant interest in the field of array processing. In the classical direction finding methods, the number of sources is normally considered to be an *a priori* parameter, which typically is not the case. To accurately estimate the DOA of noncircular signals in practice, especially when $0 < \rho < 1$ or circular and noncircular signals coexist, source enumeration has to be carried out in advance, but this issue has not been addressed. Additionally, it is natural to extend the classical optimisation methods, like ML and WSF, to noncircular signals scenario. However, the augmented matrix comprising observations and their conjugates may not fit in with the existing algorithms which only utilise the information in the covariance matrix for special signals, such as coherent, wideband, and distributed sources, special array geometries, such as circular, nonuniform linear, and L-shaped arrays, and in the presence of imperfections, such as mutual coupling, gain/phase uncertainty, and sensor location error. Additional processing procedures would need to be developed to adapt to these complex scenarios.

Conventional methods are typically linear-algebra-based methods, requiring computationally intensive matrix inversion, and cannot meet real-time requirement. Neural network, as a promising and advanced technique, can be readily implemented in analog VLSI or on special purpose massively parallel hardware. As neural methods make up for shortcomings of its linear-algebra-based counterparts with nonlinear property, adaptive learning capability, strong fault-tolerant capability, and insensitivity to uncertainty, consideration of the unconventional algorithms and the applications these impose also raises a number of questions [124–127], and noncircular signals are no exception.

Clearly, research interest in noncircular signal with sensor arrays will continue to be maintained, with the literature demonstrating a wide variety of sub-fields and a great many research questions yet to be addressed.

2.5 Conclusion

This chapter reviews the development of DOA estimation in array processing and addressed critical issues in nonideal signal models, including effects of signal coherency, unknown nonuniform and coloured noise, and signal noncircularity. Many of ideas for dealing with the problems are discussed, with important differences between the ideas highlighted. The chapter indicates some aspects of array processing research in practice, and demonstrates many of the areas currently arousing research interest, as well as indicating potential for future research.

Chapter 3

Linear Algebra Prerequisites

LINEAR algebra is an essential mathematical foundation for array signal processing. The matrix algebra presented in this chapter forms the underlying basis for all the research carried out with some important assumptions towards enabling innovations within this current research. As subspace-based DOA estimation is the emphasis of the research in the thesis, definitions and properties of subspace theory are introduced. Additionally, the Cramér-Rao lower bound, in estimation theory, is discussed to provide familiarity with this important analytical tool.

3.1 Introduction

In theoretical analysis and practical engineering applications, matrix calculations are always indispensable. Linear algebra is the most fundamental and useful mathematical tool, involving not only a number of mathematical operations, such as eigen-decomposition, derivative, inverse, Schur-Hadamard product, Kronecker product, but also many important scalar functions, such as rank, determinant, trace, norm. In fact, numerous theoretical innovations and technological developments in a broad range of disciplines, such as signal and information processing, wireless communications, electronics, system and control, pattern recognition, and aeronautics and astronautics, result from the creative extension and application of linear algebra.

This chapter introduces some basic definitions, operations, and properties which are utilised for algorithm development and theoretical analysis of DOA estimation in the subsequent chapters. In the interest of brevity, important and commonly used properties and conclusions are given directly, and the corresponding derivations and proofs are not covered here. A number of relevant titles containing such information are contained in the bibliography.

3.2 Rank of a Matrix

The column space of a matrix $\mathbf{A}_{m\times n}$ is the span of the set of its columns, denoted by $\text{span}(\mathbf{A})$. The rank of this matrix, denoted by $\text{rank}(\mathbf{A})$, is the dimension of this space, the number of linearly independent columns, i.e.,

$$\text{rank}(\mathbf{A}) = \dim[\text{span}(\mathbf{A})]. \tag{3.1}$$

Below is a list of selected properties of the rank of a matrix, which will be utilised in theoretical analysis of subsequent chapters:

1) The rank is a positive integer.

2) The rank is less than or equal to the number of rows or columns of a matrix.

3) If $\text{rank}(\mathbf{A}_{m\times n}) = m(< n)$, $\mathbf{A}$ is of full row rank.

4) If $\text{rank}(\mathbf{A}_{m\times n}) = n(< m)$, $\mathbf{A}$ is of full column rank.

5) The rank of an arbitrary matrix after pre-multiplying with a full row matrix or post-multiplying by a full column matrix remains unchanged by such an operation.

The rank of a matrix has the following common inequality relations:

1) For an arbitrary matrix $\mathbf{A}_{m\times n}$, $\text{rank}(\mathbf{A}_{m\times n}) \leq \min\{m, n\}$ always holds.

2) Let $\mathbf{A}, \mathbf{B} \in \mathbb{C}^{m\times n}$, then

$$\text{rank}(\mathbf{A}+\mathbf{B}) \leq \text{rank}([\mathbf{A}, \mathbf{B}]) \leq \text{rank}(\mathbf{A}) + \text{rank}(\mathbf{B}). \tag{3.2}$$

3) Let $\mathbf{A} \in \mathbb{C}^{m\times k}$, and let $\mathbf{B} \in \mathbb{C}^{k\times n}$, then

$$\text{rank}(\mathbf{A}) + \text{rank}(\mathbf{B}) - k \leq \text{rank}(\mathbf{AB}) \leq \min\{\text{rank}(\mathbf{A}), \text{rank}(\mathbf{B})\}. \tag{3.3}$$

4) If some rows or columns of a matrix are eliminated, then the rank of the remaining submatrix is less than or equal to the rank of the original matrix.

Additionally, common equality relations on the rank of a matrix are as follows:

1) Let $\mathbf{A} \in \mathbb{C}^{m\times n}$, then

$$\text{rank}(\mathbf{A}^H) = \text{rank}(\mathbf{A}^T) = \text{rank}(\mathbf{A}^*) = \text{rank}(\mathbf{A}). \tag{3.4}$$

2) Let $\mathbf{A} \in \mathbb{C}^{m\times n}$, and let $c \neq 0$, then $\text{rank}(c\mathbf{A}^H) = \text{rank}(\mathbf{A})$.

3) Let $\mathbf{A} \in \mathbb{C}^{m\times n}$, then

$$\text{rank}(\mathbf{A}\mathbf{A}^T) = \text{rank}(\mathbf{A}^T\mathbf{A}) = \text{rank}(\mathbf{A}) \tag{3.5}$$

$$\text{rank}(\mathbf{A}\mathbf{A}^H) = \text{rank}(\mathbf{A}^H\mathbf{A}) = \text{rank}(\mathbf{A}). \tag{3.6}$$

4) Let $\mathbf{A} \in \mathbb{C}^{m\times m}$, and let $\mathbf{C} \in \mathbb{C}^{n\times n}$, both are of full rank, then for an arbitrary matrix $\mathbf{B} \in \mathbb{C}^{m\times n}$, $\text{rank}(\mathbf{AB}) = \text{rank}(\mathbf{B}) = \text{rank}(\mathbf{BC}) = \text{rank}(\mathbf{ABC})$.

5) Let $\mathbf{A}, \mathbf{B} \in \mathbb{C}^{m\times n}$, then $\text{rank}(\mathbf{A}) = \text{rank}(\mathbf{B})$ if and only if there exist two nonsingular matrices $\mathbf{X} \in \mathbb{C}^{m\times m}$, $\mathbf{Y} \in \mathbb{C}^{n\times n}$, such that $\mathbf{B} = \mathbf{XAY}$.

3.3 Matrix Inverses

If $\mathbf{A} \in \mathbb{C}^{m \times m}$ and is of full rank, then the inverse of $\mathbf{A}$, denoted by $\mathbf{A}^{-1}$, is uniquely determined by $\mathbf{A}$ and satisfies

$$\mathbf{A}^{-1}\mathbf{A} = \mathbf{A}\mathbf{A}^{-1} = \mathbf{I} \tag{3.7}$$

where $\mathbf{I}$ is the identity matrix,

$$\mathbf{I} = \begin{bmatrix} 1 & 0 & \cdots & 0 \\ 0 & 1 & \cdots & 0 \\ \vdots & \vdots & \ddots & \vdots \\ 0 & 0 & \cdots & 1 \end{bmatrix}. \tag{3.8}$$

If the inverse does not exist (i.e., $\text{rank}(\mathbf{A}) < m$), then $\mathbf{A}$ is referred to as a singular matrix.

The inverse has the following properties:

1)

$$(\mathbf{A}^T)^{-1} = (\mathbf{A}^{-1})^T. \tag{3.9}$$

2)

$$(\mathbf{A}^H)^{-1} = (\mathbf{A}^{-1})^H. \tag{3.10}$$

3) If $\mathbf{A}$ is nonsingular, then $\mathbf{A}$ is an orthogonal matrix $\Leftrightarrow \mathbf{A}^{-1} = \mathbf{A}^T$; $\mathbf{A}$ is a unitary matrix $\Leftrightarrow \mathbf{A}^{-1} = \mathbf{A}^H$.

3.4 Moore-Penrose Pseudo-inverse

If $\mathbf{A} \in \mathbb{C}^{m \times n}$, then there exists a unique matrix $\mathbf{B} \in \mathbb{C}^{n \times m}$, if and only if which satisfies the following conditions:

$$\mathbf{A}\mathbf{B}\mathbf{A} = \mathbf{A} \tag{3.11}$$

$$\mathbf{BAB} = \mathbf{B} \tag{3.12}$$

$$(\mathbf{AB})^H = \mathbf{AB} \tag{3.13}$$

and

$$(\mathbf{BA})^H = \mathbf{BA}, \tag{3.14}$$

the matrix $\mathbf{B}$ is referred to as the Moore-Penrose pseudo-inverse, denoted by $\mathbf{A}^+$. It is readily verified that:

$$\mathbf{A}^+ = \mathbf{A}^H(\mathbf{AA}^H)^{-1}, \quad m < n \tag{3.15}$$

$$\mathbf{A}^+ = \mathbf{A}^{-1}, \quad m = n \tag{3.16}$$

$$\mathbf{A}^+ = (\mathbf{A}^H\mathbf{A})^{-1}\mathbf{A}^H, \quad m > n. \tag{3.17}$$

Furthermore, $\mathbf{A}^+$ always exists and is unique.

Let $\mathbf{A} \in \mathbb{C}^{m\times k}, \mathbf{B} \in \mathbb{C}^{k\times n}$, $(\mathbf{AB})^+ = \mathbf{B}^+\mathbf{A}^+$, if and only if either

1) $\mathbf{A}^+\mathbf{ABB}^H\mathbf{A}^H = \mathbf{BB}^H\mathbf{A}^H$ and $\mathbf{BB}^+\mathbf{A}^H\mathbf{AB} = \mathbf{A}^H\mathbf{AB}$, or

2) $\mathbf{A}^+\mathbf{ABB}^H$ and $\mathbf{A}^H\mathbf{ABB}^+$ are Hermitian, or

3) $\mathbf{A}^+\mathbf{ABB}^H\mathbf{A}^H\mathbf{ABB}^+ = \mathbf{BB}^H\mathbf{A}^H\mathbf{A}$, or

4) $\mathbf{A}^+\mathbf{AB} = \mathbf{B}(\mathbf{AB})^+\mathbf{AB}$ and $\mathbf{BB}^+\mathbf{A}^H = \mathbf{A}^H\mathbf{AB}(\mathbf{AB})^+$

is satisfied [128].

The following properties of the Moore-Penrose pseudo-inverse follow immediately from its definition and uniqueness. Let $\mathbf{A} \in \mathbb{C}^{m\times n}$, one has

$$(\mathbf{A}^H)^+ = (\mathbf{A}^+)^H \tag{3.18}$$

$$\mathbf{A}^+ = (\mathbf{A}^H\mathbf{A})^+\mathbf{A}^H = \mathbf{A}^H(\mathbf{AA}^H)^+ \tag{3.19}$$

$$\operatorname{rank}(\mathbf{A}^+) = \operatorname{rank}(\mathbf{A}^+\mathbf{A}) = \operatorname{rank}(\mathbf{AA}^+) = \operatorname{rank}(\mathbf{A}) \tag{3.20}$$

$$(\mathbf{AA}^H)^+ = (\mathbf{A}^+)^H\mathbf{A}^+ \tag{3.21}$$

$$(\mathbf{AA}^H)^+(\mathbf{AA}^H) = \mathbf{AA}^+. \tag{3.22}$$

3.5 Derivative Operations

As discussed in Section 2.2.2, a maximum likelihood estimator always attempts to maximise (or minimise) the log-likelihood (LL) function. To this end, one needs to find the vector or matrix derivatives. Another application of derivatives that we encounter in following chapters is the calculation of the CRLB which is a fundamental tool in the parameter estimation.

The gradient of a scalar $a(\boldsymbol{\theta})$ with respect to a real vector $\boldsymbol{\theta} \in \mathbb{R}^{m\times 1}$ is defined as

$$\frac{\partial}{\partial \boldsymbol{\theta}} a(\boldsymbol{\theta}) = \begin{bmatrix} \frac{\partial a(\boldsymbol{\theta})}{\partial \theta_1} \\ \frac{\partial a(\boldsymbol{\theta})}{\partial \theta_2} \\ \vdots \\ \frac{\partial a(\boldsymbol{\theta})}{\partial \theta_M} \end{bmatrix}. \tag{3.23}$$

If $\mathbf{a}(\boldsymbol{\theta}) \in \mathbb{R}^m$ is a row vector,

$$\mathbf{a}^T(\boldsymbol{\theta}) = \begin{bmatrix} a_1(\boldsymbol{\theta}), & a_2(\boldsymbol{\theta}), & \cdots, & a_n(\boldsymbol{\theta}) \end{bmatrix}, \tag{3.24}$$

the gradient is an $m \times n$ matrix, represented by

$$\begin{aligned} \frac{\partial}{\partial \boldsymbol{\theta}} \mathbf{a}^T(\boldsymbol{\theta}) &= \begin{bmatrix} \frac{\partial}{\partial \boldsymbol{\theta}} a_1(\boldsymbol{\theta}), & \frac{\partial}{\partial \boldsymbol{\theta}} a_2(\boldsymbol{\theta}), & \cdots, & \frac{\partial}{\partial \boldsymbol{\theta}} a_m(\boldsymbol{\theta}) \end{bmatrix} \\ &= \begin{bmatrix} \frac{\partial a_1(\boldsymbol{\theta})}{\partial \theta_1} & \frac{\partial a_2(\boldsymbol{\theta})}{\partial \theta_1} & \cdots & \frac{\partial a_n(\boldsymbol{\theta})}{\partial \theta_1} \\ \frac{\partial a_1(\boldsymbol{\theta})}{\partial \theta_2} & \frac{\partial a_2(\boldsymbol{\theta})}{\partial \theta_2} & \cdots & \frac{\partial a_n(\boldsymbol{\theta})}{\partial \theta_2} \\ \vdots & \vdots & \ddots & \vdots \\ \frac{\partial a_1(\boldsymbol{\theta})}{\partial \theta_m} & \frac{\partial a_2(\boldsymbol{\theta})}{\partial \theta_m} & \cdots & \frac{\partial a_n(\boldsymbol{\theta})}{\partial \theta_m} \end{bmatrix}. \end{aligned} \tag{3.25}$$

Some cases that we will encounter are:

$$\frac{\partial}{\partial \boldsymbol{\theta}} \boldsymbol{\theta}^T = \mathbf{I} \tag{3.26}$$

$$\frac{\partial}{\partial \boldsymbol{\theta}} \left(\mathbf{a}^T(\boldsymbol{\theta}) \mathbf{b}(\boldsymbol{\theta}) \right) = \left(\frac{\partial}{\partial \boldsymbol{\theta}} \mathbf{a}^T(\boldsymbol{\theta}) \right) \mathbf{b}(\boldsymbol{\theta}) + \left(\frac{\partial}{\partial \boldsymbol{\theta}} \mathbf{b}^T(\boldsymbol{\theta}) \right) \mathbf{a}(\boldsymbol{\theta}) \tag{3.27}$$

$$\frac{\partial}{\partial \boldsymbol{\theta}} \boldsymbol{\theta}^T \mathbf{Q} \boldsymbol{\theta} = 2\mathbf{Q}\boldsymbol{\theta} \tag{3.28}$$

$$\frac{\partial}{\partial \boldsymbol{\theta}} \mathbf{m}^T \mathbf{Q} \mathbf{m} = 2 \left(\frac{\partial}{\partial \boldsymbol{\theta}} \mathbf{m}^T \right) \mathbf{Q} \mathbf{m}. \tag{3.29}$$

The derivative of a scalar function of a matrix $\mathbf{X} \in \mathbb{R}^{m\times n}$, denoted by $f(\mathbf{X}) \in \mathbb{R}^{m\times n}$, with respect to $\mathbf{X}$, is defined as

$$\frac{\partial}{\partial \mathbf{X}} f(\mathbf{X}) = \begin{bmatrix} \frac{\partial f(\mathbf{X})}{\partial x_{11}} & \frac{\partial f(\mathbf{X})}{\partial x_{12}} & \cdots & \frac{\partial f(\mathbf{X})}{\partial x_{1n}} \\ \frac{\partial f(\mathbf{X})}{\partial x_{21}} & \frac{\partial f(\mathbf{X})}{\partial x_{22}} & \cdots & \frac{\partial f(\mathbf{X})}{\partial x_{2n}} \\ \vdots & \vdots & \ddots & \vdots \\ \frac{\partial f(\mathbf{X})}{\partial x_{m1}} & \frac{\partial f(\mathbf{X})}{\partial x_{m2}} & \cdots & \frac{\partial f(\mathbf{X})}{\partial x_{mn}}. \end{bmatrix}. \tag{3.30}$$

One application where we will utilise matrix gradients is in the computation of the CRLB.

Let $\mathbf{X}, f(\mathbf{X}) \in \mathbb{R}^{m\times n}, g(\mathbf{X}) \in \mathbb{R}^{n\times p}$, $\mathbf{A}$ and $\mathbf{B}$ are not functions of $\mathbf{X}$, typical functions are:

$$\frac{\partial}{\partial \mathbf{X}} \mathbf{X} = \frac{\partial}{\partial \mathbf{X}} \mathrm{tr}(\mathbf{X}) = \mathbf{I}_{mn} \tag{3.31}$$

$$\frac{\partial}{\partial \mathbf{X}} \left(f(\mathbf{X}) g(\mathbf{X})\right) = g(\mathbf{X}) \frac{\partial}{\partial \mathbf{X}} f(\mathbf{X}) + f(\mathbf{X}) \frac{\partial}{\partial \mathbf{X}} g(\mathbf{X}) \tag{3.32}$$

$$\frac{\partial}{\partial \mathbf{X}} \mathrm{tr}(\mathbf{A}\mathbf{X}) = \mathbf{A}^T \tag{3.33}$$

$$\frac{\partial}{\partial \mathbf{X}} \mathrm{tr}(\mathbf{A}\mathbf{X}^T) = \mathbf{A} \tag{3.34}$$

$$\frac{\partial}{\partial \mathbf{X}} \mathrm{tr}(\mathbf{X}^T\mathbf{A}\mathbf{X}) = (\mathbf{A} + \mathbf{A}^T)\mathbf{X} \tag{3.35}$$

$$\frac{\partial}{\partial \mathbf{X}} \mathrm{tr}(\mathbf{X}\mathbf{A}\mathbf{X}) = \mathbf{X}^T\mathbf{A}^T + \mathbf{A}^T\mathbf{X}^T \tag{3.36}$$

$$\frac{\partial}{\partial \mathbf{X}} \mathrm{tr}(\mathbf{X}\mathbf{A}\mathbf{X}^T) = \mathbf{X}(\mathbf{A} + \mathbf{A}^T) \tag{3.37}$$

$$\frac{\partial}{\partial \mathbf{X}} \mathrm{tr}(\mathbf{X}^T\mathbf{A}\mathbf{X}^T) = \mathbf{X}^T\mathbf{A} + \mathbf{A}\mathbf{X}^T. \tag{3.38}$$

3.6 Special Matrices

3.6.1 Vandermonde Matrix

A Vandermonde matrix is a matrix with the terms of a geometric progression in each row, i.e., an $m \times n$ matrix

$$\mathbf{V} = \begin{bmatrix} 1 & 1 & 1 & \cdots & 1 \\ a_1 & a_2 & a_3 & \cdots & a_n \\ a_1^2 & a_2^2 & a_3^2 & \cdots & a_n^2 \\ \vdots & \vdots & \vdots & \ddots & \vdots \\ a_1^{m-1} & a_2^{m-1} & a_3^{m-1} & \cdots & a_n^{m-1} \end{bmatrix} \tag{3.39}$$

or $\mathbf{V}_{i,j} = a_i^{j-1}, 1 \leq i \leq n, 1 \leq j \leq m$.

The determinant of a square Vandermonde matrix can be expressed as

$$\det\{\mathbf{V}\} = \prod_{1 \leq i < j \leq m} (a_j - a_i) \tag{3.40}$$

where $\prod$ denotes the operation of product. This is called the Vandermonde determinant or Vandermonde polynomial. If all the numbers a_i are distinct, then it is non-zero.

3.6.2 Toeplitz Matrix

A Toeplitz matrix has the property that all of the elements along each diagonal are identical. Thus,

$$a_{ij} = a_{i-j}. \tag{3.41}$$

For example,

$$\mathbf{A} = \begin{bmatrix} a_0 & a_{-1} & a_{-2} & \cdots & a_{-n} \\ a_1 & a_0 & a_{-1} & \cdots & a_{-n+1} \\ a_2 & a_1 & a_0 & \ddots & \vdots \\ \vdots & \vdots & \ddots & \ddots & a_{-1} \\ a_n & a_{n-1} & \cdots & a_1 & a_0 \end{bmatrix}. \tag{3.42}$$

If entries in a Toeplitz matrix $\mathbf{A}$ are complex conjugates of the entries around the principal diagonal, i.e.,

$$\mathbf{A} = \begin{bmatrix} a_0 & a_1^* & a_2^* & \cdots & a_n^* \\ a_1 & a_0 & a_1^* & \cdots & a_{n-1}^* \\ a_2 & a_1 & a_0 & \ddots & \vdots \\ \vdots & \vdots & \ddots & \ddots & a_1^* \\ a_n & a_{n-1} & \cdots & a_1 & a_0 \end{bmatrix}, \tag{3.43}$$

then $\mathbf{A}$ is called a Toeplitz Hermitian matrix.

A Toeplitz matrix has the following properties:

1) A linear combination of Toeplitz matrices is still a Toeplitz matrix.

2) If entries in a Toeplitz matrix satisfies $a_{ij} = a_{|i-j|}$, the Toeplitz matrix is symmetric.

3) Both the transpose and conjugate transpose of a Toeplitz matrices are still Toeplitz matrices.

4) A Toeplitz matrix is symmetric around the cross diagonal.

The exchange or reflection matrix $\mathbf{J}$ is a square matrix whose entries on the cross diagonal are unity and all other entries are zero. Thus,

$$\mathbf{J} = \begin{bmatrix} 0 & \cdots & 0 & 1 \\ 0 & \cdots & 1 & 0 \\ \vdots & \ddots & \vdots & \vdots \\ 1 & \cdots & 0 & 0 \end{bmatrix}, \tag{3.44}$$

considering the property of the Toeplitz matrix, it follows that

$$\mathbf{JAJ} = \mathbf{A}^T \tag{3.45}$$

$$\mathbf{JA}^T\mathbf{J} = \mathbf{A}, \tag{3.46}$$

which are widely used in FBSS and spatial differencing operations.

3.6.3 Hermitian Matrix

Most existing DOA estimation algorithms are based on SOS where the covariance matrix is Hermitian. For a square matrix $\mathbf{A}$, if its entries have complex conjugate symmetry, i.e., $\mathbf{A}^H = \mathbf{A}$, then $\mathbf{A}$ is referred to as a Hermitian matrix. If $\mathbf{A}^H = -\mathbf{A}$, then $\mathbf{A}$ is skew Hermitian. The diagonal entries of a skew Hermitian matrix are imaginary. If $\mathbf{A}$ is real and $\mathbf{A}^T = -\mathbf{A}$, then $\mathbf{A}$ is skew symmetric.

The Hermitian matrix $\mathbf{A} \in \mathbb{C}^{m\times m}$ has the following important properties:

1) The eigenvalues of $\mathbf{A}$ are all real.

2) If $\mathbf{A}$ is positive definite, i.e., $\mathbf{x}^H\mathbf{A}\mathbf{x} > 0$ (or semi-definite, i.e., $\mathbf{x}^H\mathbf{A}\mathbf{x} \geq 0$) for all $\mathbf{x} \neq \mathbf{0}$ where $\mathbf{x} \in \mathbb{C}^m$, then all eigenvalues are positive (or non-negative, and the number of positive eigenvalues equals $\text{rank}(\mathbf{A})$ and the remaining eigenvalues are zero).

3) The non-zero eigenvectors, corresponding to the unequal eigenvalues of $\mathbf{A}$, are both linearly independent and orthogonal to each other. That is, the matrix comprised of all eigenvectors $\mathbf{U} = [\mathbf{u}_1, \mathbf{u}_2, \cdots, \mathbf{u}_m]$ is a unitary matrix which satisfies $\mathbf{U}^{-1} = \mathbf{U}^H$.

4) The eigenvalues of $\mathbf{A} + \sigma^2\mathbf{I}$ are $\lambda_i + \sigma^2$ where λ_i are the eigenvalues of $\mathbf{A}$, and the eigenvectors are identical to the eigenvectors of $\mathbf{A}$.

In particular, let a matrix $\mathbf{A} \in \mathbb{C}^{m\times m}$, then it is called a centro-Hermitian matrix, if the elements of $\mathbf{A}$, $a_{i,j}$, satisfy the relation

$$a_{i,j} = a_{i,j}^* = a_{m-j+1,m-i+1} = a_{m-i+1,m-j+1}^*. \tag{3.47}$$

For example,

$$\mathbf{A} = \begin{bmatrix} a_{1,1} & a_{2,1}^* & a_{3,1}^* & a_{4,1}^* \\ a_{2,1} & a_{2,2} & a_{3,2}^* & a_{3,1}^* \\ a_{3,1} & a_{3,2} & a_{2,2} & a_{2,1}^* \\ a_{4,1} & a_{3,1} & a_{2,1} & a_{1,1} \end{bmatrix}.$$

In matrix format, the centro-Hermitian matrix $\mathbf{A}$ is rotationally Hermitian symmetric about its centre, i.e., $\mathbf{A} = \mathbf{J}\mathbf{A}^*\mathbf{J}$ where $\mathbf{J}$ is the exchange matrix.

3.7 Subspaces

Suppose that $\mathcal{V}$ is a vector space over $\mathbb{C}^n$, and that $\mathcal{W}$ is a subset of $\mathcal{V}$, then we say that $\mathcal{W}$ is a subspace of $\mathcal{V}$ if $\mathcal{W}$ forms a vector space over $\mathbb{C}^n$ under the vector addition and scalar multiplication defined in $\mathcal{V}$, i.e., for all $\mathbf{v}_1, \mathbf{v}_2 \in \mathcal{W}$ and $\alpha_1, \alpha_2 \in \mathbb{C}$ it holds that

$$\alpha_1 \mathbf{v}_1 + \alpha_2 \mathbf{v}_2 \in \mathcal{W}.$$

Suppose that $\mathbf{v}_1, \mathbf{v}_2, \cdots, \mathbf{v}_k$ are vectors in a vector space $\mathcal{V}$ over $\mathbb{C}^n$, then the set

$$\text{span}\{\mathbf{v}_1, \mathbf{v}_2, \cdots, \mathbf{v}_k\} = \{\sum_{i=1}^{k} \alpha_i \mathbf{v}_i : \alpha_i \in \mathbb{R}; i = 1, 2, \cdots, k\}$$

is called the span of the vectors $\mathbf{v}_1, \mathbf{v}_2, \cdots, \mathbf{v}_k$. We also say that the vectors $\mathbf{v}_1, \mathbf{v}_2, \cdots, \mathbf{v}_k$ span $\mathcal{V}$ if

$$\mathcal{V} = \text{span}\{\mathbf{v}_1, \mathbf{v}_2, \cdots, \mathbf{v}_k\};$$

in other words, if every vector in $\mathcal{V}$ can be expressed as a linear combination of the vectors $\mathbf{v}_1, \mathbf{v}_2, \cdots, \mathbf{v}_k$. If $\mathbf{v}_1, \mathbf{v}_2, \cdots, \mathbf{v}_k$ are linearly independent, then they form a basis for $\mathcal{V}$, and the dimension of $\mathcal{V}$ is k, denoted by $\dim(\mathcal{V}) = k$.

Consider a $m \times n$ matrix

$$\mathbf{A} = \begin{bmatrix} a_{11} & \cdots & a_{1n} \\ \vdots & \ddots & \vdots \\ a_{m1} & \cdots & a_{mn} \end{bmatrix} = \begin{bmatrix} \hat{\mathbf{a}}_1 & \hat{\mathbf{a}}_2 & \cdots & \hat{\mathbf{a}}_n \end{bmatrix} = \begin{bmatrix} \bar{\mathbf{a}}_1^H \\ \bar{\mathbf{a}}_2^H \\ \vdots \\ \bar{\mathbf{a}}_m^H \end{bmatrix} \tag{3.48}$$

with entries in $\mathbb{C}$,

1) The subspace $\text{span}\{\hat{\mathbf{a}}_1, \hat{\mathbf{a}}_2, \cdots, \hat{\mathbf{a}}_n\}$ of $\mathbb{C}^m$ is called the column space of $\mathbf{A}$, denoted by $\text{span}(\mathbf{A})$.

2) The subspace $\text{span}\{\bar{\mathbf{a}}_1^H, \bar{\mathbf{a}}_2^H, \cdots, \bar{\mathbf{a}}_m^H\}$ of $\mathbb{C}^n$ is called the row space of $\mathbf{A}$. Obviously, the row space of $\mathbf{A}$ is equivalent to the column space of $\mathbf{A}^H$, thus denoted by $\text{span}(\mathbf{A}^H)$.

3) Suppose that $\mathbf{x} \in \mathbb{C}^n$, then the range of transformation of $\mathbf{A}$ is all possible vectors $\mathbf{Ax}$, denoted by $\mathcal{R}(\mathbf{A})$, i.e.,

$$\mathcal{R}(\mathbf{A}) = \{\mathbf{Ax}|\mathbf{x} \in \mathbb{C}^n\} = \{\sum_{i=1}^{n} \hat{\mathbf{a}}_i x_i | x_i \in \mathbb{C}, i = 1, 2, \cdots, n\} \subseteq \mathbb{C}^m,$$

which is equivalent to the column space of $\mathbf{A}$.

4) The solution space of the system of homogeneous linear equations $\mathbf{Ax} = \mathbf{0}$ is called the null space of $\mathbf{A}$, denoted by $\mathcal{N}(\mathbf{A})$, i.e.,

$$\mathcal{N}(\mathbf{A}) = \{\mathbf{x} \in \mathbb{C}^n | \mathbf{Ax} = \mathbf{0}\} = \{\mathbf{x} \in \mathbb{C}^n | \bar{\mathbf{a}}_i^H \mathbf{x} = 0, i = 1, 2, \cdots, m\}.$$

A linear space $\mathcal{V}$ (for example $\mathbb{C}^n$) is a direct sum of the subspaces $\mathcal{V}_1, \mathcal{V}_2$ (i.e., $\mathcal{V}_1, \mathcal{V}_2 \subseteq \mathcal{V}$) if $\mathcal{V}_1 \cap \mathcal{V}_2 = \{\mathbf{0}\}$ and $\mathcal{V}_1 + \mathcal{V}_2 = \mathcal{V}$.[1] If the direct sum is denoted by $\mathcal{V} = \mathcal{V}_1 \oplus \mathcal{V}_2$, then every $\mathbf{v} \in \mathcal{V}$ can be written uniquely as $\mathbf{v} = \mathbf{v}_1 + \mathbf{v}_2$ where $\mathbf{v}_1 \in \mathcal{V}_1$ and $\mathbf{v}_2 \in \mathcal{V}_2$.

Let $\mathcal{V} \subseteq \mathbb{C}^n$, then the orthogonal complement of $\mathcal{V}$, denoted by $\mathcal{V}^\perp$, is the set of all vectors that are orthogonal to every vector in $\mathcal{V}$, i.e.,

$$\mathcal{V}^\perp = \{\mathbf{w} \in \mathbb{C}^n : \mathbf{w}^H \mathbf{v} = 0, \forall \mathbf{v} \in \mathcal{V}\}.$$

Obviously, $\mathcal{V}^\perp$ is the largest subset of $\mathbb{C}^n$ orthogonal to $\mathcal{V}$. The following holds:

1) $\mathcal{V}^\perp$ is a subspace.

2) $\mathbb{C}^n = \mathcal{V} \oplus \mathcal{V}^\perp$.

3) If $\dim(\mathcal{V}) = k$, then $\dim(\mathcal{V}^\perp) = n - k$.

4) $(\mathcal{V}^\perp)^\perp = \mathcal{V}$.

Considering the previously defined range and null spaces, the following orthogonality relations hold:

1) $\mathcal{R}(\mathbf{A})^\perp = \mathcal{N}(\mathbf{A}^H)$.

[1] $\mathcal{V}_1 + \mathcal{V}_2$ is the sum of subspaces $\mathcal{V}_1$ and $\mathcal{V}_2$ (see [129, pp. 268]), such as the sum of two vectors or two matrices.

2) $\mathcal{R}(\mathbf{A}^H)^\perp = \mathcal{N}(\mathbf{A})$.

3) $\mathcal{N}(\mathbf{A})^\perp = \mathcal{R}(\mathbf{A}^H)$.

4) $\mathcal{N}(\mathbf{A}^H)^\perp = \mathcal{R}(\mathbf{A})$.

Let $\mathbf{A} \in \mathbb{C}^{m\times n}$, then the following direct sums hold:

1) $\mathbb{C}^m = \mathcal{R}(\mathbf{A}) \oplus \mathcal{N}(\mathbf{A}^H)$.

2) $\mathbb{C}^n = \mathcal{R}(\mathbf{A}^H) \oplus \mathcal{N}(\mathbf{A})$.

where $\mathcal{R}(\mathbf{A}) \perp \mathcal{N}(\mathbf{A}^H)$ and $\mathcal{R}(\mathbf{A}^H) \perp \mathcal{N}(\mathbf{A})$. Furthermore, it holds that $\dim\mathcal{R}(\mathbf{A}) = \dim\mathcal{R}(\mathbf{A}^H)$.

Suppose that $\mathbf{v}_1, \mathbf{v}_2, \cdots, \mathbf{v}_k$ are vectors in a vector space $\mathcal{V}$ over $\mathbb{C}^n$, then we say that $\{\mathbf{v}_1, \mathbf{v}_2, \cdots, \mathbf{v}_k\}$ is a basis for $\mathcal{V}$ if the following two conditions are satisfied:

1) We have $\text{span}\{\mathbf{v}_1, \mathbf{v}_2, \cdots, \mathbf{v}_k\} = \mathcal{V}$.

2) The vectors $\mathbf{v}_1, \mathbf{v}_2, \cdots, \mathbf{v}_k$ are linearly independent.

Following the above definition, suppose further that $r > k$, and that the vectors $\mathbf{u}_1, \mathbf{u}_2, \cdots, \mathbf{u}_r \in \mathcal{V}$, then the vectors $\mathbf{u}_1, \mathbf{u}_2, \cdots, \mathbf{u}_r$ are linearly dependent. By this, any two bases for $\mathcal{V}$ have the same number of entries though having different bases is permissible. Recall from (3.1), the rank of a matrix $\mathbf{A} \in \mathbb{C}^{m\times n}$ is equal to the common value of the dimension of its row space and the dimension of its column space, i.e.,

$$\text{rank}(\mathbf{A}) = \dim[\text{span}(\mathbf{A})] = \dim\mathcal{R}(\mathbf{A}). \tag{3.49}$$

Finally, we introduce several relationships between matrix transformation and subspaces on an arbitrary matrix $\mathbf{A} \in \mathbb{C}^{m\times n}$:

1) Applying elementary row transformations to $\mathbf{A}$ does not change its row space $\mathcal{R}(\mathbf{A}^H)$.

2) Applying elementary column transformations to $\mathbf{A}$ does not change its column space $\mathcal{R}(\mathbf{A})$.

3) Applying elementary row transformations to $\mathbf{A}$ does not change its null space $\mathcal{N}(\mathbf{A})$.

4) Let $\mathbf{B} \in \mathbb{C}^{p\times n}, \mathbf{F} = \begin{bmatrix} \mathbf{A} \\ \mathbf{B} \end{bmatrix} \in \mathbb{C}^{(m+n)\times n}$, then $\mathbf{Fx} = \mathbf{0} \Leftrightarrow \mathbf{Ax} = \mathbf{0}$ and $\mathbf{Bx} = \mathbf{0}$, i.e. the null space of $\mathbf{F}$ is equal to the intersection of the null spaces of $\mathbf{A}$ and $\mathbf{B}$,

$$\mathcal{N}(\mathbf{F}) = \mathcal{N}(\mathbf{A}) \cap \mathcal{N}(\mathbf{B}). \tag{3.50}$$

3.8 Projection Matrices

In array processing, especially the research of DOA estimation, the optimum solution of some problems can be generalised as to extract desired signals and suppress interferences and noise. Projection techniques will play a central role in this kind of problem since they can separate one vector space into two non-overlapping subspaces to identify the useful information.

Projection techniques can be categorised into two groups: orthogonal projection and oblique projection. When two subspaces are orthogonal to each other, orthogonal projection is often exploited to conduct the optimum estimation of parameters because the projection of the signal of interest in the observations onto a subspace (i.e., the range) can be completely extracted, while other nuisance information and noise can be nulled in the same subspace. However, when two subspaces are not orthogonal to each other, orthogonal projection is not valid any more. As a more generalised projection technique, oblique projection can adapt to this case: extracting the component of observations in one subspace while eliminating components of the other subspace.

3.8.1 Orthogonal Projection

If $\mathbf{P} \in \mathbb{C}^{m\times m}$ is a square matrix such that $\mathbf{P}^2 = \mathbf{P}$, then $\mathbf{P}$ is called a projector. A matrix satisfying this property is also known as an idempotent matrix. A matrix is an orthogonal projection matrix if, and only if, it is conjugate symmetric and idempotent.

For projection onto a plane or to a subspace span$(\mathbf{A}) \in \mathbb{C}^m$ with $\mathbf{A} \in \mathbb{C}^{m \times n}$, the projection matrix, usually with a subscript indicating the range, is expressed as

$$\mathbf{P}_\mathbf{A} = \mathbf{A}(\mathbf{A}^H\mathbf{A})^{-1}\mathbf{A}^H. \tag{3.51}$$

We can also express an orthogonal projection matrix that projects a vector space onto a subspace orthogonal to the subspace defined by the columns of $\mathbf{A}$,

$$\begin{aligned}\mathbf{P}_\mathbf{A}^\perp &= \mathbf{I} - \mathbf{P}_\mathbf{A} \\ &= \mathbf{I} - \mathbf{A}(\mathbf{A}^H\mathbf{A})^{-1}\mathbf{A}^H.\end{aligned} \tag{3.52}$$

Note that, if the columns of $\mathbf{A}$ are orthogonal to each other, then

$$\mathbf{P}_\mathbf{A} = \mathbf{A}\mathbf{A}^H. \tag{3.53}$$

and

$$\mathbf{P}_\mathbf{A}^\perp = \mathbf{I} - \mathbf{A}\mathbf{A}^H. \tag{3.54}$$

In many of our applications, we will find it useful to divide the matrix vector space into the n-dimensional signal subspace, which contains both signal and noise, and an $m - n$-dimensional noise subspace, which contains noise only.

By the definitions of projection and orthogonal projection matrices, the following properties are readily verified:

$$\mathbf{P}_\mathbf{A}^H = \mathbf{P}_\mathbf{A} \tag{3.55}$$

$$(\mathbf{P}_\mathbf{A}^\perp)^H = \mathbf{P}_\mathbf{A}^\perp \tag{3.56}$$

$$\mathbf{P}_\mathbf{A}\mathbf{A} = \mathbf{A} \tag{3.57}$$

$$\mathbf{P}_\mathbf{A}^\perp\mathbf{A} = \mathbf{P}_\mathbf{A}^\perp\mathbf{P}_\mathbf{A} = \mathbf{P}_\mathbf{A}\mathbf{P}_\mathbf{A}^\perp = \mathbf{0}. \tag{3.58}$$

3.8.2 Oblique Projection

A projection matrix that does not satisfy $\mathbf{P}^H \neq \mathbf{P}$ is referred to as an oblique projection matrix. Oblique projections are represented as $\mathbf{E}$, usually with a double subscript referring first to the range and second to the null space. For an oblique projection matrix

$\mathbf{E}_{\mathbf{A}|\mathbf{B}}$ with $\mathcal{R}(\mathbf{E}_{\mathbf{A}|\mathbf{B}}) = \mathcal{R}(\mathbf{A})$ and $\mathcal{R}(\mathbf{B}) \subset \mathcal{N}(\mathbf{E}_{\mathbf{A}|\mathbf{B}})$, we have

$$\mathbf{E}_{\mathbf{A}|\mathbf{B}}^2 = \mathbf{E}_{\mathbf{A}|\mathbf{B}},\ \mathbf{E}_{\mathbf{A}|\mathbf{B}}\mathbf{A} = \mathbf{A},\ \mathbf{E}_{\mathbf{A}|\mathbf{B}}\mathbf{B} = \mathbf{0}. \tag{3.59}$$

Likewise, we have

$$\mathbf{E}_{\mathbf{B}|\mathbf{A}}^2 = \mathbf{E}_{\mathbf{B}|\mathbf{A}},\ \mathbf{E}_{\mathbf{B}|\mathbf{A}}\mathbf{B} = \mathbf{B},\ \mathbf{E}_{\mathbf{B}|\mathbf{A}}\mathbf{A} = \mathbf{0}. \tag{3.60}$$

The equations that allow projection matrices to be built from subspace spaning for desired ranges and null spaces are constructed as

$$\mathbf{E}_{\mathbf{A}|\mathbf{B}} = \mathbf{A}(\mathbf{A}^H\mathbf{P}_{\mathbf{B}}^{\perp}\mathbf{A})^{-1}\mathbf{A}^H\mathbf{P}_{\mathbf{B}}^{\perp} \tag{3.61}$$

$$\mathbf{E}_{\mathbf{B}|\mathbf{A}} = \mathbf{B}(\mathbf{B}^H\mathbf{P}_{\mathbf{A}}^{\perp}\mathbf{B})^{-1}\mathbf{B}^H\mathbf{P}_{\mathbf{A}}^{\perp}. \tag{3.62}$$

Lastly, some relationships between projection matrices are listed as follows:

$$\mathbf{E}_{\mathbf{A}|\mathbf{B}}\mathbf{E}_{\mathbf{B}|\mathbf{A}} = \mathbf{E}_{\mathbf{B}|\mathbf{A}}\mathbf{E}_{\mathbf{A}|\mathbf{B}} = \mathbf{0} \tag{3.63}$$

$$\mathbf{E}_{\mathbf{A}|\mathbf{B}} = \mathbf{P}_{\mathbf{A}}\mathbf{E}_{\mathbf{A}|\mathbf{B}},\ \mathbf{E}_{\mathbf{B}|\mathbf{A}} = \mathbf{P}_{\mathbf{B}}\mathbf{E}_{\mathbf{B}|\mathbf{A}}. \tag{3.64}$$

3.9 Conclusion

Most of the analysis that we do throughout this current research involves manipulating vectors and matrices extensively. This chapter has outlined the definitions and properties that will be useful in the remainder chapters, and also provided the vector and matrix derivatives which are the fundamental elements of Cramér-Rao lower bound (CRLB) in parameter estimation.

Chapter 4

Basis of DOA Estimation

THE signal model is the most fundamental aspect of array processing, upon which all else is built. This chapter first provides an introduction to the uncorrelated signal model, then the coherent signal model under multipath propagation. The conventional spectral-based and subspace-based algorithms for the uncorrelated signal model are introduced and the mechanisms behind the algorithms are interpreted. Then preprocessing techniques to restore rank deficiency caused by signal coherency is discussed, and the advantages of the rank restoration methods are analysed and supported by some numerical simulation results.

4.1 Introduction

DOA estimation is a key topic in spatial signal processing, and array processing techniques are widely used to address it. These have developed rapidly and continually over the past decades since they can capture and extract valuable spatial information. From the published journal papers we can see that research on DOA estimation has a wealth of content and spans a wide range of applications, covering radar, sonar, navigation, wireless communication, geophysical exploration, biomedical engineering, etc. At present, the theoretical research and implementation techniques of DOA estimation are still unfolding. In this chapter, we introduce the model of uncorrelated received signals and associated common processing techniques, and then the model of coherent incident signals and associated common pre-processing methods.

4.2 Mathematical Model of Signals Received by a Sensor Array

A sensor array has multiple sensors separately distributed in space as shown in Figure 4.1. For simplicity, we only consider a number of N narrowband far-field source impinging on a uniform linear array with M identical omnidirectional sensors.

Denote the signal from the i-th source as $s_i(t) = A_i(t)e^{j(\omega_i t+\varphi_i(t))}$ with power σ_i^2 for $i = 1, 2, \cdots, N$, where $A_i(t)$, ω_i and $\varphi_i(t)$ are the amplitude, carrier frequency and initial phase of the i-th signal, respectively. Then, the signal received at the l-th sensor can be expressed as $x_l(t) = \sum_{i=1}^{N} s_i(t+\tau_{li}) + n_l(t), l = 1, 2, \cdots, M$, where τ_{li} is the propagation time delay of the i-th signal arriving at the l-th sensor, and $n_l(t)$ is the spatially and temporally white Gaussian noise with the power σ^2 adding to the l-th sensor. Since the sources are narrowband, their amplitudes and initial phases will vary slowly with time, implying that

$$A_i(t+\tau_i) \approx A_i(t), \tag{4.1}$$

$$\varphi_i(t+\tau_i) \approx \varphi_i(t). \tag{4.2}$$

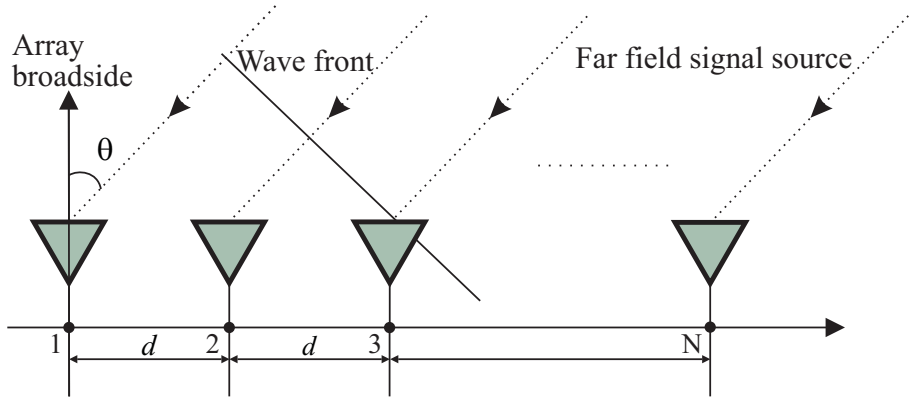

Figure 4.1. Far-field signals received by a uniform linear array (ULA).

Further, we have

$$s_i(t+\tau_{li}) \approx s_i(t)e^{j\omega_i\tau_{li}}, \tag{4.3}$$

that is, the time delays are equivalent to phase shifts. For the ULA,

$$\tau_{li} = \frac{(l-1)d}{c}\sin\theta_i \tag{4.4}$$

where c is the speed of propagation in the medium, and θ_i is the azimuth angle of the i-th incident signal. Hence, we can rewrite the received signal at the l-th sensor as

$$x_l(t) = \sum_{i=1}^{N} s_i(t)e^{j\frac{2\pi(l-1)d}{\lambda}\sin\theta_i} + n_l(t) \tag{4.5}$$

where d is the spacing between adjacent sensors, and λ is the wavelength of carrier signal.

Stacking the output of M sensors, we obtain

$$\begin{bmatrix} x_1(t) \\ x_2(t) \\ \vdots \\ x_M(t) \end{bmatrix} = \begin{bmatrix} 1 & 1 & \cdots & 1 \\ e^{j\frac{2\pi d}{\lambda}\sin\theta_1} & e^{j\frac{2\pi d}{\lambda}\sin\theta_2} & \cdots & e^{j\frac{2\pi d}{\lambda}\sin\theta_N} \\ \vdots & \vdots & & \vdots \\ e^{j\frac{2\pi(M-1)d}{\lambda}\sin\theta_1} & e^{j\frac{2\pi(M-1)d}{\lambda}\sin\theta_2} & \cdots & e^{j\frac{2\pi(M-1)d}{\lambda}\sin\theta_N} \end{bmatrix} \begin{bmatrix} s_1(t) \\ s_2(t) \\ \vdots \\ s_N(t) \end{bmatrix} + \begin{bmatrix} n_1(t) \\ n_2(t) \\ \vdots \\ n_M(t) \end{bmatrix}. \tag{4.6}$$

In matrix form, it becomes

$$\mathbf{x}(t) = \left[\mathbf{a}(\theta_1), \mathbf{a}(\theta_2), \cdots, \mathbf{a}(\theta_N)\right]\mathbf{s}(t) + \mathbf{n}(t)$$

$$= \mathbf{A}\mathbf{s}(t) + \mathbf{n}(t) \tag{4.7}$$

where $\mathbf{a}(\theta) = [1, e^{j\frac{2\pi d}{\lambda}\sin\theta}, \cdots, e^{j\frac{2\pi(M-1)d}{\lambda}\sin\theta}]^T \in \mathbb{C}^{M\times 1}$ is the steering vector, $\mathbf{A} = [\mathbf{a}(\theta_1), \mathbf{a}(\theta_2), \cdots, \mathbf{a}(\theta_N)]$ is the array manifold, $\mathbf{s}(t) = [s_1(t), s_2(t), \cdots, s_N(t)]^T$, and $\mathbf{n}(t) = [n_1(t), n_2(t), \cdots, n_N(t)]^T$. Some common assumptions on the signal model are made as follows:

A 1) The source signals $s_i(t), i = 1, 2, \cdots, N$, are statistically uncorrelated to each other and have zero-mean.

A 2) The array is calibrated, and the array manifold $\mathbf{A}$ is unambiguous, i.e., the steering vectors $\{\mathbf{a}(\theta_1), \mathbf{a}(\theta_2), \cdots, \mathbf{a}(\theta_N)\}$ are linearly independent for any set of distinct $\{\theta_1, \theta_2, \cdots, \theta_N\}$. Equivalently, the matrix $\mathbf{A}$ is of full column rank.

A 3) The noise is zero-mean wide-sense stationary (WSS), i.e., $E_t[n_l(t)n_l^*(t)] = \sigma^2$, and it is statistically uncorrelated with the signals.

A 4) Each source signal is zero-mean WSS, i.e., $E_t[s_i(t)s_i^*(t)] = \sigma_i^2$.

From (4.7), the array covariance matrix is given by

$$\mathbf{R}_x = E_t[\mathbf{x}(t)\mathbf{x}^H(t)] = \mathbf{A}\mathbf{R}_s\mathbf{A}^H + \sigma^2\mathbf{I} \tag{4.8}$$

where $\mathbf{R}_s = E_t[\mathbf{s}(t)\mathbf{s}^H(t)] = \text{diag}\{\sigma_1^2, \sigma_2^2, \cdots, \sigma_N^2\}$ is the source covariance matrix, and $\mathbf{I}$ represents the identity matrix.

In practical applications, the covariance matrix can only be estimated using the L snapshots collected at time instants of $t = 1, 2, \cdots, L$ as follows

$$\hat{\mathbf{R}}_x = \frac{1}{L}\sum_{t=1}^{L}\mathbf{x}(t)\mathbf{x}^H(t). \tag{4.9}$$

4.3 Classical DOA Estimation Algorithms of Uncorrelated Signals

Classical DOA estimation algorithms are referred to as spectral-based approaches. In this kind of method, one maximises the power of the beamforming output for given

input signals to search for the highest (separated) peaks which are related to the parameter(s) of interest, e.g., the direction of arrival (DOA). The locations of the highest (separated) peaks of the function in question are recorded as the DOA estimates. Spectral-based methods which are discussed in this section, can be classified into beamforming techniques and subspace-based methods. Conventional beamforming (CB) can form multiple beams only for widely separated sources, while minimum variance distortionless response (MVDR) can identify signals with close DOA separations under high SNRs. However, MVDR will degrade its performance to CB's levels at low SNRs, and thus more advanced high-resolution direction finding algorithms are required. Multiple signal classification (MUSIC) and estimation of signal parameters by rotational invariance techniques (ESPRIT), have emerged over time as the most representative of high resolution techniques.

4.3.1 Beamforming Techniques

The first attempt to automatically find directions of signal sources using antenna arrays was through beamforming techniques. The idea is to "steer" the array in one direction at a time and measure the output power. The steering locations which result in maximum power correspond to the DOA estimates. Consider a generic narrowband beamformer, shown in Fig. 4.2, the array response is steered by forming a linear combination of the sensor outputs as

$$y(t) = \sum_{l=1}^{M} \omega_l^* x_l(t) = \boldsymbol{\omega}^H \mathbf{x}(t). \tag{4.10}$$

Given samples $y(l), y(2), \cdots, y(L)$, the output power is measured by

$$p(\theta) = E_t[|y(t)|^2] = \boldsymbol{\omega}^H E_t[\mathbf{x}(t)\mathbf{x}^H(t)]\boldsymbol{\omega} = \boldsymbol{\omega}^H \mathbf{R}_x \boldsymbol{\omega} \tag{4.11}$$

where $\mathbf{R}_x$ is defined in (4.8). Different beamforming approaches correspond to different choices of the weighting vector $\boldsymbol{\omega}$.

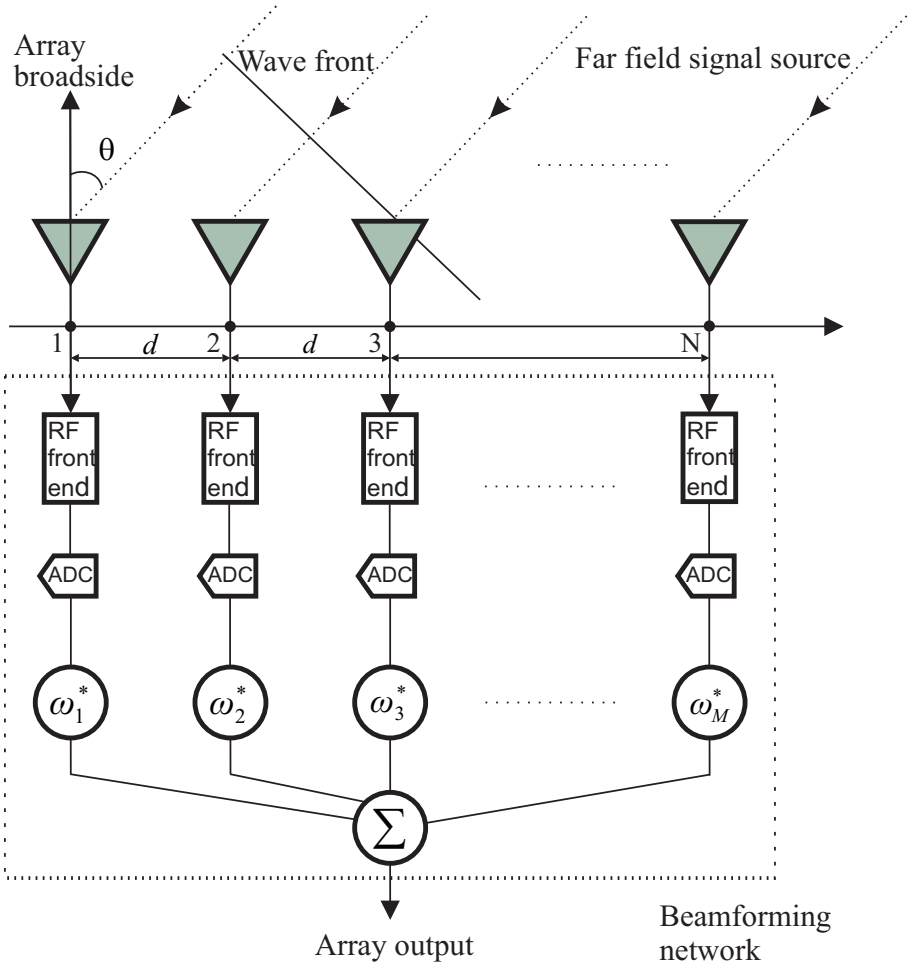

Figure 4.2. Digital beamforming network.

Conventional Beamforming

Conventional beamforming [130] is based on multiplying the output of each receiver appropriately by a phase factor prior to summing to compensate for the different times of arrival. The conventional beamformer is a natural extension of conventional spectral analysis to sensor array data. Consider the situation where multiple strong signal sources are incident upon an M-element ULA from unknown directions $\{\theta_i\}_{i=1}^{N}$, the array weights are given by

$$\boldsymbol{\omega}_{CB} = \frac{1}{M}\mathbf{a}(\theta) \tag{4.12}$$

and the output power of the array with weighting vector $\boldsymbol{\omega}_{CB}$ becomes

$$p_{CB}(\theta) = \frac{1}{M^2}\mathbf{a}^H(\theta)\mathbf{R}_x\mathbf{a}(\theta). \tag{4.13}$$

The process is typified as steering the array over $[-90^\circ, 90^\circ]$, forming many beams simultaneously and plotting the array output power against the steered direction of these beams, which will result in peaks in the directions of the signal sources. This chain of computations enable the DOA of each signal to be estimated.

Although conventional beamforming is simple to implement, it results in poor DOA estimation for sources whose angles are closer than the beamwidth. These sources cannot be resolved by the conventional beamformer, regardless of the available data quality.

MVDR

In an attempt to alleviate the limitations of the above beamformer, such as its resolving power of two sources spaced closer than a beamwidth, researchers have proposed numerous modifications. A well-known method was proposed by Capon [131], commonly called the MVDR beamformer. This approach attempts to minimise the power contributed by noise and undesired interferences, while maintaining a fixed gain in the desired direction, usually equal to unity, which is therefore stated as an optimisation problem:

$$\begin{aligned} \boldsymbol{\omega} &= \arg\min_{\boldsymbol{\omega}} \boldsymbol{\omega}^H \mathbf{R}_x \boldsymbol{\omega} \\ \text{s.t.} \quad & \boldsymbol{\omega}^H \mathbf{a}(\theta) = 1. \end{aligned} \tag{4.14}$$

By the well-known Lagrange multipliers [132], the solution is given by

$$\boldsymbol{\omega}_{MVDR} = \frac{\mathbf{R}_x^{-1}\mathbf{a}(\theta)}{\mathbf{a}^H(\theta)\mathbf{R}_x^{-1}\mathbf{a}(\theta)} \tag{4.15}$$

$$p_{MVDR}(\theta) = \frac{1}{\mathbf{a}^H(\theta)\mathbf{R}_x^{-1}\mathbf{a}(\theta)}. \tag{4.16}$$

If the array is steered over $[-90^\circ, 90^\circ]$, then the peaks formed by the maximum values of (4.16) correspond to the DOA estimates. Due to spectral leakage from closely separated sources being reduced, the MVDR beamformer has much greater resolution than the conventional beamformer. However, if the multiple signals are highly correlated, such as for multipath propagation, the resolution of the MVDR beamformer can actually become worse. In addition, the resolution capability of the MVDR beamformer is

still limited by the array aperture and the SNR. In fact, when the SNR is fairly low the resolution of MVDR deteriorates to that of the conventional beamformer.

4.3.2 Subspace-based Methods

Over the past few decades, there have been revolutionary advances in high-resolution DOA estimation problems [55, 70, 133, 134]. Among the algorithms proposed in the literature, subspace methods based on the eigen-decomposition of the sampled covariance matrix are popular because of their modest computational complexities when compared with the maximum-likelihood (ML) method [55].

The idea behind MUSIC is that the space spanned by eigenvectors of the covariance matrix may be partitioned into two orthogonal subspaces, i.e., the signal subspace and the noise subspace, and the DOA estimates can be obtained by utilising the orthogonality. Parameter estimation in these methods detects sources [135] initially and then finds the asymptotically best values of the interested parameters. MUSIC as an innovative DOA estimator initiated a new epoch in the array processing. It has later been successfully brought back to the spectral analysis/system identification problem with further developments. Based on the eigenstructure of the covariance matrix and special array geometry, ESPRIT was proposed subsequently and attracted considerable attention because of efficient computation complexity and robustness.

MUSIC

When $N < M$, taking eigen-decomposition of $\mathbf{R}_x$ produces

$$\mathbf{R}_x = \sum_{i=1}^{M} \lambda_i \mathbf{e}_i \mathbf{e}_i^H = \begin{bmatrix} \mathbf{e}_1, \mathbf{e}_2, \cdots, \mathbf{e}_N \end{bmatrix} \begin{bmatrix} \lambda_1 & & & \\ & \lambda_2 & & \\ & & \ddots & \\ & & & \lambda_N \end{bmatrix} \begin{bmatrix} \mathbf{e}_1^H \\ \mathbf{e}_2^H \\ \vdots \\ \mathbf{e}_N^H \end{bmatrix}$$
$$+ \begin{bmatrix} \mathbf{e}_{N+1}, \mathbf{e}_{N+2}, \cdots, \mathbf{e}_M \end{bmatrix} \begin{bmatrix} \lambda_{N+1} & & & \\ & \lambda_{N+2} & & \\ & & \ddots & \\ & & & \lambda_M \end{bmatrix} \begin{bmatrix} \mathbf{e}_{N+1}^H \\ \mathbf{e}_{N+2}^H \\ \vdots \\ \mathbf{e}_M^H \end{bmatrix}$$

$$= \mathbf{U}_s \mathbf{\Sigma}_s \mathbf{U}_s^H + \mathbf{U}_n \mathbf{\Sigma}_n \mathbf{U}_n^H \tag{4.17}$$

where $\lambda_1 \geq \lambda_2 \geq \cdots \lambda_N > \lambda_{N+1} = \cdots = \lambda_M = \sigma_n^2$ are eigenvalues, $\mathbf{\Sigma}_s$ is a diagonal matrix consisting of the N largest eigenvalues, and $\mathbf{\Sigma}_n$ is a diagonal matrix consisting of the remaining $M - N$ smallest eigenvalues. The columns of $\mathbf{U}_s$ are the eigenvectors corresponding to largest eigenvalues, while the columns of $\mathbf{U}_n$ are the eigenvectors corresponding to smallest eigenvalues. Referring to the subspace theory in Section 3.7, the signal subspace is spanned by the columns of $\mathbf{U}_s$, while the noise subspace is spanned by the columns of $\mathbf{U}_n$. Since the matrix $\mathbf{U} = [\mathbf{U}_s, \mathbf{U}_n]$ is unitary, $\mathbf{U}_s^H \mathbf{U}_n = \mathbf{0}$, i.e., the signal subspace is orthogonal to the noise subspace

$$\text{span}(\mathbf{U}_s) \perp \text{span}(\mathbf{U}_n). \tag{4.18}$$

From the definitions of eigenvector and eigenvalue, we have

$$\mathbf{R}_x \mathbf{U}_n = \sigma_n^2 \mathbf{U}_n. \tag{4.19}$$

Since $\mathbf{R}_x = \mathbf{A}\mathbf{R}_s\mathbf{A}^H + \sigma^2\mathbf{I}$, $\mathbf{R}_x\mathbf{U}_n$ can be obtained as

$$\mathbf{R}_x \mathbf{U}_n = \mathbf{A}\mathbf{R}_s\mathbf{A}^H\mathbf{U}_n + \sigma_n^2\mathbf{U}_n. \tag{4.20}$$

Combining (4.19) and (4.20), it is readily seen that

$$\mathbf{A}\mathbf{R}_s\mathbf{A}^H\mathbf{U}_n = \mathbf{0}_{M\times(M-N)} \tag{4.21}$$

thereby yielding $\mathbf{U}_n^H\mathbf{A}\mathbf{R}_s\mathbf{A}^H\mathbf{U}_n = \mathbf{0}_{M\times(M-N)}$. Suppose that $\mathbf{P}$ is nonsingular, then $\mathbf{t}^H\mathbf{P}\mathbf{t} = \mathbf{0}$ holds if and only if $\mathbf{t} = \mathbf{0}$, and (4.21) is consequently equivalent to

$$\mathbf{A}^H\mathbf{U}_n = \mathbf{0}_{N\times(M-N)}. \tag{4.22}$$

This means that the column vectors of array manifold $\mathbf{A}$ are all orthogonal to the noise subspace, so we have

$$\mathbf{a}^H(\theta_i)\mathbf{U}_n = \mathbf{0}_{1\times(M-N)}, \qquad i = 1, 2, \cdots, N. \tag{4.23}$$

The MUSIC "spatial spectrum" is then defined as the reciprocal of the Frobenius norm as a function of θ, i.e.,

$$p_{MUSIC}(\theta) = \frac{1}{\|\mathbf{a}^H(\theta)\mathbf{U}_n\|_F^2} = \frac{1}{\mathbf{a}^H(\theta)\mathbf{U}_n\mathbf{U}_n^H\mathbf{a}(\theta)}. \tag{4.24}$$

The peaks of $p_{MUSIC}(\theta)$, theoretically infinite, indicate DOAs $\{\theta_i\}_{i=1}^N$.

Fig. 4.3 shows a plot of the spatial spectrum for the case of four signals impinging on a 10-element ULA at an SNR $=$ 5dB. Results are displayed using CB, MVDR, and MUSIC for comparison.

From Fig. 4.3(a) we can see that all three methods can accurately identify the DOAs of four sources when the DOA separation is large, where MUSIC has the sharpest spikes and the lowest sidelobes, MVDR the second, followed by CB. For the case of close DOA separation, Fig. 4.3(b) shows that CB cannot distinguish two signals between which angular separation reduces to 9° or even less, and MVDR can separate two signals which are close to 9° but is incapable of resolving them within 5° angular separation, while MUSIC can still achieve good DOA estimation of all incident signals. The performance improvement of the MUSIC is so significant that it becomes a compelling alternative to most existing methods.

There is a problem with MUSIC as described above—one has to perform a comprehensive search over all possible directions to determine the spectral peaks. The MUSIC algorithm in general can apply to any arbitrary array regardless of the position of sensor elements. If the array geometry is restricted to ULAs, a model-based parametric MUSIC-based method, root-MUSIC [117], arises. As the name implies, it is a simplified algorithm that finds roots of a polynomial function instead of calculating the spatial spectrum and peak searching, resulting in better computational efficiency.

The steering polynomial vector is defined as $\mathbf{a}(z) = \left[1, z, \cdots, z^{M-1}\right]^T$ which is the array steering vector at $z = e^{j\frac{2\pi d}{\lambda}\sin\theta}$. To exploit the orthogonality between the signal and noise subspaces as in the previously described MUSIC technique, we want to find the zeros of the following polynomial function

$$f(z) = \mathbf{a}^T\left(z^{-1}\right)\mathbf{U}_n\mathbf{U}_n^H\mathbf{a}(z). \tag{4.25}$$

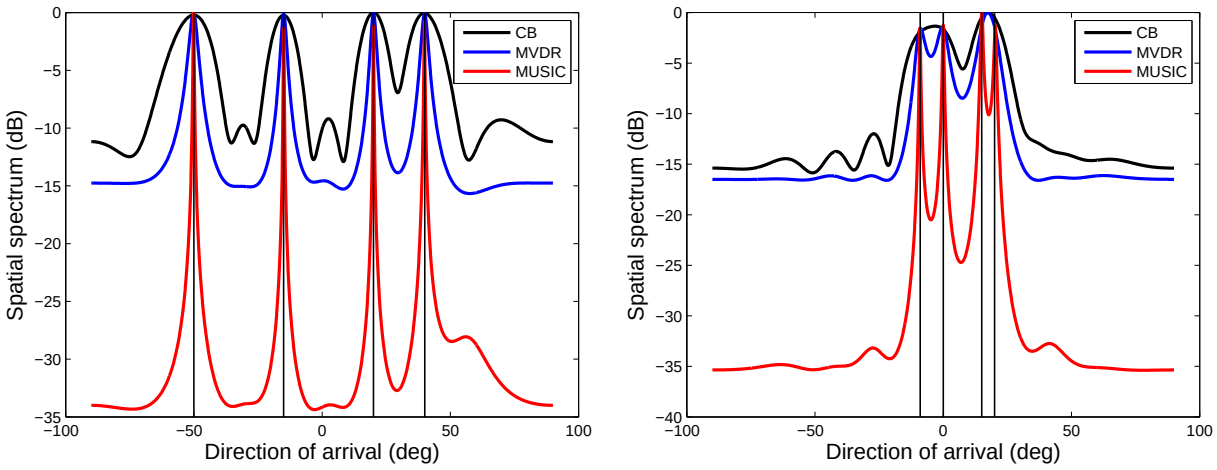

(a) Widely separated DOAs (b) Closely separated DOAs

Figure 4.3. Spatial spectrum of CB, MVDR, and MUSIC, for a 10-element ULA with $\frac{\lambda}{2}$ spacing between adjacent elements. SNR $= 5$dB, snapshots number is 500. For (a), $[\theta_1, \theta_2, \theta_3, \theta_4] = [-50°, -15°, 20°, 40°]$. For (b), $[\theta_1, \theta_2, \theta_3, \theta_4] = [-9°, 0°, 15°, 20°]$.

Theoretically the values of z on the unit circle are of interest, however, one has to compute the roots of $f(z)$ and choose the N roots that are inside the unit circle and closest to the unit circle in practice, and then the DOA estimates can be determined as

$$\theta_i = \arcsin\left[\frac{\lambda}{2\pi d}\arg(z_i)\right], \quad i = 1, 2, \cdots, N. \tag{4.26}$$

It has been shown in [136, 137] that MUSIC and root-MUSIC have identical asymptotic properties. In some cases, especially for small sample sizes, root-MUSIC may provide better performance than MUSIC. This can be attributed to a larger bias of estimates for spectral-based methods, compared to parametric techniques.

ESPRIT

The computational requirements of the MUSIC algorithm is about $[(M+1)(M-N)+1](\frac{180}{r}+1)$ complex multiplications, which is high, especially when the scanning resolution r is relative small, such as $0.1°$. To mitigate the computation cost, Roy and Kailath proposed ESPRIT (Estimation of Signal Parameters by Rotational Invariance Techniques). As the name suggests, it performs DOA estimation by exploiting the rotational invariance of the signal subspaces and array geometry rather than the orthogonality between the signal and noise subspaces.

The basic idea is as simple as it is ingenious. Consider a ULA of M sensors spaced d apart, we divide the whole array into a pair of identical subarrays. To make full use of array aperture and elements, the first subarray can be selected as the one composed of the elements $1, 2, \cdots, M-1$, and the second subarray is the one with elements $2, 3, \cdots, M$, shifted N sensors of the first subarray to the right by d.

Recall the aforementioned signal model in Section 4.2, output vectors of the two subarrays can be expressed as

$$\mathbf{x}_1(t) = \mathbf{B}_1\mathbf{x}(t) = \mathbf{A}_1\mathbf{s}(t) + \mathbf{n}_1(t) \tag{4.27}$$

$$\mathbf{x}_2(t) = \mathbf{B}_2\mathbf{x}(t) = \mathbf{A}_2\mathbf{s}(t) + \mathbf{n}_1(t) \tag{4.28}$$

where $\mathbf{B}_1 = \left[\mathbf{I}_{(M-1)\times(M-1)}, \mathbf{0}_{(M-1)\times 1}\right]$, $\mathbf{B}_2 = \left[\mathbf{0}_{(M-1)\times 1}, \mathbf{I}_{(M-1)\times(M-1)}\right]$, $\mathbf{A}_i = \mathbf{B}_i\mathbf{A}$, $\mathbf{n}_i(t) = \mathbf{B}_i\mathbf{n}(t), i = 1, 2$.

It is clear from (4.27) and (4.28) that array manifolds of the two subarrays are linked by the following relationship

$$\mathbf{A}_2 = \mathbf{A}_1\mathbf{\Phi} \tag{4.29}$$

where $\mathbf{\Phi} = \text{diag}\{e^{j\frac{2\pi d}{\lambda}\sin\theta_1}, e^{j\frac{2\pi d}{\lambda}\sin\theta_2}, \cdots, e^{j\frac{2\pi d}{\lambda}\sin\theta_N}\}$ contains all the information on the DOAs $\{\theta_i\}_{i=1}^N$. Thus, the DOA estimation problem can be simplified to finding $\mathbf{\Phi}$.

Analogously to the MUSIC algorithms, ESPRIT relies on properties of the eigendecomposition of the array covariance matrix. Let $\mathbf{U}_{s1}$ and $\mathbf{U}_{s2}$ be the $(M-1)\times N$ matrices whose column vectors are the eigenvectors of $\mathbf{R}_{x_1}$ and $\mathbf{R}_{x_2}$, respectively, corresponding to the N largest eigenvalues. As discussed in Section 3.7, $\mathbf{U}_{s1}$, $\mathbf{U}_{s2}$, and $\mathbf{A}$ span the same signal subspace, there exists a nonsingular matrix $\mathbf{T}$ such that

$$\mathbf{U}_{s1} = \mathbf{A}_1\mathbf{T}, \quad \mathbf{U}_{s2} = \mathbf{A}_1\mathbf{\Phi}\mathbf{T}. \tag{4.30}$$

Thus, one can get

$$\mathbf{U}_{s2} = \mathbf{U}_{s1}\mathbf{\Psi} \tag{4.31}$$

where the $\mathbf{\Psi} \in \mathbb{C}^{N\times N}$ is defined as

$$\mathbf{\Psi} = \mathbf{T}^{-1}\mathbf{\Phi}\mathbf{T}. \tag{4.32}$$

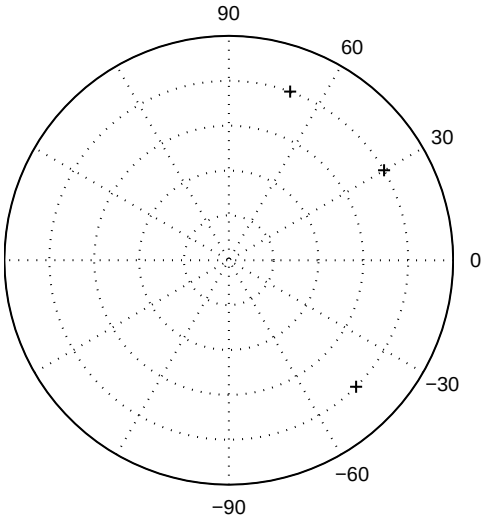

Figure 4.4. Polar of estimates using ESPRIT. $[\theta_1, \theta_2, \theta_3] = [-45°, 30°, 70°]$, SNR = 0dB, snapshots number is 200.

This implies that $\mathbf{\Psi}$ and $\mathbf{\Phi}$ are *similar* and, hence, the eigenvalues of $\mathbf{\Psi}$ must be equal to the diagonal entries of $\mathbf{\Phi}$. To obtain an estimate of $\mathbf{\Psi}$, one has to solve (4.31) which is overdetermined, and the well-known least squares solution of $\|\mathbf{U}_{s2} - \mathbf{U}_{s1}\mathbf{\Psi}\|_F^2$ is given by

$$\mathbf{\Psi} = \mathbf{U}_{s1}^{+}\mathbf{U}_{s2} = \left(\mathbf{U}_{s1}^{H}\mathbf{U}_{s1}\right)^{-1}\mathbf{U}_{s1}^{H}\mathbf{U}_{s2}. \tag{4.33}$$

Consider three signals from $[-45°, 30°, 70°]$ impinging on a 10-element ULA. Fig. 4.4 shows a polar plot of estimates of the three signals using ESPRIT when SNR = 0dB and the number of snapshots is 200.

From the algorithm description and simulation verification, it has been shown that ESPRIT can obtain the DOA estimates but does not need the spectrum calculation and peak search, which represents a significant saving in terms of computation load.

The unitary-ESPRIT is another version of ESPRIT. It has an ESPRIT-like structure, but is implemented by real-valued computations throughout, achieving a substantial reduction of the computational complexity. We start with the transformation of the data matrix from the complex to the real domain in element space. If $\mathbf{x} \in \mathbb{C}^{M\times L}$ is defined as the data matrix, then it can be transformed to the real domain as

$$\mathbf{x}_r = \mathbf{Q}_M^H \begin{bmatrix}\mathbf{x} & \mathbf{J}_M\mathbf{x}^*\mathbf{J}_L\end{bmatrix}\mathbf{Q}_{2L} \tag{4.34}$$

where $\mathbf{Q}_M$ is a sparse unitary matrix given by

$$\mathbf{Q}_m = \begin{cases} \dfrac{1}{\sqrt{2}} \begin{bmatrix} \mathbf{I}_n & j\mathbf{I}_n \\ \mathbf{J}_n & -j\mathbf{J}_n \end{bmatrix}, & m = 2n \\ \dfrac{1}{\sqrt{2}} \begin{bmatrix} \mathbf{I}_n & \mathbf{0}_{n\times 1} & j\mathbf{I}_n \\ \mathbf{0}_{n\times 1}^T & \sqrt{2} & \mathbf{0}_{n\times 1}^T \\ \mathbf{J}_n & \mathbf{0}_{n\times 1} & -j\mathbf{J}_n \end{bmatrix}, & m = 2n+1. \end{cases} \tag{4.35}$$

By performing SVD on $\mathbf{x}_r$, one then obtains the signal subspace $\mathbf{U}_{sr} \in \mathbb{R}^{M\times N}$. Similarly to ESPRIT, a rotation invariance property holds as proved by Haardt and Nossek [138] as

$$\mathbf{K}_1 \mathbf{U}_{sr} \mathbf{\Psi} = \mathbf{K}_2 \mathbf{U}_{sr} \tag{4.36}$$

where $\mathbf{K}_1 \triangleq \mathbf{Q}_{M-1}^H (\mathbf{B}_1 + \mathbf{B}_2) \mathbf{Q}_M$, $\mathbf{K}_1 \triangleq \mathbf{Q}_{M-1}^H j (\mathbf{B}_1 - \mathbf{B}_2) \mathbf{Q}_M$. Moreover, it has been proved that $\mathbf{\Psi}$ is *similar* to a diagonal matrix $\mathbf{\Phi} = \text{diag}\left\{\tan\left(\frac{\pi d}{\lambda}\sin\theta_i\right)\right\}_{i=1}^N$. Therefore, one can follow the procedures of the previously described ESPRIT to obtain the DOA estimates.

4.4 Classical DOA Estimation Algorithms of Coherent Signals

All discussions in Section 4.3 are based on the condition that the incident signals are uncorrelated to each other. However, due to various reflectors in real environments, such as the sea, hills, buildings, etc., or intentional or unintentional outside interferences, the received signals may be highly correlated or even coherent. In this section, we introduce the signal model under multipath propagation and the corresponding processing techniques.

4.4.1 Signal Model Under Multipath Propagation

Consider a number of N narrowband far-field coherent signals impinging on a uniform linear array with M identical omnidirectional sensors. Assume that these signals are

classified into K groups, which result from K statistically uncorrelated far-field sources $s_k(t), k = 1, 2, \cdots, K$ with P_k multipath signals for each source. In the k-th coherent group, the signal coming from direction θ_{kp}, $p = 1, 2, \cdots, P_k$ corresponds to the p-th multipath propagation of the source $s_k(t)$, and the complex fading coefficient is α_{kp}. It is readily seen that the total number of coherent signals satisfies $N = \sum_{k=1}^{K} P_k$. Considering the noise contamination in the array elements, the corresponding $M \times 1$ array output vector is then given by

$$\begin{aligned} \mathbf{x}(t) &= \sum_{k=1}^{K} \sum_{p=1}^{P_k} \mathbf{a}(\theta_{kp}) \alpha_{kp} s_k(t) + \mathbf{n}(t) \\ &= \mathbf{A}\boldsymbol{\Gamma}\mathbf{s}(t) + \mathbf{n}(t) \end{aligned} \tag{4.37}$$

where $\mathbf{a}(\theta) = \left[1, e^{j\frac{2\pi d}{\lambda}\sin\theta}, \cdots, e^{j\frac{2\pi(M-1)d}{\lambda}\sin\theta}\right]^T \in \mathbb{C}^M$ is the steering vector with λ and d being the wavelength of carrier signal and the spacing between adjacent elements, respectively, $\mathbf{A} = \left[\mathbf{A}_1, \cdots, \mathbf{A}_K\right]$ with $\mathbf{A}_k = \left[\mathbf{a}(\theta_{k1}), \cdots, \mathbf{a}(\theta_{kP_k})\right]$, $\boldsymbol{\Gamma} = \text{blkdiag}\{\boldsymbol{\alpha}_1, \cdots, \boldsymbol{\alpha}_K\}$ with $\boldsymbol{\alpha}_k = \left[\alpha_{k1}, \cdots, \alpha_{kP_k}\right]^T$ containing attenuation information of the k-th coherent group, $\mathbf{s}(t) = \left[s_1(t), \cdots, s_K(t)\right]^T$, and $\mathbf{n}(t)$ is white Gaussian noise with the power σ_n^2 for each entry and uncorrelated with the signals. Besides, we assume that the array manifold $\mathbf{A}$ is unambiguous, i.e., the steering vectors $\{\mathbf{a}(\theta_i)\}_{i=1}^N$ are linearly independent for any set of distinct $\{\theta_i\}_{i=1}^N$.

From (6.25), the array covariance matrix is given by

$$\mathbf{R}_x = \mathbf{A}\boldsymbol{\Gamma}\mathbf{R}_s\boldsymbol{\Gamma}^H\mathbf{A}^H + \sigma_n^2\mathbf{I}_M \tag{4.38}$$

where $\mathbf{R}_s = E_t[\mathbf{s}(t)\mathbf{s}^H(t)] = \text{diag}\{\sigma_1^2, \cdots, \sigma_K^2\}$ is the signal covariance matrix. Since $\text{rank}\,(\boldsymbol{\Gamma}) = \text{rank}\,(\mathbf{R}_s) = K < N$, that is, the dimension of the signal subspace is less than the number of coherent signals, say rank deficiency. If performing the eigendecomposition of $\mathbf{R}_x$, although $\mathcal{R}\,(\mathbf{U}_s) = \mathcal{R}\,(\mathbf{A}\boldsymbol{\Gamma})$, the standard MUSIC and ESPRIT fail to work without a prior knowledge of $\boldsymbol{\Gamma}$.

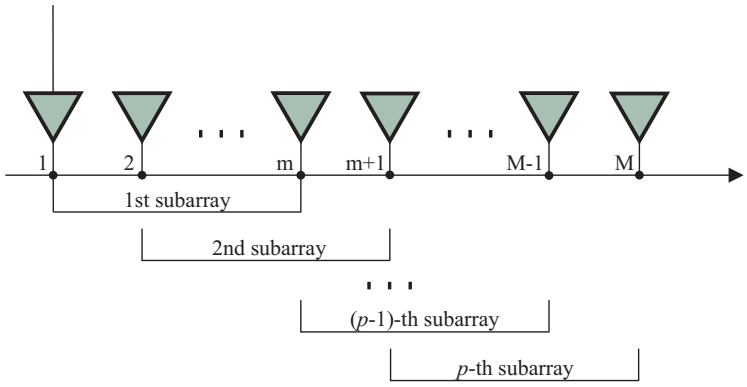

Figure 4.5. Subarrays structure with forward spatial smoothing.

4.4.2 Conventional DOA Estimation Algorithms of Coherent Signals

As we have seen in the last section, rank deficiency will give rise to a failure of standard subspace-based algorithms. Therefore, an intuitive solution of such issue is to effectively restore the rank of the signal subspace such that the resulting rank is equal to the number of coherent signals. To implement this idea, it is popular to first preprocess the array covariance matrix to restore the signal subspace to full rank, then apply the standard high-resolution algorithms, such as MUSIC and ESPRIT, to carry out the DOA estimation.

Forward/backward Spatial Smoothing

Partitioning the whole M-element array into a series of overlapping subarrays each of which consists of m sensors, as illustrated in Fig. 4.5, leads to so-called forward spatial smoothing. Let q denote the number of subarrays, then there exists $M = m + q - 1$.

For the i-th subarray, the array output and covariance matrix are given as:

$$\mathbf{x}_i^f(t) = \mathbf{A}_m \mathbf{\Phi}^{i-1} \mathbf{\Gamma} \mathbf{s}(t) + \mathbf{n}_i(t) \tag{4.39}$$

$$\mathbf{R}_{xi}^f = \mathbf{A}_m \mathbf{\Phi}^{i-1} \mathbf{\Gamma} \mathbf{R}_s \mathbf{\Gamma}^H \mathbf{\Phi}^{1-i} \mathbf{A}_m^H + \sigma_n^2 \mathbf{I} \tag{4.40}$$

where $\mathbf{\Phi} = \text{diag}\{e^{j\frac{2\pi d}{\lambda}\sin\theta_1}, \cdots, e^{j\frac{2\pi d}{\lambda}\sin\theta_N}\}$ and $\mathbf{A}_m \in \mathbb{C}^{m\times N}$ is the 1st subarray's array manifold. By averaging the covariance matrices of all subarrays, one obtains the forward smoothed covariance matrix

$$\mathbf{R}_x^f = \frac{1}{q}\sum_{i=1}^{q} \mathbf{R}_{xi}^f$$

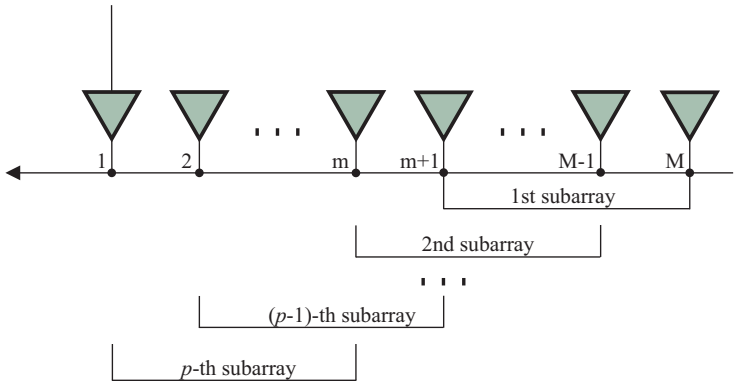

Figure 4.6. Subarrays structure with backward spatial smoothing.

$$= \mathbf{A}_m \left(\frac{1}{q} \sum_{i=1}^{q} \mathbf{\Phi}^{i-1} \mathbf{\Gamma} \mathbf{R}_s \mathbf{\Gamma}^H \mathbf{\Phi}^{1-i} \right) \mathbf{A}_m^H + \sigma_n^2 \mathbf{I}. \tag{4.41}$$

Similarly, the whole array can be divided in another way, as shown in Fig. 4.6, referred to as backward spatial smoothing. Instead of using the array outputs directly, the backward spatial smoothing makes the best of the conjugate of raw data. For the i-th subarray, one has

$$\mathbf{x}_i^b(t) = \mathbf{x}_i^*(t) = \mathbf{A}_m \mathbf{\Phi}^{2-m-i} \mathbf{\Gamma}^* \mathbf{s}^*(t) + \mathbf{n}_i^*(t) \tag{4.42}$$

$$\mathbf{R}_{xi}^b = \mathbf{A}_m \mathbf{\Phi}^{2-m-i} \mathbf{\Gamma}^* \mathbf{R}_s^* \mathbf{\Gamma}^T \mathbf{\Phi}^{i-m-2} \mathbf{A}_m^H + \sigma_n^2 \mathbf{I}. \tag{4.43}$$

Then, the backward smoothed array covariance matrix can be expressed as

$$\begin{aligned} \mathbf{R}_x^b &= \frac{1}{q} \sum_{i=1}^{q} \mathbf{R}_{xi}^b \\ &= \mathbf{A}_m \left(\frac{1}{q} \sum_{i=1}^{q} \mathbf{\Phi}^{2-m-i} \mathbf{\Gamma}^* \mathbf{R}_s^* \mathbf{\Gamma}^T \mathbf{\Phi}^{i+m-2} \right) \mathbf{A}_m^H + \sigma_n^2 \mathbf{I}. \end{aligned} \tag{4.44}$$

Combining (4.41) and (4.44), one will obtain the well-known forward/backward smoothed covariance matrix

$$\begin{aligned} \mathbf{R}_x^{fb} &= \frac{1}{2}(\mathbf{R}_x^f + \mathbf{R}_x^b) \\ &= \mathbf{A}_m \left[\frac{1}{2q} \sum_{i=1}^{q} \left(\mathbf{\Phi}^{i-1} \mathbf{\Gamma} \mathbf{R}_s \mathbf{\Gamma}^H \mathbf{\Phi}^{1-i} + \mathbf{\Phi}^{2-m-i} \mathbf{\Gamma}^* \mathbf{R}_s^* \mathbf{\Gamma}^T \mathbf{\Phi}^{i+m-2} \right) \right] \mathbf{A}_m^H + \sigma_n^2 \mathbf{I}. \end{aligned} \tag{4.45}$$

Irrespective of noise term, $\sigma_n^2 \mathbf{I}$, when $m \geq N+1$ and $2q \geq P_{max}$ where $P_{max} = \max\{P_1, P_2, \cdots, P_K\}$, $\text{rank}(\mathbf{R}_x^{fb}) = N$ for K groups of coherent signals, which has been proved

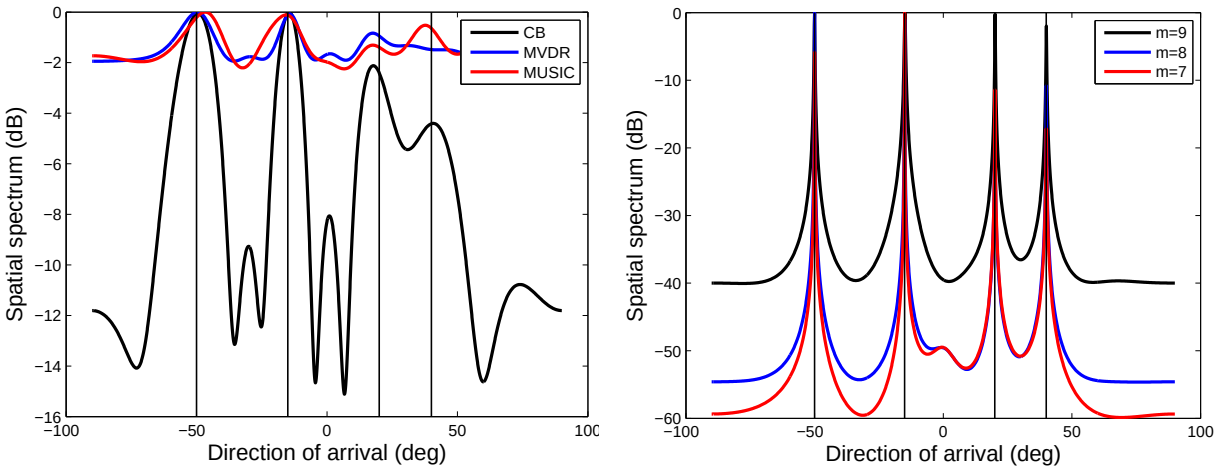

(a) Spatial spectrum without preprocessing

(b) Spatial spectrum with FBSS

Figure 4.7. Spatial spectrum comparison between (a) without rank restoration; (b) with FBSS. SNR $= 5$dB, snapshots number is 500.

in [24] under the mild restrictions that whenever equality holds among some of the members of the set $\{e^{j\frac{2\pi d}{\lambda}\sin\theta_{kp}}, k = 1, \cdots, K; p = 1, \cdots, P_k\}$, its largest subset with equal entries must be at most of size q.

As the forward/backward smoothed covariance matrix $\mathbf{R}_x^{fb}$ obtained from (4.45) has full rank, by applying high-resolution direction finding methods, such as MUSIC or ESPRIT, to $\mathbf{R}_x^{fb}$, we can get the DOA estimates of the coherent signals.

Consider one group of 4 signals from $[-50°, -15°, 20°, 40°]$ impinging on a 10-element ULA, the fading coefficients are $[0.6595 + 0.7517j, -0.4656 + 0.7702j, -0.9867 - 0.1625j, 0.6500 + 0.4664j]$, and the SNR and number of snapshots are fixed at 5dB and 500, respectively. Fig. 4.7 shows that, compared with the standard spectral-based and subspace-based methods without any preprocessing, FBSS can effectively handle the coherent signals and obtain accurate DOA estimates.

Toeplitz Matrix Reconstruction

For a ULA, considering that the covariance matrix of uncorrelated signals is Toeplitz, another rank restoration idea is to reconstruct a Toeplitz matrix using the entries of the original covariance matrix while spanning the identical signal subspace. Inspired by

this, Han and Zhang developed a Toeplitz matrix reconstruction method by exploiting the symmetric configuration of the ULA, allowing the rank of resulting matrix to only depend on the number of incident signals regardless of the correlation between them [30]. Assume that the number of sensors in a ULA is $M = 2M_1 + 1$, the multipath propagation model described in Section 4.4.1, and setting the middle sensor as a reference, then the steering vector is

$$\mathbf{a}(\theta) = \left[e^{-j\frac{2\pi M_1 d}{\lambda}\sin\theta}, \cdots, e^{-j\frac{2\pi d}{\lambda}\sin\theta}, 1, e^{j\frac{2\pi d}{\lambda}\sin\theta}, \cdots, e^{j\frac{2\pi M_1 d}{\lambda}\sin\theta}\right]^T \tag{4.46}$$

and the (i,j)-th entry of the covariance matrix can be expressed as

$$\mathbf{R}_x(i,j) = \sum_{k=1}^{K}\sum_{l=1}^{P_k}\left(\sigma_k^2\alpha_{kl}^*\sum_{p=1}^{P_k}\alpha_{kp}e^{j\frac{2\pi(i-M_1-1)d}{\lambda}\sin\theta_{kp}}\right)e^{j\frac{2\pi(M_1+1-j)d}{\lambda}\sin\theta_{kp}} + \sigma_n^2\delta_{i,j} \tag{4.47}$$

where $\delta_{i,j}$ is the Kronecker delta, i.e.,

$$\delta_{i,j} = \begin{cases} 1, & i = j \\ 0, & i \neq j. \end{cases} \tag{4.48}$$

Then, utilising the i-th row of $\mathbf{R}_x$, $i = 1, 2, \cdots, M$, one can construct the following Toeplitz matrix

$$\begin{aligned}\mathbf{R}(i) &\triangleq \begin{bmatrix} \mathbf{R}_x(i, M_1+1) & \mathbf{R}_x(i, M_1+2) & \cdots & \mathbf{R}_x(i, M) \\ \mathbf{R}_x(i, M_1) & \mathbf{R}_x(i, M_1+1) & \cdots & \mathbf{R}_x(i, M-1) \\ \vdots & \vdots & \ddots & \vdots \\ \mathbf{R}_x(i,1) & \mathbf{R}_x(i,2) & \cdots & \mathbf{R}_x(i, M_1+1) \end{bmatrix} \\ &= \mathbf{A}_1\mathbf{D}(i)\mathbf{A}_1^H + \sigma_n^2\mathbf{I}_{M_1+1,i}\end{aligned} \tag{4.49}$$

where $\mathbf{A}_1 = \left[\mathbf{0}_{(M_1+1)\times M_1}, \mathbf{I}_{M_1}\right]\mathbf{A}$, $\mathbf{D}(i) = \text{diag}\left\{d_{11}^{(i)}, \cdots, d_{1P_1}^{(i)}, \cdots, d_{KP_K}^{(i)}\right\}$ with

$$d_{kp}^{(i)} = \sigma_k^2\alpha_{kl}^*\sum_{p=1}^{P_k}\alpha_{kp}e^{j\frac{2\pi(i-M_1)d}{\lambda}\sin\theta_{kp}}, \quad k = 1, \cdots, K; \quad p = 1, \cdots, P_k \tag{4.50}$$

and $\mathbf{I}_{M_1+1,i}$ is an $(M_1+1)\times(M_1+1)$ matrix with unity entries on the ith diagonal.

As stated earlier, $\text{rank}\left(\mathbf{R}(i)\right) = N$ and the standard spectral-based algorithms can be applied accordingly, provided that $M_1 \geq N$. Note that since any row of $\mathbf{R}_x$ can be used

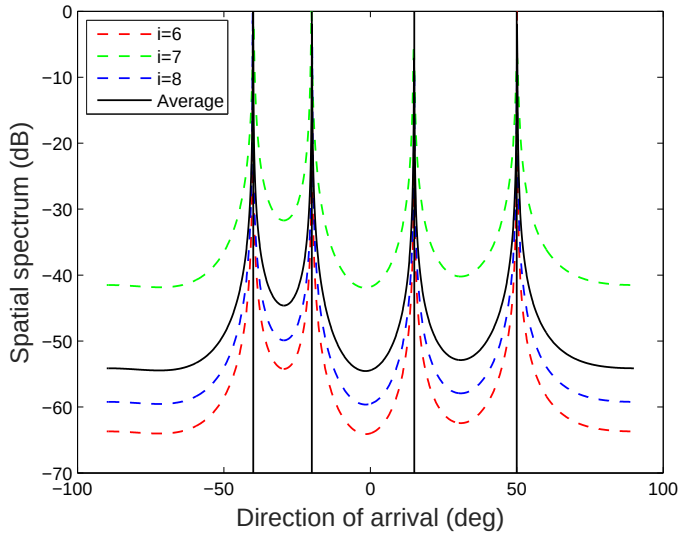

Figure 4.8. MUSIC spatial spectrum with Toeplitz matrix reconstruction.

to construct the matrix in (4.49), one can obtain M Toeplitz matrices in parallel and take the average DOA estimates as the final results, which improves the robustness as well as accuracy of the estimation.

For an 11-element ULA, take the same scenario as in Fig. 4.7, for example, the MUSIC spatial spectrum with the Toeplitz matrix reconstruction is shown in Fig. 4.8, and it is clear to see that the peaks of spatial spectrum indicate the desired DOAs of coherent signals.

4.5 Source Enumeration

As is well known, the performance of the high-resolution methods, such as MUSIC and ESPRIT, essentially relies on *a priori* knowledge of the number of sources, consequently, detection of the number of signals is both reasonable and desirable. In this area, a number of approaches have been proposed [139–144].

In [139], Wax and Kailath originally addressed this problem by employing the Akaike information criterion (AIC) and minimum description length (MDL). The MDL method is a model-dependent and eigenvalue-based estimator, yielding a consistent estimate for the number of sources, and thus it has attracted more attention than the AIC estimator that tends to overestimate the number of sources, especially when a large number

of snapshots. The idea behind is to use eigen-decomposition to separate the signal and noise subspaces, and apply selection criteria that combine likelihood-based functions and some penalty functions without adjusting the probability of false alarm, to estimate the number of sources and DOAs. MDL performs well on condition that the additive noise is a white Gaussian process with equal power, however, as reviewed in Section 2.3, this assumption may not hold in some practical applications due to the heterogeneity of the receiving channel or prevailing external noise. To improve the robustness of the ordinary MDL method, Wu et al obtained the Gerschgorin radii by performing a unitary transformation of the covariance matrix, and then used them to construct the Gerschgorin disk estimator (GDE) to separate the signal Gerschgorin disks from the noise Gerschgorin disks [140].

Although these methods have received considerable attention by virtue of their relative computational simplicity, they suffer from serious degradation when the incident signals are coherent (i.e., fully correlated) such as in multipath propagation environments, where the rank of the signal covariance matrix is smaller than the number of signals. To handle this issue, some researchers employ the spatial smoothing technique to restore the rank deficiency in covariance matrix [141–143]. Unlike these methods, Wax and Ziskind [144] have developed an MDL approach for coherent signal enumeration based on a multidimensional search. This approach first partitions the sensor data into signal and noise subspace components, and then separately calculates their MDL descriptors.

It should be stressed that source enumeration does not lie in the scope of the thesis since it is another important research field in its own right—detection theory rather than our focus estimation theory. Throughout the thesis we assume the number of signals is known *a priori* or can be obtained by using aforementioned source enumeration methods if not specified.

4.6 Conclusion

This chapter first introduced array signal model with expressions of some common terms, such as the steering vector and covariance matrix. Then, a review of the conventional DOA estimation algorithms for uncorrelated signals was presented, including conventional beamforming, MVDR, especially MUSIC which ushered in the high-resolution DOA estimation age and the follower ESPRIT, and several simple simulations were carried out to demonstrate the performance of the algorithms.

Subsequently, the coherent signal model under multipath propagation was given, and the reason why the standard spectral-based algorithms, especially MUSIC and ESPRIT, fail to work in such conditions was analysed. Conventional rank restoration techniques, including FBSS and Toeplitz matrix reconstruction, were discussed and derived, and simulations were conducted to show the performance of these approaches.

Finally, on account of the significance of detection of sources, some classical source enumeration methods were outlined for various scenarios, particularly in coloured noise or under multipath propagation, although this topic is out of the scope of the thesis.

Chapter 5

Efficient DOA Estimation Using Cumulants in Multipath

IN array processing, the forward/backward spatial smoothing (FBSS) technique is most often utilised for combating signal coherency. However, FBSS cannot distinguish independent signals from coherent signals, or coherent groups from each other, and thus the number of resolvable signals will be restricted to a large extent. In this chapter, we extend the knowledge of fourth order cumulants in this area by introducing an improved two-stage algorithm, which can separately deal with independent and coherent signals, as well as showing how temporal correlation can be exploited in a VESPA-like algorithm, both with the goal of achieving a more efficient use of degrees of freedom (DOFs) and improvement in DOA estimation performance.

5.1 Introduction

This chapter considers the DOA estimation of signals with circular statistics using fourth order cumulants (FOC) in conditions where uncorrelated and coherent signals coexist. Two improved algorithms are introduced for this scenario. Based on the literature review in Chapter 2, this particular class of algorithm is important to discuss due to the following considerations:

- Circular signal statistics are among the most general class of signals which can describe most signals encountered in array processing.
- Fourth order statistics play an important role in array processing, as they are insensitive to spatially coloured noise which is a difficult problem to deal with using second order statistics and can potentially give significantly more DOFs.
- Uncorrelated and coherent signals can coexist in practical situations when some signals are affected by multipath with delays significantly less than the inverse signal bandwidth.

As already mentioned in Chapter 2, the VESPA algorithm is the state of the art FOC-based algorithm for signals with circular statistics when multiple coherent groups exist. This algorithm can resolve the most signals for this particular scenario. It is a single-stage algorithm that blindly separates all the coherent signal into groups directly and then applies FBSS to resolve the coherent signals within each group. The blind separation of the coherent groups is achieved by constructing two different FOC matrices from which the generalised steering vectors (i.e., a linear combination of the steering vectors to the fading coefficients) can be blindly estimated using the rotation invariance property.

VESPA does spatial only processing and in this chapter we explore how the temporal correlation of signals can be exploited in the fourth order statistics to improve the DOA estimation accuracy. We introduce new augmented cumulant matrices that are based not only on spatial but also temporal correlations. These matrices maintain the same properties of rotational invariance that are exploited by VESPA to blindly separate the

coherent groups. Using temporal correlation as well as the augmented signal subspace gives significantly improved accuracy and robustness compared with the spatial only VESPA algorithm without sacrificing DOFs.

Another approach of dealing with a mixture of uncorrelated and coherent signals is based on the two-stage methods [43–47] also reviewed in Chapter 2. This class of algorithm first separates the uncorrelated from coherent signals and then applies a rank restoration technique, such as spatial smoothing, to resolve the coherent signals. These algorithms have mainly been based on second order statistics and most of them use spatial differencing followed by spatial smoothing [43, 46, 47]. Recently oblique projections have also been applied to separate the uncorrelated signals, resulting in some improvements over spatial differencing [145]. However, the two-stage techniques have rarely been combined with fourth order statistics, and we have only found one contribution in this area which is based on spatial differencing followed by spatial smoothing [49].

While the two-stage techniques cannot resolve as many signals as VESPA, they tend to be more accurate and robust, especially in low SNR environments. There is thus significant scope and motivation for improving the performance of this class of algorithm. In this chapter we introduce a new two-stage FOC algorithm that achieves significantly better performance than the previously published two-stage FOC algorithm. Improvements are made firstly in the way the FOC matrix is initially constructed. Our algorithm uses more FOC terms than the previously published algorithm to improve the robustness and accuracy of the estimates. Secondly, in the second stage, a cumulant matrix reconstruction method is used to separate the uncorrelated signals, which is more robust and loses less information than the spatial differencing applied in the previous method. Finally, a novel rank restoration technique is introduced to resolve the correlated signals which is more accurate and robust than the spatial smoothing algorithm applied in the previous method as it makes use of more entries in the cumulant matrix.

The rest of this chapter is organised as follows. In Section 5.2, we introduce the definition and properties of FOC which are significant to our research on array processing.

From the main four properties of FOC, it is clear that high order statistics can extract more information embedded in the non-Gaussian signals than SOS, which motives us to investigate how to improve the existing work on coherent signal estimation utilising FOC. In Section 5.3, we present the main model of mixed, uncorrelated and coherent, signals in the presence of multipath which is assumed in this chapter. Then in Section 5.4, we introduce a new two-stage FOC algorithm for mixed coherent and correlated signals. Our algorithm follows the framework introduced in [49] but with considerably improved accuracy and robustness. Finally in Section 5.5, we consider how to incorporate temporal correlation information into DOA estimation by proposing a novel estimator utilising space-time FOC, which can provide a more robust identification and separation of coherent groups than the spatial only VESPA algorithm. Simulation results are provided in Sections 5.4 and 5.5 to compare our new methods with previous work and final conclusions are drawn in Section 5.6.

5.2 Cumulants Preliminaries—Definitions and Properties

Conventional array processing techniques only utilise the second-order statistics of received signal snapshots. The first and second-order statistics are sufficient to depict the characteristics of signals with a Gaussian distribution. However, in wireless communication systems, most modulated signals are non-Gaussian, such as BPSK and QAM, for which the second-order statistics cannot completely characterise all of the statistical properties of the underlying signals, so it is beneficial to consider information embedded in high order moments. In this chapter, we use the fourth-order cumulant matrix instead of the conventional snapshot covariance matrix to exploit more potential information of non-Gaussian signals. The fourth-order cumulants of zero-mean stationary measurements can be defined in a balanced way as [37]

$$\begin{aligned}
&\operatorname{cum}\left\{x_{k_1}(t), x_{k_2}^*(t), x_{l_1}(t), x_{l_2}^*(t)\right\} \\
&= E_t\left[x_{k_1}(t)x_{k_2}^*(t)x_{l_1}(t)x_{l_2}^*(t)\right] - E_t\left[x_{k_1}(t)x_{k_2}^*(t)\right] E_t\left[x_{l_1}(t)x_{l_2}^*(t)\right] \\
&\quad - E_t\left[x_{k_1}(t)x_{l_1}(t)\right] E_t\left[x_{k_2}^*(t)x_{l_2}^*(t)\right] - E_t\left[x_{k_1}(t)x_{l_2}^*(t)\right] E_t\left[x_{k_2}^*(t)x_{l_1}(t)\right]
\end{aligned} \tag{5.1}$$

while another definition is also valid [146]

$$\begin{aligned}
&\operatorname{cum}\left\{x_{k_1}(t), x_{k_2}(t), x_{l_1}(t), x_{l_2}(t)\right\} \\
&= E_t\left[x_{k_1}(t)x_{k_2}(t)x_{l_1}(t)x_{l_2}(t)\right] - E_t\left[x_{k_1}(t)x_{k_2}(t)\right]E_t\left[x_{l_1}(t)x_{l_2}(t)\right] \\
&\quad - E_t\left[x_{k_1}(t)x_{l_1}(t)\right]E_t\left[x_{k_2}(t)x_{l_2}(t)\right] - E_t\left[x_{k_1}(t)x_{l_2}(t)\right]E_t\left[x_{k_2}(t)x_{l_1}(t)\right].
\end{aligned} \tag{5.2}$$

Before giving an interpretation of our work, we introduce some important properties of cumulants that are used in the sequel [38, 146]:

[CP1] If $\{\alpha_i\}_{i=1}^n$ are constants and $\{x_i\}_{i=1}^n$ are random variables, then

$$\operatorname{cum}\left\{\alpha_1 x_1, \alpha_2 x_2, \cdots, \alpha_n x_n\right\} = \left(\prod_{i=1}^{n}\alpha_i\right)\operatorname{cum}\left\{x_1, x_2, \cdots, x_n\right\}. \tag{5.3}$$

[CP2] Cumulants are additive in their arguments

$$\operatorname{cum}\left\{x_1 + y_1, x_2, \cdots, x_n\right\} = \operatorname{cum}\left\{x_1, x_2, \cdots, x_n\right\} + \operatorname{cum}\left\{y_1, x_2, \cdots, x_n\right\}. \tag{5.4}$$

[CP3] If the random variables $\{x_i\}_{i=1}^n$ are independent of the random variables $\{y_i\}_{i=1}^n$, then

$$\operatorname{cum}\left\{x_1 + y_1, x_2 + y_2, \cdots, x_n + y_n\right\} = \operatorname{cum}\left\{x_1, x_2, \cdots, x_n\right\} + \operatorname{cum}\left\{y_1, y_2, \cdots, y_n\right\}. \tag{5.5}$$

[CP4] Cumulants suppress Gaussian noise of arbitrary covariance, i.e., if $\{z_i\}_{i=1}^n$, are Gaussian random variables independent of $\{x_i\}_{i=1}^n$ and $n > 2$, we have

$$\operatorname{cum}\left\{x_1 + z_1, x_2 + z_2, \cdots, x_n + z_n\right\} = \operatorname{cum}\left\{x_1, x_2, \cdots, x_n\right\}. \tag{5.6}$$

The following sections introduce the FOC matrices and describe two DOA estimation algorithms using these matrices.

5.3 Problem Formulation

Although groups of coherent signals arise from multipath propagation, independent signals may still exist in such a scenario. It is thus reasonable to consider a more complex case where the received independent and coherent signals coexist. As a result, the

model in Section 4.4.1, which only considers coherent signals, is not applicable, and a new model is required. Here, we first introduce the mixture model of independent and coherent signals, and then the construction of the cumulant matrices.

Consider a number of N narrowband far-field signals impinging on a uniform linear array with M identical omnidirectional sensors. Assume that there are K groups of coherent signals, which come from K statistically independent far-field sources $s_k(t)$ with power σ_k^2 for $k = 1, 2, \cdots, K$, and with P_k multipath signals for each source. In the k-th coherent group, the signal coming from direction θ_{kp}, $p = 1, 2, \cdots, P_k$ corresponds to the p-th multipath propagation of the source $s_k(t)$, and the complex fading coefficient is α_{kp}. Denote the total number of coherent signals as $N_c = \sum_{k=1}^{K} P_k$, and assume the remaining $N_u = N - N_c$ sources $s_k(t)$ coming from direction θ_k with power σ_k^2, $k = N_c + 1, N_c + 2, \cdots, N$, are independent to each other and also to the coherent signals. The $M \times 1$ array output vector is then given by

$$\begin{aligned}\mathbf{x}(t) &= \sum_{k=1}^{K}\sum_{p=1}^{P_k} \mathbf{a}(\theta_{kp})\alpha_{kp}s_k(t) + \sum_{k=N_c+1}^{N} \mathbf{a}(\theta_k)s_k(t) + \mathbf{n}(t) \\ &= \mathbf{A}_c\boldsymbol{\Gamma}\mathbf{s}_c(t) + \mathbf{A}_u\mathbf{s}_u(t) + \mathbf{n}(t) = \bar{\mathbf{A}}\mathbf{s}(t) + \mathbf{n}(t) \end{aligned} \tag{5.7}$$

where $\mathbf{a}(\theta) = \left[1, e^{j\frac{2\pi d}{\lambda}\sin\theta}, \cdots, e^{j\frac{2\pi(M-1)d}{\lambda}\sin\theta}\right]^T \in \mathbb{C}^M$ is the steering vector with λ and d being the wavelength of carrier signal and the spacing between adjacent elements, respectively, $\mathbf{A}_c = \left[\mathbf{A}_{c,1}, \cdots, \mathbf{A}_{c,K}\right]$ with $\mathbf{A}_{c,k} = \left[\mathbf{a}(\theta_{k1}), \cdots, \mathbf{a}(\theta_{kP_k})\right]$, $\boldsymbol{\Gamma} = \text{blkdiag}\{\boldsymbol{\alpha}_1, \cdots, \boldsymbol{\alpha}_K\}$ with $\boldsymbol{\alpha}_k = \left[\alpha_{k1}, \cdots, \alpha_{kP_k}\right]^T$ containing attenuation information of the k-th coherent group, $\mathbf{A}_u = [\mathbf{a}(\theta_{N_c+1}), \mathbf{a}(\theta_{N_c+2}), \cdots, \mathbf{a}(\theta_N)]$, $\mathbf{s}_c(t) = \left[s_1(t), \cdots, s_K(t)\right]^T$, $\mathbf{s}_u(t) = \left[s_{N_c+1}(t), \cdots, s_N(t)\right]^T$, $\bar{\mathbf{A}} = \left[\mathbf{A}_c\boldsymbol{\Gamma}, \mathbf{A}_u\right] = \left[\bar{\mathbf{a}}_1, \cdots, \bar{\mathbf{a}}_{K+N_u}\right]$, $\mathbf{s}(t) = \left[\mathbf{s}_c^T(t), \mathbf{s}_u^T(t)\right]^T$, and $\mathbf{n}(t)$ is spatially coloured Gaussian noise with an unknown covariance matrix. Besides, we assume that the array is calibrated, and the array manifold $\bar{\mathbf{A}}$ is unambiguous, i.e., the steering vectors $\{\mathbf{a}(\theta_i)\}_{i=1}^N$ are linearly independent for any set of distinct $\{\theta_i\}_{i=1}^N$. Equivalently, the matrix $\bar{\mathbf{A}}$ is of full column rank.

According to the definition of cumulants (5.1), there are totally M^2 combinations of cumulants, so the size of full cumulant matrix is $M^2 \times M^2$. However, only subsets of

these can be used for rank restoration, say FBSS, due to the subarray structure requirement [38, 49]. The possible subsets of cumulant terms $\mathbf{C}_{x,i}$, corresponding to the i-th subset, can be generated by the following equation

$$\mathbf{C}_{x,i} \triangleq \text{cum}\{x_i(t), x_i^*(t), \mathbf{x}(t), \mathbf{x}^H(t)\}, \quad i = 1, 2, \cdots, M \tag{5.8}$$

whose entry $\mathbf{C}_x(m,n)$ is given by

$$\begin{aligned}\mathbf{C}_{x,i}(m,n) &= \text{cum}\{x_i(t), x_i^*(t), x_m(t), x_n^*(t)\} \\ &= E_t[x_i(t)x_i^*(t)x_m(t)x_n^*(t)] - E_t[x_i(t)x_i^*(t)]E_t[x_m(t)x_n^*(t)] \\ &\quad - E_t[x_i(t)x_m(t)]E_t[x_i^*(t)x_n^*(t)] - E_t[x_i(t)x_n^*(t)]E_t[x_i^*(t)x_m(t)].\end{aligned} \tag{5.9}$$

We now derive an expression for the averaged cumulant matrix based on our signal model. As seen in (5.8) that there are M different cumulant matrices available. However, only $\mathbf{C}_{x,1}$ is used in [49]. In order to improve the robustness of cumulants matrix estimates, one can take an average over multiple $\mathbf{C}_{x,i}$ as the final estimate.

Based on (5.7) and recalling the property of cumulants [CP4] in the last section, one gets

$$\begin{aligned}\mathbf{C}_{x,i} &= \text{cum}\left\{\bar{\mathbf{A}}(i,:)\mathbf{s}(t), (\bar{\mathbf{A}}(i,:)\mathbf{s}(t))^*, \bar{\mathbf{A}}\mathbf{s}(t), (\bar{\mathbf{A}}\mathbf{s}(t))^H\right\} \\ &\quad + \text{cum}\{n_i(t), n_i^*(t), \mathbf{n}(t), \mathbf{n}^H(t)\} \\ &= \text{cum}\left\{\bar{\mathbf{A}}(i,:)\mathbf{s}(t), (\bar{\mathbf{A}}(i,:)\mathbf{s}(t))^*, \bar{\mathbf{A}}\mathbf{s}(t), (\bar{\mathbf{A}}\mathbf{s}(t))^H\right\}\end{aligned} \tag{5.10}$$

where the FOC matrix of noise $\text{cum}\{n_i(t), n_i^*(t), \mathbf{n}(t), \mathbf{n}^H(t)\}$ is zero under the Gaussian assumption and thus can be omitted. Substituting $\sum_{i=1}^{K+N_u} \bar{\mathbf{a}}_i s_i(t)$ for $\bar{\mathbf{A}}\mathbf{s}(t)$ into (5.10) and utilising the properties of cumulants [CP1]-[CP4] in the last section, one can further get

$$\begin{aligned}\mathbf{C}_{x,i} = \text{cum}\Bigg\{&\sum_{p=1}^{K+N_u} \bar{\mathbf{A}}(i,p)s_p(t), \sum_{q=1}^{K+N_u} \bar{\mathbf{A}}^*(i,q)s_q^*(t), \\ &\sum_{m=1}^{K+N_u} \bar{\mathbf{a}}_m s_m(t), \sum_{n=1}^{K+N_u} \bar{\mathbf{a}}_n^H s_n^*(t)\Bigg\} \\ = &\sum_{p=1}^{K+N_u}\sum_{q=1}^{K+N_u}\sum_{m=1}^{K+N_u}\sum_{n=1}^{K+N_u} \bar{\mathbf{A}}(i,p)\bar{\mathbf{A}}^*(i,q)\bar{\mathbf{a}}_m\bar{\mathbf{a}}_n^H \text{cum}\{s_p(t),\end{aligned}$$

$$
\begin{aligned}
& s_q^*(t), s_m(t), s_n^*(t)\} \\
&= \sum_{k=1}^{K+N_u} |\bar{\mathbf{A}}(i,k)|^2 \bar{\mathbf{a}}_k \bar{\mathbf{a}}_k^H \mathrm{cum}\{s_k(t), s_k^*(t), s_k(t), s_k^*(t)\} \\
&= \sum_{k=1}^{K+N_u} \gamma_k |\bar{\mathbf{A}}(i,k)|^2 \bar{\mathbf{a}}_k \bar{\mathbf{a}}_k^H = \bar{\mathbf{A}} \mathbf{C}_{s,i} \bar{\mathbf{A}}^H
\end{aligned} \tag{5.11}
$$

where $\gamma_k \triangleq \mathrm{cum}\{s_k(t), s_k^*(t), s_k(t), s_k^*(t)\}$ is the kurtosis of the k-th signal, and $\mathbf{C}_{s,i} = \mathrm{diag}\{\gamma_1 |\bar{\mathbf{A}}(i,1)|^2, \cdots, \gamma_{K+N_u} |\bar{\mathbf{A}}(i,K+N_u)|^2\}$. We assume γ_k is nonzero, otherwise it is impossible to distinguish the signal subspace from the noise subspace as the zero singular values correspond to the two subspaces simultaneously.

Averaging over the M different cumulant matrices gives

$$
\mathbf{C}_x = \frac{1}{M} \sum_{i=1}^{M} \mathbf{C}_{x,i} = \bar{\mathbf{A}} \mathbf{C}_s \bar{\mathbf{A}}^H \tag{5.12}
$$

where

$$
\begin{aligned}
\mathbf{C}_s &\triangleq \frac{1}{M} \sum_{i=1}^{M} \mathbf{C}_{s,i} \\
&= \mathrm{diag}\left\{ \frac{\gamma_1}{M} \sum_{i=1}^{M} |\bar{\mathbf{A}}(i,1)|^2, \cdots, \frac{\gamma_{K+N_u}}{M} \sum_{i=1}^{M} |\bar{\mathbf{A}}(i,K+N_u)|^2 \right\} \\
&= \mathrm{diag}\left\{ \bar{\gamma}_1, \cdots, \bar{\gamma}_{K+N_u} \right\}.
\end{aligned} \tag{5.13}
$$

Since the required computations for different cumulant matrices $\mathbf{C}_{x,i}$ are independent, they can be implemented in parallel, which means that this method does not require additional computation time.

5.4 Two-stage Processing for Mixed Signals Under Multipath Propagation

This section describes a new two-stage DOA estimation algorithm which first estimates the DOAs of independent signals in stage 1 and then extracts and restores the rank of coherent signals in stage 2. The algorithm utilises averaged cumulant matrix $\mathbf{C}_x$ introduced in Section 5.3, which gives better performance than the previous method which only adopts $\mathbf{C}_{x,1}$.

5.4.1 Stage 1: DOA Estimation of the Uncorrelated Signals

When $K + N_u < M$, the singular value decomposition (SVD) of $\mathbf{C}_x$ is given by

$$\mathbf{C}_x = \mathbf{U}\boldsymbol{\Sigma}\mathbf{V}^H \tag{5.14}$$

where $\boldsymbol{\Sigma} = \text{diag}\{\lambda_1, \lambda_2, \cdots, \lambda_M\}$ consists of M singular values satisfying $\lambda_1 \geq \cdots \geq \lambda_{K+N_u} > \lambda_{K+N_u+1} = \cdots = \lambda_M = 0$ and $\mathbf{V} \in \mathbb{C}^{M\times M}$ consists of the right singular vectors. The columns of $\mathbf{U}_s \triangleq \mathbf{U}(:, 1 : K + N_u)$ are the left singular vectors corresponding to the $K + N_u$ largest singular values, while the columns of $\mathbf{U}_n \triangleq \mathbf{U}(:, K + N_u + 1 : M)$ are the left singular vectors corresponding to the $M - K - N_u$ singular values which are all zero. The signal subspace is spanned by the columns of $\mathbf{U}_s$, while the noise subspace is spanned by the columns of $\mathbf{U}_n$. Because the signal subspace is orthogonal to the noise subspace, we have

$$\left\|(\mathbf{A}_{c,k}\boldsymbol{\alpha}_k)^H\mathbf{U}_n\right\|_F^2 = 0, \quad \text{for } k = 1, 2, \cdots, K \tag{5.15}$$

$$\left\|\mathbf{a}^H(\theta)\mathbf{U}_n\right\|_F^2 = 0, \quad \text{for } \theta = \theta_i, i = N_c + 1, N_c + 2, \cdots, N. \tag{5.16}$$

Proposition 1. *$A_{c,k}\boldsymbol{\alpha}_k$ cannot be a nonzero scalar multiple of $\boldsymbol{a}(\theta_0)$ for any direction of arrival θ_0.*

Proof: If $\mathbf{A}_{c,k}\boldsymbol{\alpha}_k$ can result in another steering vector multiplied by a nonzero scalar, i.e., $\mathbf{A}_{c,k}\boldsymbol{\alpha}_k = \beta\mathbf{a}(\theta_0)$, then we have

$$\begin{bmatrix}\mathbf{a}(\theta_{k1}) & \mathbf{a}(\theta_{k2}) & \cdots & \mathbf{a}(\theta_{kP_k})\end{bmatrix}\begin{bmatrix}\alpha_{k1}\\ \alpha_{k2}\\ \vdots\\ \alpha_{kP_k}\end{bmatrix} = \beta\mathbf{a}(\theta_0)$$

$$\Leftrightarrow \alpha_{k1}\mathbf{a}(\theta_{k1}) + \alpha_{k2}\mathbf{a}(\theta_{k2}) + \cdots + \alpha_{kP_k}\mathbf{a}(\theta_{kP_k}) = \beta\mathbf{a}(\theta_0) \tag{5.17}$$

which indicates that $\mathbf{a}(\theta_0)$ is a linear combination of $\mathbf{a}(\theta_{k1}), \mathbf{a}(\theta_{k2}), \cdots, \mathbf{a}(\theta_{kP_k})$, so the matrix $\tilde{\mathbf{A}}_k \triangleq \begin{bmatrix}\mathbf{a}(\theta_{k1}) & \mathbf{a}(\theta_{k2}) & \cdots & \mathbf{a}(\theta_{kP_k}), \mathbf{a}(\theta_0)\end{bmatrix} \in \mathbb{C}^{K\times P_k+1}$ must be deficient in column rank. Next, we prove that $\theta_0 \notin \{\theta_i\}_{i=k1}^{kP_k}$. This follows from the fact that there must

be at least two signals in each coherent group, i.e., $P_k \geq 2$, otherwise it would be simplified to uncorrelated signal case. If $\theta_0 \in \{\theta_i\}_{i=k1}^{kP_k}$, without loss of generality, we assume $\theta_0 = \theta_{k1}$. From (5.17), one obtains $(\alpha_{k1} - \beta)\,\mathbf{a}(\theta_{k1}) + \alpha_{k2}\mathbf{a}(\theta_{k2}) + \cdots + \alpha_{kP_k}\mathbf{a}(\theta_{kP_k}) = \mathbf{0}$. It is well known that any $m \times n$ $(m \geq n)$ Vandermonde matrix

$$\mathbf{V} = \begin{bmatrix} 1 & 1 & 1 & \cdots & 1 \\ a_1 & a_2 & a_3 & \cdots & a_n \\ a_1^2 & a_2^2 & a_3^2 & \cdots & a_n^2 \\ \vdots & \vdots & \vdots & \ddots & \vdots \\ a_1^{m-1} & a_2^{m-1} & a_3^{m-1} & \cdots & a_n^{m-1} \end{bmatrix}$$

has full column rank as long as the values of a_i are distinct [147], which implies that all columns of $\mathbf{A}_{c,k}$ are linearly independent in our case. As a result, $(\alpha_{k1} - \beta)\,\mathbf{a}(\theta_{k1}) + \alpha_{k2}\mathbf{a}(\theta_{k2}) + \cdots + \alpha_{kP_k}\mathbf{a}(\theta_{kP_k}) = \mathbf{0}$ holds if and only if $\alpha_{k1} - \beta = \alpha_{k2} = \cdots = \alpha_{kP_k} = 0$, however, this contradicts the assumption that there are P_k coherent signals impinging on the array, i.e., all the α_i are nonzero. Hence, we say $\theta_0 \notin \{\theta_i\}_{i=k1}^{kP_k}$. Recalling the previously described property of Vandermonde matrix, one further deduces that the matrix $\tilde{\mathbf{A}}_k$ has full column rank as the entries on the second row of $\tilde{\mathbf{A}}_k$ are distinct to each other, which contradicts the previous conclusion that $\tilde{\mathbf{A}}_k$ is deficient in column rank. Therefore, the initial assumption $\mathbf{A}_{c,k}\boldsymbol{\alpha}_k = \beta\mathbf{a}(\theta_0)$ does not hold, i.e., $\mathbf{A}_{c,k}\boldsymbol{\alpha}_k \neq \beta\mathbf{a}(\theta_0)$. ■

Now denote $z = e^{j\frac{2\pi d}{\lambda}\sin\theta}$, then $\mathbf{a}(z) = \left[1, z, \cdots, z^{M-1}\right]^T$. Referring to [136] a root-MUSIC polynomial can be constructed as

$$f(z) \triangleq \mathbf{a}^T(z^{-1})\mathbf{U}_n\mathbf{U}_n^H\mathbf{a}(z). \tag{5.18}$$

It follows from Proposition 1 that $f(z)$ will not go to 0 for any coherent signal DOA. Therefore, combined with (5.16), the roots of (5.18) z_i which are closest to the unit circle indicate the desired DOAs of uncorrelated sources. The DOA estimates related to the signal roots can be determined as

$$\theta_i = \arcsin\left[\frac{\lambda}{2\pi d}\arg(z_i)\right]. \tag{5.19}$$

Since $K+N_u$ singular values are much larger than the remaining ones, one can detect $K+N_u$ far-field sources using the popular source enumeration methods [139,140]. However, we will obtain the K roots associated with the K groups of the coherent signals in addition to the roots of the N_u independent signals, which means we have K false DOA estimates. If the number of independent signals is known in advance, then the DOA estimates with the N_u smallest values of $\eta_i = \left\|\mathbf{a}^H(\hat{\theta}_i)\mathbf{U}_n\right\|_F^2$, $i = 1,2,\cdots,K+N_u$, correspond to the independent signals. However, in practice, the number of independent signals may not be known *a priori*. As a consequence, it is necessary to provide a more robust criterion to identify the DOA of independent signals from the false ones. Here, we carry out independent signal enumeration inspired by second order statistic of eigenvalues (SORTE) which is a cluster enumeration strategy [148]. Suppose the values of η_i are sorted decreasingly:

$$\eta_1 \geq \eta_2 \geq \cdots \geq \eta_K > \eta_{K+1} = \cdots = \eta_{K+N_u}. \tag{5.20}$$

To detect the number of independent signals, we define a gap measure:

$$\text{SORTE}\,(k) = \begin{cases} \dfrac{\text{var}\left(\{\nabla\eta_i\}_{i=k+1}^{K+N_u-1}\right)}{\text{var}\left(\{\nabla\eta_i\}_{i=k}^{K+N_u-1}\right)}, & \text{var}\left(\{\nabla\eta_i\}_{i=k}^{K+N_u-1}\right) \neq 0 \\ +\infty, & \text{var}\left(\{\nabla\eta_i\}_{i=k}^{K+N_u-1}\right) = 0 \end{cases} \tag{5.21}$$

where $k = 1,2,\cdots,K+N_u-2$, $\nabla\eta_i = \eta_i - \eta_{i+1}$, and $\text{var}\left(\{\nabla\eta_i\}_{i=k}^{K+N_u-1}\right) = \frac{1}{K+N_u-k}$ $\times \sum_{i=k}^{K+N_u-1}\left(\nabla\eta_i - \frac{1}{K+N_u-k}\sum_{l=k}^{K+N_u-1}\nabla\eta_l\right)^2$. Then the number of independent signal is $\hat{N}_u = K + N_u - \arg\min_k \text{SORTE}\,(k)$.

Remark 1. It can be seen that the proposed method utilises root-MUSIC to classify coherency, and polynomial rooting is adopted for the sake of computational efficiency, which avoids spectrum calculation and peak searching. Unlike our approach, the authors in [49] partition the whole array into three overlapping subarrays, use ESPRIT to obtain $N_u + K$ DOA estimates, then use a pair matching method to sift the DOA estimates of independent sources. Since that scheme requires an extra subarray, there is a loss of one DOF and reduced array aperture, resulting in a larger DOA estimation error and resolution compared to our technique, especially at low SNRs or limited

snapshots. Additionally, since the source enumeration method presented above can distinguish the number of of independent signals from the coherent ones, it is applicable to the case without such *a priori* information which FSDS is not valid for.

5.4.2 Stage 2: DOA Estimation of the Coherent Signals

Next we will deal with the coherent signals. The coherent signal DOAs are estimated by first removing the independent signals from the the FOC matrix $\mathbf{C}_x$ and then resolving the coherent signals using a novel matrix reconstruction technique for rank restoration. In this way, the proposed method classifies the signal types and provides improved estimation accuracy. The first step in removing the independent signals is estimating their contributions, $\{\bar{\gamma}_i\}_{i=1}^{N_u}$, to the cumulant matrix.

Performing the compact SVD of $\bar{\mathbf{A}}$, we have

$$\bar{\mathbf{A}} = \sum_{k=1}^{K+N_u} \eta_k \mathbf{u}_k \mathbf{v}_k^H \tag{5.22}$$

where $\{\eta_k\}_{k=1}^{K+N_u}, \{\mathbf{u}_k\}_{k=1}^{K+N_u}, \{\mathbf{v}_k\}_{k=1}^{K+N_u}$ are the non-zero singular values, left singular vectors, and right singular vectors, respectively. Accordingly, the pseudo-inverse of $\bar{\mathbf{A}}$ is

$$\bar{\mathbf{A}}^+ = \sum_{k=1}^{K+N_u} \eta_k^{-1} \mathbf{v}_k \mathbf{u}_k^H. \tag{5.23}$$

This allows us to expand the term $\mathbf{a}^H(\theta_i)\mathbf{C}_x^+\mathbf{a}(\theta_i)$ as

$$\begin{aligned} \mathbf{a}^H(\theta_i)\mathbf{C}_x^+\mathbf{a}(\theta_i) &= \mathbf{a}^H(\theta_i)\left(\bar{\mathbf{A}}^H\right)^+ \mathbf{C}_s^{-1}\bar{\mathbf{A}}^+\mathbf{a}(\theta_i) \\ &= \left(\bar{\mathbf{A}}^+\mathbf{a}(\theta_i)\right)^H \mathbf{C}_s^{-1}\bar{\mathbf{A}}^+\mathbf{a}(\theta_i) \end{aligned} \tag{5.24}$$

where we use the fact that $\mathbf{C}_x^+ = \left(\bar{\mathbf{A}}^H\right)^+ \mathbf{C}_s^{-1}\bar{\mathbf{A}}^+$ (see Appendix A.1 for proof). Note that $\bar{\mathbf{A}} = \left[\mathbf{a}(\theta_i), \mathbf{B}\right]$, $i = 1, 2, \cdots, N_u$, where $\mathbf{B}$ is the remaining part of $\bar{\mathbf{A}}$, one has $\mathbf{a}(\theta_i) = \bar{\mathbf{A}}\mathbf{e}_i$ where $\mathbf{e}_i \in \mathbb{R}^{K+N_u}$ is a column vector with 1 at the i-th entry and 0 elsewhere, then substituting back to (5.24) gives

$$\mathbf{a}^H(\theta_i)\mathbf{C}_x^+\mathbf{a}(\theta_i) = \left(\sum_{k=1}^{K+N_u} \eta_k^{-1}\mathbf{v}_k\mathbf{u}_k^H \sum_{k=1}^{K+N_u} \eta_k \mathbf{u}_k \mathbf{v}_k^H \mathbf{e}_i\right)^H \mathbf{C}_s^{-1}$$

$$\times \sum_{k=1}^{K+N_u} \eta_k^{-1} \mathbf{v}_k \mathbf{u}_k^H \sum_{k=1}^{K+N_u} \eta_k \mathbf{u}_k \mathbf{v}_k^H \mathbf{e}_i$$
$$= \mathbf{e}_i^H \mathbf{C}_s^{-1} \mathbf{e}_i$$
$$= \mathbf{e}_i^H \mathrm{diag}\{\bar{\gamma}_1^{-1}, \cdots, \bar{\gamma}_{K+N_u}^{-1}\} \mathbf{e}_i$$
$$= \bar{\gamma}_i^{-1}. \tag{5.25}$$

Therefore,

$$\bar{\gamma}_i = \frac{1}{\mathbf{a}^H(\theta_i) \mathbf{C}_x^{+} \mathbf{a}(\theta_i)}, \quad i = 1, 2, \cdots, N_u. \tag{5.26}$$

From (5.26), we define $\mathbf{C}_{su} \triangleq \mathrm{diag}\{\bar{\gamma}_1, \cdots, \bar{\gamma}_{N_u}\}$. Given $\mathbf{A}_u$ and $\mathbf{C}_{su}$, we can form a matrix $\mathbf{C}_{xc}$ as

$$\begin{aligned} \mathbf{C}_{xc} &\triangleq \mathbf{C}_x - \mathbf{A}_u \mathbf{C}_{su} \mathbf{A}_u^H \\ &= \mathbf{A}_c \mathbf{\Gamma} \mathrm{diag}\{\bar{\gamma}_{N_u+1}, \bar{\gamma}_{N_u+2}, \cdots, \bar{\gamma}_{N_u+K}\} (\mathbf{A}_c \mathbf{\Gamma})^H \\ &= \mathbf{A}_c \mathbf{\Gamma} \mathbf{C}_{sc} (\mathbf{A}_c \mathbf{\Gamma})^H. \end{aligned} \tag{5.27}$$

Clearly, $\mathbf{C}_{xc}$ only contains the information of coherent signals. Note that the FOC of coloured noise will not go to zero in practice due to a limited number of snapshots, which means that the impact of noise can be mitigated but not completely removed, so it is not negligible. For this reason, the smallest singular values $\lambda_{K+N_u+1}, \lambda_{K+N_u+2}, \cdots, \lambda_M$ in (5.14) are not identical to zero, and their contribution to the cumulants can be calculated as $\mathbf{C}_{pn} = \mathbf{U}_n \mathbf{\Sigma}_n \mathbf{V}_n^H$ where $\mathbf{\Sigma}_n = \mathrm{diag}\{\lambda_{K+N_u+1}, \lambda_{K+N_u+2}, \cdots, \lambda_M\}$. To alleviate the effect of noise on $\mathbf{C}_{xc}$, the matrix $\mathbf{C}_x$ in (5.26) and (5.27) is rectified as $\mathbf{C}_x - \mathbf{C}_{pn}$.

Remark 2. The previous method in [49] has implemented this step of eliminating the uncorrelated signal contribution from $\mathbf{C}_x$ using spatial differencing. However, part of the coherent signal information (i.e., the entries along the cross diagonal of $\mathbf{C}_x$) will be canceled out in this process as well. As a result, the performance of DOA estimation for coherent signals suffers. In contrast, our proposed method achieves the same goal through subtraction of the reconstructed cumulant matrix of uncorrelated sources from $\mathbf{C}_x$ without removing any coherent signal information.

After removing the uncorrelated source components from $\mathbf{C}_x$, the rank of the remaining coherent signals in $\mathbf{C}_{xc}$ is restored using a matrix reconstruction method. Other approaches such as in [49] typically adopt a spatial smoothing technique in this step.

Here we define a vector $\mathbf{g}_{i,r} \in \mathbb{C}^m$ as

$$\mathbf{g}_{i,r} \triangleq \begin{bmatrix} \mathbf{C}_{xc}(i, m+r-1) \\ \mathbf{C}_{xc}(i, m+r-2) \\ \vdots \\ \mathbf{C}_{xc}(i, r) \end{bmatrix}, \quad r = 1, 2, \cdots, L \tag{5.28}$$

where $L = M + 1 - m$, and construct a matrix $\mathbf{G}_{i,r} = \mathbf{g}_{i,r}\mathbf{g}_{i,r}^H$ accordingly.

Since $\mathbf{C}_{xc}$ only contains the information of coherent signals, from the received data model given in (5.7) the snapshot of coherent signals at the i-th sensor can be expressed as

$$x_{c,i}(t) = \sum_{k=1}^{K} \sum_{p=1}^{P_k} \alpha_{kp} s_k(t) e^{j\frac{2\pi(i-1)d}{\lambda}\sin\theta_{kp}}. \tag{5.29}$$

Combining with (5.9) we have

$$\begin{aligned}
\mathbf{C}_{xc}(i, m+r-n) &= \frac{1}{M}\sum_{q=1}^{M} \mathrm{cum}\{x_{c,q}(t), x_{c,q}^*(t), x_{c,i}(t), x_{c,m+r-n}^*(t)\} \\
&= \frac{1}{M}\sum_{q=1}^{M} \mathrm{cum}\left\{ \sum_{k=1}^{K}\sum_{p=1}^{P_k} \alpha_{kp} s_k(t) e^{j\frac{2\pi(q-1)d}{\lambda}\sin\theta_{kp}}, \right. \\
&\quad \sum_{k=1}^{K}\sum_{p=1}^{P_k} \alpha_{kp}^* s_k^*(t) e^{-j\frac{2\pi(q-1)d}{\lambda}\sin\theta_{kp}}, \sum_{k=1}^{K}\sum_{p=1}^{P_k} \alpha_{kp} s_k(t) e^{j\frac{2\pi(i-1)d}{\lambda}\sin\theta_{kp}}, \\
&\quad \left. \sum_{k=1}^{K}\sum_{p=1}^{P_k} \alpha_{kp}^* s_k^*(t) e^{-j\frac{2\pi(m+r-n-1)d}{\lambda}\sin\theta_{kp}} \right\} \\
&= \frac{1}{M}\sum_{q=1}^{M}\sum_{k=1}^{K}\sum_{l=1}^{P_k} \alpha_{kl} e^{j\frac{2\pi(q-1)d}{\lambda}\sin\theta_{kl}} \\
&\quad \times \sum_{u=1}^{P_k} \alpha_{ku}^* e^{-j\frac{2\pi(q-1)d}{\lambda}\sin\theta_{ku}} \sum_{v=1}^{P_k} \alpha_{kv} e^{j\frac{2\pi(i-1)d}{\lambda}\sin\theta_{kv}} \\
&\quad \times \sum_{p=1}^{P_k} \alpha_{kp}^* e^{-j\frac{2\pi(m+r-n-1)d}{\lambda}\sin\theta_{kp}} \mathrm{cum}\{s_k(t), s_k^*(t), s_k(t), s_k^*(t)\}
\end{aligned}$$

$$= \sum_{k=1}^{K}\sum_{p=1}^{P_k}\frac{1}{M}\gamma_k\alpha_{kp}^{*}e^{-j\frac{2\pi(m+r-n-1)d}{\lambda}\sin\theta_{kp}} \times \sum_{q=1}^{M}\sum_{l=1}^{P_k}\alpha_{kl}e^{j\frac{2\pi(q-1)d}{\lambda}\sin\theta_{kl}}\sum_{u=1}^{P_k}\alpha_{ku}^{*}e^{-j\frac{2\pi(q-1)d}{\lambda}\sin\theta_{ku}} \times \sum_{v=1}^{P_k}\alpha_{kv}e^{j\frac{2\pi(i-1)d}{\lambda}\sin\theta_{kv}}. \tag{5.30}$$

If we define $a_{kp} \triangleq e^{j\frac{2\pi(n-1)d}{\lambda}\sin\theta_{kp}}$, $\mathbf{d}_i \triangleq \left[d_{11}^{(i)},\cdots,d_{1P_1}^{(i)},\cdots,d_{K1}^{(i)},\cdots,d_{KP_K}^{(i)}\right]^T$ with

$$d_{kp}^{(i)} = \frac{1}{M}\gamma_k\alpha_{kp}^{*}e^{-j\frac{2\pi(m-1)d}{\lambda}\sin\theta_{kp}}\sum_{q=1}^{M}\sum_{l=1}^{P_k}\alpha_{kl}e^{j\frac{2\pi(q-1)d}{\lambda}\sin\theta_{kl}} \times \sum_{u=1}^{P_k}\alpha_{ku}^{*}e^{-j\frac{2\pi(q-1)d}{\lambda}\sin\theta_{ku}}\sum_{v=1}^{P_k}\alpha_{kv}e^{j\frac{2\pi(i-1)d}{\lambda}\sin\theta_{kv}} \tag{5.31}$$

the above equation can be rewritten in the following compact format

$$\mathbf{C}_{xc}(i,m+r-n) = \left[a_{11},\cdots,a_{1P_1},\cdots,a_{K1},\cdots,a_{KP_K}\right]\mathbf{\Phi}^{1-r}\mathbf{d}_i \tag{5.32}$$

where $\mathbf{\Phi} = \text{diag}\{e^{j\frac{2\pi d}{\lambda}\sin\theta_1}, e^{j\frac{2\pi d}{\lambda}\sin\theta_2},\cdots,e^{j\frac{2\pi d}{\lambda}\sin\theta_{N_c}}\}$. Stacking $\mathbf{C}_{xc}(i,m+r-1), \mathbf{C}_{xc}(i,m+r-2),\cdots,\mathbf{C}_{xc}(i,r)$ in a column, we obtain

$$\begin{aligned}\mathbf{g}_{i,r} &= \mathbf{F}\left[\mathbf{A}_{c,1},...,\mathbf{A}_{c,K}\right]\mathbf{\Phi}^{1-r}\mathbf{d}_i \\ &= \mathbf{B}_c\mathbf{\Phi}^{1-r}\mathbf{d}_i, \quad r=1,2,\cdots,L\end{aligned} \tag{5.33}$$

where $\mathbf{F} = \left[\mathbf{I}_{(M-L+1)}, \mathbf{0}_{(M-L+1)\times(L-1)}\right]$, $\mathbf{B}_c = \mathbf{F}\left[\mathbf{A}_{c,1}, \mathbf{A}_{c,2}, ..., \mathbf{A}_{c,K}\right]$, and further $\mathbf{G}_{i,r} = \mathbf{B}_c\mathbf{\Phi}^{1-r}\mathbf{d}_i\mathbf{d}_i^H\mathbf{\Phi}^{r-1}\mathbf{B}_c^H$. The proof of (5.33) is given in Appendix A.2.

Since $\mathbf{B}_c$ is a Vandermonde matrix, it can be readily seen that $\mathbf{J}\mathbf{B}_c^{*} = \mathbf{B}_c\mathbf{\Phi}^{1-m}$ where $\mathbf{J} \in \mathbb{R}^{m\times m}$ is an exchange matrix (see Appendix A.3 for proof). Then a new matrix from the i-th row of $\mathbf{C}_{xc}$ is constructed as

$$\begin{aligned}\bar{\mathbf{C}}_i &= \frac{1}{L}\sum_{r=1}^{L}\left(\mathbf{G}_{i,r} + \mathbf{J}\mathbf{G}_{i,r}^{*}\mathbf{J}\right) \\ &= \mathbf{B}_c\left(\frac{1}{L}\sum_{r=1}^{L}\left(\mathbf{\Phi}^{1-r}\mathbf{d}_i\mathbf{d}_i^H\mathbf{\Phi}^{r-1} + \mathbf{\Phi}^{r-m}\mathbf{d}_i^{*}\mathbf{d}_i^T\mathbf{\Phi}^{m-r}\right)\right)\mathbf{B}_c^H \\ &= \mathbf{B}_c\mathbf{D}_i\mathbf{B}_c^H\end{aligned} \tag{5.34}$$

where

$$\mathbf{D}_i = \frac{1}{L}\sum_{r=1}^{L}\left\{\mathbf{\Phi}^{1-r}\mathbf{d}_i\mathbf{d}_i^H\mathbf{\Phi}^{r-1} + \mathbf{\Phi}^{r-m}\mathbf{d}_i^*\mathbf{d}_i^T\mathbf{\Phi}^{m-r}\right\} \tag{5.35}$$

and $\mathbf{J} \in \mathbb{R}^{m\times m}$ denotes an exchange matrix that has unity entries on the cross diagonal and zeros elsewhere.

To further restore rank and smooth out the effects of noise and limited snapshots, the information of all M rows of $\mathbf{C}_{xc}$ are then utilised to construct an overall smoothed matrix $\bar{\mathbf{C}}$ which is given by

$$\bar{\mathbf{C}} = \sum_{i=1}^{M}\mathbf{B}_c\mathbf{D}_i\mathbf{B}_c^H. \tag{5.36}$$

Next we examine whether the rank of $\bar{\mathbf{C}}$ has been restored sufficiently to resolve N_c coherent signals.

Proposition 2. *When $m \geq N_c + 1$ and $2L \geq P_{max}$, $rank(\bar{\mathbf{C}}) = N_c$ for K groups of coherent signals, where $P_{max} = max\{P_1, P_2, \cdots, P_K\}$.*

Proof: As seen above, $\mathbf{B}_c \in \mathbb{C}^{m\times N_c}$ is a Vandermonde matrix. Since $m > N_c$, $\mathbf{B}_c$ must be of full column rank, i.e., $\text{rank}(\mathbf{B}_c) = N_c$. Since $\mathbf{D}_i$ can be rewritten as

$$\begin{aligned}\mathbf{D}_i &= \frac{1}{L}\left[\mathbf{\Phi}^{1-L}\mathbf{d}_i, \mathbf{\Phi}^{2-L}\mathbf{d}_i, \cdots, \mathbf{d}_i, \mathbf{\Phi}^{1-m}\mathbf{d}_i^*, \mathbf{\Phi}^{2-m}\mathbf{d}_i^*, \cdots, \mathbf{\Phi}^{L-m}\mathbf{d}_i^*\right] \\ &\quad\times\left[\mathbf{\Phi}^{1-L}\mathbf{d}_i, \mathbf{\Phi}^{2-L}\mathbf{d}_i, \cdots, \mathbf{d}_i, \mathbf{\Phi}^{1-m}\mathbf{d}_i^*, \mathbf{\Phi}^{2-m}\mathbf{d}_i^*, \cdots, \mathbf{\Phi}^{L-m}\mathbf{d}_i^*\right]^H \\ &= \frac{1}{L}\mathbf{T}_i\left[\mathbf{V}, \mathbf{HV}\right]\left[\mathbf{V}, \mathbf{HV}\right]^H\mathbf{T}_i^H\end{aligned} \tag{5.37}$$

where $\mathbf{T}_i = \text{diag}\left\{e^{j\frac{2\pi(1-L)d}{\lambda}\sin\theta_{11}}d_{11}^{(i)}, \cdots, e^{j\frac{2\pi(1-L)d}{\lambda}\sin\theta_{1P_1}}d_{1P_1}^{(i)}, \cdots, e^{j\frac{2\pi(1-L)d}{\lambda}\sin\theta_{K1}}d_{K1}^{(i)}, \cdots, e^{j\frac{2\pi(1-L)d}{\lambda}\sin\theta_{KP_K}}d_{KP_K}^{(i)}\right\}$, $\mathbf{V} = \mathbf{A}_c^T(1:L, 1:N_c)$, and $\mathbf{H} = \text{diag}\left\{\frac{d_{11}^{*(i)}}{d_{11}^{(i)}}e^{j\frac{2\pi(1-m)d}{\lambda}\sin\theta_{11}}, \cdots, \frac{d_{1P_1}^{*(i)}}{d_{1P_1}^{(i)}}e^{j\frac{2\pi(1-m)d}{\lambda}\sin\theta_{1P_1}}, \cdots, \frac{d_{K1}^{*(i)}}{d_{K1}^{(i)}}e^{j\frac{2\pi(1-m)d}{\lambda}\sin\theta_{K1}}, \cdots, \frac{d_{KP_K}^{*(i)}}{d_{KP_K}^{(i)}}e^{j\frac{2\pi(1-m)d}{\lambda}\sin\theta_{KP_K}}\right\} \triangleq \text{diag}\{h_1, h_2, \cdots, h_{N_c}\}$, it is easy to identify that $\text{rank}(\mathbf{T}_i) = \text{rank}(\mathbf{H}) = N_c, \text{rank}(\mathbf{V}) = \min(L, N_c)$. The proof of (5.37) is provided in Appendix A.4. By the same setup on Page 11 of [24], we know that $\text{rank}(\mathbf{D}_i) = \text{rank}\left(\left[\mathbf{V}, \mathbf{HV}\right]\right) = \min\{2L, N_c\} \geq P_{max}$ under the mild restriction that whenever equality holds among some of the members of the set $\{h_i\}_{i=1}^{N_c}$, the largest subset with equal entries must at most be of size L.

We know that $\mathbf{C}_{xc} = \mathbf{A}_c\mathbf{\Gamma}\mathbf{C}_{sc}(\mathbf{A}_c\mathbf{\Gamma})^H, \text{rank}(\mathbf{A}_c) = N_c, \text{rank}(\mathbf{\Gamma}) = \text{rank}(\mathbf{C}_{sc}) = K$, so $\text{rank}(\mathbf{C}_{xc}) = K$. This implies that the size of the largest collection of linearly independent rows of $\mathbf{C}_{xc}$ is K. Without loss of generality, we assume the largest collection of linearly independent rows is $\{\mathbf{C}_{xc}(i,:)\}_{i=1}^{K}$. Since the matrix $\Big[\mathbf{C}_{xc}(1,:), \mathbf{C}_{xc}(2,:), \cdots, \mathbf{C}_{xc}(K,:)\Big] = \Big[\mathbf{B}_c\mathbf{\Psi}\mathbf{d}_1, \mathbf{B}_c\mathbf{\Psi}\mathbf{d}_2, \cdots, \mathbf{B}_c\mathbf{\Psi}\mathbf{d}_K\Big] = \mathbf{B}_c\mathbf{\Psi}\Big[\mathbf{d}_1, \mathbf{d}_2, \cdots, \mathbf{d}_K\Big]$ where $\mathbf{\Psi} = \text{diag}\left\{e^{-j\frac{2\pi(M-m)d}{\lambda}\sin\theta_1}, e^{-j\frac{2\pi(M-m)d}{\lambda}\sin\theta_2}, \cdots, e^{-j\frac{2\pi(M-m)d}{\lambda}\sin\theta_{N_c}}\right\}$, the vectors $\{\mathbf{d}_i\}_{i=1}^{K}$ are linearly independent to each other, and further matrices $\{\mathbf{T}_i\}_{i=1}^{K}$ are linearly independent to each other as well.

Denote $\mathbf{W} = \Big[\mathbf{V}, \mathbf{H}\mathbf{V}\Big]$, we have

$$\sum_{i=1}^{K}\mathbf{D}_i = \frac{1}{L}\Big[\mathbf{T}_1\mathbf{W}, \mathbf{T}_2\mathbf{W}, \cdots, \mathbf{T}_K\mathbf{W}\Big]\Big[\mathbf{T}_1\mathbf{W}, \mathbf{T}_2\mathbf{W}, \cdots, \mathbf{T}_K\mathbf{W}\Big]^H. \tag{5.38}$$

As discussed above, $c_1\mathbf{T}_1 + c_2\mathbf{T}_2 + \cdots + c_K\mathbf{T}_K = \mathbf{0}$ holds if and only if $c_1 = c_2 = \cdots = c_K = 0$, and thus $(c_1\mathbf{T}_1 + c_2\mathbf{T}_2 + \cdots + c_K\mathbf{T}_K)\mathbf{W} = c_1\mathbf{T}_1\mathbf{W} + c_2\mathbf{T}_2\mathbf{W} + \cdots + c_K\mathbf{T}_K\mathbf{W} = \mathbf{0}$ under the same condition. This implies that matrices $\{\mathbf{T}_i\mathbf{W}\}_{i=1}^{K}$ are linearly independent to each other. Therefore, $\text{rank}\left(\sum_{i=1}^{K}\mathbf{D}_i\right) = \text{rank}\left(\Big[\mathbf{T}_1\mathbf{W}, \mathbf{T}_2\mathbf{W}, \cdots, \mathbf{T}_K\mathbf{W}\Big]\right) = \min\{2KL, N_c\} = N_c$. As it is known that the total number of coherent signals is N_c, the rank of the smoothed cumulant matrix $\bar{\mathbf{D}} \triangleq \sum_{i=1}^{M}\mathbf{D}_i$ can be restored up to N_c but not larger, which implies that $\text{rank}\left(\sum_{i=1}^{M}\mathbf{D}_i\right) = \text{rank}\left(\Big[\mathbf{T}_1\mathbf{W}, \mathbf{T}_2\mathbf{W}, \cdots, \mathbf{T}_M\mathbf{W}\Big]\right) = \text{rank}\left(\Big[\mathbf{T}_1\mathbf{W}, \mathbf{T}_2\mathbf{W}, \cdots, \mathbf{T}_K\mathbf{W}\Big]\right) = N_c$, i.e., each of the remaining matrices $\{\mathbf{T}_i\mathbf{W}\}_{i=K+1}^{M}$ must be a linear combination of $\{\mathbf{T}_i\mathbf{W}\}_{i=1}^{K}$.

It can be seen that $\{\mathbf{D}_i\}_{i=K+1}^{M}$ do not contribute to the rank recovery as each of the remaining matrices $\{\mathbf{T}_i\mathbf{W}\}_{i=K+1}^{M}$ can be expressed as a linear combination of $\{\mathbf{T}_i\mathbf{W}\}_{i=1}^{K}$, and consequently $\text{rank}\,(\bar{\mathbf{C}}) = \text{rank}\left(\sum_{i=1}^{M}\mathbf{D}_i\right) = N_c$. This completes the proof of Proposition 3. ■

One can subsequently follow similar procedures as discussed in Section 5.4.1 to resolve the DOA estimates of the coherent signals. Particularly, note that $\mathbf{J}\bar{\mathbf{C}}^*\mathbf{J} = \bar{\mathbf{C}}$, which means that $\bar{\mathbf{C}}$ is centro-Hermitian (see definition in Section 3.6.3), thus one can transform $\bar{\mathbf{C}}$ into the field of real numbers for the sake of computational efficiency. We define a new matrix $\mathbf{C}_T$ as

$$\mathbf{C}_T = \mathbf{Q}_m^H\bar{\mathbf{C}}\mathbf{Q}_m \tag{5.39}$$

where $\mathbf{Q}_m$ is a sparse unitary matrix given by

$$\mathbf{Q}_m = \begin{cases} \dfrac{1}{\sqrt{2}} \begin{bmatrix} \mathbf{I}_n & j\mathbf{I}_n \\ \mathbf{J}_n & -j\mathbf{J}_n \end{bmatrix}, & m = 2n \\ \dfrac{1}{\sqrt{2}} \begin{bmatrix} \mathbf{I}_n & \mathbf{0}_{n\times 1} & j\mathbf{I}_n \\ \mathbf{0}_{n\times 1}^T & \sqrt{2} & \mathbf{0}_{n\times 1}^T \\ \mathbf{J}_n & \mathbf{0}_{n\times 1} & -j\mathbf{J}_n \end{bmatrix}, & m = 2n+1. \end{cases} \tag{5.40}$$

Referring to Theorem 3 in [149], we can see that $\mathbf{C}_T$ is a real matrix. Performing the SVD of $\mathbf{C}_T$, one has

$$\mathbf{C}_T = \mathbf{U}_T \mathbf{\Sigma}_T \mathbf{V}_T^H \tag{5.41}$$

where $\mathbf{U}_T = \left[\mathbf{U}_{Ts}, \mathbf{U}_{Tn}\right] \in \mathbb{R}^{m\times m}$ is a matrix whose columns are the left singular vectors of $\mathbf{C}_T$, and $\mathbf{\Sigma}_T = \text{diag}\{\lambda_{T1}, \lambda_{T2}, \cdots, \lambda_{Tm}\}$ consists of the corresponding m singular values. The columns of $\mathbf{U}_{Ts}$ span the N_c dimensional signal subspace of $\mathbf{Q}_m\mathbf{B}_c$, while the columns of $\mathbf{U}_n$ span the noise subspace. Then the unitary root-MUSIC polynomial can be expressed as

$$f_U(z) \triangleq \tilde{\mathbf{b}}^T(z^{-1})\mathbf{U}_{Tn}\mathbf{U}_{Tn}^H\tilde{\mathbf{b}}(z) \tag{5.42}$$

where $\tilde{\mathbf{b}}(z) = \mathbf{Q}_m^H\mathbf{b}(z)$ with $\mathbf{b}(z) = \left[1, z, \cdots, z^{m-1}\right]^T$. Then the DOA estimates related to the roots $\{z_i\}_{i=1}^{N_c}$ of (5.42) can be determined by (5.18) accordingly.

Remark 3. The standard FBSS always exploits the partial information of all rows of $\mathbf{C}_{xc}$ by averaging the cumulants of the subarrays, e.g. submatrices along the main diagonal of $\mathbf{C}_{xc}$, but not utilising the cross correlations between the subarrays, e.g. upper and lower triangular parts of $\mathbf{C}_{xc}$, to resolve the coherent signals, and thus the estimation performance will be compromised to some extent [150]. In contrast, our method exploits all entries of the cumulants matrix of the coherent signals for rank restoration, which means more information has been utilised and better accuracy can be expected. Additionally, our algorithm applies a unitary transformation in conjunction with the root-MUSIC algorithm which results in real-valued computations, while the counterparts, such as FSDS, VESPA, and FBSS, employ the standard high-resolution algorithms which perform complex-valued computations, resulting in higher computational complexity [151].

5.4.3 Separable Signal Number

This section discusses the maximum number of separable signals by the proposed scheme. The independent and coherent signals are resolved separately, which makes best use of the DOFs of the original ULA and allows more signals than sensors ($N \geq M$) to be estimated, i.e., the so-called underdetermined DOA estimation problem [152, 153]. Compared with the standard FBSS which estimates the independent and coherent signals simultaneously, the maximum number of signals estimated by our method can be increased beyond the traditional limit. If $M > K + N_u$, $m > N_c$, and $2L \geq P_{max}$, we can estimate a maximum number of $M - K - 1$ independent sources plus $M - \lceil \frac{P_{max}}{2} \rceil$ coherent signals since $M \geq N_c + \lceil \frac{P_{max}}{2} \rceil$, while the FBSS can estimate at most $M - \lceil \frac{P_{max}}{2} \rceil$ mixed signals since $M \geq N_u + N_c + \lceil \frac{P_{max}}{2} \rceil$, where $\lceil \cdot \rceil$ is the ceiling operator. Although in general spatial differencing methods for separating the coherent signals from independent sources can also process more signals than array sensors, they have shortcomings in the coherent signal estimation step. First, the differencing operation will give rise to a loss of information as explained in Remark 2. Besides, extra processing procedures are required to identify and alleviate pseudo-DOA estimates which are also caused by the differencing operation [49]. A rectified smoothing technique such as FSDS can achieve the same number of coherent signals as our proposed method, but it is less accurate. Chen et al [154] used a Toeplitz matrix constructed from the cumulants matrix, referred to as CTMR, to improve the accuracy of DOA estimates no matter whether the sources are coherent or not, but at the cost of halving the DOFs and effective array aperture. In general, the loss of DOFs in CTMR outweighs the gain in accuracy. By exploiting a quite different approach, VESPA in [38, 39] achieves much better discrimination of coherent groups, which gives more DOFs for estimation with an upper limit of $M - K - 1$ uncorrelated sources plus $K\lfloor \frac{2M}{3} \rfloor$ coherent signals, where $\lfloor \cdot \rfloor$ is the flooring operator.

Table 6.1 lists the minimum number of array elements required to resolve a given number of signals by the five methods. For simplicity, we assume that each group has the

Table 5.1. Minimum number of array elements required

Indepe-ndent signals	Coherent signals		Total signals	Number of array elements				
	Groups	Signals in each group		CTMR	FBSS	FSDS	VESPA	PROPO-SED
2	1	2	4	9	5	5	4	4
2	2	2	6	13	7	6	5	5
4	1	4	8	17	10	7	6	6
4	2	2	8	17	9	8	7	7
5	3	2	11	23	12	10	9	9
3	3	3	12	25	14	11	7	11
7	2	4	15	31	17	11	10	10
3	4	4	19	39	21	18	8	18

same number of coherent signals. We can see that our method can use less array elements than most algorithms except VESPA, to estimate the same number of signals.

5.4.4 Simulation Results and Discussion

In this section, a series of numerical experiments under different conditions are conducted to examine the performance of the proposed method. Simulations are carried out for a ULA with half-wavelength spacing between adjacent elements. For simplicity, we assume that all signals, independent and coherent, have identical power. Similar to the settings in [49], the signals are modeled as $\mathbf{s}(t) = \mathbf{F}(t)\mathbf{r}(t)$, where $\mathbf{F}(t) = \text{diag}\{f_1(t), \cdots, f_N(t)\}$, $\mathbf{r}(t) = [r_1(t), \cdots, r_N(t)]^T$. $f_i(t)$ and $r_i(t)$ are zero-mean Gaussian processes with unit-variance and σ_s^2-variance, respectively. The noise is assumed to be a first order spatial autoregressive process, and the (m,n)-th entry of the noise covariance matrix is given by $\mathbf{R}(m,n) = \sigma_n^2 0.8^{|m-n|} e^{j\frac{\pi(m-n)}{16}}$ [85,90]. In order to describe the performance of the source enumeration method we developed in Section 5.4.1, the detection accuracy is defined as

$$\text{Detection accuracy} = \frac{F_d}{F} \tag{5.43}$$

where F is the number of trials, and F_r is the number of times that the number of independent signals N_u is successfully detected. The accuracy of the DOA estimates is measured from 800 Monte Carlo runs in terms of the root mean square error (RMSE) which is defined as

$$\text{RMSE} = \sqrt{\frac{1}{800N}\sum_{n=1}^{800}\sum_{i=1}^{N}(\hat{\theta}_i^{(n)} - \theta_i)^2} \tag{5.44}$$

where $\hat{\theta}_i^{(n)}$ is the estimate of θ_i for the n-th trial, and N is the number of all independent or coherent signals. Additionally, to assess the overall reliability of all the algorithms, the probability of resolution is defined as

$$\text{Probability of resolution} = \frac{F_r}{F} \tag{5.45}$$

where F_r is the number of successful estimations for which the absolute DOA estimation errors of both independent and coherent signals are within 1.5°.

Source Enumeration

In the first scenario, we consider three independent sources from $[-52^\circ, -25^\circ, 27^\circ]$ and two groups of five coherent signals from $[-13^\circ, 37^\circ]$ and $[-39^\circ, 1^\circ, 10^\circ]$, respectively, impinging on an eleven-element array. The fading amplitudes of the coherent signals are $[1, 0.8]$ and $[1, 0.7, 0.6]$, while the fading phases are $[122.16^\circ, 30.52^\circ]$ and $[326.45^\circ, 211.82^\circ, 336.19^\circ]$, respectively. In this case, suppose that this number of independent signals is unknown and we need to detect it. The detection accuracy of the proposed method using as a function of SNR or the number of snapshots are plotted in Fig. 5.1. Since both FSDS and VESPA do not provide explicit source enumeration methods, there are no counterparts for comparison. We can see that the detection accuracy of our method improves dramatically with increasing SNR or number of snapshots, and achieves a 100% successful detection above -6dB or 1900 snapshots, which means the enumeration method we developed can even work well under adverse conditions (e.g. relatively low SNRs or few snapshots) for the cumulants.

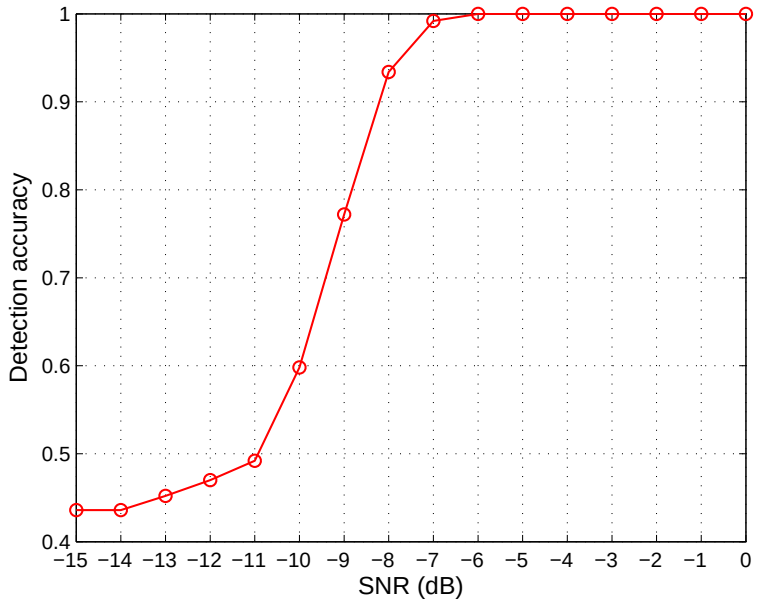

(a)

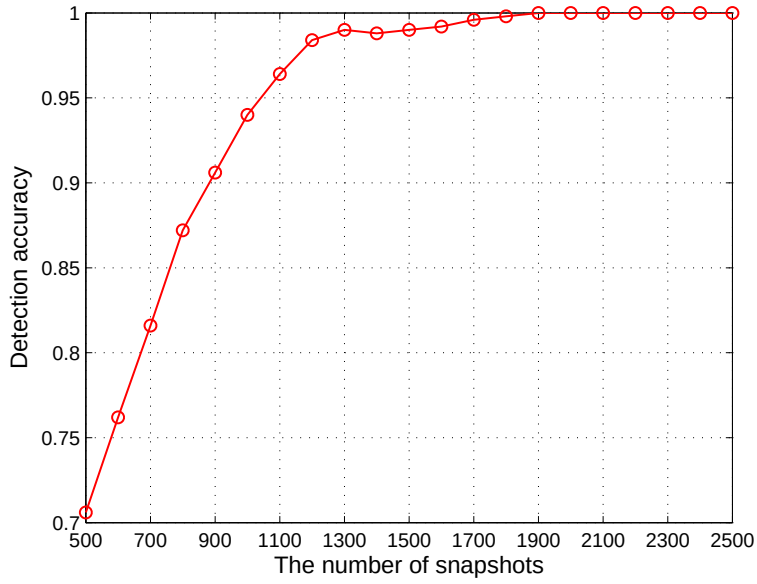

(b)

Figure 5.1. Detection accuracy versus (a) SNR when the number of snapshots is 2000; (b) the number of snapshots when SNR $= -6$dB.

Overdetermined DOA estimation

Since RMSE defined before can only be collected when the numbers of signals, both independent and coherent, are given, we assume such information is known in advance,

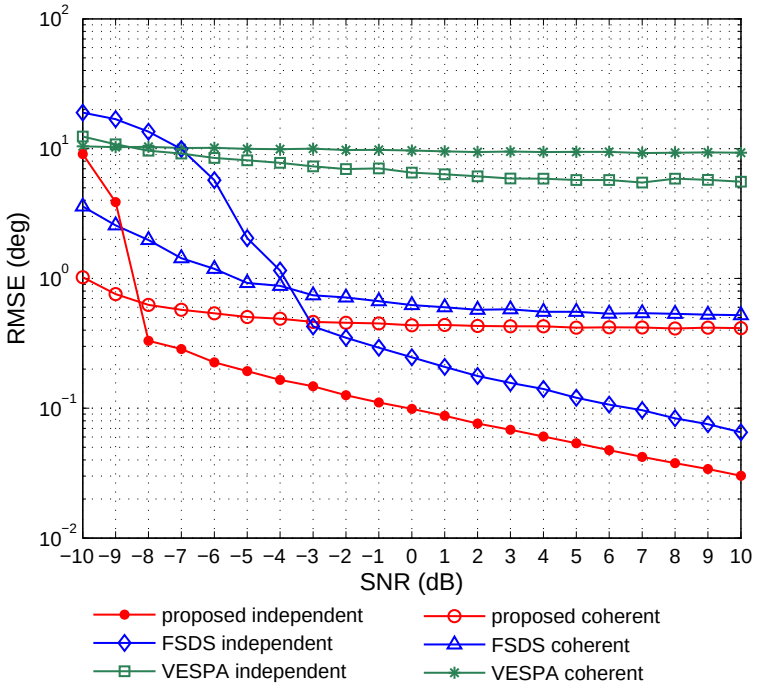

(a)

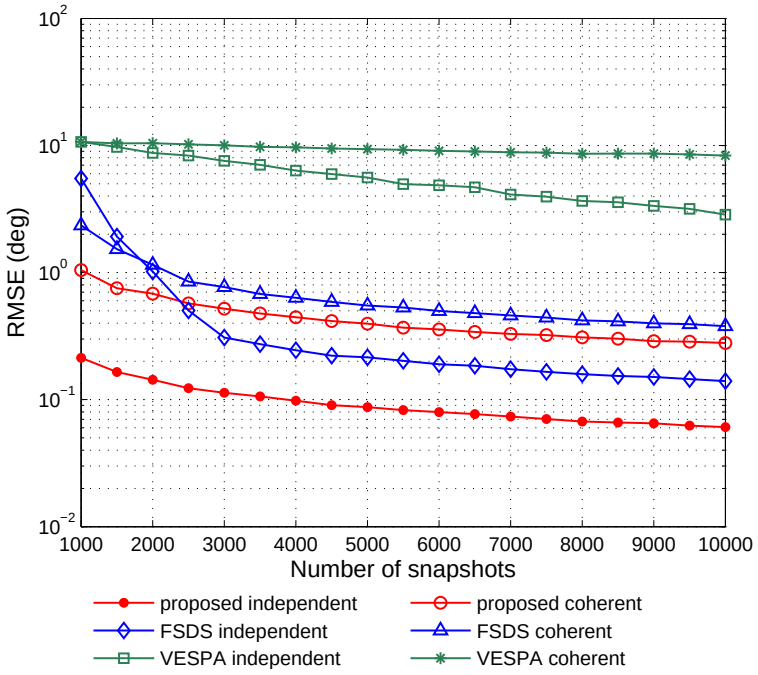

(b)

Figure 5.2. RMSE of the DOA estimates in the overdetermined case versus (a) SNR when the number of snapshots is 4000; (b) the number of snapshots when SNR = 0dB.

or the number of independent signals has been detected successfully using the proposed enumeration approach, and then the number of coherent signals is obtained by the method in [141]. We consider the same scenario as in the source enumeration simulation and select $m = 9$ for the reconstruction of $\bar{\mathbf{C}}$. FSDS and VESPA are chosen for comparison. Fig. 5.2(a) depicts the RMSE of the DOA estimates versus input SNR. The number of snapshots is fixed to 4000. From this figure, we can see that the proposed algorithm has the lowest RMSE for both independent and coherent signals, among all the algorithms for all SNRs. With an increase in SNR, the estimation accuracy of all three algorithms improves, and the RMSE of the independent signals is better than that of coherent signals except for VESPA. Although VESPA can separate coherent groups and achieve more DOFs for coherent signal estimation, its performance is not satisfactory due to the large errors introduced by using the rotational invariance property to estimate the generalised steering vector. In Fig. 5.2(b) we show the RMSE performance of all three methods when the number of snapshots increases, fixing the SNR at 0dB. It is observed that our technique is still superior to FSDS and VESPA, especially when the number of snapshots is less than 3000 for the independent signal case, whereas the performance of FSDS for coherent signal estimation approaches that of the proposed algorithm asymptotically with increasing snapshots. The remaining algorithm, VESPA, however, improves slowly with increasing snapshots and has a relatively large bias for both independent and coherent signals compared with our technique and FSDS even for a relatively large number of samples.

The results of the empirical probability of resolution versus input SNR and the number of snapshots are shown in Fig. 5.3. It can be observed that the proposed method and FSDS attain over 90% successful estimation above 5dB. As the SNR decreases, the probability of successful estimation starts dropping for each method at a certain point, known as the SNR threshold, until it eventually becomes zero. The proposed method has the lowest SNR threshold, followed by FSDS and then VESPA which has the highest SNR threshold. Even if the SNR rises to 15dB, VESPA can barely reach 10% success probability due to the big error in independent signal identification. When the SNR is fixed at 0dB, both our approach and FSDS can achieve over 90% probability above 5000 snapshots, whereas VESPA can barely reach 20% success probability even if the

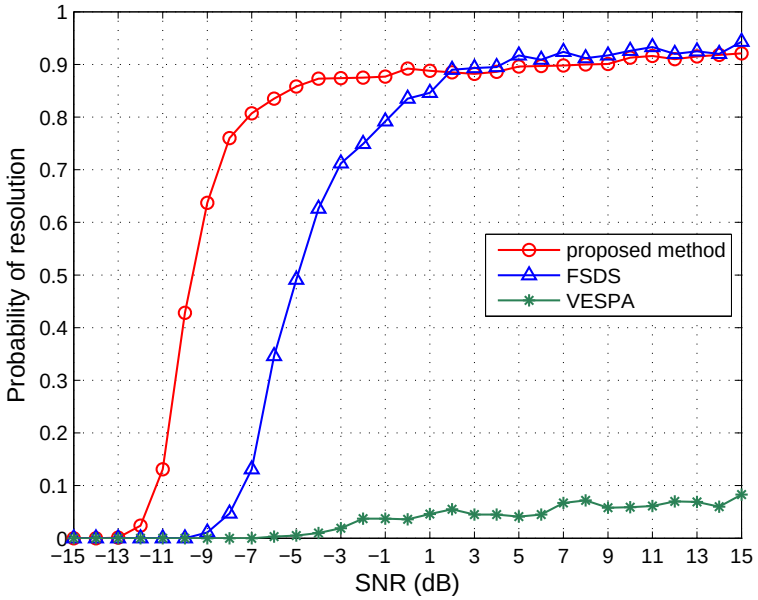

(a)

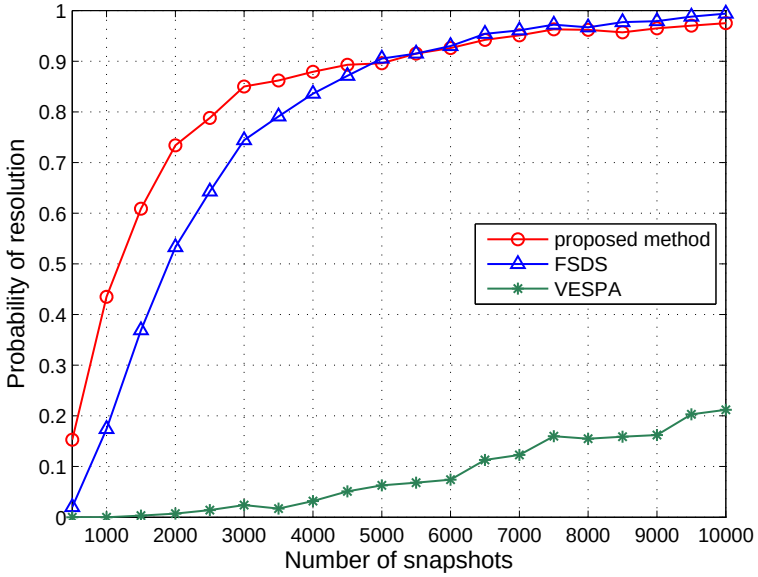

(b)

Figure 5.3. Probability of resolution of the DOA estimates in the overdetermined case versus (a) SNR when the number of snapshots is 4000; (b) the number of snapshots when SNR = 0dB.

number of snapshots is greater than 10000. The proposed method outperforms FSDS, especially at low SNRs or few snapshots, but is somewhat inferior to FSDS when the SNR or the size of snapshots is large.

Underdetermined DOA estimation

We consider six independent signals from $[-45°, -26°, -8°, 9°, 24°, 50°]$ and one group of five coherent signals from $[-53°, -33°, -1°, 15°, 41°]$ impinging on a ten-element array. The fading amplitudes and phases of the coherent signals are $[1, 0.7, 0.8, 0.9, 0.6]$ and $[245.97°, 201.89°, 47.96°, 122.01°, 294.69°]$, respectively. We select $m = 7$ in this scenario where the total number of signals exceeds the number of array elements.

Fig. 5.4 depicts the RMSE of DOA estimates in the underdetermined case. From this figure, we can see that as the SNR and the number of snapshots increase, the RMSE of DOA estimation decreases gradually for all of the methods. The proposed method is significantly superior to FSDS and VESPA, especially at low SNRs and few snapshots, mainly because the independent and coherent signals are processed separately while avoiding the elimination of partial coherent information. Although FSDS outperforms VESPA, there is a larger discrepancy between these two and the proposed method even for SNRs up to 10dB as shown in Fig. 5.4(a), compared with the first scenario.

Next, in Fig. 5.5 we plot the probability of resolution of the three methods by varying the SNR and total number of snapshots. Evidently the proposed method is superior to the counterparts for all SNRs and number of snapshots considered. Although FSDS outperforms VESPA, both have poor reliability, and there is a clear discrepancy between these two and the proposed method even for snapshot sizes up to 10000 or beyond 0dB as shown in the figure.

Effect of the Number of Cumulant Matrices

Next, we test the algorithm in the cases of different numbers of cumulant matrices, denoted as T_m. Consider an independent signal from $-30°$ and one group of three coherent signals from $[-12°, 10°, 33°]$ impinging on a six-element array. The fading amplitudes and phases of the coherent signals are $[1, 0.8, 0.4]$ and $[218.43°, 106.64°, 47.96°]$, respectively. To compare with FSDS, we select $T_m = 1, 6$ for the proposed algorithm. Fig. 5.6 shows the RMSEs for different values of T_m with respect to SNR and snapshot size, respectively. It can be found that the proposed method is superior to FSDS even though the performance improvement with $T_m = 1$ is not as significant as with $T_m = 6$.

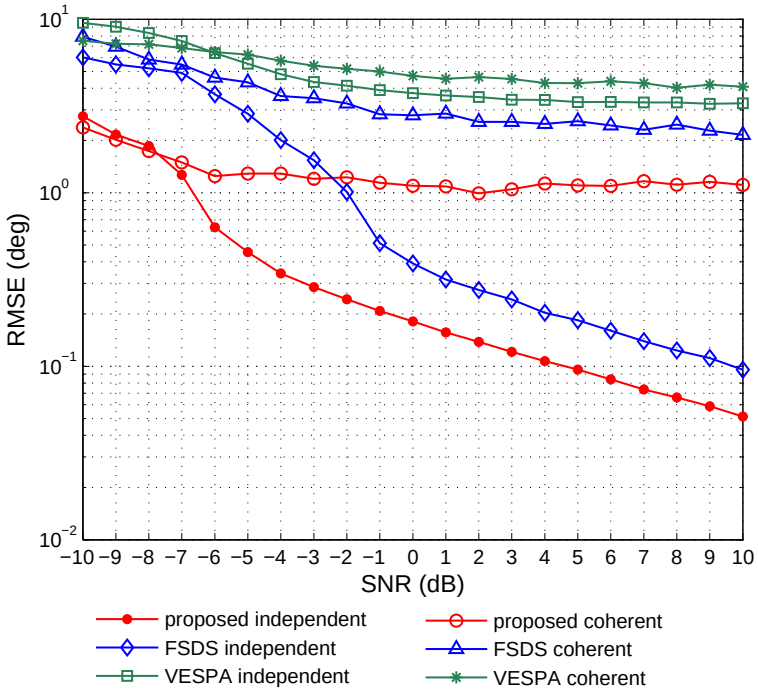

(a)

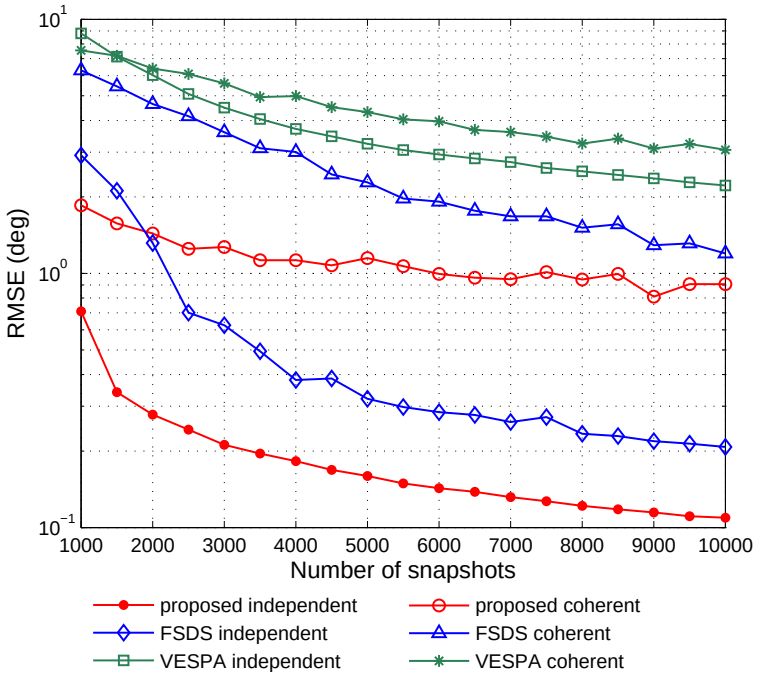

(b)

Figure 5.4. RMSE of the DOA estimates in the underdetermined case versus (a) SNR when the number of snapshots is 4000; (b) the number of snapshots when SNR = 0dB.

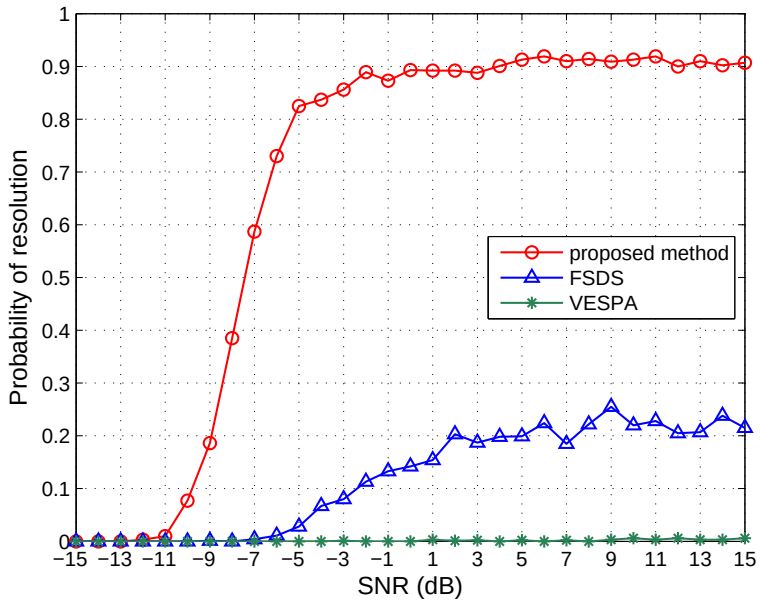

(a)

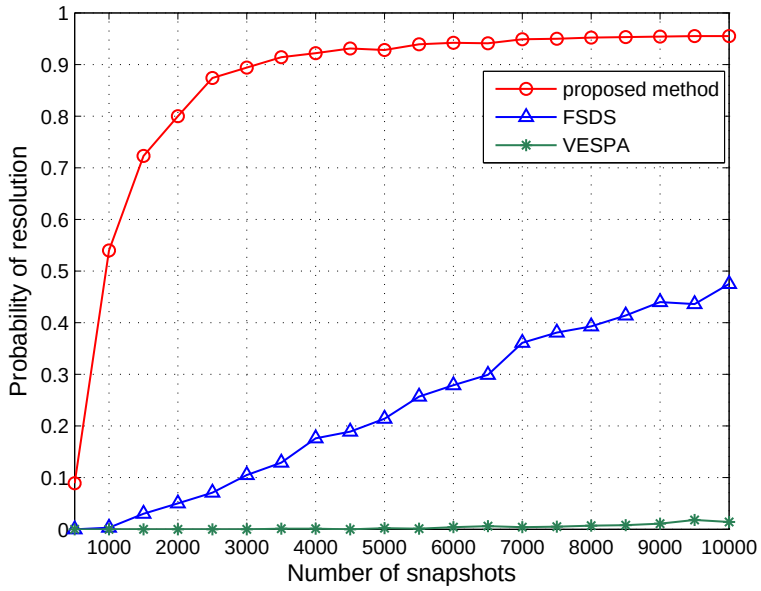

(b)

Figure 5.5. Probability of resolution of the DOA estimates in the underdetermined case versus (a) SNR when the number of snapshots is 4000; (b) the number of snapshots when SNR = 0dB.

It is also worth mentioning that exploiting more cumulant matrices has a clear advantage on coherent signal estimation, compared with independent signal estimation.

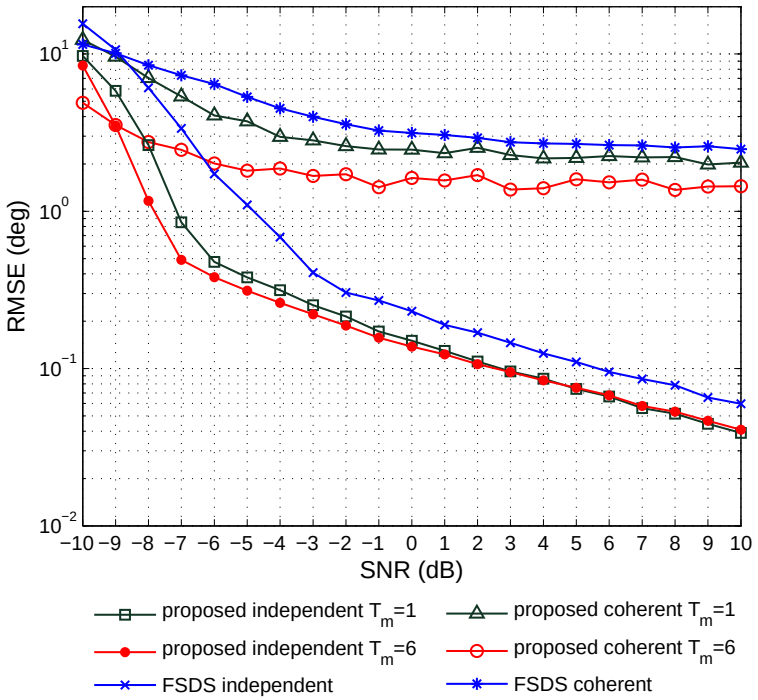

(a)

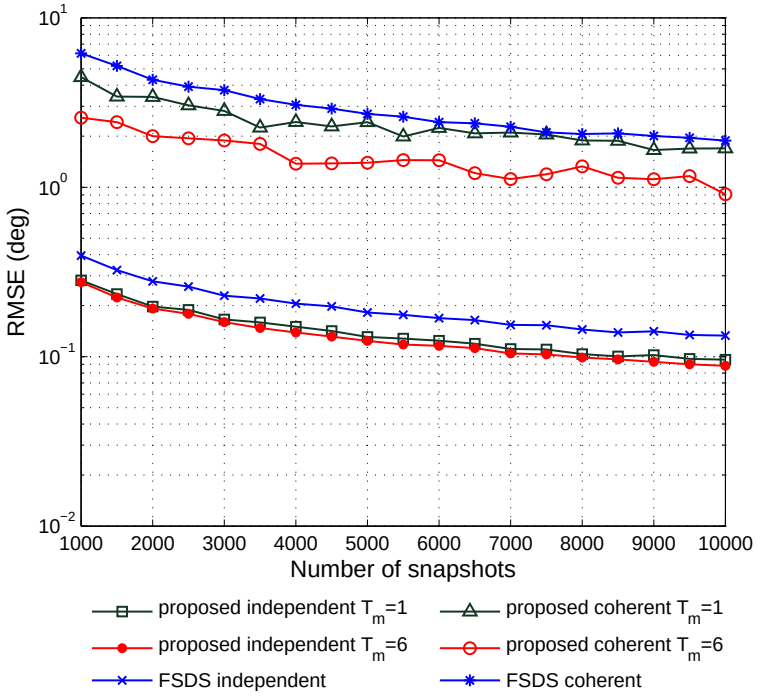

(b)

Figure 5.6. RMSE of the DOA estimates for T_m versus (a) SNR when the number of snapshots is 4000; (b) the number of snapshots when SNR = 0dB.

Effect of the Small Snapshot Sizes

Finally, we investigate the effect of the the small snapshot sizes, say several hundreds, on the proposed approach. We consider the same scenario as in the effect of the number of cumulant matrices. The resulting RMSEs versus SNR and the number of snapshots are exhibited respectively in Fig. 5.6. As expected, the performances of all three methods, i.e, the proposed one, FSDS, and VESPA, are very poor except that our method can achieve satisfactory accuracy with respect to the DOA estimation of independent signals. This is mainly due to the fact that fourth order statistics require a relatively large number of snapshots to "cumulate", otherwise it cannot suppress the unknown coloured noise, and the signal kurtosis is not large enough to the noise level either. As this effect has been known to signal processing society, we will not consider the case of the small snapshot sizes when discussing FOC hereafter.

5.5 DOA Estimation in the Presence of Multipath with Fewer Sensors

Employing the proposed two-stage processing technique, one can improve the DOFs and resolve more signals than the number of sensors, provided that the mixed model is valid, i.e., uncorrelated and coherent signals coexist. Note that all the coherent signals are still resolved by our method simultaneously, which implies that no improvement of DOFs for coherent signal has been achieved. As reviewed in Section 2.2.1, Mendel et al suggested that the scaled generalised array manifold (i.e., the product of original array manifold and fading coefficient matrix) can be obtained by using the rotational invariance between signal subspaces of two cumulant matrices, and then the standard FBSS can be applied to each Hermitian matrix constructed by the resulting generalised steering vectors to restore the rank deficiency. This algorithm, VESPA, can estimate more signals than our two-stage approach since the generalised manifold inherently separates coherent signals into different groups which can then be dealt with individually.

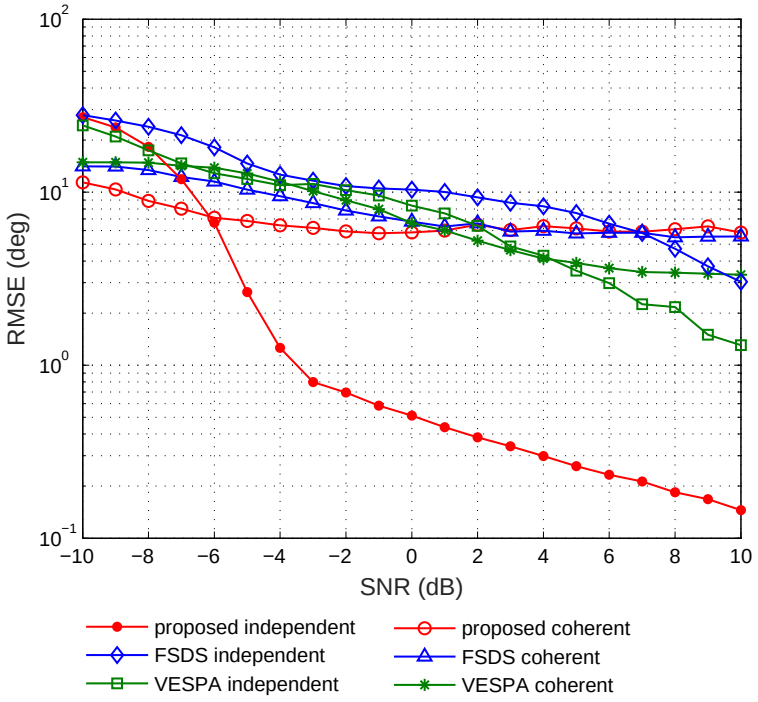

(a)

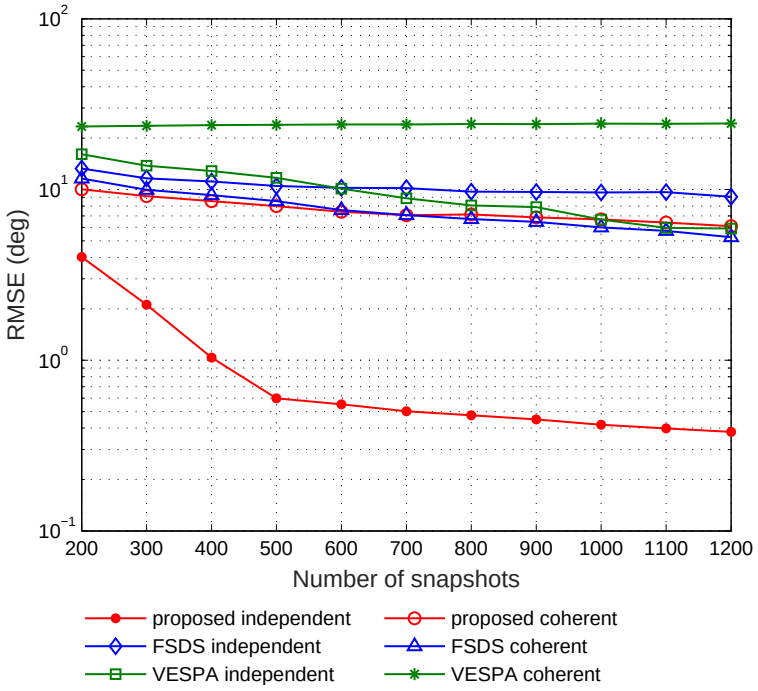

(b)

Figure 5.7. RMSE of the DOA estimates versus in the case of the small snapshot sizes (a) SNR when the number of snapshots is 700; (b) the number of snapshots when SNR = 0dB.

In this section, we consider how temporal correlation can be incorporated into the framework proposed in VESPA by forming space-time cumulant matrices, and then separating coherent groups through a more robust rotation invariance between the signal subspaces of the cumulant matrices. To demonstrate the utility of this technique, continuous wave (CW) signals are adopted as they are fully correlated in time domain. In practice, narrowband signals whose bandwidths (to sampling rate) are less than the inverse of the snapshot length can be used.

5.5.1 Space-time Cumulant Matrix

We utilise the same signal model as Section 5.3, but without loss of generality, here we only consider K groups of multiple coherent signals (independent signals can be regarded as coherent groups each of which only include one signal). Let the coherent signal arising from the k-th direct path be denoted as $s_{kp}(t) = \alpha_{kp} s_k(t) = \alpha_{kp} A_k e^{j(\omega_c+\omega_k)t}$, where ω_c is the carrier frequency, ω_k is a small frequency offset for the k-th signal with $\omega_k \ll \omega_c$, A_k is the amplitude of the k-th signal, and α_{kp} is the fading coefficient of the kp-th multipath channel [155]. After demodulation to IF, the coherent signal due to the k-th source becomes $s_{kp}(t) = \alpha_{kp} A_k e^{j\omega_k t}$. We assume that source signals (direct paths) are mutually independent, the noises are spatially coloured and temporally white to each other, and also statistically independent to the signals.

For an array with M physical sensors, the cross-correlation functions $\mathbf{R}_{x_m x_1}(\tau)$ between signal outputs $\{x_m(t)\}_{m=1}^{M}$ and $x_1(t)$ can be expressed as

$$\begin{aligned} R_{x_m x_1}(\tau) &= E_t\left[x_m\left(t+\frac{\tau}{2}\right) x_1^*\left(t-\frac{\tau}{2}\right)\right] \\ &= E_t\left[\left(\sum_{k=1}^{K}\sum_{p=1}^{P_k} \alpha_{kp} e^{j\frac{2\pi(m-1)d}{\lambda}\sin\theta_{kp}} s_k\left(t+\frac{\tau}{2}\right) + n_m\left(t+\frac{\tau}{2}\right)\right)\right. \\ &\quad \left.\times\left(\sum_{k=1}^{K}\sum_{p=1}^{P_k} \alpha_{kp}^* s_k^*\left(t-\frac{\tau}{2}\right) + n_1^*\left(t-\frac{\tau}{2}\right)\right)\right] \\ &= \sum_{k=1}^{K}\sum_{l=1}^{P_k} \alpha_{kl}^* R_{s_k s_k}(\tau) \sum_{p=1}^{P_k} \alpha_{kp} e^{j\frac{2\pi(m-1)d}{\lambda}\sin\theta_{kp}} + R_{n_m n_1}(\tau). \end{aligned} \tag{5.46}$$

The auto-correlation function in (5.46) can be evaluated as

$$\begin{aligned} R_{s_k s_k}(\tau) &= E_t\left[s_k\left(t+\frac{\tau}{2}\right)s_k^*\left(t-\frac{\tau}{2}\right)\right] \\ &= E_t\left[A_k e^{j\omega_k\left(t+\frac{\tau}{2}\right)}A_k e^{-j\omega_k\left(t-\frac{\tau}{2}\right)}\right] \\ &= A_k^2 e^{j\omega_k\tau} \end{aligned} \tag{5.47}$$

and is found to have the same form as the source signals. The second term in (5.46) is evaluated as

$$\begin{aligned} R_{n_m n_1}(\tau) &= E_t\left[n_m\left(t+\frac{\tau}{2}\right)n_1^*\left(t-\frac{\tau}{2}\right)\right] \\ &= \sigma_n^2\delta(\tau)\delta(m-1). \end{aligned} \tag{5.48}$$

Stacking $R_{x_1x_1}(\tau), R_{x_2x_1}(\tau), \cdots, R_{x_Mx_1}(\tau)$ in a column, one obtain

$$\begin{aligned} \mathbf{R}_x(\tau) &= \left[R_{x_1x_1}(\tau), R_{x_2x_1}(\tau), \cdots, R_{x_Mx_1}(\tau)\right]^T \\ &= \mathbf{A}\boldsymbol{\Gamma}\mathbf{R}_s(\tau) + \left[R_{n_1n_1}(\tau), R_{n_2n_1}(\tau), \cdots, R_{n_Mn_1}(\tau)\right]^T \\ &= \overline{\mathbf{A}}\mathbf{R}_s(\tau) + \mathbf{R}_n(\tau) \end{aligned} \tag{5.49}$$

where $\overline{\mathbf{A}} = \mathbf{A}\boldsymbol{\Gamma} = [\bar{\mathbf{a}}_1, \cdots, \bar{\mathbf{a}}_K]$ is the generlised array manifold, $\mathbf{A} = [\mathbf{A}_1, \cdots, \mathbf{A}_K]$ with $\mathbf{A}_k = \left[\mathbf{a}(\theta_{k1}), \cdots, \mathbf{a}(\theta_{kP_k})\right]$, $\boldsymbol{\Gamma}$ is the fading coefficient matrix, and $\mathbf{R}_s(\tau) = [R_{s_1s_1}(\tau), R_{s_2s_2}(\tau), \cdots, R_{s_Ks_K}(\tau)]^T$.

Following the approach in [156], we form the pseudo-data matrix of $\mathbf{R}_x(\tau)$ for different lags

$$\begin{aligned} \overline{\mathbf{R}} &= \left[\mathbf{R}_x\left(-L_pT_s\right), \mathbf{R}_x\left(-\left(L_p-1\right)T_s\right), \cdots, \mathbf{R}_x\left(L_pT_s\right)\right] \\ &= \overline{\mathbf{A}}\left[\mathbf{R}_s\left(-L_pT_s\right), \mathbf{R}_s\left(-\left(L_p-1\right)T_s\right), \cdots, \mathbf{R}_s\left(L_pT_s\right)\right] \\ &\quad + \left[\mathbf{R}_n\left(-L_pT_s\right), \mathbf{R}_n\left(-\left(L_p-1\right)T_s\right), \cdots, \mathbf{R}_n\left(L_pT_s\right)\right] \\ &= \overline{\mathbf{A}}\mathbf{R}_s + \mathbf{R}_n \end{aligned} \tag{5.50}$$

where T_s is the pseudo sampling period. Clearly, $\overline{\mathbf{R}} \in \mathbb{C}^{M\times(2L_p+1)}$ contains $2L_p+1$ pseudo snapshots.

Next we proceed to the estimation of generalised steering vectors. To this end, the cumulant matrix is constructed by averaging over pseudo snapshots as

$$\begin{aligned}\mathbf{C}_1 &\triangleq \text{cum}\left\{\bar{r}_1(t), \bar{r}_1^*(t), \overline{\mathbf{R}}(t), \overline{\mathbf{R}}^H(t)\right\} \\ &= \text{cum}\left\{\overline{\mathbf{A}}(1,:)\mathbf{R}_s(t), \left(\overline{\mathbf{A}}(1,:)\mathbf{R}_s(t)\right)^*, \overline{\mathbf{A}}\mathbf{R}_s(t), \left(\overline{\mathbf{A}}\mathbf{R}_s(t)\right)^H\right\} \\ &\quad + \text{cum}\left\{r_{n,1}(t), r_{n,1}^*(t), \mathbf{R}_n(t), \mathbf{R}_n^H(t)\right\} \end{aligned} \tag{5.51}$$

where t denotes the index of pseudo snapshots, $t = -L_pT_s, -\left(L_p-1\right)T_s, \cdots, L_pT_s$, $\bar{r}_1(t)$ and $r_{n,1}(t)$ are the first entries of $\overline{\mathbf{R}}(t)$ and $\mathbf{R}_n(t)$, respectively.

It is well known that the product of Gaussian probability density functions (PDFs) are also Gaussian functions [157], so the second term in the above equation is a zero matrix by the property of cumulants [CP4]. Substituting $\sum_{i=1}^{K}\bar{\mathbf{a}}_i r_{s,i}(t)$ for $\overline{\mathbf{A}}\mathbf{R}_s(t)$ and by applying the properties of cumulants [CP1]-[CP3] in the Section 5.2, (5.51) can be rewritten as

$$\begin{aligned}\mathbf{C}_1 &= \text{cum}\left\{\sum_{p=1}^{K}\overline{\mathbf{A}}(1,p)r_{s,p}(t), \sum_{q=1}^{K}\overline{\mathbf{A}}^*(1,q)r_{s,q}^*(t),\right. \\ &\quad \left.\sum_{m=1}^{K}\bar{\mathbf{a}}_m r_{s,m}(t), \sum_{n=1}^{K}\bar{\mathbf{a}}_n^H r_{s,n}^*(t)\right\} \\ &= \sum_{p=1}^{K}\sum_{q=1}^{K}\sum_{m=1}^{K}\sum_{n=1}^{K}\overline{\mathbf{A}}(1,p)\overline{\mathbf{A}}^*(1,q)\bar{\mathbf{a}}_m\bar{\mathbf{a}}_n^H\text{cum}\{r_{s,p}(t), \\ &\quad r_{s,q}^*(t), r_{s,m}(t), r_{s,n}^*(t)\} \\ &= \sum_{k=1}^{K}|\overline{\mathbf{A}}(1,k)|^2\bar{\mathbf{a}}_k\bar{\mathbf{a}}_k^H\text{cum}\{r_{s,k}(t), r_{s,k}^*(t), r_{s,k}(t), r_{s,k}^*(t)\} \\ &= \sum_{k=1}^{K}\gamma_k|\overline{\mathbf{A}}(1,k)|^2\bar{\mathbf{a}}_k\bar{\mathbf{a}}_k^H = \overline{\mathbf{A}}\mathbf{C}_s\overline{\mathbf{A}}^H \end{aligned} \tag{5.52}$$

where $\gamma_k \triangleq \text{cum}\left\{r_{s,p}(t), r_{s,q}^*(t), r_{s,m}(t), r_{s,n}^*(t)\right\}$ and $\mathbf{C}_s = \text{diag}\left\{\gamma_1|\bar{\mathbf{A}}(1,1)|^2, \cdots, \gamma_K|\bar{\mathbf{A}}(1,K)|^2\right\}$.

Proceeding similarly, another three cumulant matrices are given as follows:

$$\begin{aligned}\mathbf{C}_2 &\triangleq \text{cum}\left\{\bar{r}_2(t), \bar{r}_1^*(t), \overline{\mathbf{R}}(t), \overline{\mathbf{R}}^H(t)\right\} \\ &= \sum_{k=1}^{K}\gamma_k\overline{\mathbf{A}}(2,k)\overline{\mathbf{A}}^*(1,k)\bar{\mathbf{a}}_k\bar{\mathbf{a}}_k^H \end{aligned}$$

$$= \overline{\mathbf{A}}\mathbf{D}_1\mathbf{C}_s\overline{\mathbf{A}}^H \tag{5.53}$$

$$\begin{aligned}\mathbf{C}_3 &\triangleq \text{cum}\left\{\bar{r}_1(t), \bar{r}_2^*(t), \overline{\mathbf{R}}(t), \overline{\mathbf{R}}^H(t)\right\} \\ &= \sum_{k=1}^{K} \gamma_k \overline{\mathbf{A}}(1,k)\overline{\mathbf{A}}^*(2,k)\bar{\mathbf{a}}_k\bar{\mathbf{a}}_k^H \\ &= \overline{\mathbf{A}}\mathbf{D}_2\mathbf{C}_s\overline{\mathbf{A}}^H \end{aligned} \tag{5.54}$$

$$\begin{aligned}\mathbf{C}_4 &\triangleq \text{cum}\left\{\bar{r}_2(t), \bar{r}_2^*(t), \overline{\mathbf{R}}(t), \overline{\mathbf{R}}^H(t)\right\} \\ &= \sum_{k=1}^{K} \gamma_k |\overline{\mathbf{A}}(2,k)|^2 \bar{\mathbf{a}}_k\bar{\mathbf{a}}_k^H \\ &= \overline{\mathbf{A}}\mathbf{D}_3\mathbf{C}_s\overline{\mathbf{A}}^H \end{aligned} \tag{5.55}$$

where $\mathbf{D}_1 = \text{diag}\left\{\frac{\overline{\mathbf{A}}(2,1)}{\overline{\mathbf{A}}(1,1)}, \cdots, \frac{\overline{\mathbf{A}}(2,K)}{\overline{\mathbf{A}}(1,K)}\right\}$, $\mathbf{D}_2 = \text{diag}\left\{\frac{\overline{\mathbf{A}}^*(2,1)}{\overline{\mathbf{A}}^*(1,1)}, \cdots, \frac{\overline{\mathbf{A}}^*(2,K)}{\overline{\mathbf{A}}^*(1,K)}\right\}$, and $\mathbf{D}_3 = \text{diag}\left\{\left|\frac{\overline{\mathbf{A}}(2,1)}{\overline{\mathbf{A}}(1,1)}\right|^2, \cdots, \left|\frac{\overline{\mathbf{A}}(2,K)}{\overline{\mathbf{A}}(1,K)}\right|^2\right\}$.

From (5.52), (5.53), (5.54), (5.55), one can form two augmented matrices, say

$$\begin{aligned}\widetilde{\mathbf{C}}_1 &\triangleq \begin{bmatrix}\mathbf{C}_1 \\ \mathbf{C}_3\end{bmatrix} \\ &= \begin{bmatrix}\overline{\mathbf{A}} \\ \overline{\mathbf{A}}\mathbf{D}_2\end{bmatrix}\mathbf{C}_s\overline{\mathbf{A}}^H \end{aligned} \tag{5.56}$$

$$\begin{aligned}\widetilde{\mathbf{C}}_2 &\triangleq \begin{bmatrix}\mathbf{C}_2 \\ \mathbf{C}_4\end{bmatrix} \\ &= \begin{bmatrix}\overline{\mathbf{A}} \\ \overline{\mathbf{A}}\mathbf{D}_2\end{bmatrix}\mathbf{D}_1\mathbf{C}_s\overline{\mathbf{A}}^H. \end{aligned} \tag{5.57}$$

Now, consider the matrix pencil [158]

$$\widetilde{\mathbf{C}}_2 - \lambda\widetilde{\mathbf{C}}_1 = \begin{bmatrix}\overline{\mathbf{A}} \\ \overline{\mathbf{A}}\mathbf{D}_2\end{bmatrix}(\mathbf{D}_1 - \lambda\mathbf{I})\,\mathbf{C}_s\overline{\mathbf{A}}^H \tag{5.58}$$

where $\mathbf{I} \in \mathbb{R}^{K\times K}$ is the identity matrix. One can show that rank $\left\{\widetilde{\mathbf{C}}_2 - \lambda\widetilde{\mathbf{C}}_1\right\} = K$, provided that $K \leq M$. However, if $\lambda = \frac{\overline{\mathbf{A}}(2,k)}{\overline{\mathbf{A}}(1,k)}, k = 1, 2, \cdots, K$, the k-th row of $\mathbf{D}_1 - \lambda\mathbf{I}$ is zero (see Appendix A.5 for proof), then rank $\left\{\widetilde{\mathbf{C}}_2 - \lambda\widetilde{\mathbf{C}}_1\right\} = K - 1$. Therefore,

the diagonal entry $\frac{\overline{\mathbf{A}}^*(2,k)}{\overline{\mathbf{A}}^*(1,k)}$ can be found as the generalised singular value of the matrix pair $\{\widetilde{\mathbf{C}}_1, \widetilde{\mathbf{C}}_2\}$. The solution to the problem is simplified to the standard eigen-decomposition problem, i.e., $\frac{\overline{\mathbf{A}}(2,k)}{\overline{\mathbf{A}}(1,k)}$ is the eigenvalue of $\widetilde{\mathbf{C}}_1^+ \widetilde{\mathbf{C}}_2$.

From the eigen-decomposition $\widetilde{\mathbf{C}}_1^+ \widetilde{\mathbf{C}}_2 = \mathbf{U}\mathbf{D}_1\mathbf{U}^H$ where the columns of $\mathbf{U}$ are the eigenvectors corresponding to the eigenvalues in $\mathbf{D}_2$, one has

$$\widetilde{\mathbf{C}}_2\mathbf{U} = \widetilde{\mathbf{C}}_1\mathbf{U}\mathbf{D}_1. \tag{5.59}$$

Considering (5.56) and (5.57), it follows that $\mathbf{U} = \left(\mathbf{C}_s\overline{\mathbf{A}}^H\right)^+ \mathbf{Z}^{-1}$, where $\mathbf{Z}$ is an arbitrary diagonal matrix with nonzero entries. Therefore, multiplying (5.56) and (5.57) by $\mathbf{U}$ and $\mathbf{U}\mathbf{D}_1^{-1}$, one finds that

$$\widetilde{\mathbf{C}}_1\mathbf{U} = \begin{bmatrix} \overline{\mathbf{A}} \\ \overline{\mathbf{A}}\mathbf{D}_2 \end{bmatrix} \mathbf{Z}^{-1} \triangleq \begin{bmatrix} \mathbf{F}_{11} \\ \mathbf{F}_{12} \end{bmatrix} \tag{5.60}$$

$$\widetilde{\mathbf{C}}_2\mathbf{U}\mathbf{D}_1^{-1} = \begin{bmatrix} \overline{\mathbf{A}} \\ \overline{\mathbf{A}}\mathbf{D}_2 \end{bmatrix} \mathbf{Z}^{-1} \triangleq \begin{bmatrix} \mathbf{F}_{21} \\ \mathbf{F}_{22} \end{bmatrix}. \tag{5.61}$$

Finally, an improved estimate of $\overline{\mathbf{A}}$ is obtained by averaging these results as

$$\overline{\mathbf{A}}\mathbf{Z}^{-1} = \frac{1}{2}\left(\mathbf{F}_{11} + \mathbf{F}_{21}\right). \tag{5.62}$$

Note that $\mathbf{Z}$ is a diagonal matrix, $\overline{\mathbf{A}}\mathbf{Z}^{-1}$ has scaled column vectors as in $\overline{\mathbf{A}}$. By denoting $\overline{\mathbf{A}}\mathbf{Z}^{-1} = [\mathbf{b}_1, \cdots, \mathbf{b}_K]$, it is readily seen that the column vector $\mathbf{b}_k = z_k^{-1}\bar{\mathbf{a}}_k = z_k^{-1}\mathbf{A}_k\boldsymbol{\alpha}_k, k = 1, \cdots, K$, where z_k is the k-th diagonal entry of $\mathbf{Z}$. Once one has the estimate of $\mathbf{b}_k$, exactly following the same procedure in [39], FBSS can be applied to a Hermitian matrix constructed from $\mathbf{b}_k$ as follows

$$\begin{aligned} \overline{\mathbf{C}}_k &= \frac{1}{2q}\sum_{i=1}^{q}\left[\boldsymbol{\Pi}_i\mathbf{b}_k\mathbf{b}_k^H\boldsymbol{\Pi}_i^H + \mathbf{J}\left(\boldsymbol{\Pi}_i\mathbf{b}_k\mathbf{b}_k^H\boldsymbol{\Pi}_i^H\right)^*\mathbf{J}\right] \\ &= \boldsymbol{\Pi}_1\mathbf{A}_k\left[\frac{1}{2q|z_k|}\sum_{i=1}^{q}\left(\boldsymbol{\Phi}^{i-1}\boldsymbol{\alpha}\boldsymbol{\alpha}^H\boldsymbol{\Phi}^{1-i} + \boldsymbol{\Phi}^{2-m-i}\boldsymbol{\alpha}^*\boldsymbol{\alpha}^T\boldsymbol{\Phi}^{i+m-2}\right)\right]\mathbf{A}_k^H\boldsymbol{\Pi}_1^H \end{aligned} \tag{5.63}$$

where $\boldsymbol{\Pi}_i = \left[\mathbf{0}_{m\times(i-1)}, \mathbf{I}_m, \mathbf{0}_{m\times(q-i)}\right]$ with $q = M+1-m$, and $\mathbf{J} \in \mathbb{R}^{m\times m}$ is the exchange matrix.

It has been shown that rank $\{\overline{\mathbf{C}}_k\} = P_k$, provided that $m \geq P_k + 1$ and $2q \geq P_k$ [39]. As proved in [24], up to $\lfloor \frac{2M}{3} \rfloor$ coherent signals in the k-th group can be resolved. Therefore, considering at most $M-1$ coherent groups can be separated, it is possible to estimate a maximum of $(M-1)\lfloor \frac{2M}{3} \rfloor$ signals.

To reduce the computational load, one can make use of $\mathbf{J}\overline{\mathbf{C}}_k^*\mathbf{J} = \overline{\mathbf{C}}_k$, where $\overline{\mathbf{C}}_k$ is the centro-Hermitian matrix, to define a new matrix $\mathbf{T}_k$ as

$$\mathbf{T}_k = \mathbf{Q}_m^H \overline{\mathbf{C}}_k \mathbf{Q}_m \tag{5.64}$$

where $\mathbf{Q}_m$ is defined in (5.40). Referring to Theorem 3 in [149], $\mathbf{T}_k$ is a real matrix, and thus one can resort to unitary ESPRIT [138] to resolve the DOA estimates of the coherent signals.

5.5.2 Computational Complexity

We compare the major computations of FBSS, VESPA and STFOC, which involve in the fourth order and the second order statistical matrices construction, eigen-decomposition, and SVD. In order to facilitate the analysis, we assume that the effective apertures of smoothed cumulant or covariance matrices are identical to m elements. For FBSS, the major computations involved are to form one $M \times M$ FOC matrix and to perform the SVD of the smoothed $m \times m$ cumulant matrix, which require $\mathcal{O}\left(9M^2L_s + m^3\right)$ flops where L_s is the number of snapshots.[2] Here, a flop stands for a complex-valued floating point multiplication operation. VESPA constructs two $M \times M$ cumulant matrices and performs the SVDs of one $2M \times M$ matrix and one $M \times 2K$ matrix, respectively, and the eigen-decomposition of one $K \times K$ matrix to estimate the generalised steering vectors. Then, VESPA forms K smoothed covariance matrices and carries out the eigen-decompositions of these matrices to finally determine the DOA estimates of coherent signals. As a result, it needs $\mathcal{O}\left(18M^2L_s + 2M^3 + \min\{2M^2K, 4MK^2\} + K^3 + M^2K + m^3 \times K\right)$ flops in total. By comparison, the proposed STFOC establishes $2L_p + 1$ pseudo snapshots which involves $\mathcal{O}\left(\sum_{i=-L_p}^{L_p} M\left(L_s - \mid iT_s \mid\right)\right) = \mathcal{O}\left(2M\left(L_pL_s - \frac{L_p(L_p+1)}{2}T_s\right)\right.$

[2] The computational complexity of SVD is known as $\mathcal{O}\left(\min\{kl^2, k^2l\}\right)$ for an arbitrary matrix $\mathbf{B} \in \mathbb{C}^{k\times l}$.

$+ML_s)$ flops, the construction of four $M \times M$ cumulant matrices by such pseudo snapshots needs $\mathcal{O}\left(36M^2\left(2L_p+1\right)\right)$ flops, and the eigen-decomposition of one $M \times M$ matrix takes about $\mathcal{O}\left(M^3\right)$ flops. Additionally, STFOC also constructs K smoothed covariance matrices and performs the eigen-decompositions of these matrices, which involve $\mathcal{O}\left(M^2K+m^3K\right)$ flops. The resulting flops required are in order of $\mathcal{O}\Big(2M\left(L_pL_s-\frac{L_p(L_p+1)}{2}T_s\right)+ML_s+36M^2\left(2L_p+1\right)+M^3+M^2K+m^3K\Big)$.

5.5.3 Simulation Results and Discussion

We now evaluate the DOA estimation performance of STFOC for a few scenarios by computer simulation. Specifically, the runtime of the algorithm, estimation accuracy and reliability of overdetermined and underdetermined problems are studied. Cumulant-based FBSS and VESPA are chosen for comparison with the proposed STFOC. Consider an eight-element ULA with sensor separation $\frac{\lambda}{2}$. For simplicity, we assume that each coherent group contains the same number of signals, i.e., $P_1 = P_2 = \cdots = P_K$. In addition, let L_s and L_p denote the number of snapshots and pseudo snapshots, respectively.

Runtime Comparison

This scenario is designed to compare the running time for the cumulant-based FBSS, VESPA, and STFOC estimator. Table 5.2 records the average elapsed time of one hundred trial runs for various numbers of sensors M. Here, we assume that there are $K = 2$ coherent groups, $P_1 = P_2 = 3$, and $L_s = 3000$, $L_p = 180$, $T_s = 1$, and $m = 7$, respectively. The simulations are performed using MATLAB R2013a running on an Intel Core i7-2600, 3.4 GHz processor with 16 GB of memory, under Windows 7 64-bit. Table 5.2 shows that for the same value of M, STFOC has a much longer runtime than FBSS and VESPA, and the runtime of VESPA appears to be approximately twice that of FBSS. The higher computational complexity of STFOC is mainly subject to its larger number of pseudo snapshots generated from the temporal correlation as well as the cumulant matrices arising from these pseudo snapshots.

Table 5.2. Average runtime (in seconds)

M	FBSS	VESPA	STFOC
6	N/A	0.0215	0.2408
7	N/A	0.0288	0.2862
8	0.0193	0.0378	0.3390
9	0.0243	0.0470	0.3812
10	0.0302	0.0586	0.4346
11	0.0358	0.0698	0.4785

Overdetermined DOA Estimation

In the second scenario, we consider two groups of three coherent signals from $[-42°, -13°, 37°]$ and $[-29°, 20°, 50°]$ impinge on the array. The fading amplitudes and phases of the coherent signals are $[1, 0.9, 0.8]$ and $[1, 0.7, 0.6]$, while the fading phases are $[48.74°, 121.15°, 35.66°]$ and $[9.35°, 251.47°, 103.56°]$, respectively. We select $m = 7$ for rank restoration of the generalised steering vectors $\{\mathbf{b}_k\}_{k=1}^{2}$. Fig. 5.8 shows the estimation results of 50 independent trials. The solid lines indicate the true DOAs. It can be seen that each group of DOAs can be accurately determined, and there is no failure among the 50 experiments.

Since both VESPA and STFOC have to estimate $\mathbf{D}_1$ in the course of the generalised steering vector estimation, and the generalised steering vectors and $\mathbf{D}_1$ closely relate to each other as the relationship between eigenvalue and eigenvector, it is necessary to examine the estimates of diagonal entries of $\mathbf{D}_1$, denoted as $\{\xi_k\}_{k=1}^{K}$, which influence the estimation accuracy of the generalised steering vectors (see (5.61) in Section 5.5.1 and (25) in [38]) and to some extend reflect the accuracy of estimates of generalised steering vectors. The estimated ξ_1 and ξ_2 under different SNRs are listed in Table 5.3 to Table 5.6. All measurements are obtained from 1000 Monte Carlo runs. The above results show that the bias of ξ_1 and ξ_2 estimates are quite small, so both VESPA and STFOC can achieve satisfactory estimation accuracy of $\mathbf{D}_1$ for moderate SNRs.

In terms of estimation accuracy, we calculated the RMSE of each coherent group for the three methods. The results are given in Fig. 5.9. For all SNRs and number of snapshots, our STFOC method gives substantially better angle estimates than FBSS and VESPA.

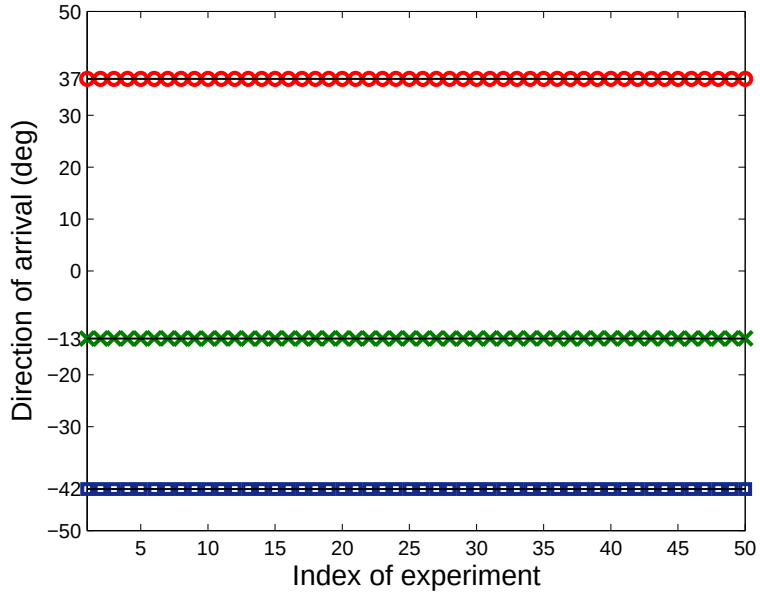

(a) The first coherent group

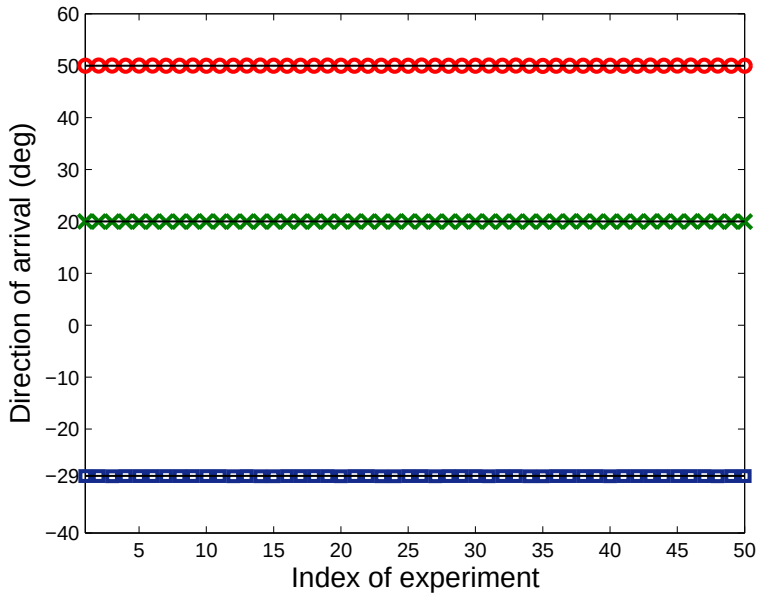

(b) The second coherent group

Figure 5.8. DOA estimation results of 50 runs in the overdetermined case. SNR $= 0$**dB,** $L_s = 5000$**, and** $L_p = 300$**.** Two groups of coherent signals from $[\theta_1, \theta_2, \theta_3] = [-42°, -13°, 37°]$, $[\theta_4, \theta_5, \theta_6] = [-29°, 20°, 50°]$, respectively.

To be specific, the RMSE of the first coherent group is always very small, i.e., lower than $0.02°$, and the RMSE of the second group falls off dramatically and stabilises for SNR values greater than -5dB. On the other hand, the RMSE of the first coherent

Table 5.3. Estimated amplitude of ξ_1 versus SNR in the overdetermined case (True value $\rho_1 = 0.7522$)

	VESPA		STFOC	
SNR	$\hat{\rho}_1$	$\lvert\rho_1 - \hat{\rho}_1\rvert \times 10^{-3}$	$\hat{\rho}_1$	$\lvert\rho_1 - \hat{\rho}_1\rvert \times 10^{-3}$
0	0.7517	0.4768	0.7522	0.02527
2	0.7523	0.1214	0.7522	0.02598
4	0.7520	0.1342	0.7522	0.02703
6	0.7521	0.0433	0.7522	0.02451
8	0.7522	0.0436	0.7522	0.02722
10	0.7522	0.0230	0.7522	0.02645

Table 5.4. Estimated amplitude of ξ_2 versus SNR in the overdetermined case (True value $\rho_2 = 0.9821$)

	VESPA		STFOC	
SNR	$\hat{\rho}_2$	$\lvert\rho_2 - \hat{\rho}_2\rvert \times 10^{-3}$	$\hat{\rho}_2$	$\lvert\rho_2 - \hat{\rho}_2\rvert \times 10^{-3}$
0	0.9824	0.3736	0.9833	1.2421
2	0.9823	0.2269	0.9831	0.9996
4	0.9825	0.4711	0.9829	0.8715
6	0.9813	0.7559	0.9829	0.8353
8	0.9820	0.0957	0.9829	0.8311
10	0.9820	0.0483	0.9829	0.8238

Table 5.5. Estimated phase of ξ_1 versus SNR in the overdetermined case (True value $\psi_1 = 2.1533$rad)

	VESPA		STFOC	
SNR	$\hat{\psi}_1$	$\lvert\psi_1 - \hat{\psi}_1\rvert \times 10^{-3}$	$\hat{\psi}_1$	$\lvert\psi_1 - \hat{\psi}_1\rvert \times 10^{-3}$
0	2.1526	0.6385	2.1533	0.01479
2	2.1530	0.3062	2.1533	0.01463
4	2.1536	0.3145	2.1533	0.01731
6	2.1532	0.0376	2.1533	0.02264
8	2.1532	0.0208	2.1533	0.02012
10	2.1532	0.0724	2.1533	0.02086

group from VESPA is much smaller than FBSS at low SNRs, but slightly greater at 2dB and above. The RMSE of the second coherent group using VESPA is greater than

Table 5.6. Estimated phase of ξ_2 versus SNR in the overdetermined case (True value $\psi_2 = 1.9644$rad)

	VESPA		STFOC	
SNR	$\hat{\psi}_2$	$\lvert\psi_2 - \hat{\psi}_2\rvert \times 10^{-3}$	$\hat{\psi}_2$	$\lvert\psi_2 - \hat{\psi}_2\rvert \times 10^{-3}$
0	1.9648	0.4107	1.9684	3.9652
2	1.9646	0.1794	1.9685	4.1135
4	1.9644	0.0510	1.9685	4.0721
6	1.9648	0.3679	1.9685	4.0651
8	1.9646	0.2155	1.9685	4.1176
10	1.9640	0.3899	1.9685	4.1089

FBSS when the SNR is lower than 5dB, while it tends to give equal performance as the SNR increases. The three algorithms have similar performance as in Fig. 5.9(a) by varying the number of snapshots shown in Fig. 5.9(b), and one subtle difference is that the accuracy of STFOC is getting better with the rise of pseudo snapshots, whereas remains unchanged with a fixed number of snapshots even if SNR ascends to 15dB. One concludes, therefore, STFOC is more sensitive to the number of pseudo snapshots than to the SNR.

Underdetermined DOA Estimation

In the third scenario, we consider three groups of three coherent signals from $[-47^\circ, -24^\circ, 9^\circ]$, $[-70^\circ, 30^\circ, 60^\circ]$, and $[8^\circ, 23^\circ, 45^\circ]$ impinging on the array. The fading amplitudes and phases of the coherent signals are $[1, 0.9, 0.8]$, $[1, 0.7, 0.6]$, and $[1, 0.7, 0.4]$, while the fading phases are $[48.74^\circ, 121.15^\circ, 35.66^\circ]$, $[9.35^\circ, 251.47^\circ, 103.56^\circ]$ and $[130.21^\circ, 16.88^\circ, 319.69^\circ]$, respectively. We select $m = 7$ for rank restoration of the generalised steering vectors $\{\mathbf{b}_k\}_{k=1}^3$. Fig. 5.10 shows estimation results of 50 independent trials. Like the overdetermined case, all three groups of coherent signals can be correctly estimated, even though the total number of signals is larger than the number of sensors.

We now examine the estimation accuracy of $\mathbf{D}_1$. The estimated ξ_1, ξ_2, and ξ_3 under different SNRs are listed in Table 5.7 to Table 5.12. The results show that the bias of the $\{\xi_k\}_{k=1}^3$ estimates by STFOC decrease more quickly than for VESPA, and remain

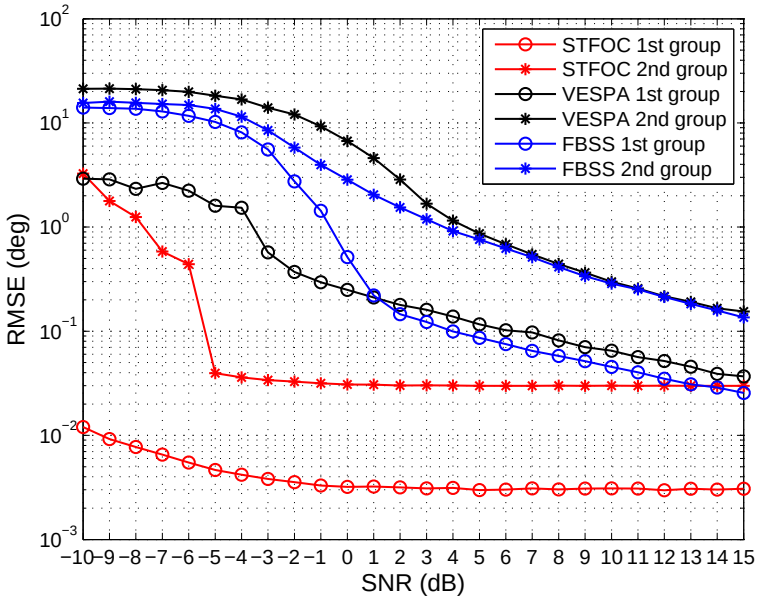

(a)

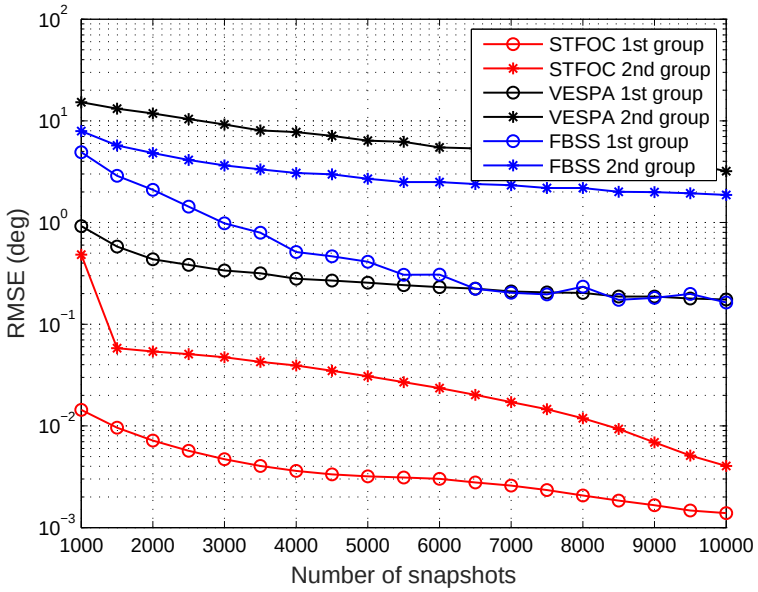

(b)

Figure 5.9. RMSE of DOA estimates in the overdetermined case. (a) $L_s = 5000$**, and** $L_p = 300$**. (b) SNR** $= 0$**dB, and** $L_p = \frac{3}{50}L_s$**.**

lower than 3% of the relative estimation error. At high SNRs, VESPA can give as good performance as STFOC does, while it is significantly inferior to STFOC at low SNRs.

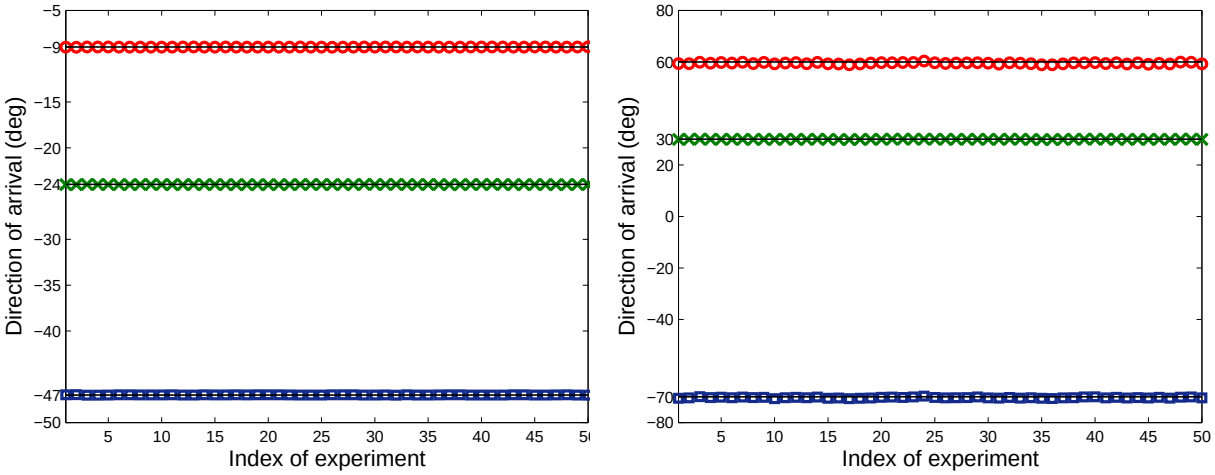

(a) The first coherent group

(b) The second coherent group

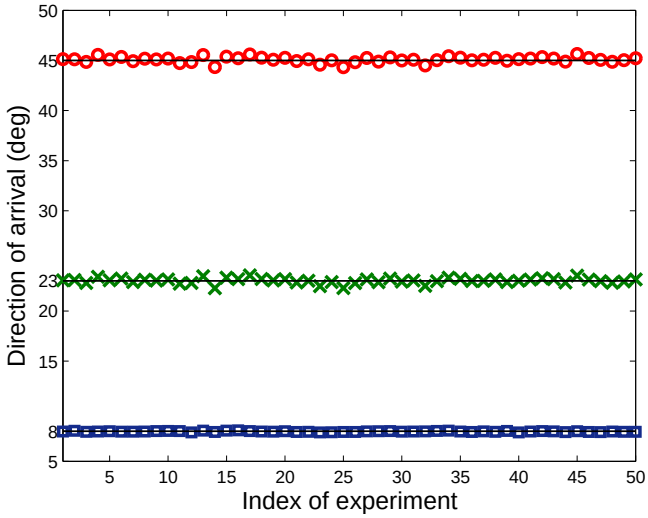

(c) The third coherent group

Figure 5.10. DOA estimation results of 50 runs in the underdetermined case. SNR $= 0$dB, $L_s = 5000$, and $L_p = 300$. Three groups of coherent signals from $[\theta_1, \theta_2, \theta_3] = [-47°, -24°, -9°]$, $[\theta_4, \theta_5, \theta_6] = [-70°, 30°, 60°]$, and $[\theta_7, \theta_8, \theta_9] = [8°, 23°, 45°]$, respectively.

The RMSE of the DOA estimates are calculated and displayed in Fig. 5.11 as a function of SNR and the number of snapshots. It follows similarly to Fig. 5.9 that STFOC achieves satisfactory performance at a much lower SNR and number of snapshots than VESPA. The RMSE of STFOC is less than $1°$ for all three groups at SNRs greater than -5dB and more than 2000 snapshots for an SNR of 0dB. To achieve comparable performance, VESPA requires more than 8dB SNR for 5000 snapshots and much more than

Table 5.7. Estimated amplitude of ξ_1 versus SNR in the underdetermined case (True value $\rho_1 = 0.7386$)

	VESPA		STFOC	
SNR	$\hat{\rho}_1$	$\lvert\rho_1 - \hat{\rho}_1\rvert \times 10^{-3}$	$\hat{\rho}_1$	$\lvert\rho_1 - \hat{\rho}_1\rvert \times 10^{-3}$
0	0.7389	0.3293	0.7522	0.6473
2	0.7387	0.1102	0.7522	0.6566
4	0.7390	0.4240	0.7522	0.6565
6	0.7387	0.0792	0.7522	0.6589
8	0.7384	0.1882	0.7522	0.6160
10	0.7385	0.0761	0.7522	0.6410

Table 5.8. Estimated amplitude of ξ_2 versus SNR in the underdetermined case (True value $\rho_2 = 1.5385$)

	VESPA		STFOC	
SNR	$\hat{\rho}_2$	$\lvert\rho_2 - \hat{\rho}_2\rvert$	$\hat{\rho}_2$	$\lvert\rho_2 - \hat{\rho}_2\rvert$
0	1.1597	0.3788	1.5191	0.0193
2	1.2421	0.2963	1.5353	0.0032
4	1.3539	0.1846	1.5359	0.0026
6	1.4151	0.1233	1.5358	0.0027
8	1.4677	0.0708	1.5357	0.0028
10	1.5034	0.0350	1.5359	0.0025

Table 5.9. Estimated amplitude of ξ_3 versus SNR in the underdetermined case (True value $\rho_3 = 1.8732$)

	VESPA		STFOC	
SNR	$\hat{\rho}_3$	$\lvert\rho_3 - \hat{\rho}_3\rvert$	$\hat{\rho}_3$	$\lvert\rho_2 - \hat{\rho}_2\rvert$
0	1.3824	0.4908	1.8634	0.0098
2	1.5134	0.3598	1.8817	0.0084
4	1.6557	0.2175	1.8815	0.0082
6	1.7290	0.1443	1.8816	0.0083
8	1.7918	0.0814	1.8812	0.0079
10	1.8335	0.0398	1.8813	0.0081

10000 snapshots at an SNR of 0dB. In addition, we found that the estimation accuracy of the first group is always superior to the remaining group for both VESPA and

Table 5.10. Estimated phase of ξ_1 versus SNR in the underdetermined case (True value $\psi_1 = 1.6613$rad)

	VESPA		STFOC	
SNR	$\hat{\psi}_1$	$\lvert\psi_1 - \hat{\psi}_1\rvert \times 10^{-3}$	$\hat{\psi}_1$	$\lvert\psi_1 - \hat{\psi}_1\rvert \times 10^{-3}$
0	1.6609	0.3845	1.6621	0.7423
2	1.6610	0.3328	1.6621	0.7593
4	1.6615	0.1700	1.6622	0.8276
6	1.6612	0.1752	1.6621	0.7847
8	1.6612	0.1692	1.6622	0.8403
10	1.6614	0.0373	1.6621	0.8082

Table 5.11. Estimated phase of ξ_2 versus SNR in the underdetermined case (True value $\psi_2 = -0.7055$rad)

	VESPA		STFOC	
SNR	$\hat{\psi}_2$	$\lvert\psi_2 - \hat{\psi}_2\rvert$	$\hat{\psi}_2$	$\lvert\psi_2 - \hat{\psi}_2\rvert$
0	-1.1373	0.4318	-0.6950	0.0105
2	-0.9785	0.2730	-0.6855	0.0200
4	-0.8509	0.1454	-0.6853	0.0201
6	-0.7945	0.0890	-0.6853	0.0202
8	-0.7552	0.0498	-0.6854	0.0201
10	-0.7295	0.0240	-0.6853	0.0201

Table 5.12. Estimated phase of ξ_3 versus SNR in the underdetermined case (True value $\psi_3 = -2.4933$rad)

	VESPA		STFOC	
SNR	$\hat{\psi}_3$	$\lvert\psi_3 - \hat{\psi}_3\rvert$	$\hat{\psi}_3$	$\lvert\psi_3 - \hat{\psi}_3\rvert$
0	-2.1950	0.2983	-2.5176	0.0243
2	-2.3087	0.1847	-2.5239	0.0306
4	-2.3948	0.0986	-2.5241	0.0308
6	-2.4323	0.0610	-2.5240	0.0307
8	-2.4597	0.0336	-2.5240	0.0307
10	-2.4772	0.0161	-2.5240	0.0307

STFOC, which is consistent with Fig. 5.9. The estimator performance using generalised steering vectors is determined by the robustness of the signal subspace eigenvectors of

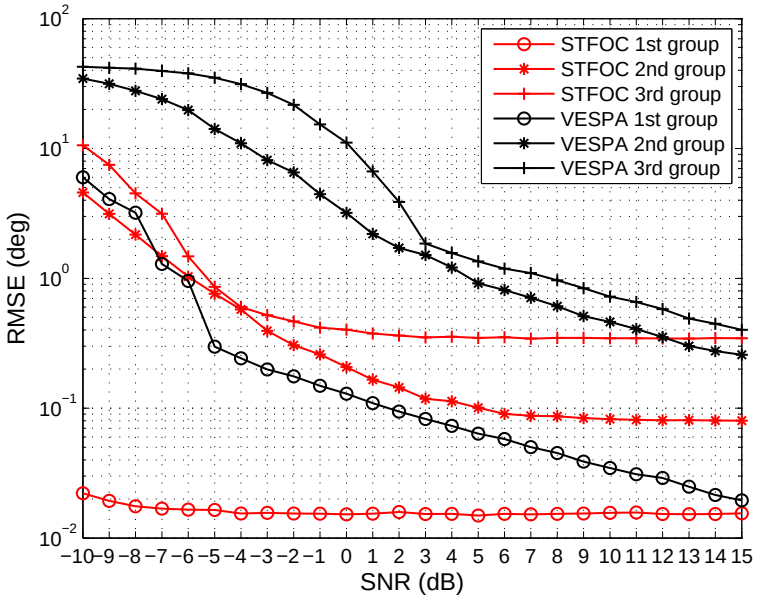

(a)

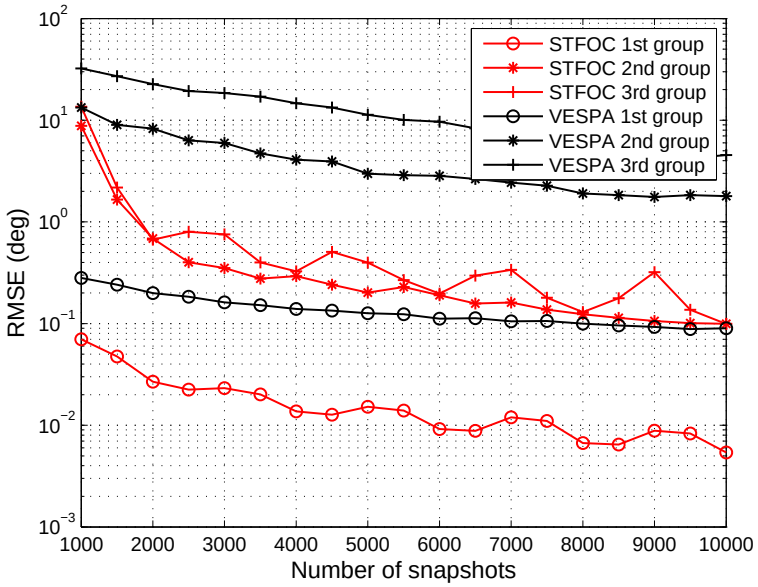

(b)

Figure 5.11. RMSE of DOA estimates in the underdetermined case. (a) $L_s = 5000$**, and** $L_p = 300$**. (b) SNR** $= 0$**dB,and** $L_p = \frac{3}{50}L_s$**.**

$\{\mathbf{b}_k\}_{k=1}^{K}$ to noise perturbation. The more robust the eigenvectors, the better the performance. The robustness of $\mathbf{b}_k$ is determined by its condition number, as described in [159, chap. 8]. The smaller the condition number, the more robust the eigenvector. Since $\widetilde{\mathbf{C}}_1^{+}\widetilde{\mathbf{C}}_2$ is Hermitian, the condition number of the eigenvector is the reciprocal of the smallest absolute difference between the corresponding eigenvalue and any other

eigenvalue [159, pp. 399]. Normally, the smallest "gap" between the first eigenvalue and any others is the largest, so $\mathbf{b}_1$ in our simulation, the generalised steering vector of the first coherent group, corresponding to the the first eigenvalue, is the most robust, resulting in the lowest RMSEs of DOA estimates.

5.6 Conclusion

In this Chapter, an FOC-based two-stage matrix reconstruction algorithm is proposed first in Section 5.4 for DOA estimation of mixed independent and coherent signals. The algorithm makes efficient use of the cumulants of sensor outputs of a ULA, and enables us to separately deal with two different types of signals, thus resolving more signals than the number of array elements. In the first stage, the root-MUSIC algorithm is utilised to estimate the DOA of the independent signals as root-MUSIC is only a function of the DOA of the independent sources while the coherent signals are ignored. In the second stage, the independent components are removed from the cumulant matrix of the received data based on the DOA estimates of the independent sources. Then a matrix reconstruction is performed to restore the rank deficiency in the cumulant matrix of the coherent signals, and finally their DOAs are resolved using a unitary transformation to reduce computation complexity. Compared with previous two-stage FOC-based methods, the proposed solution is efficient in the sense that it achieves a more reasonable classification of the signal types, alleviates the array DOFs and aperture loss in previous methods, as well as improving the estimation accuracy of both independent and coherent signals.

Secondly in Section 5.5, we develop a new DOA estimator called space-time fourth order cumulants (STFOC) method. The basic idea of STFOC is to use the second-order statistics of the received signals to get the pseudo snapshots which contain the temporal correlation information. This, together with the array manifold structure, is used to find the fourth-order cumulants. It makes use of temporal as well as spatial information when estimating directions. The source directions are obtained from the fourth order cumulants using the unitary ESPRIT algorithm. STFOC can resolve the same number of directions as VESPA. Simulation results show that the estimation accuracy,

robustness to coherent group separation, and immunity to noise are evidently superior to VESPA, although at the cost of greater computations.

Chapter 6

Noncircularity to Array: Novel Approaches with Enhanced DOFs

MOST DOA estimators assume circular signal statistics. However the noncircular statistics of modern wireless communication signals can be exploited to develop new estimators which can deal with more signals than is possible with circular statistics. This is typically achieved by utilising the rotational invariance of the augmented covariance matrix constructed from this class of signals. In this chapter we introduce a new noncircular FOC estimator that can deal with more signals than previously published FOC methods. We also consider how the noncircularity can be exploited in the previously introduced two-stage DOA estimation methods based on second order statistics. The simulation results demonstrate the advantages of our novel approaches over existing methods.

6.1 Introduction

DOA estimation for noncircular signals has been drawing increasing attention over the past few years. These signals arise in radar, wireless communications, and satellite systems and include amplitude modulation (AM), binary phase shift keying (BPSK), amplitude shift keying (ASK), offset quadrature phase shift keying (OQPSK), and pulse amplitude modulation (PAM) signals. The previous literature has shown that exploitation of the noncircularity of the incident signals helps to improve the performance of general DOA estimation methods [20, 105, 106, 108, 113, 114]. Noncircular signal estimators based on SOS can extend the effective array aperture and resolve at most twice as many sources as the circular signal estimators. Combining high order cumulants and noncircularity, Liu et al recently proposed the NC-2q-MUSIC algorithm which is an extension of standard 2q-MUSIC [118] to noncircular signals, which can further extend the effective array aperture and give better performance compared with the original [20]. However, similar to the algorithms using SOS reviewed in Chapter 2, none of the aforementioned noncircular DOA estimation methods are able to work properly when uncorrelated and coherent signals coexist, as the spatial covariance matrix becomes rank deficient. Two interesting questions arise as a result: a) Is it possible to further improve the effective aperture and estimation capacity by utilising noncircularity and FOC? b) Does noncircularity help with direction finding of the mixed uncorrelated and coherent signals?

To this end, in Section 6.2 we first introduce and evaluate a new FOC-based DOA estimation method for noncircular signals, called augmented NC-FOC, which can handle an additional $M-1$ (M is the number of sensors) sources compared with the NC-2q approach and has lower estimation errors because of a better utilisation of noncircular information in the FOC by constructing two cumulant matrices corresponding to a virtual array which has the fewest overlapping sensors.

To the best of our knowledge, the previous literature has not considered DOA estimation of noncircular signals containing a mixture of uncorrelated and coherent signals. The techniques considered in Section 6.3 exploit the properties of noncircular signals

to enable more sources to be resolved when the uncorrelated and coherent signals coexist. A subspace-based method is first applied to resolve the uncorrelated sources from the overall mixed signals. It exploits the orthogonality between the signal and noise subspaces to classify the signal types. By reconstructing the covariance matrix of the uncorrelated noncircular sources, their contribution can be removed from the covariance matrix of the received data. Then a spatial smoothing technique is developed to resolve the remaining coherent signals. As we shall show in Section 6.3.2, the proposed method is capable of handling many more signals compared with existing two-stage processing algorithms. In addition, we present the deterministic direction of arrival estimation CRLB for the noncircular signals in the multipath case. The derivation of the CRLB can be viewed as a natural extension of the well-known results derived in [56, 160] for the noncircular signal model. The CRLB for strict sense noncircular uncorrelated sources (no multipath) has been derived in [112], however, it does not show the bound expression for noncircularity phase, nor is it applicable to coherent signals arising from multipath propagation.

6.2 DOA Estimation of Noncircular Signals with Fewer Sensors: A Cumulant-based Approach

As reviewed in Section 2.4, DOA estimation of strict sense noncircular signals, i.e., $\rho = 1$ (see definition in Section 2.4.1), based on the second-order statistics applying either MUSIC- or ESPRIT-type algorithms, can estimate up to $2(M-1)$ sources [105, 106, 108, 113, 114], or $3(M-1)$ sources if fourth order cumulants are used [20]. By revisiting the approach by Liu et al [20], we find that the limits of estimation capacity, i.e., the degrees of freedom, can be further extended using noncircularity. In this Chapter, we assume that all signals are strictly second-order noncircular, i.e., the case of $\rho = 1$.

6.2.1 Signal Model for Independent Noncircular Sources

Consider a number of N narrowband far-field noncircular signals impinging on a uniform linear array with M identical omnidirectional sensors. Assume that all sources

$s_i(t) = e^{j\frac{\phi_i}{2}} s_{i,0}(t)$ coming from directions $\theta_i, i = 1, 2, \cdots, N$, are independent to each other. The $M \times 1$ array output vector is then given by

$$\begin{aligned} \mathbf{x}(t) &= \sum_{i=1}^{N} \mathbf{a}(\theta_i) e^{j\frac{\phi_i}{2}} s_{i,0}(t) + \mathbf{n}(t) \\ &= \mathbf{A}\mathbf{\Psi}\mathbf{s}_0(t) + \mathbf{n}(t) \end{aligned} \tag{6.1}$$

where $\mathbf{a}(\theta) = \left[1, e^{j\frac{2\pi d}{\lambda}\sin\theta}, \cdots, e^{j\frac{2\pi(M-1)d}{\lambda}\sin\theta}\right]^T \in \mathbb{C}^M$ is the steering vector with λ and d being the wavelength of the carrier signal and the spacing between adjacent elements, respectively, $\mathbf{A} = [\mathbf{a}(\theta_1), \mathbf{a}(\theta_2), \cdots, \mathbf{a}(\theta_N)]$, $\mathbf{\Psi} = \text{diag}\left\{e^{j\frac{\phi_1}{2}}, e^{j\frac{\phi_2}{2}}, \cdots, e^{j\frac{\phi_N}{2}}\right\}$, $\mathbf{s}_0(t) = \left[s_{1,0}(t), \cdots, s_{N,0}(t)\right]^T$, and $\mathbf{n}(t)$ is white Gaussian noise. Besides, we assume that the array is calibrated, and the array manifold $\mathbf{A}$ is unambiguous, i.e., the steering vectors $\{\mathbf{a}(\theta_i)\}_{i=1}^N$ are linearly independent for any set of distinct $\{\theta_i\}_{i=1}^N$. Equivalently, the matrix $\mathbf{A}$ is of full column rank.

6.2.2 Improved Noncircular Signals Direction Finding Using FOC

Considering the definition of cumulants in (5.2), we start with constructing two cumulant matrices as

$$\begin{aligned} \mathbf{C}_{x1} &\triangleq \text{cum}\left\{\mathbf{x}^*(t), \mathbf{x}^T(t), \mathbf{x}^*(t), \mathbf{x}^T(t)\right\} \\ &= \text{cum}\left\{\sum_{p=1}^{N} \mathbf{a}^*(\theta_p) e^{-j\frac{\phi_p}{2}} s_{p,0}^*(t), \sum_{m=1}^{N} \mathbf{a}^T(\theta_m) e^{j\frac{\phi_m}{2}} s_{m,0}(t),\right. \\ &\quad \left.\sum_{q=1}^{N} \mathbf{a}^*(\theta_q) e^{-j\frac{\phi_q}{2}} s_{q,0}^*(t), \sum_{n=1}^{N} \mathbf{a}^T(\theta_n) e^{j\frac{\phi_n}{2}} s_{n,0}(t)\right\} \\ &= \sum_{p=1}^{N}\sum_{m=1}^{N}\sum_{q=1}^{N}\sum_{n=1}^{N} \left(\left(\mathbf{a}^*(\theta_p) e^{-j\frac{\phi_p}{2}}\right) \otimes \left(\mathbf{a}^*(\theta_q) e^{-j\frac{\phi_q}{2}}\right)\right) \\ &\quad \times \left(\left(\mathbf{a}(\theta_m) e^{j\frac{\phi_m}{2}}\right) \otimes \left(\mathbf{a}(\theta_n) e^{j\frac{\phi_n}{2}}\right)\right)^T \text{cum}\left\{s_{p,0}^*(t), s_{m,0}(t), s_{q,0}^*(t), s_{n,0}(t)\right\} \\ &= \sum_{i=1}^{N} \left(\left(\mathbf{a}^*(\theta_i) e^{-j\frac{\phi_i}{2}}\right) \otimes \left(\mathbf{a}^*(\theta_i) e^{-j\frac{\phi_i}{2}}\right)\right) \left(\left(\mathbf{a}(\theta_i) e^{j\frac{\phi_i}{2}}\right) \otimes \left(\mathbf{a}(\theta_i) e^{j\frac{\phi_i}{2}}\right)\right)^T \\ &\quad \times \text{cum}\left\{s_{i,0}(t), s_{i,0}(t), s_{i,0}(t), s_{i,0}(t)\right\} \\ &= \sum_{i=1}^{N} \gamma_i \left(\mathbf{a}^*(\theta_i) \otimes \mathbf{a}^*(\theta_i)\right) \left(\mathbf{a}(\theta_i) \otimes \mathbf{a}(\theta_i)\right)^T \end{aligned}$$

$$
\begin{aligned}
&= \left(\mathbf{A}^* \circ \mathbf{A}^*\right) \operatorname{diag}\left\{\gamma_1, \gamma_2, \cdots, \gamma_N\right\} \left(\mathbf{A} \circ \mathbf{A}\right)^T \\
&= \mathbf{A}_1 \mathbf{C}_s \mathbf{A}_1^H \qquad (6.2)
\end{aligned}
$$

$$
\begin{aligned}
\mathbf{C}_{x2} &\triangleq \operatorname{cum}\left\{\mathbf{x}(t), \mathbf{x}^T(t), \mathbf{x}(t), \mathbf{x}^T(t)\right\} \\
&= \operatorname{cum}\left\{\sum_{p=1}^{N} \mathbf{a}\left(\theta_p\right) e^{j\frac{\phi_p}{2}} s_{p,0}(t), \sum_{m=1}^{N} \mathbf{a}^T\left(\theta_m\right) e^{j\frac{\phi_m}{2}} s_{m,0}(t),\right. \\
&\quad \left.\sum_{q=1}^{N} \mathbf{a}\left(\theta_q\right) e^{j\frac{\phi_q}{2}} s_{q,0}(t), \sum_{n=1}^{N} \mathbf{a}^T\left(\theta_n\right) e^{j\frac{\phi_n}{2}} s_{n,0}(t)\right\} \\
&= \sum_{p=1}^{N}\sum_{m=1}^{N}\sum_{q=1}^{N}\sum_{n=1}^{N} \left(\left(\mathbf{a}\left(\theta_p\right) e^{j\frac{\phi_p}{2}}\right) \otimes \left(\mathbf{a}\left(\theta_q\right) e^{j\frac{\phi_q}{2}}\right)\right) \\
&\quad \times \left(\left(\mathbf{a}\left(\theta_m\right) e^{j\frac{\phi_m}{2}}\right) \otimes \left(\mathbf{a}\left(\theta_n\right) e^{j\frac{\phi_n}{2}}\right)\right)^T \operatorname{cum}\left\{s_{p,0}(t), s_{m,0}(t), s_{q,0}(t), s_{n,0}(t)\right\} \\
&= \sum_{i=1}^{N} \left(\left(\mathbf{a}\left(\theta_i\right) e^{j\frac{\phi_i}{2}}\right) \otimes \left(\mathbf{a}\left(\theta_i\right) e^{j\frac{\phi_i}{2}}\right)\right) \left(\left(\mathbf{a}\left(\theta_i\right) e^{j\frac{\phi_i}{2}}\right) \otimes \left(\mathbf{a}\left(\theta_i\right) e^{j\frac{\phi_i}{2}}\right)\right)^T \\
&\quad \times \operatorname{cum}\left\{s_{i,0}(t), s_{i,0}(t), s_{i,0}(t), s_{i,0}(t)\right\} \\
&= \sum_{i=1}^{N} \gamma_i e^{j2\phi_i} \left(\mathbf{a}\left(\theta_i\right) \otimes \mathbf{a}\left(\theta_i\right)\right) \left(\mathbf{a}\left(\theta_i\right) \otimes \mathbf{a}\left(\theta_i\right)\right)^T \\
&= \left(\mathbf{A} \circ \mathbf{A}\right) \operatorname{diag}\left\{\gamma_1, \gamma_2, \cdots, \gamma_N\right\} \operatorname{diag}\left\{e^{j\frac{\phi_1}{2}}, e^{j\frac{\phi_2}{2}}, \cdots, e^{j\frac{\phi_N}{2}}\right\}^4 \left(\mathbf{A} \circ \mathbf{A}\right)^T \\
&= \left(\mathbf{A} \circ \mathbf{A}\right) \mathbf{C}_s \mathbf{\Psi}^4 \left(\mathbf{A}^* \circ \mathbf{A}^*\right)^H \\
&= \mathbf{A}_2 \mathbf{\Psi}^2 \mathbf{C}_s \mathbf{\Psi}^2 \mathbf{A}_1^H \qquad (6.3)
\end{aligned}
$$

where

$$\gamma_i = \operatorname{cum}\left\{s_{i,0}(t), s_{i,0}(t), s_{i,0}(t), s_{i,0}(t)\right\} \qquad (6.4)$$

$$\mathbf{A}_1 = \mathbf{A}^* \circ \mathbf{A}^* = \left[\mathbf{a}^*(\theta_1) \otimes \mathbf{a}^*(\theta_1), \mathbf{a}^*(\theta_2) \otimes \mathbf{a}^*(\theta_2), \cdots, \mathbf{a}^*(\theta_N) \otimes \mathbf{a}^*(\theta_N)\right] \in \mathbb{C}^{M^2 \times N} \qquad (6.5)$$

$$\mathbf{A}_2 = \mathbf{A} \circ \mathbf{A} = \left[\mathbf{a}(\theta_1) \otimes \mathbf{a}(\theta_1), \mathbf{a}(\theta_2) \otimes \mathbf{a}(\theta_2), \cdots, \mathbf{a}(\theta_N) \otimes \mathbf{a}(\theta_N)\right] \in \mathbb{C}^{M^2 \times N} \qquad (6.6)$$

$$\mathbf{C}_s = \operatorname{cum}\left\{\mathbf{s}_0(t), \mathbf{s}_0(t), \mathbf{s}_0(t), \mathbf{s}_0(t)\right\} = \operatorname{diag}\left\{\gamma_1, \gamma_2, \cdots, \gamma_N\right\} \in \mathbb{R}^{N \times N}. \qquad (6.7)$$

As discussed in the context of aperture extension via FOC in [37], some rows of $\mathbf{A}_1$ and $\mathbf{A}_2$ are redundant to the rest in the case of a ULA and can be removed, resulting in the effective array aperture being $2M-1$ elements. Let $\mathbf{G} \triangleq \begin{bmatrix} \mathbf{I}_M & \mathbf{0}_{M \times (M^2-M)} \\ \mathbf{0}_{(M-1)\times(M^2-M+1)} & \mathbf{I}_{M-1} \end{bmatrix}$,

then one can reduce the problem size by performing a transformation

$$\mathbf{G}\mathbf{C}_{x1}\mathbf{G}^H = \mathbf{G}\mathbf{A}_1\mathbf{C}_s\mathbf{A}_1^H\mathbf{G}^H = \widetilde{\mathbf{A}}_1\mathbf{C}_s\widetilde{\mathbf{A}}_1^H \tag{6.8}$$

$$\mathbf{G}\mathbf{C}_{x2}\mathbf{G}^H = \mathbf{G}\mathbf{A}_2\mathbf{\Psi}^2\mathbf{C}_s\mathbf{\Psi}^2\mathbf{A}_1^H\mathbf{G}^H = \widetilde{\mathbf{A}}_2\mathbf{\Psi}^2\mathbf{C}_s\mathbf{\Psi}^2\widetilde{\mathbf{A}}_1^H \tag{6.9}$$

where $\widetilde{\mathbf{A}}_1 = [\tilde{\mathbf{a}}(\theta_1), \tilde{\mathbf{a}}(\theta_2), \cdots, \tilde{\mathbf{a}}(\theta_N)]$ with $\tilde{\mathbf{a}}(\theta_i) = \left[1, e^{-j\frac{2\pi d}{\lambda}\sin\theta}, \cdots, e^{-j\frac{2\pi 2(M-1)d}{\lambda}\sin\theta}\right]^T \in \mathbb{C}^{2M-1}$, $\widetilde{\mathbf{A}}_2 = \widetilde{\mathbf{A}}_1^*$. Interpretation of $\mathbf{G}$ and corresponding examples are given in Appendix B.1.

Then, one can form an augmented matrix as

$$\mathbf{C}_a = \begin{bmatrix} \mathbf{J}\mathbf{C}_{x1}\mathbf{J} & \mathbf{J}\mathbf{C}_{x2}^H \\ \mathbf{C}_{x2}\mathbf{J} & \mathbf{C}_{x1}^* \end{bmatrix} \tag{6.10}$$

$$= \begin{bmatrix} \mathbf{J}\widetilde{\mathbf{A}}_1\mathbf{\Psi}^{-2} \\ \widetilde{\mathbf{A}}_2\mathbf{\Psi}^2 \end{bmatrix} \mathbf{C}_s \begin{bmatrix} \mathbf{J}\widetilde{\mathbf{A}}_1\mathbf{\Psi}^{-2} \\ \widetilde{\mathbf{A}}_2\mathbf{\Psi}^2 \end{bmatrix}^H. \tag{6.11}$$

Performing the SVD of $\mathbf{C}_a$, one has

$$\mathbf{C}_a = \mathbf{U}\mathbf{\Sigma}_s\mathbf{V}^H \tag{6.12}$$

where $\mathbf{\Sigma} = \mathrm{diag}\{\lambda_1, \lambda_2, \cdots, \lambda_{2M-1}\}$ consists of $2M-1$ singular values. The columns of $\mathbf{U}_s \triangleq \mathbf{U}(:, 1:N)$ are the singular vectors corresponding to the N largest singular values. Because the columns of $\mathbf{U}_s$ share the same signal subspace with $\begin{bmatrix} \mathbf{J}\widetilde{\mathbf{A}}_1\mathbf{\Psi}^{-2} \\ \widetilde{\mathbf{A}}_2\mathbf{\Psi}^2 \end{bmatrix}$, there is a nonsingular matrix $\mathbf{T} \in \mathbb{C}^{N\times N}$ that satisfies

$$\mathbf{U}_s = \begin{bmatrix} \mathbf{J}\widetilde{\mathbf{A}}_1\mathbf{\Psi}^{-2} \\ \widetilde{\mathbf{A}}_2\mathbf{\Psi}^2 \end{bmatrix} \mathbf{T}. \tag{6.13}$$

Here the signal subspace $\mathbf{U}_s$ can be divided into two matrices $\mathbf{U}_{s1} = \begin{bmatrix} \mathbf{U}_s(1:2M-2,:) \\ \mathbf{U}_s(2M:4M-3,:) \end{bmatrix}$, $\mathbf{U}_{s2} = \begin{bmatrix} \mathbf{U}_s(2:2M-1,:) \\ \mathbf{U}_s(2M+1:4M-2,:) \end{bmatrix} \in \mathbb{C}^{4(M-1)\times N}$. Evidently the structure in (6.13) is also valid to $\mathbf{U}_{s1}$ and $\mathbf{U}_{s2}$. Defining $\mathbf{B}_1 = \begin{bmatrix} \mathbf{J}\widetilde{\mathbf{A}}_1(1:2M-2,:)\mathbf{\Psi}^{-2} \\ \widetilde{\mathbf{A}}_2(2M:4M-3,:)\mathbf{\Psi}^2 \end{bmatrix}$, $\mathbf{B}_2 = \begin{bmatrix} \mathbf{J}\widetilde{\mathbf{A}}_1(2:2M-1,:)\mathbf{\Psi}^{-2} \\ \widetilde{\mathbf{A}}_2(2M+1:4M-2,:)\mathbf{\Psi}^2 \end{bmatrix}$,

because $\mathbf{J}\widetilde{\mathbf{A}}_1(2:2M-1,:) = \mathbf{J}\widetilde{\mathbf{A}}_1(1:2M-2,:)\mathbf{\Phi}$ and $\widetilde{\mathbf{A}}_2(2M+1:4M-2,:) = \widetilde{\mathbf{A}}_2(2M:4M-3,:)\mathbf{\Phi}$, then $\mathbf{B}_2 = \mathbf{B}_1\mathbf{\Phi}$ holds and

$$\begin{bmatrix}\mathbf{U}_{s1}\\ \mathbf{U}_{s2}\end{bmatrix} = \begin{bmatrix}\mathbf{B}_1\\ \mathbf{B}_2\end{bmatrix}\mathbf{T} = \begin{bmatrix}\mathbf{B}_1\\ \mathbf{B}_1\mathbf{\Phi}\end{bmatrix}\mathbf{T}. \tag{6.14}$$

This shows that $\mathbf{U}_{s1}$ and $\mathbf{U}_{s2}$ share a common column space of dimension N, and thus rank $([\mathbf{U}_{s1}, \mathbf{U}_{s2}]) = N$. Thus, there is a full column rank matrix $\mathbf{F} \in \mathbb{C}^{2N\times N}$ such that

$$\begin{aligned}\left[\mathbf{U}_{s1}, \mathbf{U}_{s2}\right]\mathbf{F} &= \left[\mathbf{U}_{s1}, \mathbf{U}_{s2}\right]\begin{bmatrix}\mathbf{F}_1\\ \mathbf{F}_2\end{bmatrix}\\ &= \mathbf{B}_1\mathbf{T}\mathbf{F}_1 + \mathbf{B}_1\mathbf{\Phi}\mathbf{T}\mathbf{F}_2\\ &= \mathbf{0}_{4(M-1)\times N}\end{aligned} \tag{6.15}$$

where the columns of $\mathbf{F}$ are the eigenvectors corresponding to the N smallest eigenvalues of $\left[\mathbf{U}_{s1}, \mathbf{U}_{s2}\right]^H\left[\mathbf{U}_{s1}, \mathbf{U}_{s2}\right]$, $\mathbf{F}_1 = \mathbf{F}(1:N,:)$, and $\mathbf{F}_2 = \mathbf{F}(N+1:2N,:)$.

Since $\mathbf{B}_1 \in \mathbb{C}^{4(M-1)\times N}$ is of full column rank, (6.15) results in $\mathbf{T}\mathbf{F}_1 + \mathbf{\Phi}\mathbf{T}\mathbf{F}_2 = \mathbf{0}$, which is equivalent to

$$-\mathbf{F}_1\mathbf{F}_2^{-1} = \mathbf{T}^{-1}\mathbf{\Phi}\mathbf{T}. \tag{6.16}$$

Note that $\mathbf{\Phi}$ and $-\mathbf{F}_1\mathbf{F}_2^{-1}$ are similar matrices and have identical eigenvalues. Thus, let $\{\eta_i\}_{i=1}^N$ be the N eigenvalues of $-\mathbf{F}_1\mathbf{F}_2^{-1}$, the DOAs can be determined as follows

$$\hat{\theta}_i = \arcsin\left(\frac{\lambda}{2\pi d}\arg(\eta_i)\right), \quad i = 1, \cdots, N. \tag{6.17}$$

6.2.3 Connection with Other Work

Upon exploring how to extend the virtual array aperture, we became aware of existing work by other researchers who, in a similar spirit to this work, have noticed and sought to exploit the link and differences between them.

In [37], the authors first pointed out that FOC cooperating with ESPRIT, so-called VESPA, can effectively enhance the array's DOFs, and thus more signals can be resolved. The key idea behind the innovation is that the extra information obtained

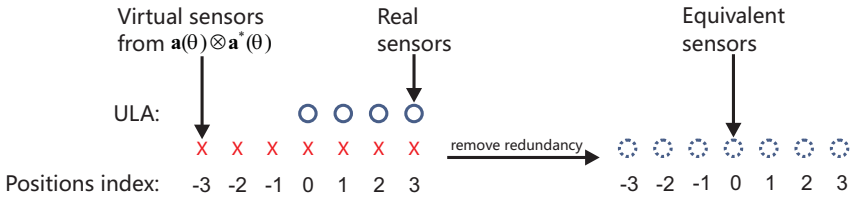

(a) Extended virtual aperture of a ULA.

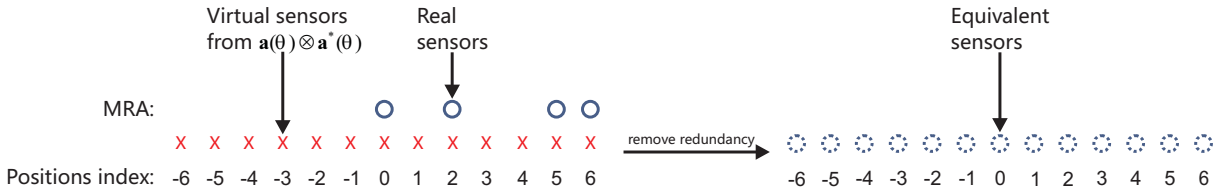

(b) Extended virtual aperture of an MRA.

Figure 6.1. The schematics of virtual aperture extension for circular signals.

from the FOC can be interpreted as coming from additional virtual sensors. The FOC for circular signals are based on the the Kronecker product between two steering vectors, $\mathbf{a}(\theta_i) \otimes \mathbf{a}^*(\theta_i)$. Expanding this Kronecker product results in a steering vector with additional entries. For example if $\mathbf{a}(\theta_1) = \left[1, e^{j\frac{2\pi d}{\lambda}\sin\theta_1}, e^{j\frac{2\pi 2d}{\lambda}\sin\theta_1}\right]^T$ for one signal impinging on a three-element ULA, then the Kroneker product has the following terms

$$\mathbf{a}(\theta_1) \otimes \mathbf{a}^*(\theta_1) = \left[1, e^{-j\frac{2\pi d}{\lambda}\sin\theta_1}, e^{-j\frac{2\pi 2d}{\lambda}\sin\theta_1}, e^{j\frac{2\pi d}{\lambda}\sin\theta_1}, 1, e^{-j\frac{2\pi d}{\lambda}\sin\theta_1}, e^{j\frac{2\pi 2d}{\lambda}\sin\theta_1}, e^{j\frac{2\pi d}{\lambda}\sin\theta_1}, 1\right]^T \tag{6.18}$$

In general these additional entries can be interpreted as the same signal coming from virtual sensor elements as shown in Fig. 6.1(a). Note that some entries are duplicate in (6.18), which means the number of effective virtual sensors cannot reach M^2. For a ULA, it is proved that the aperture can be extended to $2M-1$ elements without redundancy. These principles can also be applied to minimum redundancy arrays (MRAs) as shown in Fig. 6.1(b) where the upper bound on aperture extension is $M^2 - M + 1$ elements.

Later on authors in [118] also noted that even higher order cumulants can process more sources. They initially focused on 6th-order cumulant direction finding method and also extended the technique to an arbitrary even order $2q$ ($q \geq 1$) case, called $2q$-MUSIC methods. The steering vector for the $2q$-th order cumulants is $\mathbf{a}^{\otimes l}(\theta_i) \otimes \mathbf{a}^{*\otimes(q-l)}(\theta_i)$ where l is an arbitrary integer such that $0 \leq l \leq q$ and $\mathbf{a}^{\otimes l}(\theta_i) \triangleq \mathbf{a}(\theta_i) \otimes \mathbf{a}(\theta_i) \otimes \cdots \otimes$

$\mathbf{a}(\theta_i)$ where the number of Kronecker products is equal to $l-1$. Their study showed that 6-MUSIC has better performances than 2- and 4-MUSIC with respect to angular resolution, robustness to modeling errors, and estimation capacity, while comes along with higher variance. In particular, it has been shown that, for a ULA, the $2q$-MUSIC method can process up to $q\,(M-1)$ sources.

Note that the underlying assumption in both papers [37,118] is that signals processed have circular statistics, so only circular cumulants, defined in (5.1), have been utilised.

More recently researchers in [20] extend $2q$-MUSIC directly to noncircular signals and found that the DOFs limit can be further relaxed on the condition of the signal noncircularity. By exploiting noncircularity, the FOC can now be formed from a virtual array with more elements not only arising from the steering vector as $\mathbf{a}(\theta_i)\otimes\mathbf{a}^*(\theta_i)$ but also $\mathbf{a}^*(\theta_i)\otimes\mathbf{a}^*(\theta_i)$. This gives rise to the additional virtual array elements as shown in Fig. 6.2(a). It should be noted that $\mathbf{a}^*(\theta_i)\otimes\mathbf{a}^*(\theta_i)$ is also valid for circular signals but cannot directly couple with $\mathbf{a}(\theta_i)\otimes\mathbf{a}^*(\theta_i)$ to extend the effective array aperture due to rank deficiency. For $q=2$, the authors of [20] chose $\mathbf{C}_{x1}$, defined in (6.2) and the following two cumulant matrices

$$\check{\mathbf{C}}_{x2}=\operatorname{cum}\left\{\mathbf{x}(t),\mathbf{x}^H(t),\mathbf{x}^H(t),\mathbf{x}(t)\right\}=\check{\mathbf{A}}_2\mathbf{C}_s\check{\mathbf{A}}_2^H \tag{6.19}$$

$$\check{\mathbf{C}}_{x3}=\operatorname{cum}\left\{\mathbf{x}(t),\mathbf{x}^T(t),\mathbf{x}^H(t),\mathbf{x}(t)\right\}=\check{\mathbf{A}}_2\mathbf{C}_s\boldsymbol{\Psi}^2\mathbf{A}_1^H \tag{6.20}$$

to construct an augmented matrix as

$$\mathbf{C}_l=\begin{bmatrix}\check{\mathbf{C}}_{x2} & \check{\mathbf{C}}_{x3}\\ \check{\mathbf{C}}_{x3}^H & \mathbf{C}_{x1}\end{bmatrix} \tag{6.21}$$

$$=\begin{bmatrix}\check{\mathbf{A}}_2\\ \mathbf{A}_1\boldsymbol{\Psi}^{-2}\end{bmatrix}\mathbf{C}_s\begin{bmatrix}\check{\mathbf{A}}_2\\ \mathbf{A}_1\boldsymbol{\Psi}^{-2}\end{bmatrix}^H \tag{6.22}$$

where

$$\check{\mathbf{A}}_2=\mathbf{A}\circ\mathbf{A}^*=[\mathbf{a}(\theta_1)\otimes\mathbf{a}^*(\theta_1),\mathbf{a}(\theta_2)\otimes\mathbf{a}^*(\theta_2),\cdots,\mathbf{a}(\theta_N)\otimes\mathbf{a}^*(\theta_N)]\in\mathbb{C}^{M^2\times N}. \tag{6.23}$$

With the help of $\check{\mathbf{C}}_{x3}$ containing the noncircular information, this is equivalent to the covariance matrix from a virtual array based on $\mathbf{a}(\theta_i)\otimes\mathbf{a}^*(\theta_i)$ as well as $\mathbf{a}^*(\theta_i)\otimes\mathbf{a}^*(\theta_i)$,

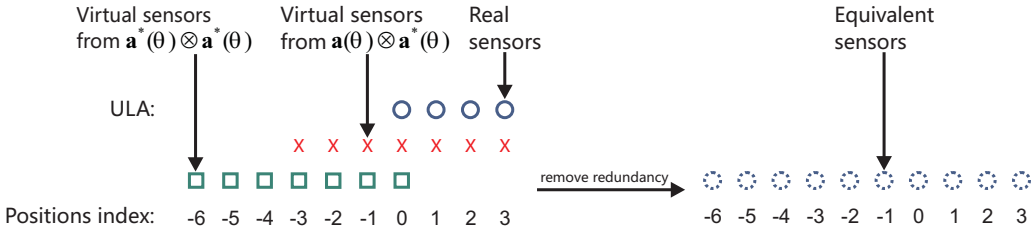

(a) Extended virtual aperture by the NC-2q method.

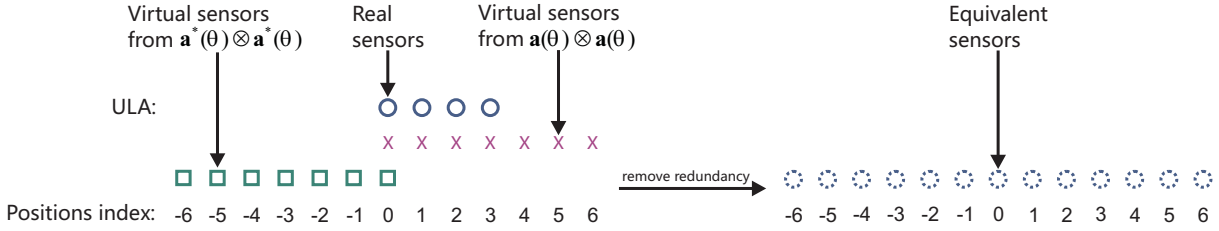

(b) Extended virtual aperture by the proposed method.

Figure 6.2. The schematics of virtual aperture extension for noncircular signals.

which has a larger array aperture as illustrated in Fig. 6.2(a). However, it is also evident that the aperture of $\mathbf{a}(\theta_i) \otimes \mathbf{a}^*(\theta_i)$ overlaps with $\mathbf{a}^*(\theta_i) \otimes \mathbf{a}^*(\theta_i)$ by M elements.

The main contribution in our approach is to avoid the overlap between virtual elements to the greatest degree. The key innovation step is coupling $\mathbf{a}(\theta_i) \otimes \mathbf{a}(\theta_i)$ with $\mathbf{a}^*(\theta_i) \otimes \mathbf{a}^*(\theta_i)$ in the FOC matrices, which appears to have been ignored in all previous research. The virtual array, resulting from $\mathbf{a}(\theta_i) \otimes \mathbf{a}(\theta_i)$ combined with $\mathbf{a}^*(\theta_i) \otimes \mathbf{a}^*(\theta_i)$, gives a larger aperture as well as more non-redundant virtual elements, as shown in Fig. 6.2(b). As a result, our method has up to $4M-3$ virtual sensors compared with $3M-2$ available from the NC-2q method. Thus, we can process up to $M-1$ additional noncircular signals.

6.2.4 Simulation Results and Discussion

In this section, we provide some numerical simulation results to illustrate the performance of the proposed DOA estimator, named as augmented NC-FOC method. We assume a ULA of 3 omnidirectional sensors spaced half a wavelength apart, receiving equal-power statistically independent BPSK signals in the presence of complex additive white Gaussian noise. NC-2q ($q = 2$) and VESPA are chosen for comparison. The accuracy of the DOA estimate is measured from 1000 Monte Carlo runs in terms of

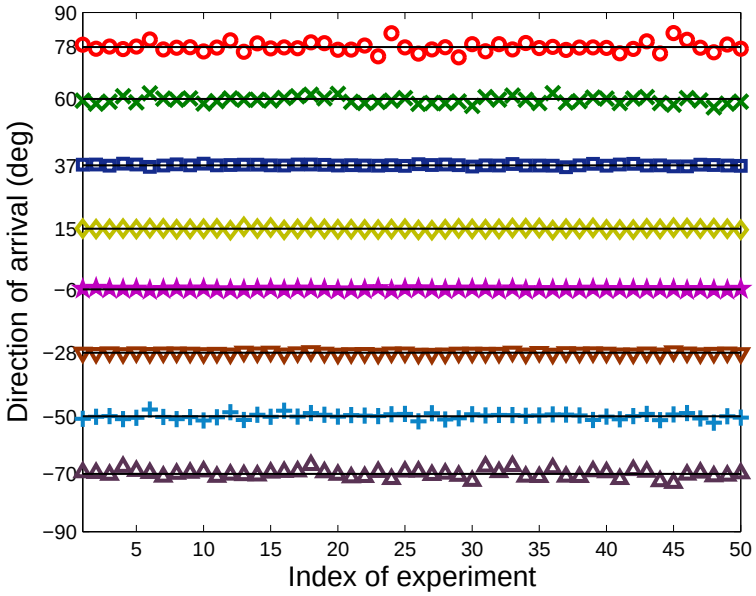

Figure 6.3. DOA estimation results of 50 runs under the maximum processing capacity. SNR $= 20$dB, the number of snapshot is 20000.

RMSE in (5.44). Additionally, to assess the overall reliability of the algorithms, the probability of resolution is defined as

$$\text{Probability of resolution} = \frac{F_r}{F} \tag{6.24}$$

where F is the number of trials, and F_r is the number of successful estimations for which the absolute DOA estimation errors are within 1°.

Estimation Capacity

The estimation capacity of augmented NC-FOC is $4(M-1) = 8$ while $3(M-1) = 6$ and $2(M-1) = 4$ for NC-2q and VESPA, respectively. First assume 8 incident signals from $[-70^\circ, -50^\circ, -28^\circ, -6^\circ, 15^\circ, 37^\circ, 60^\circ, 78^\circ]$, respectively, so NC-2$q$ and VESPA fail to resolve all the sources in this case. It is assumed that the SNR is 20dB and the number of snapshots is 20000 which is chosen to be massive to simulate the upper bond. Fig. 6.3 depicts the estimation results of 50 independent experiments by the proposed augmented NC-FOC. The solid lines indicate the true DOAs. It can be seen that each DOA can be correctly determined, and there is no failure among the 50 experiments.

Overdetermined DOA Estimation

To quantify the influence of both SNR and the number of snapshots on the performance of augmented NC-FOC, NC-2q and VESPA, we assume that two statistically independent BPSK sources $[-70°, -58°]$ with initial phases $[205.78°, 129.56°]$ have the same symbol duration. Under these assumptions, Fig. 6.4(a) exhibits, for a moderately angular separation and overdetermined case, behaviors of the three algorithms with variations of SNR from -5 to 15dB. Fig. 6.4(b) depicts how the number of snapshots affects the RMSE performance of the algorithms when the input SNR is fixed at 5dB. The RMSEs are measured from 1000 Monte Carlo realisations. It is obvious from Fig. 6.4 that the estimation accuracy of the augmented NC-FOC algorithm is better than NC-2q and VESPA for all SNRs and snapshots sizes, followed by NC-2q and then VESPA. Augmented NC-FOC has lower RMSEs than NC-2q because of its improved aperture extension capability. A similar analysis can be done for NC-2q with respect to VESPA. These results confirm that, in the overdetermined case, with moderate angular separation, augmented NC-FOC may offer better performances than NC-2q and VESPA for noncircular signals.

To quantify the influence of the SNR and number of snapshots on the reliability of the three algorithms, we consider the same simulation scenarios as above. Fig. 6.5 shows the variations of probability of resolution, as a function of SNR and the number of snapshots, for augmented NC-FOC, NC-2q and VESPA, respectively. As in Fig.6.4, augmented NC-FOC outperforms NC-2q and VESPA, and can achieve 100% probability as long as the SNR is greater than 8dB assuming 10000 snapshots or SNR $=$ 10dB for snapshot sizes larger than 4000. These results are consistent with those in Fig.6.4, and show that augmented NC-FOC has better accuracy than NC-2q and VESPA as it achieves a larger effective aperture, allowing more DOFs to be utilised in the estimation of subspaces. Similar reason explains why NC-2q performs better than VESPA.

Underdetermined DOA Estimation

To illustrate the case when the number of sources is greater than the number of sensor elements, we assume that four statistically independent BPSK sources from $[-70°, -50°,$

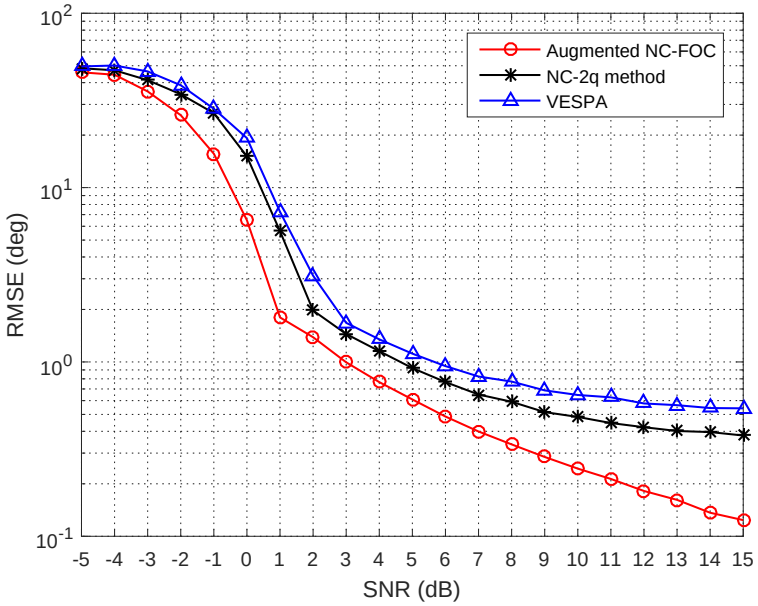

(a) RMSE versus input SNR

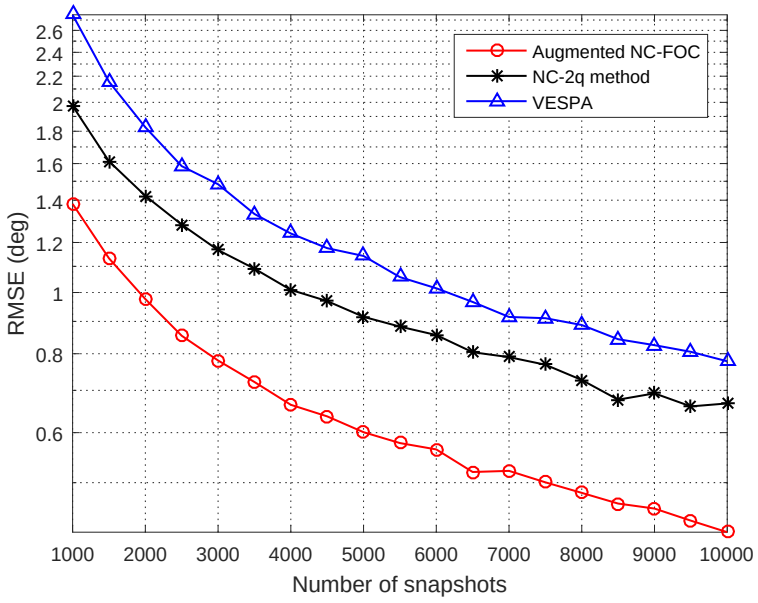

(b) RMSE versus the number of snapshots

Figure 6.4. RMSE of the DOA estimates in the overdetermined case versus (a) SNR when the number of snapshots is 5000**; (b) the number of snapshots when SNR** $= 5$**dB.** Two signals from $[\theta_1, \theta_2] = [-70°, -58°]$.

$-24°, -9°]$ with initial phases $[205.78°, 129.56°, 80.96°, 82.01°]$ have the same symbol duration. Under these assumptions, Fig. 6.6 shows the variations of the RMSE of three algorithms, as a function of SNR and the number of snapshots for the underdetermined

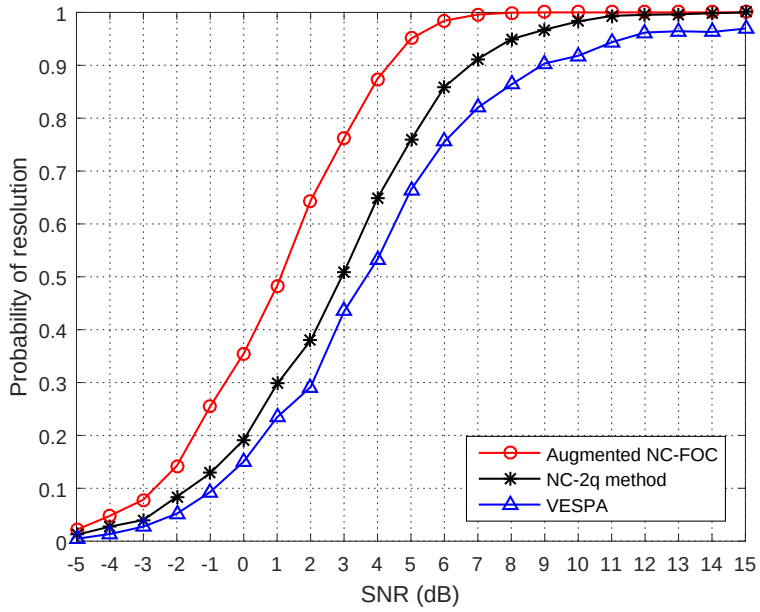

(a) Probability of resolution versus input SNR

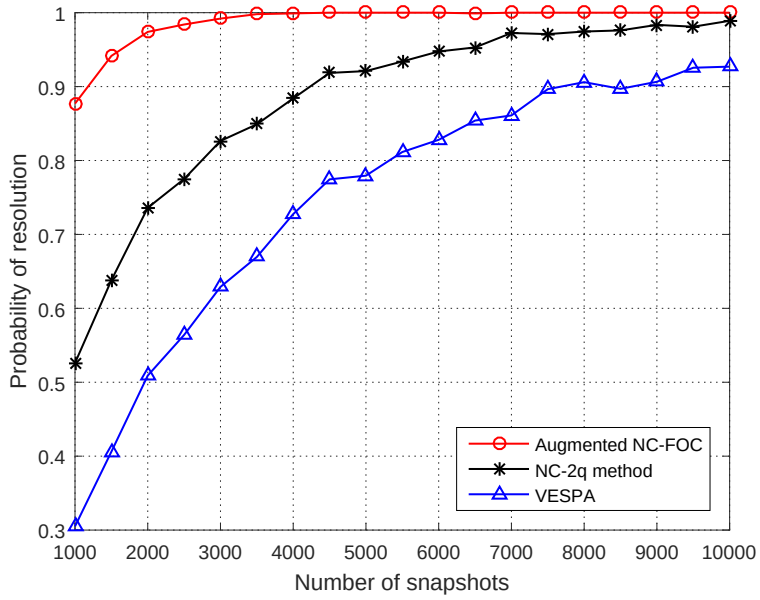

(b) Probability of resolution versus the number of snapshots

Figure 6.5. Probability of resolution in the overdetermined case versus (a) SNR when the number of snapshots is 10000; (b) the number of snapshots when SNR $= 10$dB. Two signals from $[\theta_1, \theta_2] = [-70°, -58°]$.

case. Note the good behavior of augmented NC-FOC which succeeds in estimating the DOA of the four sources when the SNR becomes greater than 4dB or the number of snapshots increase above 4000, and the poor behavior of VESPA, which has relatively

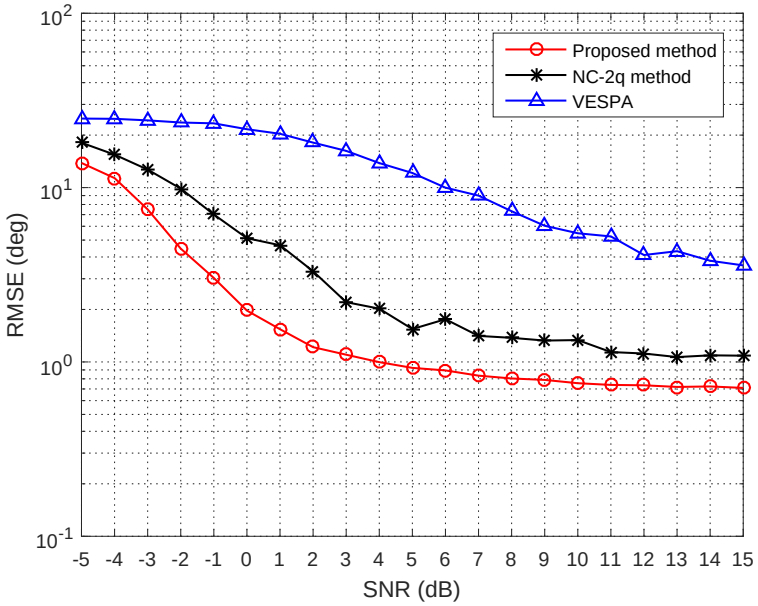

(a) RMSE versus input SNR

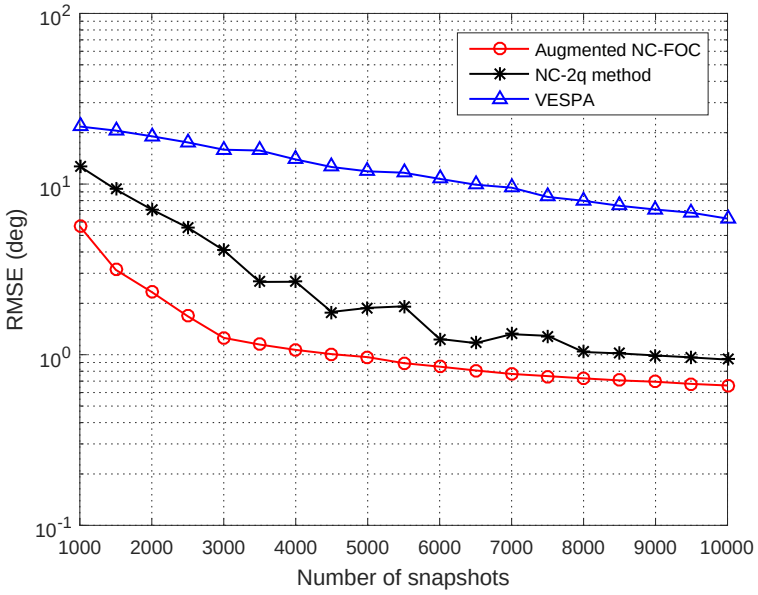

(b) RMSE versus the number of snapshots

Figure 6.6. RMSE of the DOA estimates in the underdetermined case versus (a) SNR when the number of snapshots is 5000; (b) the number of snapshots when SNR $= 5$dB. Four signals from $[\theta_1, \theta_2, \theta_3, \theta_4] = [-70°, -50°, -24°, -9°]$.

large estimation errors, since the dimensions of null space associated with augmented NC-FOC and VESPA are 5 and 1, respectively, i.e., VESPA reaches its upper bound

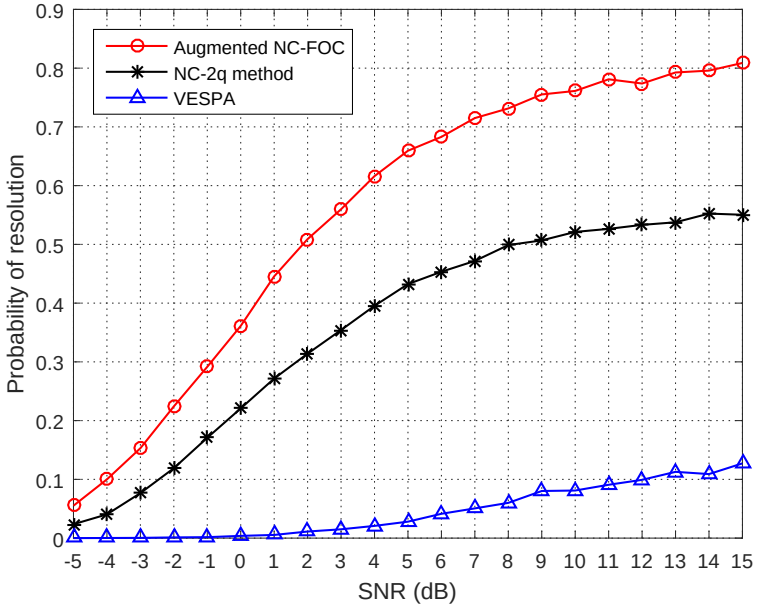

(a) Probability of resolution versus input SNR

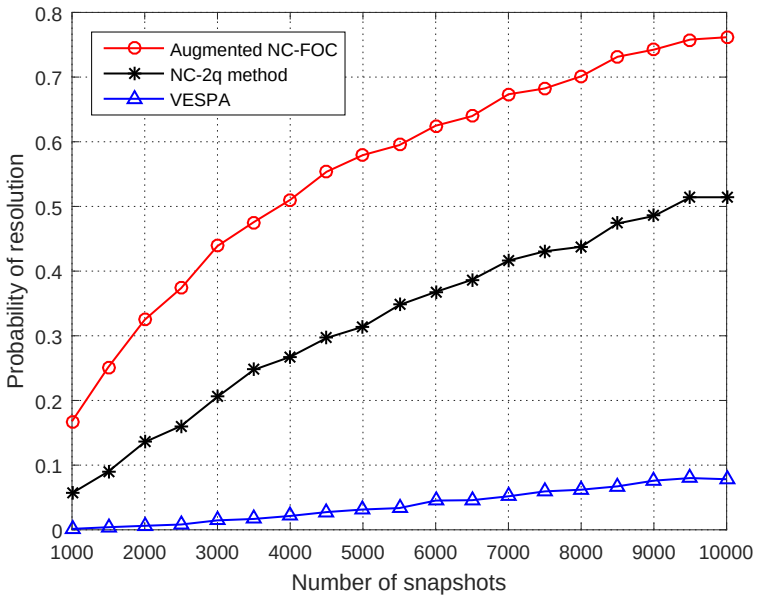

(b) Probability of resolution versus the number of snapshots

Figure 6.7. Probability of resolution in the underdetermined case versus (a) SNR when the number of snapshots is 10000**; (b) the number of snapshots when SNR** $= 10$**dB.** Four signals from $[\theta_1, \theta_2, \theta_3, \theta_4] = [-70°, -50°, -24°, -9°]$.

of estimation capacity. NC-2q outperforms VESPA but is still strictly inferior to augmented NC-FOC due to its dimension of null space being 3, half way between 1 and 5.

Finally, we examine the probability of successful estimation of the three methods by varying the SNR and total number of snapshots for the same scenario in Fig. 6.7. It can be observed that, as the SNR and snapshots size increase, the probability of successful estimation grows for each method, and augmented NC-FOC rises the quickest, followed by NC-2q, and VESPA. Evidently, although no method reaches 100% probability, the proposed one has a notable advantage over the counterparts. Even if the SNR and number of snapshots are relatively large such as 15dB and 10000, respectively, the NC-2q algorithm can barely achieve 50% success probability, while VESPA only hits about 10%, which means nine estimations in ten are not satisfactory.

6.3 Direction Finding of Noncircular Signals in the Presence of Multipath Propagation

In this section we present a novel DOA estimation method by utilising the noncircularity of the signal to separately estimate uncorrelated and coherent signals.

6.3.1 Array Model for Noncircular Signals

Consider a number of N narrowband noncircular signals impinging on a uniform linear array (ULA) with M identical omnidirectional sensors. Assume that there are K groups of coherent signals, which come from K statistically independent far-field sources $s_k(t)$ with power σ_k^2 for $k = 1, 2, \cdots, K$, and with P_k multipath signals for each source. In the k-th coherent group, the signal coming from direction θ_{kp}, $p = 1, 2, \cdots, P_k$ corresponds to the p-th multipath propagation of the source $s_k(t)$, and the complex fading coefficient is α_{kp}. Denote the total number of coherent signals as $N_c = \sum_{k=1}^{K} P_k$, and assume the remaining $N_u = N - N_c$ sources $s_k(t)$ coming from direction θ_k with power σ_k^2, $k = N_c + 1, N_c + 2, \cdots, N$, are uncorrelated to each other and also to the coherent signals. The $M \times 1$ array output vector is then given by

$$\mathbf{x}(t) = \sum_{k=1}^{K} \sum_{p=1}^{P_k} \mathbf{a}(\theta_{kp}) \alpha_{kp} e^{j\frac{\phi_k}{2}} s_{k,0}(t)$$

$$
\begin{aligned}
&+ \sum_{k=N_c+1}^{N} \mathbf{a}(\theta_k) e^{j\frac{\phi_k}{2}} s_{k,0}(t) + \mathbf{n}(t) \\
&= \mathbf{A}_c \mathbf{\Gamma} \mathbf{\Psi}_c \mathbf{s}_{c,0}(t) + \mathbf{A}_u \mathbf{\Psi}_u \mathbf{s}_{u,0}(t) + \mathbf{n}(t) \\
&= \mathbf{A} \mathbf{Y} \mathbf{\Psi} \mathbf{s}_0(t) + \mathbf{n}(t)
\end{aligned} \tag{6.25}
$$

where $\mathbf{a}(\theta) = \left[1, e^{j\frac{2\pi d}{\lambda}\sin\theta}, \cdots, e^{j\frac{2\pi(M-1)d}{\lambda}\sin\theta}\right]^T \in \mathbb{C}^M$ is the steering vector with λ and d being the wavelength of carrier signal and the spacing between adjacent elements, respectively, $\mathbf{A}_c = \left[\mathbf{A}_{c,1}, \cdots, \mathbf{A}_{c,K}\right]$ with $\mathbf{A}_{c,k} = \left[\mathbf{a}(\theta_{k1}), \cdots, \mathbf{a}(\theta_{kP_k})\right]$, $\mathbf{\Gamma} = \text{blkdiag}\{\boldsymbol{\alpha}_1, \cdots, \boldsymbol{\alpha}_K\}$ with $\boldsymbol{\alpha}_k = \left[\alpha_{k1}, \cdots, \alpha_{kP_k}\right]^T$ containing attenuation information of the k-th coherent group, $\mathbf{A}_u = [\mathbf{a}(\theta_{N_c+1}), \mathbf{a}(\theta_{N_c+2}), \cdots, \mathbf{a}(\theta_N)]$, $\mathbf{\Psi}_c = \text{diag}\left\{e^{j\frac{\phi_1}{2}}, e^{j\frac{\phi_2}{2}}, \cdots, e^{j\frac{\phi_K}{2}}\right\}$, $\mathbf{\Psi}_u = \text{diag}\left\{e^{j\frac{\phi_{K+1}}{2}}, e^{j\frac{\phi_{K+2}}{2}}, \cdots, e^{j\frac{\phi_{K+N_u}}{2}}\right\}$, $\mathbf{s}_{c,0}(t) = [s_{1,0}(t), s_{2,0}(t), \cdots, s_{K,0}(t)]^T \in \mathbb{R}^K$, $\mathbf{s}_{u,0}(t) = [s_{K+1,0}(t), s_{K+2,0}(t), \cdots, s_{K+N_u}(t)]^T \in \mathbb{R}^{N_u}$, $\mathbf{A} = [\mathbf{A}_c, \mathbf{A}_u]$, $\mathbf{Y} = \text{blkdiag}\{\mathbf{\Gamma}, \mathbf{I}\}$, $\mathbf{\Psi} = \text{blkdiag}\{\mathbf{\Psi}_c, \mathbf{\Psi}_u\}$, $\mathbf{s}_0(t) = \left[\mathbf{s}_{c,0}^T(t), \mathbf{s}_{u,0}^T(t)\right]^T$, and $\mathbf{n}(t)$ is white Gaussian noise with the power σ_n^2 for each entry. Besides, we assume that the array is calibrated, and the array manifold $\mathbf{A}$ is unambiguous, i.e., the steering vectors $\{\mathbf{a}(\theta_i)\}_{i=1}^N$ are linearly independent for any set of distinct $\{\theta_i\}_{i=1}^N$. Equivalently, the matrix $\mathbf{A}$ is of full column rank.

In order to exploit the second-order noncircularity of $\mathbf{x}(t)$ more conveniently, we construct an augmented observation vector

$$
\begin{aligned}
\tilde{\mathbf{x}}(t) &= \begin{bmatrix} \mathbf{J}\mathbf{x}^*(t) \\ \mathbf{x}(t) \end{bmatrix} \\
&= \begin{bmatrix} \mathbf{J}\mathbf{A}_c^* \mathbf{\Gamma}^* \mathbf{\Psi}_c^* \\ \mathbf{A}_c \mathbf{\Gamma} \mathbf{\Psi}_c \end{bmatrix} \mathbf{s}_{c,0}(t) + \begin{bmatrix} \mathbf{J}\mathbf{A}_u^* \mathbf{\Psi}_u^* \\ \mathbf{A}_u \mathbf{\Psi}_u \end{bmatrix} \mathbf{s}_{u,0}(t) + \begin{bmatrix} \mathbf{J}\mathbf{n}^*(t) \\ \mathbf{n}(t) \end{bmatrix} \\
&= \begin{bmatrix} \mathbf{A}_c \mathbf{\Phi}_c^{1-M} \mathbf{\Gamma}^* \mathbf{\Psi}_c^* \\ \mathbf{A}_c \mathbf{\Gamma} \mathbf{\Psi}_c \end{bmatrix} \mathbf{s}_{c,0}(t) + \begin{bmatrix} \mathbf{A}_u \mathbf{\Phi}_u^{1-M} \mathbf{\Psi}_u^* \\ \mathbf{A}_u \mathbf{\Psi}_u \end{bmatrix} \mathbf{s}_{u,0}(t) + \begin{bmatrix} \mathbf{J}\mathbf{n}^*(t) \\ \mathbf{n}(t) \end{bmatrix} \\
&= \tilde{\mathbf{A}}_c \mathbf{s}_{c,0}(t) + \tilde{\mathbf{A}}_u \mathbf{s}_{u,0}(t) + \tilde{\mathbf{n}}(t)
\end{aligned} \tag{6.26}
$$

where $\mathbf{J} \in \mathbb{R}^{M\times M}$ denotes an exchange matrix that has unity entries on the cross diagonal and zeros elsewhere, $\tilde{\mathbf{A}}_c = \left[\left(\mathbf{A}_c \mathbf{\Phi}_c^{1-M} \mathbf{\Gamma}^* \mathbf{\Psi}_c^*\right)^T, \left(\mathbf{A}_c \mathbf{\Gamma} \mathbf{\Psi}_c\right)^T\right]^T$, $\tilde{\mathbf{A}}_u = \left[\left(\mathbf{A}_u \mathbf{\Phi}_u^{1-M} \mathbf{\Psi}_u^*\right)^T, \left(\mathbf{A}_u \mathbf{\Psi}_u\right)^T\right]^T$, $\mathbf{\Phi}_c = \text{blkdiag}\{\mathbf{\Phi}_{c1}, \mathbf{\Phi}_{c2}, \cdots, \mathbf{\Phi}_{cK}\}$ with $\mathbf{\Phi}_{ck} = \text{diag}\left\{e^{j\frac{2\pi d}{\lambda}\sin\theta_{k1}}, e^{j\frac{2\pi d}{\lambda}\sin\theta_{k2}},\right.$

$\cdots, e^{j\frac{2\pi d}{\lambda}\sin\theta_{kP_k}}\Big\}$, $\mathbf{\Phi}_u = \text{diag}\Big\{e^{j\frac{2\pi d}{\lambda}\sin\theta_{N_c+1}}, e^{j\frac{2\pi d}{\lambda}\sin\theta_{N_c+2}}, \cdots, e^{j\frac{2\pi d}{\lambda}\sin\theta_N}\Big\}$, and $\tilde{\mathbf{n}}(t) = \left[\left(\mathbf{J}\mathbf{n}^*(t)\right)^T, \mathbf{n}^T(t)\right]^T$.

The covariance matrix $\tilde{\mathbf{R}}$ of the newly constructed vector $\tilde{\mathbf{x}}(t)$ is then given by

$$\tilde{\mathbf{R}} = E_t[\tilde{\mathbf{x}}(t)\tilde{\mathbf{x}}^H(t)] = \tilde{\mathbf{A}}_c\mathbf{R}_c\tilde{\mathbf{A}}_c^H + \tilde{\mathbf{A}}_u\mathbf{R}_u\tilde{\mathbf{A}}_u^H + \sigma_n^2\mathbf{I} \tag{6.27}$$

where $\mathbf{R}_c = E_t\left[\mathbf{s}_{c,0}(t)\mathbf{s}_{c,0}^H(t)\right] = \text{diag}\left\{\sigma_1^2, \sigma_2^2, \cdots, \sigma_K^2\right\}$, $\mathbf{R}_u = E_t\left[\mathbf{s}_{u,0}(t)\mathbf{s}_{u,0}^H(t)\right] = \text{diag}\left\{\sigma_{K+1}^2, \sigma_{K+2}^2, \cdots, \sigma_{K+N_u}^2\right\}$, and $\mathbf{I}$ represents a $2M \times 2M$ identity matrix. In the case of finite snapshots, the array covariance matrix can be calculated as $\hat{\mathbf{R}} = \frac{1}{L}\sum_{t=1}^{L}\tilde{\mathbf{x}}(t)\tilde{\mathbf{x}}^H(t)$, where L is the total number of snapshots.

When $K + N_u \leq 2(M-1)$, the eigen-decomposition of $\tilde{\mathbf{R}}$ is given by

$$\tilde{\mathbf{R}} = \mathbf{U}\mathbf{\Sigma}\mathbf{U}^H = \mathbf{U}_s\mathbf{\Sigma}_s\mathbf{U}_s^H + \mathbf{U}_n\mathbf{\Sigma}_n\mathbf{U}_n^H \tag{6.28}$$

where $\mathbf{\Sigma} = \text{blkdiag}\{\mathbf{\Sigma}_s, \mathbf{\Sigma}_n\} = \text{diag}\{\lambda_1, \lambda_2, \cdots, \lambda_{2M}\}$ consists of $2M$ eigenvalues satisfying $\lambda_1 \geq \cdots \geq \lambda_{K+N_u} > \lambda_{K+N_u+1} = \cdots = \lambda_{2M}$. The columns of $\mathbf{U}_s \triangleq \mathbf{U}(:, 1:K+N_u)$ are the eigenvectors corresponding to the $K+N_u$ largest eigenvalues, while the columns of $\mathbf{U}_n \triangleq \mathbf{U}(:, K+N_u+1:M)$ are the eigenvectors corresponding to the rest $2M-K-N_u$ eigenvalues. Because the columns of $\mathbf{U}_s$ span the same signal subspace as that spanned by $[\tilde{\mathbf{A}}_c, \tilde{\mathbf{A}}_u]$, there is a nonsingular matrix $\mathbf{T} \in \mathbb{C}^{(K+N_u)\times(K+N_u)}$ that makes

$$\mathbf{U}_s = \left[\tilde{\mathbf{A}}_c, \tilde{\mathbf{A}}_u\right]\mathbf{T}. \tag{6.29}$$

Here the signal subspace $\mathbf{U}_s$ can be divided into two matrices $\mathbf{U}_{s1} = \begin{bmatrix}\mathbf{U}_s(1:M-1,:)\\ \mathbf{U}_s(M+1:2M-1,:)\end{bmatrix}$, $\mathbf{U}_{s2} = \begin{bmatrix}\mathbf{U}_s(2:M,:)\\ \mathbf{U}_s(M+2:2M,:)\end{bmatrix} \in \mathbb{C}^{2(M-1)\times(K+N_u)}$. Evidently the structure in (6.29) is also valid for $\mathbf{U}_{s1}$ and $\mathbf{U}_{s2}$. If define $\tilde{\mathbf{A}}_{c1} = \begin{bmatrix}\tilde{\mathbf{A}}_c(1:M-1,:)\\ \tilde{\mathbf{A}}_c(M+1:2M-1,:)\end{bmatrix}$, $\tilde{\mathbf{A}}_{c2} = \begin{bmatrix}\tilde{\mathbf{A}}_c(2:M,:)\\ \tilde{\mathbf{A}}_c(M+2:2M,:)\end{bmatrix}$, $\tilde{\mathbf{A}}_{u1} = \begin{bmatrix}\tilde{\mathbf{A}}_u(1:M-1,:)\\ \tilde{\mathbf{A}}_u(M+1:2M-1,:)\end{bmatrix}$, $\tilde{\mathbf{A}}_{u2} = \begin{bmatrix}\tilde{\mathbf{A}}_u(2:M,:)\\ \tilde{\mathbf{A}}_u(M+2:2M,:)\end{bmatrix}$, $\tilde{\mathbf{\Gamma}} = \begin{bmatrix}\mathbf{\Phi}_c^{1-M}\mathbf{\Gamma}^*\mathbf{\Psi}_c^*\\ \mathbf{\Gamma}\mathbf{\Psi}_c\end{bmatrix}$ and

$\tilde{\mathbf{\Phi}}_c = \mathbf{I}_2 \otimes \mathbf{\Phi}_c$, one has $\left[\tilde{\mathbf{A}}_{c1}, \tilde{\mathbf{A}}_{u1}\right] = \left[\left(\mathbf{I}_2 \otimes \mathbf{A}_{c1}\right)\tilde{\mathbf{\Gamma}}, \tilde{\mathbf{A}}_{u1}\right]$. It is readily shown that $\mathbf{U}_{s1}^{+} = \left(\left[\tilde{\mathbf{A}}_{c1}, \tilde{\mathbf{A}}_{u1}\right]\mathbf{T}\right)^{+} = \mathbf{T}^{-1}\left[\left(\mathbf{I}_2 \otimes \mathbf{A}_{c1}\right)\tilde{\mathbf{\Gamma}}, \tilde{\mathbf{A}}_{u1}\right]^{+}$ as we have used the fact that $(\mathbf{BC})^{+} = \mathbf{C}^{+}\mathbf{B}^{+}$ holds on condition that $\mathbf{B}$ is of full column rank and $\mathbf{C}$ is of full row rank and, hence

$$
\begin{aligned}
\mathbf{U}_{s1}^{+}\mathbf{U}_{s2} &= \mathbf{T}^{-1}\left[\tilde{\mathbf{A}}_{c1}, \tilde{\mathbf{A}}_{u1}\right]^{+}\left[\tilde{\mathbf{A}}_{c2}, \tilde{\mathbf{A}}_{u1}\mathbf{\Phi}_u\right]\mathbf{T} \\
&= \mathbf{T}^{-1}\left(\left[\left(\mathbf{I}_2 \otimes \mathbf{A}_{c1}\right)\tilde{\mathbf{\Gamma}}, \tilde{\mathbf{A}}_{u1}\right]^{H}\left[\left(\mathbf{I}_2 \otimes \mathbf{A}_{c1}\right)\tilde{\mathbf{\Gamma}}, \tilde{\mathbf{A}}_{u1}\right]\right)^{-1} \\
&\quad \times \left[\left(\mathbf{I}_2 \otimes \mathbf{A}_{c1}\right)\tilde{\mathbf{\Gamma}}, \tilde{\mathbf{A}}_{u1}\right]^{H}\left[\left(\mathbf{I}_2 \otimes \mathbf{A}_{c1}\right)\tilde{\mathbf{\Phi}}_c\tilde{\mathbf{\Gamma}}, \tilde{\mathbf{A}}_{u1}\mathbf{\Phi}_u\right]\mathbf{T} \\
&= \mathbf{T}^{-1}\begin{bmatrix} \tilde{\mathbf{\Gamma}}^{H}\left(\mathbf{I}_2 \otimes \left(\mathbf{A}_{c1}^{H}\mathbf{A}_{c1}\right)\right)\tilde{\mathbf{\Gamma}} & \tilde{\mathbf{\Gamma}}^{H}\left(\mathbf{I}_2 \otimes \mathbf{A}_{c1}^{H}\right)\tilde{\mathbf{A}}_{u1} \\ \tilde{\mathbf{A}}_{u1}^{H}\left(\mathbf{I}_2 \otimes \mathbf{A}_{c1}\right)\tilde{\mathbf{\Gamma}} & \tilde{\mathbf{A}}_{u1}^{H}\tilde{\mathbf{A}}_{u1} \end{bmatrix}^{-1} \\
&\quad \times \begin{bmatrix} \tilde{\mathbf{\Gamma}}^{H}\left(\mathbf{I}_2 \otimes \left(\mathbf{A}_{c1}^{H}\mathbf{A}_{c1}\right)\right)\tilde{\mathbf{\Phi}}_c\tilde{\mathbf{\Gamma}} & \tilde{\mathbf{\Gamma}}^{H}\left(\mathbf{I}_2 \otimes \mathbf{A}_{c1}^{H}\right)\tilde{\mathbf{A}}_{u1}\mathbf{\Phi}_u \\ \tilde{\mathbf{A}}_{u1}^{H}\left(\mathbf{I}_2 \otimes \mathbf{A}_{c1}\right)\tilde{\mathbf{\Phi}}_c\tilde{\mathbf{\Gamma}} & \tilde{\mathbf{A}}_{u1}^{H}\tilde{\mathbf{A}}_{u1}\mathbf{\Phi}_u \end{bmatrix}\mathbf{T} \\
&= \mathbf{T}^{-1}\begin{bmatrix} \tilde{\mathbf{\Gamma}}^{H}\left(\mathbf{I}_2 \otimes \left(\mathbf{A}_{c1}^{H}\mathbf{A}_{c1}\right)\right)\tilde{\mathbf{\Gamma}} & \tilde{\mathbf{\Gamma}}^{H}\left(\mathbf{I}_2 \otimes \mathbf{A}_{c1}^{H}\right)\tilde{\mathbf{A}}_{u1} \\ \tilde{\mathbf{A}}_{u1}^{H}\left(\mathbf{I}_2 \otimes \mathbf{A}_{c1}\right)\tilde{\mathbf{\Gamma}} & \tilde{\mathbf{A}}_{u1}^{H}\tilde{\mathbf{A}}_{u1} \end{bmatrix}^{-1} \\
&\quad \times \begin{bmatrix} \tilde{\mathbf{\Gamma}}^{H}\left(\mathbf{I}_2 \otimes \left(\mathbf{A}_{c1}^{H}\mathbf{A}_{c1}\right)\right)\tilde{\mathbf{\Gamma}} & \tilde{\mathbf{\Gamma}}^{H}\left(\mathbf{I}_2 \otimes \mathbf{A}_{c1}^{H}\right)\tilde{\mathbf{A}}_{u1} \\ \tilde{\mathbf{A}}_{u1}^{H}\left(\mathbf{I}_2 \otimes \mathbf{A}_{c1}\right)\tilde{\mathbf{\Gamma}} & \tilde{\mathbf{A}}_{u1}^{H}\tilde{\mathbf{A}}_{u1} \end{bmatrix}\begin{bmatrix} \mathbf{F}_1 & \mathbf{0}_{K\times N_u} \\ \mathbf{F}_2 & \mathbf{\Phi}_u \end{bmatrix}\mathbf{T} \\
&= \mathbf{T}^{-1}\begin{bmatrix} \mathbf{F}_1 & \mathbf{0}_{K\times N_u} \\ \mathbf{F}_2 & \mathbf{\Phi}_u \end{bmatrix}\mathbf{T}
\end{aligned}
\tag{6.30}
$$

where

$$
\begin{aligned}
\begin{bmatrix} \mathbf{F}_1 \\ \mathbf{F}_2 \end{bmatrix} &= \begin{bmatrix} \tilde{\mathbf{\Gamma}}^{H}\left(\mathbf{I}_2 \otimes \left(\mathbf{A}_{c1}^{H}\mathbf{A}_{c1}\right)\right)\tilde{\mathbf{\Gamma}} & \tilde{\mathbf{\Gamma}}^{H}\left(\mathbf{I}_2 \otimes \mathbf{A}_{c1}^{H}\right)\tilde{\mathbf{A}}_{u1} \\ \tilde{\mathbf{A}}_{u1}^{H}\left(\mathbf{I}_2 \otimes \mathbf{A}_{c1}\right)\tilde{\mathbf{\Gamma}} & \tilde{\mathbf{A}}_{u1}^{H}\tilde{\mathbf{A}}_{u1} \end{bmatrix}^{-1} \\
&\quad \times \begin{bmatrix} \tilde{\mathbf{\Gamma}}^{H}\left(\mathbf{I}_2 \otimes \left(\mathbf{A}_{c1}^{H}\mathbf{A}_{c1}\right)\right)\tilde{\mathbf{\Phi}}_c\tilde{\mathbf{\Gamma}} \\ \tilde{\mathbf{A}}_{u1}^{H}\left(\mathbf{I}_2 \otimes \mathbf{A}_{c1}\right)\tilde{\mathbf{\Phi}}_c\tilde{\mathbf{\Gamma}} \end{bmatrix}.
\end{aligned}
\tag{6.31}
$$

This result shows that $\mathbf{U}_{s1}^{+}\mathbf{U}_{s2}$ is *similar* to $\begin{bmatrix} \mathbf{F}_1 & \mathbf{0}_{K\times N_u} \\ \mathbf{F}_2 & \mathbf{\Phi}_u \end{bmatrix}$. Hence, the eigenvalues of these two matrices are identical to each other.

By definition, an eigenvalue η of the block matrix $\begin{bmatrix} \mathbf{F}_1 & \mathbf{0}_{K\times N_u} \\ \mathbf{F}_2 & \mathbf{\Phi}_u \end{bmatrix} \in \mathbb{C}^{(K+N_u)\times(K+N_u)}$ satisfies $\det\left\{\begin{bmatrix} \mathbf{F}_1 & \mathbf{0}_{K\times N_u} \\ \mathbf{F}_2 & \mathbf{\Phi}_u \end{bmatrix} - \eta\mathbf{I}_{K+N_u}\right\} = \det\left\{\begin{bmatrix} \mathbf{F}_1 - \eta\mathbf{I}_K & \mathbf{0}_{K\times N_u} \\ \mathbf{F}_2 & \mathbf{\Phi}_u - \eta\mathbf{I}_{N_u} \end{bmatrix}\right\} = 0$. Using the identity $\det\left\{\begin{bmatrix} \mathbf{B}_{1,1} & \mathbf{0}_{m\times n} \\ \mathbf{B}_{2,1} & \mathbf{B}_{2,2} \end{bmatrix}\right\} = \det\{\mathbf{B}_{1,1}\}\det\{\mathbf{B}_{2,2}\}$ where $\mathbf{B}_{1,1} \in \mathbb{C}^{m\times m}$, $\mathbf{B}_{2,1} \in \mathbb{C}^{n\times m}$, and $\mathbf{B}_{2,2} \in \mathbb{C}^{n\times n}$, one has $\det\left\{\begin{bmatrix} \mathbf{F}_1 & \mathbf{0}_{K\times N_u} \\ \mathbf{F}_2 & \mathbf{\Phi}_u \end{bmatrix} - \eta\mathbf{I}_{K+N_u}\right\} = \det\{\mathbf{F}_1 - \eta\mathbf{I}_K\}$ $\times\det\{\mathbf{\Phi}_u - \eta\mathbf{I}_{N_u}\} = 0$. Thus we say that if η is an eigenvalue of $\begin{bmatrix} \mathbf{F}_1 & \mathbf{0}_{K\times N_u} \\ \mathbf{F}_2 & \mathbf{\Phi}_u \end{bmatrix}$, then either $\det\{\mathbf{F}_1 - \eta\mathbf{I}_K\} = 0$ or $\det\{\mathbf{\Phi}_u - \eta\mathbf{I}_{N_u}\} = 0$ and, hence η is also an eigenvalue of $\mathbf{F}_1$ or $\mathbf{\Phi}_u$. It is concluded that the N_u diagonal entries of $\mathbf{\Phi}_u$ are included in the non-zero eigenvalues of $\begin{bmatrix} \mathbf{F}_1 & \mathbf{0}_{K\times N_u} \\ \mathbf{F}_2 & \mathbf{\Phi}_u \end{bmatrix}$. However, we can obtain the K eigenvalues associated with the K groups of the coherent noncircular signals in addition to the eigenvalues of the N_u uncorrelated noncircular signals. As a consequence, it is necessary to provide a more robust criterion to identify the DOA of uncorrelated noncircular signals from the false ones.

Firstly, if the eigenvalues of $\mathbf{U}_{s1}^{+}\mathbf{U}_{s2}$ are denoted as $\{\eta_k\}_{k=1}^{K+N_u}$, all DOA estimate candidates, $\hat{\theta}_k$, of uncorrelated noncircular signals can be obtained by

$$\hat{\theta}_k = \arcsin\left(\frac{\lambda}{2\pi d}\arg(\eta_k)\right), \quad k = 1, 2, \cdots, K+N_u. \tag{6.32}$$

Then, let us define a spatial spectrum function

$$f(\theta,\phi) \triangleq \tilde{\mathbf{a}}(\theta,\phi)^H\mathbf{U}_n\mathbf{U}_n^H\tilde{\mathbf{a}}(\theta,\phi) \tag{6.33}$$

where

$$\tilde{\mathbf{a}}(\theta,\phi) = \begin{bmatrix} \mathbf{a}(\theta)e^{j\frac{2\pi(1-M)d}{\lambda}\sin\theta}e^{-j\frac{\phi}{2}} \\ \mathbf{a}(\theta)e^{j\frac{\phi}{2}} \end{bmatrix}. \tag{6.34}$$

To separate parameterisation for noncircular phase and DOA, (6.34) can be rewritten as

$$\begin{aligned}\tilde{\mathbf{a}}(\theta,\phi) &= \begin{bmatrix}\mathbf{a}(\theta)e^{j\frac{2\pi(1-M)d}{\lambda}\sin\theta} & \\ & \mathbf{a}(\theta)\end{bmatrix}\begin{bmatrix}e^{-j\frac{\phi}{2}}\\ e^{j\frac{\phi}{2}}\end{bmatrix}\\ &= \mathbf{E}(\theta)\mathbf{c}(\phi)\end{aligned} \tag{6.35}$$

where $\mathbf{E}(\theta) \triangleq \text{blkdiag}\left\{\mathbf{a}(\theta)e^{j\frac{2\pi(1-M)d}{\lambda}\sin\theta}, \mathbf{a}(\theta)\right\} \in \mathbb{C}^{2M\times 2}$ and $\mathbf{c}(\phi) \triangleq \left[e^{-j\frac{\phi}{2}}, e^{j\frac{\phi}{2}}\right]^T$. Then, substituting (6.35) into (6.33), one gets

$$f(\theta,\phi) = \mathbf{c}^H(\phi)\mathbf{M}(\theta)\mathbf{c}(\phi) \tag{6.36}$$

where

$$\mathbf{M}(\theta) = \mathbf{E}(\theta)^H\mathbf{U}_n\mathbf{U}_n^H\mathbf{E}(\theta). \tag{6.37}$$

The function $f(\theta,\phi)$ will only go to 0 at the DOAs and noncircularity phases of the uncorrelated sources because of the orthogonality between the signal subspace and noise subspace. This indicates that the DOA estimates of the uncorrelated signals can thus be obtained by checking which of the $\{\hat{\theta}_k\}_{k=1}^{K+N_u}$ make (6.36) equal to 0. Until now, we have not obtained the noncircularity phase estimates, and this motivates us to investigate whether we can identify the true DOA estimates of uncorrelated signals from $\mathbf{M}(\theta)$ which does not include any information of noncircularity phase.

We now show how to verify the true DOA estimates of uncorrelated signals based on the determinant or the smallest eigenvalue of $\mathbf{M}(\theta)$. One should first note that since $\mathbf{c} \neq \mathbf{0}$, (6.36) can hold true only if the matrix $\mathbf{M}(\theta)$ is rank deficient or, equivalently, its determinant (as well as its smallest eigenvalue) is equal to zero [161–163]. Secondly $\mathbf{M}(\theta) \in \mathbb{C}^{2\times 2}$ is of full rank for the coherent signal groups and rank deficient for the uncorrelated signals. It can be found that the dimension of $\mathbf{E}(\theta)^H\mathbf{U}_n$ is $2 \times (2M - K - N_u)$. Because of the condition $K + N_u \leq 2(M-1)$, i.e., $2 \leq (2M - K - N_u)$, the matrix $\mathbf{E}(\theta)^H\mathbf{U}_n$, in general, is of full row rank and $\mathbf{M}(\theta)$ is of full rank. However, due to the orthogonality between the signal subspace spanned by $\tilde{\mathbf{A}}_u$ and the noise subspace spanned by $\mathbf{U}_n$, which only holds for the uncorrelated signals, when θ coincides with

any one of the N_u desired DOAs of uncorrelated signals, i.e., $\theta = \hat{\theta}_k$ ($k = K+1, K+2, \cdots, K+N_u$), the function $f(\theta, \phi)$ in (6.36) becomes zero. In the finite snapshots case, the true DOA estimates of the N_u uncorrelated signals correspond to the minima of the verification equation $\det\{\mathbf{M}(\hat{\theta})\}$ which remains large for the remaining K false estimates. In this way, the true estimates can be selected and the false ones can be effectively eliminated.

The noncircularity phases of the uncorrelated signals are subsequently given by the minima of (6.33). By partitioning $\mathbf{U}_n$ into the two submatrices with the same dimension $\mathbf{U}_{n1} = \mathbf{U}_n(1:M,:)$, $\mathbf{U}_{n2} = \mathbf{U}_n(M+1:2M,:)$, and setting the partial derivative of (6.33) to zero, i.e., $\frac{\partial f(\theta,\phi)}{\partial \theta} = 0$, we find that when

$$e^{j\phi} = -\frac{\mathbf{a}^H(\theta)\mathbf{U}_{n2}\mathbf{U}_{n1}^H\mathbf{a}(\theta)e^{j\frac{2\pi(1-M)d}{\lambda}\sin\theta}}{\left|\mathbf{a}^H(\theta)\mathbf{U}_{n2}\mathbf{U}_{n1}^H\mathbf{a}(\theta)e^{j\frac{2\pi(1-M)d}{\lambda}\sin\theta}\right|}, \tag{6.38}$$

(6.33) will achieve its minima. Once the true DOA estimates of uncorrelated signals are obtained, the corresponding noncircularity phases will be estimated accordingly.

DOA Estimation of the Coherent Noncircular Signals

Next we will deal with the coherent noncircular signals. The coherent signal DOAs are estimated by first removing the uncorrelated signals from the the covariance matrix $\tilde{\mathbf{R}}$ and then resolving the coherent signals by performing spatial smoothing on the eigenvectors of the resulting covariance matrix for rank restoration. In this way, the proposed method separates the two types of signals and provides improved estimation accuracy.

After obtaining the DOA and noncircularity phase estimates of the uncorrelated signals, one can construct the following vector

$$\mathbf{b}(\theta,\phi) = \begin{bmatrix} \mathbf{a}(\theta)e^{j\frac{2\pi(1-M)d}{\lambda}\sin\theta} \\ \mathbf{a}(\theta)e^{j\phi} \end{bmatrix} = e^{j\frac{\phi}{2}}\tilde{\mathbf{a}}(\theta,\phi) \tag{6.39}$$

which has the same subspace as $\tilde{\mathbf{a}}(\theta,\phi)$. Performing the compact singular value decomposition (SVD) of $\bar{\mathbf{A}} \triangleq \left[\tilde{\mathbf{A}}_c, \tilde{\mathbf{A}}_u\right] = \left[\mathbf{E}, \tilde{\mathbf{a}}(\theta_k,\phi_k)\right], k = K+1, \cdots, K+N_u$, where $\mathbf{E}$

is the remaining part of $\bar{\mathbf{A}}$ excluding $\tilde{\mathbf{a}}(\theta_k, \phi_k)$, we have

$$\bar{\mathbf{A}} = \sum_{i=1}^{K+N_u} \eta_i \mathbf{u}_i \mathbf{v}_i^H \tag{6.40}$$

where $\{\eta_i\}_{i=1}^{K+N_u}, \{\mathbf{u}_i\}_{i=1}^{K+N_u}, \{\mathbf{v}_i\}_{i=1}^{K+N_u}$ are the non-zero singular values, left singular vectors, and right singular vectors, respectively. Accordingly, the pseudo-inverse of $\bar{\mathbf{A}}$ is

$$\bar{\mathbf{A}}^+ = \sum_{i=1}^{K+N_u} \eta_i^{-1} \mathbf{v}_i \mathbf{u}_i^H. \tag{6.41}$$

Since $\tilde{\mathbf{R}} - \sigma_n^2 \mathbf{I} = \bar{\mathbf{A}} \mathbf{R}_0 \bar{\mathbf{A}}^H$ where $\mathbf{R}_0 = \text{diag}\left\{\sigma_1^2, \sigma_2^2, \cdots, \sigma_{K+N_u}^2\right\}$, where σ_n^2 can be estimated as the mean of the $2M - K - N_u$ smallest eigenvalues of $\tilde{\mathbf{R}}$, and $\mathbf{b}(\theta, \phi) = e^{j\frac{\phi}{2}} \tilde{\mathbf{a}}(\theta, \phi)$, this allows us to expand the term

$$\begin{aligned} &\mathbf{b}^H(\theta_k, \phi_k) \left(\tilde{\mathbf{R}} - \sigma_n^2 \mathbf{I}\right)^+ \mathbf{b}(\theta_k, \phi_k) \\ &= \tilde{\mathbf{a}}^H(\theta_k, \phi_k) \left(\bar{\mathbf{A}}^H\right)^+ \mathbf{R}_0^{-1} \bar{\mathbf{A}}^+ \tilde{\mathbf{a}}(\theta_k, \phi_k). \end{aligned} \tag{6.42}$$

Note that $\tilde{\mathbf{a}}(\theta_k, \phi_k) = \bar{\mathbf{A}} \mathbf{e}_k$ where $\mathbf{e}_k \in \mathbb{R}^{K+N_u}$ is a column vector with 1 at the k-th entry and 0 elsewhere, then substituting back to (6.42) gives

$$\begin{aligned} &\mathbf{b}^H(\theta_k, \phi_k) \left(\tilde{\mathbf{R}} - \sigma_n^2 \mathbf{I}\right)^+ \mathbf{b}(\theta_k, \phi_k) \\ &= \left(\sum_{i=1}^{K+N_u} \eta_i^{-1} \mathbf{v}_i \mathbf{u}_i^H \sum_{i=1}^{K+N_u} \eta_i \mathbf{u}_i \mathbf{v}_i^H \mathbf{e}_k\right)^H \mathbf{R}_0^{-1} \\ &\quad \times \sum_{i=1}^{K+N_u} \eta_i^{-1} \mathbf{v}_i \mathbf{u}_i^H \sum_{i=1}^{K+N_u} \eta_i \mathbf{u}_i \mathbf{v}_i^H \mathbf{e}_k \\ &= \mathbf{e}_k^H \mathbf{R}_0^{-1} \mathbf{e}_k \\ &= \mathbf{e}_k^H \text{diag}\{\sigma_1^{-2}, \sigma_2^{-2}, \cdots, \sigma_{K+N_u}^{-2}\} \mathbf{e}_k \\ &= \sigma_k^{-2}. \end{aligned} \tag{6.43}$$

Therefore, the power of the uncorrelated signals can be estimated by

$$\begin{aligned} \sigma_k^2 = \frac{1}{\mathbf{b}^H(\theta_k, \phi_k) \left(\tilde{\mathbf{R}} - \sigma_n^2 \mathbf{I}\right)^+ \mathbf{b}(\theta_k, \phi_k)}, \\ k = K+1, \cdots, K+N_u. \end{aligned} \tag{6.44}$$

From (6.44), we define $\mathbf{R}_{su} \triangleq \text{diag}\{\sigma^2_{K+1}, \cdots, \sigma^2_{K+N_u}\}$ and $\mathbf{B}_u \triangleq [\mathbf{b}(\theta_{K+1}, \phi_{K+1}), \cdots, \mathbf{b}(\theta_{K+N_u}, \phi_{K+N_u})] = \tilde{\mathbf{A}}_u \boldsymbol{\Psi}_u$. Given $\mathbf{B}_u$ and $\mathbf{R}_{su}$, we can form a matrix $\mathbf{R}_{xc}$ as

$$\begin{aligned}\mathbf{R}_{xc} &\triangleq \tilde{\mathbf{R}} - \mathbf{B}_u \mathbf{R}_{su} \mathbf{B}_u^H - \sigma_n^2 \mathbf{I} \\ &= \tilde{\mathbf{R}} - \tilde{\mathbf{A}}_u \boldsymbol{\Psi}_u \mathbf{R}_{su} \boldsymbol{\Psi}_u^H \tilde{\mathbf{A}}_u^H - \sigma_n^2 \mathbf{I} \\ &= \tilde{\mathbf{R}} - \tilde{\mathbf{A}}_u \mathbf{R}_{su} \tilde{\mathbf{A}}_u^H - \sigma_n^2 \mathbf{I} \\ &= \tilde{\mathbf{A}}_c \mathbf{R}_c \tilde{\mathbf{A}}_c^H. \end{aligned} \tag{6.45}$$

Clearly, $\mathbf{R}_{xc}$ only contains the information of coherent signals.

After removing the uncorrelated source components from $\tilde{\mathbf{R}}$, the rank of the remaining coherent signals in $\mathbf{R}_{xc}$ is restored using a spatial smoothing technique.

Rather than the commonly used FBSS technique in [24], we carry out spatial smoothing on the eigenvectors and tailor them to fit the noncircular signal case for two reasons. Firstly, the standard FBSS, only averages the covariance matrices of the subarrays but ignores the information between subarrays, like cross-correlation, to resolve the coherent signals, which limits estimation performance, especially at low SNRs and few snapshots [150]; Secondly, the subarrays, if directly partitioned by the standard FBSS, are not completely identical to each other due to the different noncircularity effects working on the whole array as in (6.26), compared with that in (6.25).

Performing the eigen-decomposition of $\mathbf{R}_{xc}$, we have

$$\mathbf{R}_{xc} = \mathbf{U}_c \boldsymbol{\Sigma}_c \mathbf{U}_c^H \tag{6.46}$$

where $\mathbf{U}_c \in \mathbb{C}^{2M \times K}$ is a matrix whose columns are the eigenvectors corresponding to the K largest eigenvalues. Combining (6.45) and (6.46), the columns of $\mathbf{U}_c$ span the K dimensional subspace of $\tilde{\mathbf{A}}_c$, and it can be shown that $\mathbf{U}_c = \tilde{\mathbf{A}}_c \mathbf{T}$ where $\mathbf{T} \in \mathbb{C}^{K \times K}$ is a nonsingular matrix. Then we can readily verify that $\mathbf{u}_i = \tilde{\mathbf{A}}_c \boldsymbol{\beta}_i$ where $\mathbf{u}_i$ is the i-th eigenvector and $\boldsymbol{\beta}_i = [\beta_{i1}, \beta_{i2}, \cdots, \beta_{iK}]^T \in \mathbb{C}^K$ is the i-th column vector of $\mathbf{T}$. Here, we divide the i-th eigenvector and construct multiple $2m \times 1$ subvectors as

$$\mathbf{u}_{ir} = \begin{bmatrix} \mathbf{u}_i(r : r+m-1) \\ \mathbf{u}_i(r+M : r+m-1+M) \end{bmatrix} \tag{6.47}$$

and then $q = M - m + 1$ subvectors become available. Since $\mathbf{u}_i = \tilde{\mathbf{A}}_c \boldsymbol{\beta}_i$, one has $\mathbf{u}_i(r : r+m-1) = \mathbf{B}_c \boldsymbol{\Phi}_c^{r-M} \boldsymbol{\Gamma}^* \boldsymbol{\Psi}_c^* \boldsymbol{\beta}_i$, $\mathbf{u}_i(r+M : r+m-1+M) = \mathbf{B}_c \boldsymbol{\Phi}_c^{r-1} \boldsymbol{\Gamma} \boldsymbol{\Psi}_c \boldsymbol{\beta}_i$ where $\mathbf{B}_c = \mathbf{F}\left[\mathbf{A}_{c,1}, \mathbf{A}_{c,2}, ..., \mathbf{A}_{c,K}\right]$ with $\mathbf{F} = \left[\mathbf{I}_{(M-q+1)}, \mathbf{0}_{(M-q+1)\times(q-1)}\right]$. The spatial smoothed covariance matrix is given by

$$
\begin{aligned}
\mathbf{R}_{ss} &= \frac{1}{q}\sum_{i=1}^{K}\sum_{r=1}^{q} \mathbf{u}_{ir}\mathbf{u}_{ir}^H \\
&= \frac{1}{q}\sum_{i=1}^{K}\sum_{r=1}^{q} \begin{bmatrix} \mathbf{B}_c \boldsymbol{\Phi}_c^{r-M} \boldsymbol{\Gamma}^* \boldsymbol{\Psi}_c^* \\ \mathbf{B}_c \boldsymbol{\Phi}_c^{r-1} \boldsymbol{\Gamma} \boldsymbol{\Psi}_c \end{bmatrix} \boldsymbol{\beta}_i \boldsymbol{\beta}_i^H \begin{bmatrix} \mathbf{B}_c \boldsymbol{\Phi}_c^{r-M} \boldsymbol{\Gamma}^* \boldsymbol{\Psi}_c^* \\ \mathbf{B}_c \boldsymbol{\Phi}_c^{r-1} \boldsymbol{\Gamma} \boldsymbol{\Psi}_c \end{bmatrix}^H \\
&= \frac{1}{q}\sum_{r=1}^{q} \begin{bmatrix} \mathbf{B}_c \boldsymbol{\Phi}_c^{r-M} \boldsymbol{\Gamma}^* \boldsymbol{\Psi}_c^* \\ \mathbf{B}_c \boldsymbol{\Phi}_c^{r-1} \boldsymbol{\Gamma} \boldsymbol{\Psi}_c \end{bmatrix} \left[\boldsymbol{\beta}_1, \cdots, \boldsymbol{\beta}_K\right] \\
&\quad \times \left[\boldsymbol{\beta}_1, \cdots, \boldsymbol{\beta}_K\right]^H \begin{bmatrix} \mathbf{B}_c \boldsymbol{\Phi}_c^{r-M} \boldsymbol{\Gamma}^* \boldsymbol{\Psi}_c^* \\ \mathbf{B}_c \boldsymbol{\Phi}_c^{r-1} \boldsymbol{\Gamma} \boldsymbol{\Psi}_c \end{bmatrix}^H \\
&= \frac{1}{q}\sum_{r=1}^{q} \begin{bmatrix} \mathbf{B}_c \boldsymbol{\Phi}_c^{r-M} \boldsymbol{\Gamma}^* \boldsymbol{\Psi}_c^* \\ \mathbf{B}_c \boldsymbol{\Phi}_c^{r-1} \boldsymbol{\Gamma} \boldsymbol{\Psi}_c \end{bmatrix} \mathbf{T}\mathbf{T}^H \begin{bmatrix} \mathbf{B}_c \boldsymbol{\Phi}_c^{r-M} \boldsymbol{\Gamma}^* \boldsymbol{\Psi}_c^* \\ \mathbf{B}_c \boldsymbol{\Phi}_c^{r-1} \boldsymbol{\Gamma} \boldsymbol{\Psi}_c \end{bmatrix}^H .
\end{aligned} \tag{6.48}
$$

Next we examine whether the rank of $\mathbf{R}_{ss}$ has been restored sufficiently to resolve N_c coherent noncircular signals.

Proposition 3. *When $2m \geq N_c + 1$ and $q \geq P_{max}$, rank $(\boldsymbol{R}_{ss}) = N_c$ for K groups of coherent noncircular signals, where $P_{max} = max\{P_1, P_2, \cdots, P_K\}$.*

Proof: Under the assumptions that $\mathbf{A}_c$ is unambiguous and $m \geq N_c + 1$, the rank of the Vandermonde matrix $\mathbf{B}_c$ is given by $\text{rank}(\mathbf{B}_c) = N_c$. If we define

$$
\mathbf{G}_i = \frac{1}{q}\sum_{r=1}^{q} \begin{bmatrix} \mathbf{B}_c \boldsymbol{\Phi}_c^{r-M} \boldsymbol{\Gamma}^* \boldsymbol{\Psi}_c^* \\ \mathbf{B}_c \boldsymbol{\Phi}_c^{r-1} \boldsymbol{\Gamma} \boldsymbol{\Psi}_c \end{bmatrix} \boldsymbol{\beta}_i \boldsymbol{\beta}_i^H \begin{bmatrix} \mathbf{B}_c \boldsymbol{\Phi}_c^{r-M} \boldsymbol{\Gamma}^* \boldsymbol{\Psi}_c^* \\ \mathbf{B}_c \boldsymbol{\Phi}_c^{r-1} \boldsymbol{\Gamma} \boldsymbol{\Psi}_c \end{bmatrix}^H \tag{6.49}
$$

it can be rewritten as

$$
\begin{aligned}
\mathbf{G}_i = &\begin{bmatrix} \mathbf{B}_c \boldsymbol{\Phi}_c^{1-M} \boldsymbol{\Gamma}^* \boldsymbol{\Psi}_c^* \boldsymbol{\beta}_i, \mathbf{B}_c \boldsymbol{\Phi}_c^{2-M} \boldsymbol{\Gamma}^* \boldsymbol{\Psi}_c^* \boldsymbol{\beta}_i, \cdots, \mathbf{B}_c \boldsymbol{\Phi}_c^{q-M} \boldsymbol{\Gamma}^* \boldsymbol{\Psi}_c^* \boldsymbol{\beta}_i \\ \mathbf{B}_c \boldsymbol{\Gamma} \boldsymbol{\Psi}_c \boldsymbol{\beta}_i, \mathbf{B}_c \boldsymbol{\Phi}_c \boldsymbol{\Gamma} \boldsymbol{\Psi}_c \boldsymbol{\beta}_i, \cdots, \mathbf{B}_c \boldsymbol{\Phi}_c^{q-1} \boldsymbol{\Gamma} \boldsymbol{\Psi}_c \boldsymbol{\beta}_i \end{bmatrix} \\
&\times \begin{bmatrix} \mathbf{B}_c \boldsymbol{\Phi}_c^{1-M} \boldsymbol{\Gamma}^* \boldsymbol{\Psi}_c^* \boldsymbol{\beta}_i, \mathbf{B}_c \boldsymbol{\Phi}_c^{2-M} \boldsymbol{\Gamma}^* \boldsymbol{\Psi}_c^* \boldsymbol{\beta}_i, \cdots, \mathbf{B}_c \boldsymbol{\Phi}_c^{q-M} \boldsymbol{\Gamma}^* \boldsymbol{\Psi}_c^* \boldsymbol{\beta}_i \\ \mathbf{B}_c \boldsymbol{\Gamma} \boldsymbol{\Psi}_c \boldsymbol{\beta}_i, \mathbf{B}_c \boldsymbol{\Phi}_c \boldsymbol{\Gamma} \boldsymbol{\Psi}_c \boldsymbol{\beta}_i, \cdots, \mathbf{B}_c \boldsymbol{\Phi}_c^{q-1} \boldsymbol{\Gamma} \boldsymbol{\Psi}_c \boldsymbol{\beta}_i \end{bmatrix}^H
\end{aligned}
$$

$$= \begin{bmatrix} \mathbf{B}_c \boldsymbol{\Phi}_c^{1-M} \mathbf{D}^* \mathbf{H}_i \\ \mathbf{B}_c \mathbf{D} \mathbf{H}_i \end{bmatrix} \mathbf{V}\mathbf{V}^H \begin{bmatrix} \mathbf{B}_c \boldsymbol{\Phi}_c^{1-M} \mathbf{D}^* \mathbf{H}_i \\ \mathbf{B}_c \mathbf{D} \mathbf{H}_i \end{bmatrix}^H$$
$$\triangleq \tilde{\mathbf{B}}_{ci} \mathbf{V}\mathbf{V}^H \tilde{\mathbf{B}}_{ci}^H \tag{6.50}$$

where $\mathbf{D} = \text{diag}\{d_{11}, \cdots, d_{1P_1}, \cdots, d_{K1}, \cdots, d_{KP_K}\}$ with $d_{kp_k} = \alpha_{kp_k} e^{j\frac{\phi_k}{2}}$, $\mathbf{H}_i = \text{blkdiag}\{\mathbf{h}_{i1}, \mathbf{h}_{i2}, \cdots, \mathbf{h}_{iK}\}$ with $\mathbf{h}_{ik} = \text{diag}\{\beta_{ik}, \beta_{ik}, \cdots, \beta_{ik}\} \in \mathbb{C}^{P_k \times P_k}$, and $\mathbf{V} = \mathbf{A}_c^T(1:q, 1:N_c)$. It is easy to identify that $\text{rank}(\boldsymbol{\Phi}_c) = \text{rank}(\mathbf{D}) = \text{rank}(\mathbf{H}_i) = N_c, \text{rank}(\mathbf{V}) = \min(N_c, q)$. Since the row vectors of $\mathbf{B}_c \boldsymbol{\Phi}_c^{1-M}$ and $\mathbf{B}_c$ are linearly independent to each other, one has $\text{rank}\left(\tilde{\mathbf{B}}_{ci}\right) = \min\{2m, N_c\} = N_c$ and $\text{rank}\left(\mathbf{G}_i\right) = \min\{N_c, q\} \geq P_{max}$. Further, we know that $\mathbf{T}$ is of full column rank, which implies that $\{\boldsymbol{\beta}_i\}_{i=1}^K$ are linearly independent to each other, and $\mathbf{R}_{ss} = \sum_{i=1}^K \mathbf{G}_i$, so $\text{rank}\left(\mathbf{R}_{ss}\right) = \min\{N_c, Kq\} = N_c$, which means that the rank deficiency in $\mathbf{R}_{xc}$ has been completely restored. This completes the proof of Proposition 3. ■

One can subsequently follow prevailing subspace methods, such as MUSIC or ESPRIT, to resolve the DOA estimates of the coherent signals.

6.3.2 Separable Signal Number

This section discusses the maximum number of separable signals by the proposed scheme. The uncorrelated and coherent noncircular signals are resolved separately, which makes best use of the DOFs of the original ULA and allows more signals than sensors ($N \geq M$) to be estimated, i.e., the so-called underdetermined DOA estimation problem [152, 153]. Compared with the standard FBSS, which estimates the uncorrelated and coherent signals simultaneously, and spatial difference smoothing method in [43], referred to as SDS, which cannot extend the effective aperture for uncorrelated signals, the maximum number of signals estimated by our method can be increased beyond the traditional limit. If $2(M-1) \geq K + N_u$, $2m > N_c$, and $q \geq P_{max}$, we can estimate a maximum number of $2M - K - 2$ uncorrelated noncircular sources plus $2\left(M - P_{max}\right)$ coherent noncircular signals since $M \geq \lceil \frac{N_c}{2} \rceil + P_{max}$, while the FBSS can estimate at most $M - \lceil \frac{P_{max}}{2} \rceil$ mixed signals, and SDS can achieve the upper bound of $M - K - 1$ uncorrelated signals plus $M - \lceil \frac{P_{max}}{2} \rceil$ coherent signals on condition that

Table 6.1. Minimum number of array elements required.

Uncorrelated signals	Coherent signals		Total signals	Number of array elements			
	groups	Signals in each group		FBSS	SDS	RSDS	PROPOSED
2	2	2	6	7	6	5	4
4	1	4	8	10	7	6	6
4	2	2	8	9	8	7	4
3	3	2	9	10	8	7	6
5	2	3	11	13	9	8	5
5	3	2	11	12	10	9	6
6	3	3	15	17	12	11	8

$M-1 \geq K+N_u, m > N_c$ and $2q \geq P_{max}$, where $\lceil \cdot \rceil$ is the ceiling operator. Although in general spatial differencing methods for separating the coherent signals from uncorrelated sources can also process more signals than array sensors, they ignore the noncircularity of the incident signals, and thus cannot increase the DOFs for uncorrelated noncircular signal estimation. Besides, spatial differencing will eliminate part of the coherent signal information (i.e., the entries along the cross diagonal of the covariance matrix of $\mathbf{x}(t)$) in addition to the uncorrelated signal components. Thirdly, extra processing procedures are required to identify and alleviate pseudo-DOA estimates which are also caused by the differencing operation [43]. A rectified spatial differencing technique [46], referred to as RSDS, can achieve one more DOF for resolving coherent signals than SDS after rank restoration, but it is less accurate.

Table 6.1 compares the minimum number of array elements required to resolve a given number of signals of the proposed method with three approaches mentioned above. For simplicity, we assume that each group has the same number of coherent signals. We can see that our method can use fewer array elements than any of the other algorithms to estimate the same number of signals. This is due to exploiting the noncircular statistics of the signals.

6.3.3 Computational Complexity

Regarding the computational complexity, we consider the major part, i.e., multiplications, involved in covariance matrix construction, eigen-decomposition, and MUSIC spectrum calculation. To facilitate the analysis, we assume that the effective apertures of smoothed covariance matrices of FBSS, SDS, RSDS, and the proposed one are identical to m elements. FBSS constructs one $M \times M$ covariance matrix and then utilises ESPRIT to deal with the smoothed $m \times m$ covariance matrix, which require $\mathcal{O}\left(M^2L + m^3 + N^2m + N^3\right)$ flops where L is the number of snapshots. Here, a flop stands for a complex-valued floating point multiplication operation. For the SDS method, the major computations involved are to form one $M \times M$ covariance matrix, to multiply two $m \times m$ covariance matrices twice, to conduct the eigen-decomposition of the smoothed $m \times m$ covariance matrix, and to do one-dimensional MUSIC spectral search twice, one for uncorrelated signals and the other for coherent signals. Summing them up, we can determine the computational load of SDS as $\mathcal{O}\left(M^2L + 3m^3 + \frac{180}{\varepsilon}(M+1)\right.$ $\left.(M-K-N_u) + \frac{180}{\varepsilon}(m+1)\,(m-N_c)\right)$ flops where ε is the search step size. Instead of MUSIC, the computational complexity of RSDS in conjunction with ESPRIT needs $\mathcal{O}\left(M^2L + 4\,(M-1)^2\,L + 8\,(M-1)^3 + 8\,(K+N_u)^3 + N_u^3 + M^3 + m^3 + N_c^2m + N_c^3\right)$ flops. For the proposed method, the major computations involved are to form $\tilde{\mathbf{R}} \in \mathbb{C}^{2M\times 2M}$, to perform the eigen-decompositions of $\tilde{\mathbf{R}}$, to multiply $\mathbf{U}_{s1}^{+} \in \mathbb{C}^{(K+N_u)\times(2M-1)}$ by $\mathbf{U}_{s2} \in \mathbb{C}^{(2M-1)\times(K+N_u)}$, to perform the eigen-decompositions of $\mathbf{U}_{s1}^{+}\mathbf{U}_{s2}$, to calculate $\left\{\mathbf{M}(\hat{\theta}_k)\right\}_{k=1}^{K+N_u}$, to reconstruct one $2M \times 2M$ covariance matrix of uncorrelated noncircular signals, to perform the eigen-decompositions of $\mathbf{R}_{xc} \in \mathbb{C}^{2M\times 2M}$, to form $\mathbf{R}_{ss} \in \mathbb{C}^{m\times m}$, and to apply ESPRIT to it. The resulting flops required are in order of $\mathcal{O}\Big(4M^2L + 8M^3 + (K+N_u)^2\,(2M-1) + (K+N_u)^3 + 4\,(K+N_u)\,(M+1)(2M-K+$ $N_u) + 2MN_u(1+2M) + 8M^3 + 4M^2K + m^3 + N_c^2m + N_c^3\Big)$. It is clear that the computational complexity of the proposed algorithm is higher than FBSS and RSDS due to the extended array aperture, but lower than the SDS approach especially when ε is relatively small, say less than 0.1°.

6.3.4 Derivation of Deterministic CRLB for the Noncircular Signals in the Presence of Multipath

In the problem of direction finding of noncircular signals under multipath propagation, the vector including all unknown parameters is

$$\boldsymbol{\eta} = \left[\boldsymbol{\theta}^T, \boldsymbol{\alpha}^T, \boldsymbol{\phi}^T, \mathbf{s}_0^T(1), \cdots, \mathbf{s}_0^T(L), \sigma_n^2\right]^T \tag{6.51}$$

where $\boldsymbol{\theta}, \boldsymbol{\alpha}, \boldsymbol{\phi}, \mathbf{s}_0(1), \cdots, \mathbf{s}_0(L)$ are the vectors of unknown DOAs, fading coefficients, noncircularity phases, signal snapshots, respectively, and σ_n^2 is the unknown noise power.[3]

In the deterministic case, the (m,n)-th entry of the Fisher information matrix (FIM) is given by[4] [56, 164]

$$\begin{aligned}\mathbf{F}_{mn} = &\sum_{i=1}^{L} \mathrm{tr}\left\{\mathbf{R}_n^{-1}\frac{\partial \mathbf{R}_n}{\partial \boldsymbol{\eta}_m}\mathbf{R}_n^{-1}\frac{\partial \mathbf{R}_n}{\partial \boldsymbol{\eta}_n}\right\} \\ &+ 2\sum_{i=1}^{L} \mathrm{Re}\left\{\frac{\partial \mathbf{y}^H}{\partial \boldsymbol{\eta}_m}\mathbf{R}_n^{-1}\frac{\partial \mathbf{y}}{\partial \boldsymbol{\eta}_n}\right\}\end{aligned} \tag{6.52}$$

where $\mathbf{R}_n = \sigma_n^2\mathbf{I}$ and the $M \times 1$ vector

$$\begin{aligned}\mathbf{y} &= \mathbf{A}\boldsymbol{\Upsilon}\boldsymbol{\Psi}\mathbf{s}_0(i) \\ &= \mathbf{A}_c\boldsymbol{\Gamma}\boldsymbol{\Psi}_c\mathbf{s}_{c,0}(i) + \mathbf{A}_u\boldsymbol{\Psi}_u\mathbf{s}_{u,0}(i).\end{aligned} \tag{6.53}$$

For convenience of formulation, we define the following notations:

$$\dot{\mathbf{A}} = \left[\left.\frac{d\mathbf{a}(\theta)}{d\theta}\right|_{\theta=\theta_1}, \left.\frac{d\mathbf{a}(\theta)}{d\theta}\right|_{\theta=\theta_2}, \cdots, \left.\frac{d\mathbf{a}(\theta)}{d\theta}\right|_{\theta=\theta_N}\right] \tag{6.54}$$

$$\boldsymbol{\Pi} = \mathrm{blkdiag}\left\{\mathbf{1}_{P_1}, \mathbf{1}_{P_2}, \cdots, \mathbf{1}_{P_K}\right\} \tag{6.55}$$

$$\dot{\boldsymbol{\Psi}} = \mathrm{diag}\left\{\left.\frac{de^{j\frac{\phi}{2}}}{d\phi}\right|_{\phi=\phi_1}, \left.\frac{de^{j\frac{\phi}{2}}}{d\phi}\right|_{\phi=\phi_2}, \cdots, \left.\frac{de^{j\frac{\phi}{2}}}{d\phi}\right|_{\phi=\phi_{K+N_u}}\right\} \tag{6.56}$$

$$\hat{\mathbf{P}} = \frac{1}{L}\sum_{i=1}^{L}\mathbf{s}_0(i)\mathbf{s}_0^H(i) \tag{6.57}$$

[3] The interpretation of (6.51) can be found in Appendix B.2.

[4] The interpretation of this equation can be found in Appendix B.3.

$$\hat{\mathbf{P}}_c = \frac{1}{L}\sum_{i=1}^{L}\mathbf{s}_{c,0}(i)\mathbf{s}_{c,0}^H(i) \tag{6.58}$$

$$\hat{\mathbf{P}}_d = \frac{1}{L}\sum_{i=1}^{L}\mathbf{s}_{c,0}(i)\mathbf{s}_{0}^H(i) \tag{6.59}$$

$$\begin{aligned}\mathbf{Q}(i) = \operatorname{diag}\Big\{&\alpha_{11}e^{j\frac{\phi_1}{2}}s_{1,0}(i),\cdots,\alpha_{1P_1}e^{j\frac{\phi_1}{2}}s_{1,0}(i),\cdots,\\ &\alpha_{K1}e^{j\frac{\phi_K}{2}}s_{K,0}(i),\cdots,\alpha_{KP_K}e^{j\frac{\phi_K}{2}}s_{K,0}(i),\\ &e^{j\frac{\phi_{K+1}}{2}}s_{K+1,0}(i),\cdots,e^{j\frac{\phi_{K+N_u}}{2}}s_{K+N_u,0}(i)\Big\}\end{aligned} \tag{6.60}$$

$$\begin{aligned}\mathbf{Q}_c(i) = \operatorname{diag}\Big\{&\alpha_{11}e^{j\frac{\phi_1}{2}}s_{1,0}(i),\cdots,\alpha_{1P_1}e^{j\frac{\phi_1}{2}}s_{1,0}(i),\cdots,\\ &\alpha_{K1}e^{j\frac{\phi_K}{2}}s_{K,0}(i),\cdots,\alpha_{KP_K}e^{j\frac{\phi_K}{2}}s_{K,0}(i)\Big\}\end{aligned} \tag{6.61}$$

$$\mathbf{W}(i) = \operatorname{diag}\left\{s_{1,0}(i), s_{2,0}(i),\cdots,s_{K+N_u,0}(i)\right\} \tag{6.62}$$

where $\mathbf{1}_l$ is a $l\times 1$ vector with all the entries being 1. Additionally, define $\boldsymbol{\mu} = \operatorname{Re}\{\boldsymbol{\alpha}\}$ and $\boldsymbol{\nu} = \operatorname{Im}\{\boldsymbol{\alpha}\}$.

In this section, all blocks of the FIM corresponding to the unknown parameters required to calculate the CRLB are derived. The idea behind the derivation can be found in [56, 59] and, hence, the detailed derivations are omitted here for simplicity.[5]

$$\mathbf{F}_{\boldsymbol{\theta\theta}} = \frac{2L}{\sigma_n^2}\operatorname{Re}\left\{\left(\dot{\mathbf{A}}^H\dot{\mathbf{A}}\right)\odot\left(\boldsymbol{\Upsilon}\boldsymbol{\Psi}\hat{\mathbf{P}}\boldsymbol{\Psi}^H\boldsymbol{\Upsilon}^H\right)^T\right\} \tag{6.63}$$

$$\begin{aligned}\mathbf{F}_{\boldsymbol{\mu\mu}} &= \mathbf{F}_{\boldsymbol{\nu\nu}}\\ &= \frac{2L}{\sigma_n^2}\operatorname{Re}\left\{\left(\mathbf{A}_c^H\mathbf{A}_c\right)\odot\left(\boldsymbol{\Pi}\boldsymbol{\Psi}_c\hat{\mathbf{P}}_c\boldsymbol{\Psi}_c^H\boldsymbol{\Pi}^H\right)^T\right\}\end{aligned} \tag{6.64}$$

$$\mathbf{F}_{\boldsymbol{\phi\phi}} = \frac{2L}{\sigma_n^2}\operatorname{Re}\left\{\left(\dot{\boldsymbol{\Psi}}^H\boldsymbol{\Upsilon}^H\mathbf{A}^H\mathbf{A}\boldsymbol{\Upsilon}\dot{\boldsymbol{\Psi}}\right)\odot\hat{\mathbf{P}}^T\right\} \tag{6.65}$$

$$\mathbf{F}_{\mathbf{s}_0(i)\mathbf{s}_0(k)} = \frac{2}{\sigma_n^2}\operatorname{Re}\left\{\boldsymbol{\Psi}^H\boldsymbol{\Upsilon}^H\mathbf{A}^H\mathbf{A}\boldsymbol{\Upsilon}\boldsymbol{\Psi}\right\}\delta_{i,k} \tag{6.66}$$

$$\mathbf{F}_{\mathbf{s}_0\mathbf{s}_0} = \operatorname{blkdiag}\left\{\mathbf{F}_{\mathbf{s}_0(1)\mathbf{s}_0(1)}, \mathbf{F}_{\mathbf{s}_0(2)\mathbf{s}_0(2)},\cdots,\mathbf{F}_{\mathbf{s}_0(L)\mathbf{s}_0(L)}\right\} \tag{6.67}$$

$$\mathbf{F}_{\sigma_n^2\sigma_n^2} = \frac{ML}{\sigma_n^4} \tag{6.68}$$

$$\begin{aligned}\mathbf{F}_{\boldsymbol{\theta\mu}} &= \mathbf{F}_{\boldsymbol{\mu\theta}}^T\\ &= \frac{2L}{\sigma_n^2}\operatorname{Re}\left\{\left(\dot{\mathbf{A}}^H\mathbf{A}_c\right)\odot\left(\boldsymbol{\Pi}\boldsymbol{\Psi}_c\hat{\mathbf{P}}_d\boldsymbol{\Psi}^H\boldsymbol{\Upsilon}^H\right)^T\right\}\end{aligned} \tag{6.69}$$

[5] Some blocks are derived in Appendix B.4.

$$\mathbf{F}_{\theta\nu} = -\mathbf{F}_{\nu\theta}^T = -\frac{2L}{\sigma_n^2}\mathrm{Im}\left\{\left(\dot{\mathbf{A}}^H\mathbf{A}_c\right)\odot\left(\mathbf{\Pi}\mathbf{\Psi}_c\hat{\mathbf{P}}_d\mathbf{\Psi}^H\mathbf{\Upsilon}^H\right)^T\right\} \tag{6.70}$$

$$\mathbf{F}_{\theta\phi} = \mathbf{F}_{\phi\theta}^T = \frac{2L}{\sigma_n^2}\mathrm{Re}\left\{\left(\dot{\mathbf{A}}^H\mathbf{A}\mathbf{\Upsilon}\dot{\mathbf{\Psi}}\right)\odot\left(\hat{\mathbf{P}}\mathbf{\Psi}^H\mathbf{\Upsilon}^H\right)^T\right\} \tag{6.71}$$

$$\mathbf{F}_{\theta\mathbf{s}_0(i)} = \mathbf{F}_{\mathbf{s}_0(i)\theta}^T = \frac{2}{\sigma_n^2}\mathrm{Re}\left\{\mathbf{Q}^H(i)\dot{\mathbf{A}}^H\mathbf{A}\mathbf{\Upsilon}\mathbf{\Psi}\right\} \tag{6.72}$$

$$\mathbf{F}_{\theta\mathbf{s}_0} = \mathbf{F}_{\mathbf{s}_0\theta}^T = \left[\mathbf{F}_{\theta\mathbf{s}_0(1)}, \mathbf{F}_{\theta\mathbf{s}_0(2)}, \cdots, \mathbf{F}_{\theta\mathbf{s}_0(L)}\right] \tag{6.73}$$

$$\mathbf{F}_{\mu\nu} = -\mathbf{F}_{\nu\mu}^T = -\frac{2L}{\sigma_n^2}\mathrm{Im}\left\{\left(\mathbf{A}^H\mathbf{A}_c\right)\odot\left(\mathbf{\Pi}\mathbf{\Psi}_c\hat{\mathbf{P}}_c\mathbf{\Psi}_c^H\mathbf{\Pi}^H\right)^T\right\} \tag{6.74}$$

$$\mathbf{F}_{\mu\phi} = \mathbf{F}_{\phi\mu}^T = \frac{2L}{\sigma_n^2}\mathrm{Re}\left\{\left(\mathbf{A}_c^H\mathbf{A}\mathbf{\Upsilon}\dot{\mathbf{\Psi}}\right)\odot\left(\hat{\mathbf{P}}_d^H\mathbf{\Psi}_c^H\mathbf{\Pi}^H\right)^T\right\} \tag{6.75}$$

$$\mathbf{F}_{\mu\mathbf{s}_0(i)} = \mathbf{F}_{\mathbf{s}_0(i)\mu}^T = \frac{2}{\sigma_n^2}\mathrm{Re}\left\{\mathbf{Q}_c^H(i)\mathbf{A}_c^H\mathbf{A}\mathbf{\Upsilon}\mathbf{\Psi}\right\} \tag{6.76}$$

$$\mathbf{F}_{\mu\mathbf{s}_0} = \mathbf{F}_{\mathbf{s}_0\mu}^T = \left[\mathbf{F}_{\mu\mathbf{s}_0(1)}, \mathbf{F}_{\mu\mathbf{s}_0(2)}, \cdots, \mathbf{F}_{\mu\mathbf{s}_0(L)}\right] \tag{6.77}$$

$$\mathbf{F}_{\nu\phi} = -\mathbf{F}_{\phi\nu}^T = \frac{2L}{\sigma_n^2}\mathrm{Im}\left\{\left(\mathbf{A}_c^H\mathbf{A}\mathbf{\Upsilon}\dot{\mathbf{\Psi}}\right)\odot\left(\hat{\mathbf{P}}_d^H\mathbf{\Psi}_c^H\mathbf{\Pi}^H\right)^T\right\} \tag{6.78}$$

$$\mathbf{F}_{\nu\mathbf{s}_0(i)} = -\mathbf{F}_{\mathbf{s}_0(i)\nu}^T = \frac{2}{\sigma_n^2}\mathrm{Im}\left\{\mathbf{Q}_c^H(i)\mathbf{A}_c^H\mathbf{A}\mathbf{\Upsilon}\mathbf{\Psi}\right\} \tag{6.79}$$

$$\mathbf{F}_{\nu\mathbf{s}_0} = -\mathbf{F}_{\mathbf{s}_0\nu}^T = \left[\mathbf{F}_{\nu\mathbf{s}_0(1)}, \mathbf{F}_{\nu\mathbf{s}_0(2)}, \cdots, \mathbf{F}_{\nu\mathbf{s}_0(L)}\right] \tag{6.80}$$

$$\mathbf{F}_{\phi\mathbf{s}_0(i)} = \mathbf{F}_{\mathbf{s}_0(i)\phi}^T = \frac{2}{\sigma_n^2}\mathrm{Re}\left\{\mathbf{W}^H(i)\dot{\mathbf{\Psi}}^H\mathbf{\Upsilon}^H\mathbf{A}^H\mathbf{A}\mathbf{\Upsilon}\mathbf{\Psi}\right\} \tag{6.81}$$

$$\begin{aligned}\mathbf{F}_{\boldsymbol{\phi}\mathbf{s}_0} &= \mathbf{F}_{\mathbf{s}_0\boldsymbol{\phi}}^T \\ &= \left[\mathbf{F}_{\boldsymbol{\phi}\mathbf{s}_0(1)}, \mathbf{F}_{\boldsymbol{\phi}\mathbf{s}_0(2)}, \cdots, \mathbf{F}_{\boldsymbol{\phi}\mathbf{s}_0(L)}\right].\end{aligned} \tag{6.82}$$

As a result, the FIM can be expressed as

$$\mathbf{F} = \begin{bmatrix} \mathbf{F}_{\theta\theta} & \mathbf{F}_{\theta\mu} & \mathbf{F}_{\theta\nu} & \mathbf{F}_{\theta\boldsymbol{\phi}} & \mathbf{F}_{\theta\mathbf{s}_0} & \mathbf{0} \\ \mathbf{F}_{\mu\theta} & \mathbf{F}_{\mu\mu} & \mathbf{F}_{\mu\nu} & \mathbf{F}_{\mu\boldsymbol{\phi}} & \mathbf{F}_{\mu\mathbf{s}_0} & \mathbf{0} \\ \mathbf{F}_{\nu\theta} & \mathbf{F}_{\nu\mu} & \mathbf{F}_{\nu\nu} & \mathbf{F}_{\nu\boldsymbol{\phi}} & \mathbf{F}_{\nu\mathbf{s}_0} & \mathbf{0} \\ \mathbf{F}_{\boldsymbol{\phi}\theta} & \mathbf{F}_{\boldsymbol{\phi}\mu} & \mathbf{F}_{\boldsymbol{\phi}\nu} & \mathbf{F}_{\boldsymbol{\phi}\boldsymbol{\phi}} & \mathbf{F}_{\boldsymbol{\phi}\mathbf{s}_0} & \mathbf{0} \\ \mathbf{F}_{\mathbf{s}_0\theta} & \mathbf{F}_{\mathbf{s}_0\mu} & \mathbf{F}_{\mathbf{s}_0\nu} & \mathbf{F}_{\mathbf{s}_0\boldsymbol{\phi}} & \mathbf{F}_{\mathbf{s}_0\mathbf{s}_0} & \mathbf{0} \\ \mathbf{0} & \mathbf{0} & \mathbf{0} & \mathbf{0} & \mathbf{0} & \mathbf{F}_{\sigma_n^2\sigma_n^2} \end{bmatrix}. \tag{6.83}$$

Consequently, the CRLB can be obtained by taking the inverse of the FIM as

$$\mathrm{CRLB}_{\theta_c} = \sqrt{\frac{1}{N_c}\sum_{i=1}^{N_c}[\mathbf{F}^{-1}]_{ii}} \tag{6.84}$$

$$\mathrm{CRLB}_{\theta_u} = \sqrt{\frac{1}{N_u}\sum_{i=N_c+1}^{N}[\mathbf{F}^{-1}]_{ii}} \tag{6.85}$$

$$\mathrm{CRLB}_{\phi_u} = \sqrt{\frac{1}{N_u}\sum_{i=N+2N_c+1}^{N+2N_c+N_u}[\mathbf{F}^{-1}]_{ii}}. \tag{6.86}$$

6.3.5 Simulation Results and Discussion

In this section, a series of numerical experiments under different conditions are conducted to examine the performance of the proposed method. Simulations are carried out for a ten-element ULA with half-wavelength spacing between adjacent elements. For simplicity, we assume that all noncircular signals are BPSK modulated with the same symbol duration, and these BPSK signals, uncorrelated and coherent, have identical power σ_s^2, and the input SNR is defined as $10\log_{10}(\sigma_s^2/\sigma_n^2)$. RSDS, SDS, and FBSS are chosen for comparison. The accuracy of the estimates is measured from 1000 Monte Carlo runs in terms of the root mean square error (RMSE) which is defined as

$$\mathrm{RMSE}_{\theta} = \sqrt{\frac{1}{1000I}\sum_{n=1}^{1000}\sum_{i=1}^{I}(\hat{\theta}_i^{(n)} - \theta_i)^2} \tag{6.87}$$

Table 6.2. Average runtime (in milli-seconds)

M	FBSS	SDS	RSDS	PROP-OSED
6	N/A	61.2	0.6181	1.6
8	0.4714	61.8	0.6504	1.8
10	0.4821	62.4	0.7027	2.2
12	0.5204	63.0	0.7360	2.4
14	0.5876	64.5	0.9090	2.8
16	0.6347	65.3	0.9543	3.2

$$\mathrm{RMSE}_{\phi} = \sqrt{\frac{1}{1000J}\sum_{n=1}^{1000}\sum_{j=1}^{J}(\hat{\phi}_j^{(n)} - \phi_j)^2} \tag{6.88}$$

where $\hat{\theta}_i^{(n)}$ is the estimate of θ_i for the n-th trial, I is the number of all uncorrelated or coherent signals, and J is the number of noncircularity phases of the uncorrelated signals. Note that here we use different indices i for the signals, since they are estimated at different stages.

Runtime Comparison

This scenario is designed to compare the running time for FBSS cooperating with ESPRIT, SDS, RSDS, and the proposed estimator. Table 6.2 records the average elapsed time of two hundred trial runs for various numbers of sensors M. Here, we assume two uncorrelated and one group of three coherent signals impinging on the ULA, and the number of snapshots is fixed at 500. The simulations are performed using MATLAB R2013a running on an Intel Core i7-2600, 3.4 GHz processor with 16 GB of memory, under Windows 7 64-bit. Table 5.2 shows that for the same M, SDS has a much longer runtime than the other three, and the runtime of ours is approximately three times as long as RSDS. The higher computational complexity of SDS is mainly subject to its spatial spectrum calculation and peak searching, i.e., the MUSIC algorithm [133], for signal estimation at both two stages. FBSS combined with ESPRIT takes the shortest time to complete the estimation due to its single processing stage.

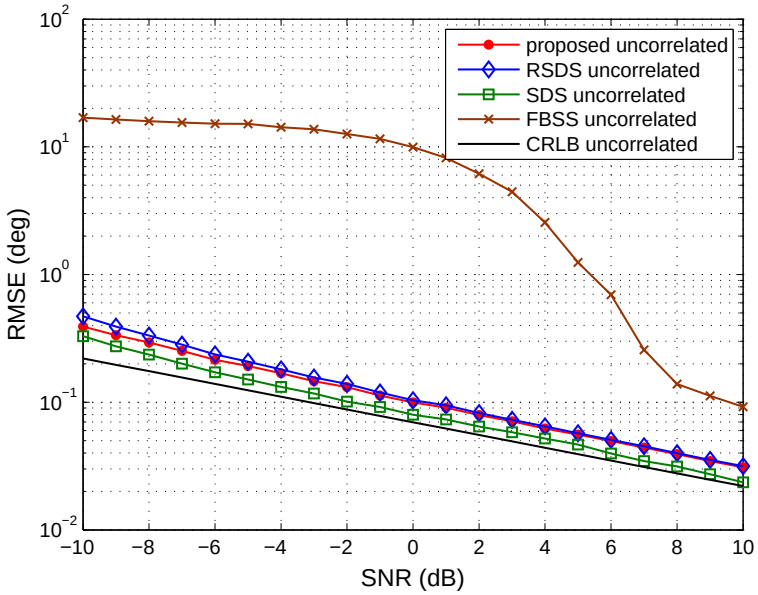

(a)

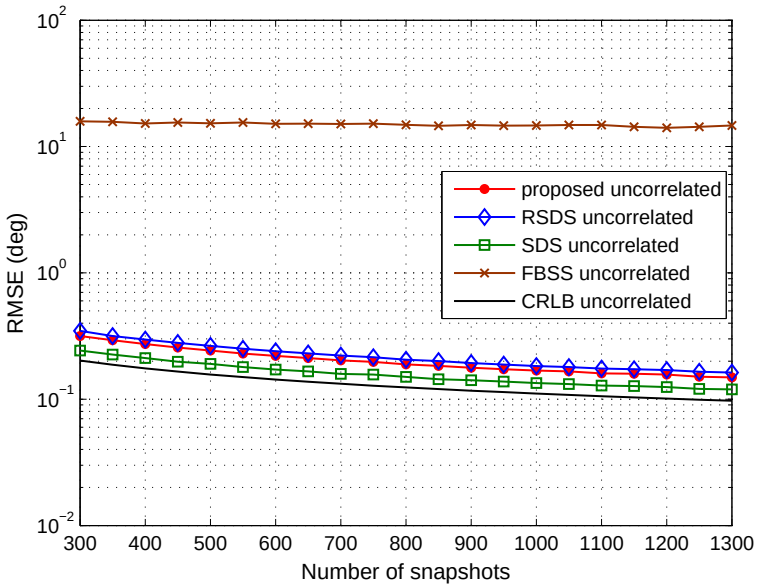

(b)

Figure 6.8. RMSE of the uncorrelated signal estimates in the overdetermined case versus (a) SNR when the number of snapshots is 800; (b) the number of snapshots when SNR $= -5$dB.

Overdetermined DOA Estimation and Corresponding Noncircularity Phase Estimation of Uncorrelated Signals

In the first scenario, we consider three uncorrelated sources from $[55°, 16°, -18°]$ and a group of four coherent signals from $[-10°, -2°, 28°, 36°]$, impinging on the array. The

fading amplitudes and phases of the coherent signals are $[1, 0.9, 0.7, 0.6]$ and $[189.35°, 92.79°, 38.07°, 170.28°]$, respectively. The noncircularity phases are $[51.55°, 259.13°, 161.93°, 164.02°]$. We select $m = 7$ for rank restoration of $\mathbf{R}_{xc}$. Fig. 6.8 depicts the RMSE of the DOA estimates of uncorrelated signals versus input SNR and the number of snapshots. Additionally, we plot the deterministic CRLB for the noncircular uncorrelated signals under multipath propagation, which is derived in Section 6.3.4. From this figure, we can see that although the proposed method is somewhat inferior to SDS in the uncorrelated case, mainly because SDS applies MUSIC to uncorrelated signal estimation, the computational complexity of our method is significantly lower than MUSIC and the overall performance is satisfactory. With an increase in SNR, estimation accuracies of all four algorithms improve asymptotically. Although FBSS can simultaneously resolve uncorrelated and coherent signals, its performance is barely acceptable since it does not take full advantage of the array elements, compared with the two-stage-based methods. As a result, it has the worst estimation accuracy for uncorrelated signals.

The RMSE of the noncircularity phase estimates versus input SNR and number of snapshots is shown in Fig. 6.9. The results illustrate that the performance of noncircularity phase estimation approaches the CRLB asymptotically with increasing SNR and number of snapshots, resulting in a good reconstruction of the covariance matrix of uncorrelated signals for the second stage processing.

In Fig. 6.10 we exhibit the RMSE performance of all four methods for the coherent signal estimation as the SNR and the number of snapshots increase. It is observed that the proposed algorithm has the lowest RMSE for coherent signals, among all the algorithms for all SNRs and snapshots, followed by SDS, RSDS, and then FBSS. FBSS only ameliorates at high SNRs and has a relatively large bias for coherent signals compared with the other three algorithms even for a relatively large number of snapshots at a moderate SNR.

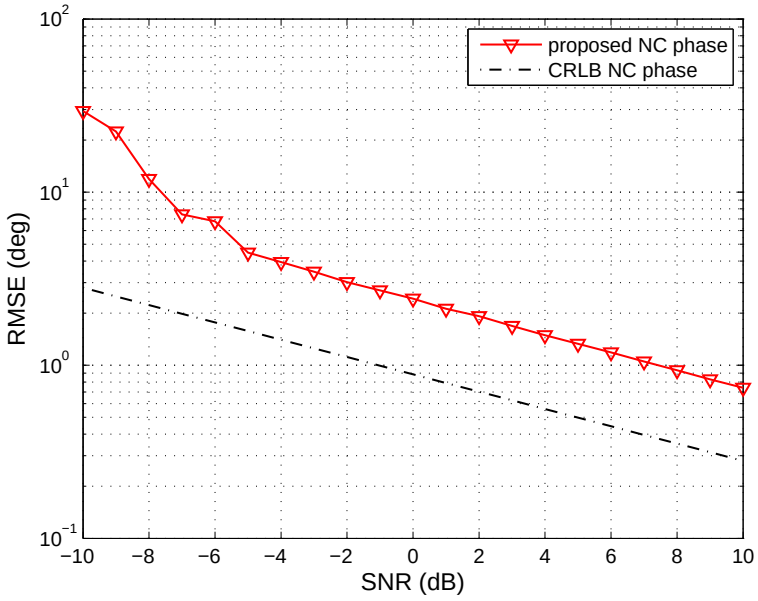

(a)

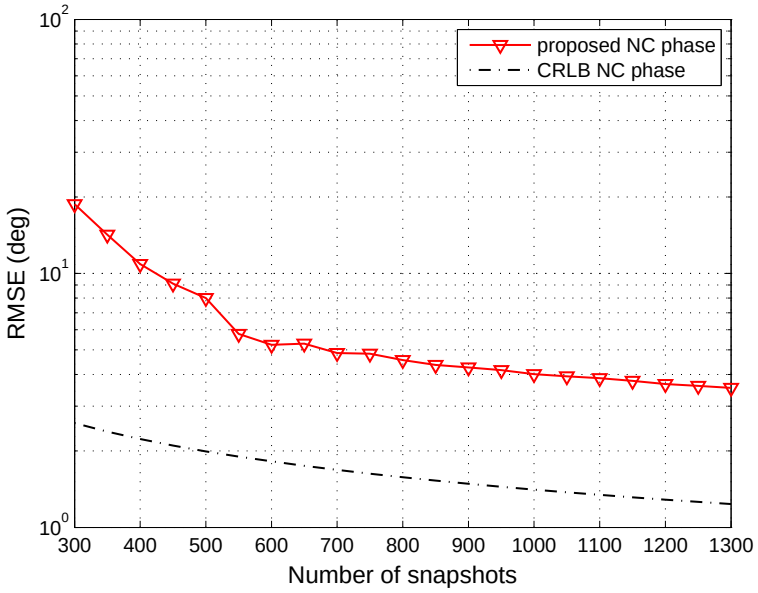

(b)

Figure 6.9. RMSE of the noncircularity phase estimates for 3 uncorrelated signals. (a) The number of snapshots is 800. (b) The SNR $= -5$dB.

Underdetermined DOA Estimation and Corresponding Noncircularity Phase Estimation of Uncorrelated Signals

We consider five uncorrelated signals from $[-41^\circ, -19^\circ, 5^\circ, 38^\circ, 50^\circ]$ and two groups of three coherent signals from $[-48^\circ, -33^\circ, -10^\circ]$ and $[14^\circ, 25^\circ, 57^\circ]$ impinging on the

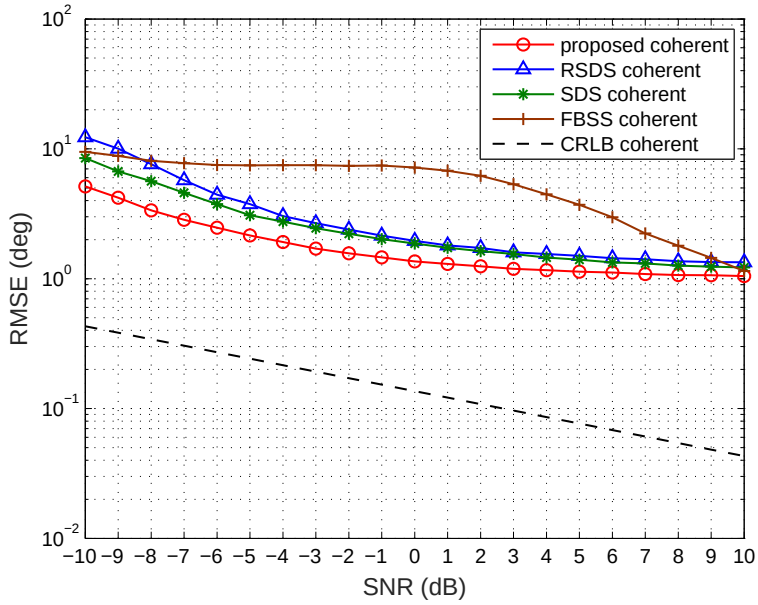

(a)

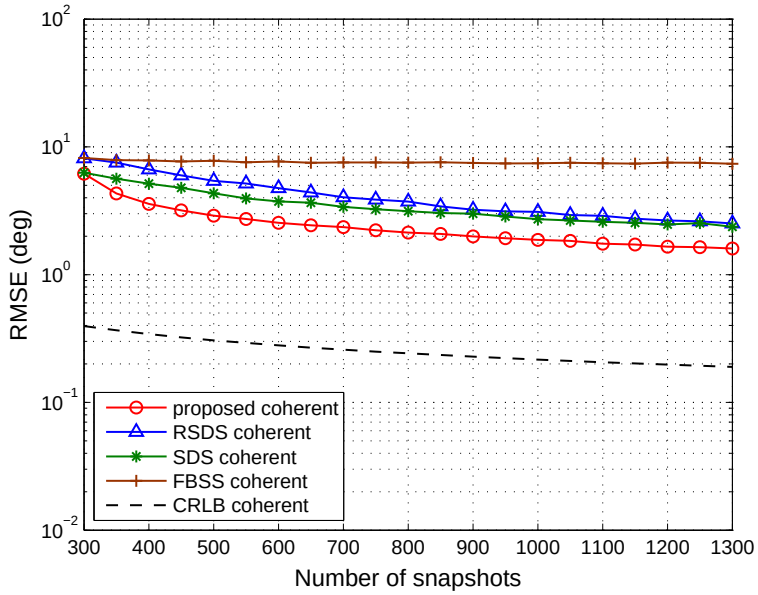

(b)

Figure 6.10. RMSE of the coherent signal estimates in the overdetermined case versus (a) SNR when the number of snapshots is 800; (b) the number of snapshots when SNR $= -5$dB.

ULA. The fading amplitudes of the coherent signals are $[1, 0.9, 0.7]$ and $[1, 0.8, 0.6]$, while the fading phases are $[48.74°, 121.15°, 71.47°]$ and $[189.35°, 35.66°, 283.56°]$, respectively. The noncircularity phases are $[51.55°, 259.13°, 161.93°, 164.02°, 40.75°, 15.19°, 263.59°]$. We select $m = 7$ in this scenario.

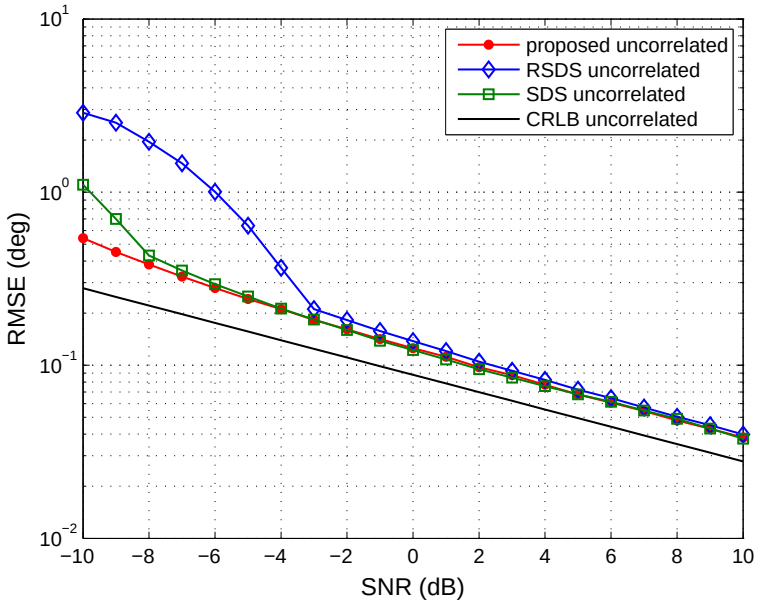

(a)

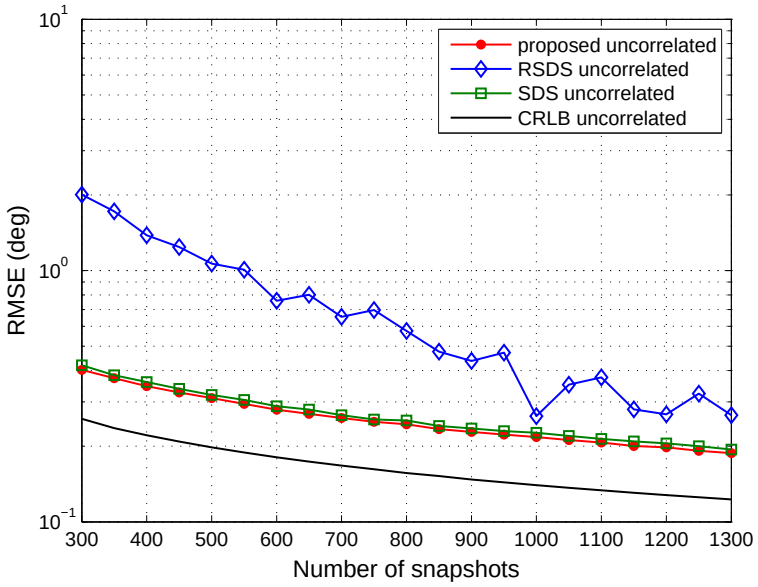

(b)

Figure 6.11. RMSE of the uncorrelated signal estimates in the underdetermined case versus (a) SNR when the number of snapshots is 800; (b) the number of snapshots when SNR $= -5$dB.

Based on these settings, the simulation results of the RMSE of the uncorrelated signal estimates by varying SNR and the number of snapshots are illustrated in Fig. 6.11. The total number of signals exceeds the number of array elements, and thus FBSS fails to work. As is shown in Fig. 6.11, the proposed approach achieves the best performance

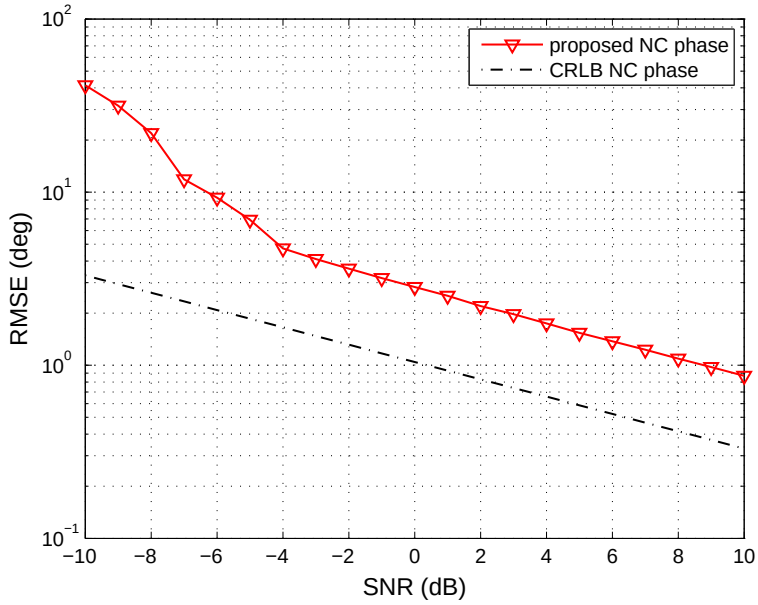

(a)

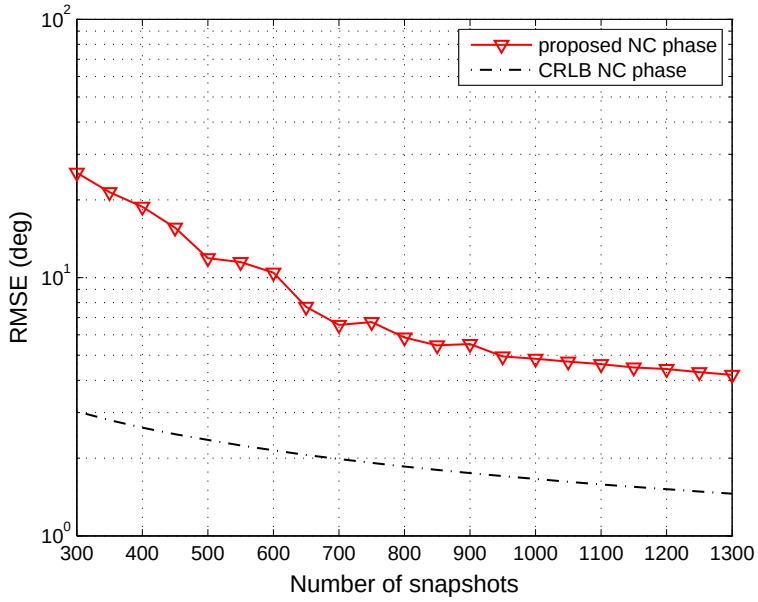

(b)

Figure 6.12. RMSE of the noncircularity phase estimates for 5 uncorrelated signals. (a) The number of snapshots is 800. (b) The SNR $= -5$dB.

over the range of SNR values and the number of snapshots for the uncorrelated signal estimation. Under this more challenging scenario, the proposed approach even outperforms SDS for the uncorrelated case, especially at low SNRs. This is because our method constructs a virtual array with twice as many elements, which plays an

important role in estimating uncorrelated signals under DOFs-constrained conditions. The smaller noise subspace of the SDS algorithm results in larger estimation errors, as the orthogonality between the signal and noise subspace is affected more by finite data effects. However, consistent with the overdetermined case, SDS is still superior to RSDS for the uncorrelated signal estimation because of its one dimensional search of the spatial spectrum.

In the same scenario, the RMSE of the noncircularity phase estimates versus input SNR and number of snapshots is shown in Fig. 6.12. Similar to Fig. 6.9, the performance of the noncircularity phase estimation approaches the CRLB asymptotically with increasing SNR and number of snapshots, only with a slightly worse accuracy than that of the first scenario due to more estimations requiring to be carried out.

In Fig. 6.13 we plot the performance of the three methods for the coherent signal estimation as well as CRLB as a function of SNR and the total number of snapshots. It can be seen that the proposed method has a greater advantage over the other two algorithms than the first scenario shown in Fig. 6.10 for all SNRs and number of snapshots. Among the other approaches, the RSDS algorithm performs better than SDS for coherent signal estimation up to -2dB, but worse above -2dB. When fixing SNR $= -5$dB, as observed in Fig. 6.13(b), the performance of SDS for coherent signal estimation improves faster than that of RSDS with increasing snapshots, and approaches RSDS when the number of snapshots is larger than 1100.

6.4 Conclusion

In this Chapter, two novel DOA estimation methods have been proposed for independent noncircular signals and the mixed (i.e., uncorrelated and coherent) signals, respectively.

In Section 6.2, we introduced an augmented FOC-based algorithm for noncircular signal estimation. Both the theoretical formulation and computer simulations show that

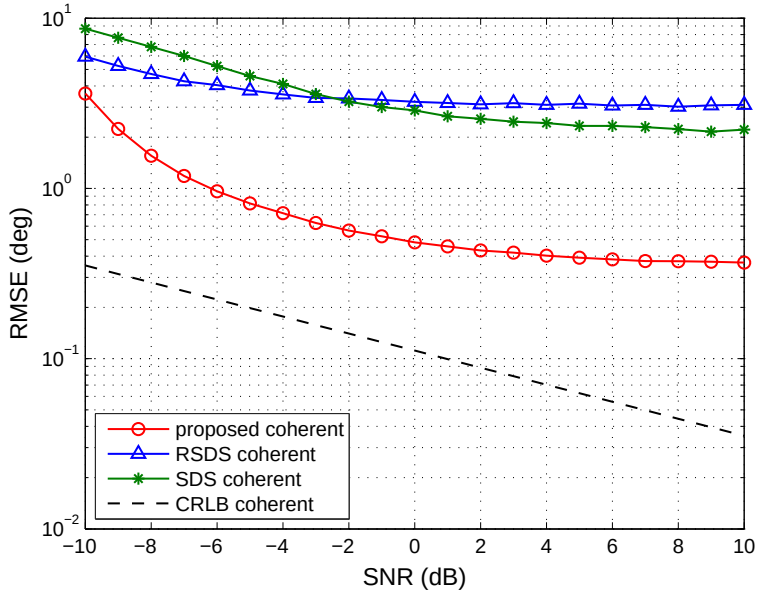

(a)

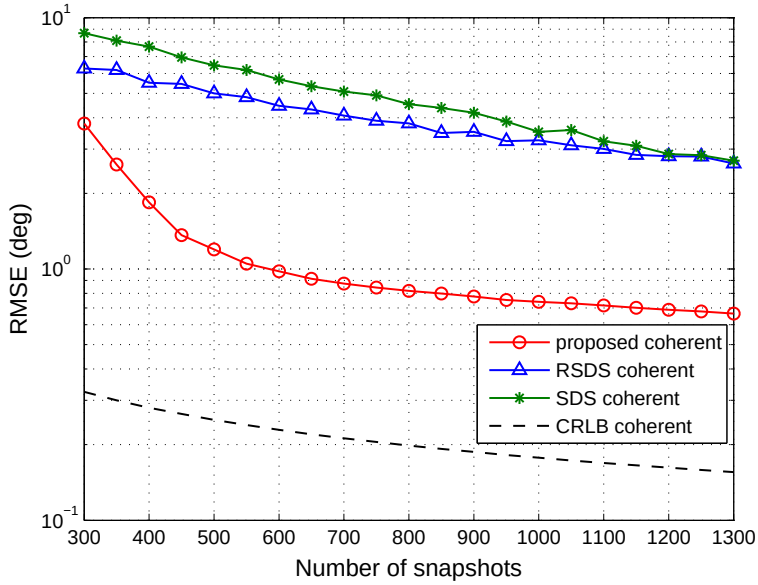

(b)

Figure 6.13. RMSE of the coherent signal estimates in the underdetermined case versus (a) SNR when the number of snapshots is 800; (b) the number of snapshots when SNR $= -5$dB.

the augmented NC-FOC estimator has better performances in terms of RMSE and estimation capacity than existing techniques. To conclude this chapter, we note that the proposed algorithm can be easily extended to higher even orders, e.g., sixth-order.

The DOA estimation of noncircular signals under multipath is addressed in Section 6.3, and a two-stage DOA estimation algorithm is proposed for this case. The algorithm makes efficient use of the DOFs of a ULA, and enables us to separately deal with two different types of signals, thus resolving more signals than the number of array elements. At the first stage, we construct an augmented matrix of array outputs, then use the eigenvectors of the augmented covariance matrix, corresponding to the signal subspace, to resolve the uncorrelated signals with our proposed criterion. Our theoretical identifiability analysis has revealed that the proposed method can uniquely make a reasonable classification of the source types. After the first stage, the uncorrelated components are removed from the covariance matrix of the augmented data based on the DOA and noncircularity phase estimates of the uncorrelated sources. Then a spatial smoothing on eigenvectors is performed to restore the rank deficiency in the covariance matrix of the coherent signals, and finally their DOAs are resolved using a similar procedure as for uncorrelated sources. Compared with previous two-stage-based methods, the proposed solution is efficient in the sense that by exploitation of the noncircularity of the incident signals it achieves a more reasonable classification of the signal types, alleviates the array DOFs and aperture loss, as well as improving the estimation accuracy of both uncorrelated and coherent signals. Besides, it is more robust under adverse noise conditions (SNR) and data availability (the number of snapshots).

Chapter 7

Conclusions and Future Work

THIS chapter collects and categorises the main contributions of this thesis, and offers a road map for further research. It very briefly summarises the material contained in this thesis, thereby concluding this research on sensor array processing.

7.1 Review of Research Results

The main focus of this thesis has been on enhancing the performance of DOA estimation techniques by better utilising the available DOFs. These extra DOFs have been obtained by mining extra information in the signal structure and have enabled more signals to be estimated with improved estimation accuracy for a given sensor array. We have mainly considered algorithms that exploit FOC, and developed two improved algorithms in this area using circular signal statistics in Chapter 5. However, significantly more DOFs can be obtained by exploiting the noncircularity of modern wireless communication signals and in Chapter 6 we also proposed two new algorithms which demonstrated the potential gains from this approach.

For circular signals, there are two classes of state of the art algorithms based on FOC. The first are two-stage methods that separate coherent from independent signals to achieve more DOFs than standard cumulant-based FBSS. The second class is termed VESPA [38,39] which separates the coherent groups directly and can accomplish even more DOFs at a cost of degraded robustness and accuracy.

In Chapter 5, we first introduced a new two-stage FOC-based DOA estimation algorithm for the case where independent and coherent signals coexist. Our algorithm employed DOFs more efficiently than the previous two-stage method [49], achieving higher accuracy, robustness and the ability to deal with more signals. The extra DOFs were obtained by exploiting the orthogonality between the signal and noise subspaces to distinguish the independent signal from the coherent ones. After reconstructing the cumulant matrix of the estimated independent signals, they were removed from the original cumulant matrix to deal with the remaining coherent signals. By introducing a new matrix construction approach and utilising it to restore the deficient rank caused by signal coherency, the desired coherent signals can then be resolved by common subspace-based DOA estimators.

In the second part of Chapter 5, we introduced a new algorithm that can estimate the same number of signals as VESPA but with improved accuracy. It follows the similar idea as VESPA by separating the signals directly in accordance with coherency, then restoring the rank of the signals in each coherent group. A key contribution is to show

that if the non-Gaussian signal is temporal correlated, then by using this correlation information and rotation invariance between the newly constructed augmented cumulant matrices, a more robust coherent group separation can be obtained, although the upper bound of estimation identifiability is not improved.

Only limited work has been done on exploiting the noncircular characteristics of modern wireless communication signals and in Chapter 6 we further extend the state of the art algorithms in this area for both fourth and second order statistics.

In the first half of Chapter 6, we introduced a new FOC-based DOA estimation algorithm that is able to estimate up to $4(M-1)$ uncorrelated sources. This is significantly more than the VESPA algorithm which does not exploit the noncircularity of the received signals. The state of the art algorithm in this area which does exploit the noncircular properties is termed NC-2q method and can only resolve at most $3(M-1)$ sources. It exploited the noncircularity to obtain virtual arrays that were used in the FOC matrices to give more DOFs. Our algorithm, termed augmented NC-FOC, is inspired by the NC-2q method but takes advantage of a novel choice of virtual arrays to gain the extra DOFs. Our algorithm can also be extended to even higher order cumulants in a similar fashion to the NC-2q method, allowing up to $2q(M-1)$ sources identifiable. Numerical simulations demonstrated that the proposed augmented NC-FOC technique is significantly better than existing methods in dealing with underdetermined DOA estimation.

In the last part of of Chapter 6, we considered improving the state of the art algorithms for noncircular signals based on second order statistics. In particular we focused on the two-stage algorithms covered in Chapter 5 where circular statistics were assumed. These algorithms are able to resolve more sources when uncorrelated and coherent signals coexist, however, noncircular properties do not appear to have been exploited in these algorithms to date. We introduced a novel two-stage algorithm that integrates the noncircularity to further increase DOFs. By expanding the signal subspace from an augmented array output, the DOA estimates of the uncorrelated sources were obtained first, then the covariance matrix of uncorrelated signals was reconstructed and removed. Secondly, a spatial smoothing technique was performed on the eigenvectors

of the covariance matrix to restore the rank deficiency in the covariance of the remaining coherent signals. The two-stage processing strategy used the rotation invariance between the signal subspaces to classify the signal types. The separation of the uncorrelated and coherent signals gave rise to more DOFs than the number of physical sensors. The theoretical analysis showed that the number of signals that can be identifiable is larger than the current algorithms. Additionally, new deterministic CRLBs were derived for the considered mixture model of noncircular signals. Extensive simulation results demonstrated the validity and efficiency of the proposed method.

7.2 Recommendations on Future Work

Throughout the thesis, we assume isotropic sensors and point source scenarios. In future research, we could extend the work in the following directions.

- In Chapter 5, we only considered the problem of rank restoration by using the structure of a uniform linear array. The optimum orientation of a nonuniform linear array to contribute to recover rank deficiency is worth further investigation. Moreover, the array we assume is placed along the x axis and only 1-D bearing information can be obtained. The problem will become even more interesting if a 2-D array can be utilised to resist multipath propagation, i.e., taking the elevation angle into account.

- The proposed STFOC algorithm is valid for non-Gaussian signals but not for Gaussian distribution. The consideration of Gaussian signals will make the coherent group separation problem much more involved than for the non-Gaussian case. New DOA estimation algorithms considering temporal correlation in signals may need to be developed in order to solve this problem, which presents an exciting challenge for the future research.

- The noise model in Chapter 5 is assumed to be spatially coloured with an unknown covariance matrix. This is a general and robust model but does not accommodate much information for noise suppression. In several real applications, the

estimation performance can be further improved by considering signals in structured noise, such as nonuniform white noise and coloured noise in sparse sensor arrays which are common in sonar and seismology applications. Correspondingly, new methods need to be developed to achieve targeted noise mitigation while preserving good estimation performance.

- The investigation of virtual arrays for DOA estimation of noncircular signals was conducted in Chapter 6. There are some open issues that deserve further research: (a) For nonuniform linear arrays, such as MRAs and recently emerging co-prime arrays, finding the upper bound of estimation identifiability and developing high-resolution DOA estimation methods are very important; (b) Mathematically speaking, the rotation noncircular phase matrix $\mathbf{\Psi}$ in our model $\mathbf{x}(t) = \mathbf{A}\mathbf{\Psi}\mathbf{s}_0(t) + \mathbf{n}(t)$ has to be stationary. In the case without frequency syncronisation in multicarrier wireless communication systems, all the signals have slightly different frequencies and thus frequency offsets in the baseband due to jitter, Doppler for nonstationary sources etc. In this case, the rotation phases contained in $\mathbf{\Psi}$ change slowly over time (snapshots). Thus work can be done on analysing such an effect. For instance, it would be interesting to know what the maximum frequency offset can be for the algorithms to still work and when they break down; (c) Applying the virtual array concept to MIMO radar related applications is another interesting and promising topic.

- Last but not least, throughout this thesis, we solved the problem of DOA estimation from the ideal array manifold, i.e., on which there are no perturbations or errors—mutual coupling and gain/phase uncertainties, for example. In practice, it is impossible to guarantee a perfect array calibration and obtain exact knowledge of the array manifold. Therefore, taking such array model errors into account is necessary and pragmatic. The array manifold errors can be characterised by perturbation coefficient matrices but with different structures. It should be noted that the inclusion of the perturbation coefficient matrices will increase the

difficulty of DOA estimation. Also, it is assumed that the number of incident signals is known *a priori*. If such prior information is not available, it gives rise to another important topic—source enumeration. Several popular enumeration methods have been extensively studied, such as Akaike information criterion (AIC), the minimum description length (MDL), Gerschgorin disk estimator (GDE), etc, but most of them are not either applicable to or developed specialised for coherent signals and, hence, new source enumeration methods are much in demand but more challenging.

7.3 Conclusion

This chapter summarises the research carried out in the duration of the Ph.D study. According to the discussion in Section 7.1, the research done in this thesis contributes to knowledge in sensor array processing into two aspects. Firstly, the thesis provides two methods for (a) the mixture of uncorrelated and coherent circular signals under multipath propagation and (b) improving coherent group separation utilising temporal and spatial correlation. Second, the thesis gives two new perspectives on enhancing DOFs by considering noncircularity contained in signals, i.e., achieving virtual arrays by noncircular cumulants and expanding the signal subspace to improve estimation performance when uncorrelated and coherent signals coexist. Both aspects of the contributions could be used by other researchers in this field and related applications. The work in this thesis and the recommendations on future work in Section 7.2 will create more research possibilities for advancing the state of the art in sensor array processing.

Appendix A

Proof of Equations and Statements in Chapter 5

THIS appendix contains the details of intermediate steps for some equations and statements developed in Chapter 5.

A.1 Proof of $\mathbf{C}_x^+$ in (5.24)

Recall the representation of the pseudo-inverse in equation (3.17), evidently $\bar{\mathbf{A}}^+\bar{\mathbf{A}} = \mathbf{I}_{K+N_u}$. Let $\mathbf{B} \triangleq \left(\bar{\mathbf{A}}^H\right)^+ \mathbf{C}_s^{-1}\bar{\mathbf{A}}^+$, by the property (3.18), one can verify that $\mathbf{B}$ satisfies

$$\begin{aligned}
\mathbf{C}_x\mathbf{B}\mathbf{C}_x &= \bar{\mathbf{A}}\mathbf{C}_s\bar{\mathbf{A}}^H\left(\bar{\mathbf{A}}^H\right)^+\mathbf{C}_s^{-1}\bar{\mathbf{A}}^+\bar{\mathbf{A}}\mathbf{C}_s\bar{\mathbf{A}}^H \\
&= \bar{\mathbf{A}}\mathbf{C}_s\bar{\mathbf{A}}^H\left(\bar{\mathbf{A}}^+\right)^H\mathbf{C}_s^{-1}\mathbf{C}_s\bar{\mathbf{A}}^H \\
&= \bar{\mathbf{A}}\mathbf{C}_s\left(\bar{\mathbf{A}}^+\bar{\mathbf{A}}\right)^H\bar{\mathbf{A}}^H \\
&= \bar{\mathbf{A}}\mathbf{C}_s\bar{\mathbf{A}}^H \\
&= \mathbf{C}_x \qquad \text{(A.1)} \\
\mathbf{B}\mathbf{C}_x\mathbf{B} &= \left(\bar{\mathbf{A}}^H\right)^+\mathbf{C}_s^{-1}\bar{\mathbf{A}}^+\bar{\mathbf{A}}\mathbf{C}_s\bar{\mathbf{A}}^H\left(\bar{\mathbf{A}}^H\right)^+\mathbf{C}_s^{-1}\bar{\mathbf{A}}^+ \\
&= \left(\bar{\mathbf{A}}^H\right)^+\mathbf{C}_s^{-1}\mathbf{C}_s\left(\bar{\mathbf{A}}^+\bar{\mathbf{A}}\right)^H\mathbf{C}_s^{-1}\bar{\mathbf{A}}^+ \\
&= \left(\bar{\mathbf{A}}^H\right)^+\mathbf{C}_s^{-1}\bar{\mathbf{A}}^+ \\
&= \mathbf{B} \qquad \text{(A.2)} \\
(\mathbf{C}_x\mathbf{B})^H &= \left(\bar{\mathbf{A}}\mathbf{C}_s\bar{\mathbf{A}}^H\left(\bar{\mathbf{A}}^H\right)^+\mathbf{C}_s^{-1}\bar{\mathbf{A}}^+\right)^H \\
&= \left(\bar{\mathbf{A}}\mathbf{C}_s^H\left(\bar{\mathbf{A}}^+\bar{\mathbf{A}}\right)^H\mathbf{C}_s^{-1}\bar{\mathbf{A}}^+\right)^H \\
&= \mathbf{I}_{K+N_u}^H \\
&= \mathbf{I}_{K+N_u} \\
&= \bar{\mathbf{A}}\mathbf{C}_s^H\left(\bar{\mathbf{A}}^+\bar{\mathbf{A}}\right)^H\mathbf{C}_s^{-1}\bar{\mathbf{A}}^+ \\
&= \mathbf{C}_x\mathbf{B} \qquad \text{(A.3)} \\
(\mathbf{B}\mathbf{C}_x)^H &= \left(\left(\bar{\mathbf{A}}^H\right)^+\mathbf{C}_s^{-1}\bar{\mathbf{A}}^+\bar{\mathbf{A}}\mathbf{C}_s\bar{\mathbf{A}}^H\right)^H \\
&= \left(\left(\bar{\mathbf{A}}^+\right)^H\bar{\mathbf{A}}^H\right)^H \\
&= \left(\left(\bar{\mathbf{A}}\bar{\mathbf{A}}^+\right)^H\right)^H \\
&= \bar{\mathbf{A}}\bar{\mathbf{A}}^+ \\
&= \left(\bar{\mathbf{A}}\bar{\mathbf{A}}^+\right)^H = \mathbf{B}\mathbf{C}_x \qquad \text{(A.4)}
\end{aligned}$$

where $\bar{\mathbf{A}}\bar{\mathbf{A}}^{+} = \left(\bar{\mathbf{A}}\bar{\mathbf{A}}^{+}\right)^{H}$ since condition (3.13) in Section 3.4 holds for $\bar{\mathbf{A}}^{+}$. As $\mathbf{B}$ satisfies all four pseudo-inverse conditions introduced in Section 3.4, we say that $\mathbf{B}$ must be the pseudo-inverse of $\mathbf{C}_x$, i.e. $\mathbf{C}_x^{+} = \left(\bar{\mathbf{A}}^{H}\right)^{+} \mathbf{C}_s^{-1}\bar{\mathbf{A}}^{+}$. Therefore, equations (5.24)–(5.26) hold.

A.2 Proof of (5.33)

Considering equation (5.32) and stacking $\mathbf{C}_{xc}(i, m+r-1), \mathbf{C}_{xc}(i, m+r-2), \cdots, \mathbf{C}_{xc}(i, r)$ in a column, one obtains

$$\begin{aligned}
\mathbf{g}_{i,r} &= \begin{bmatrix} \mathbf{C}_{xc}(i, m+r-1) \\ \mathbf{C}_{xc}(i, m+r-2) \\ \vdots \\ \mathbf{C}_{xc}(i, r) \end{bmatrix} \\
&= \underbrace{\begin{bmatrix} 1 & \cdots & 1 & \cdots & 1 & \cdots & 1 \\ e^{j\frac{2\pi d}{\lambda}\sin\theta_{11}} & \cdots & e^{j\frac{2\pi d}{\lambda}\sin\theta_{1P_1}} & \cdots & e^{j\frac{2\pi d}{\lambda}\sin\theta_{K1}} & \cdots & e^{j\frac{2\pi d}{\lambda}\sin\theta_{KP_K}} \\ \vdots & & & & & & \\ e^{j\frac{2\pi(m-1)d}{\lambda}\sin\theta_{11}} & \cdots & e^{j\frac{2\pi(m-1)d}{\lambda}\sin\theta_{1P_1}} & \cdots & e^{j\frac{2\pi(m-1)d}{\lambda}\sin\theta_{K1}} & \cdots & e^{j\frac{2\pi(m-1)d}{\lambda}\sin\theta_{KP_K}} \end{bmatrix}}_{\mathbf{A}_c(1{:}m,:)} \\
&\quad \times \mathbf{\Phi}^{1-r}\mathbf{d}_i. \qquad \text{(A.5)}
\end{aligned}$$

If define $\mathbf{F} = \left[\mathbf{I}_{(M-L+1)}, \mathbf{0}_{(M-L+1)\times(L-1)}\right]$, recalling $m = M - L + 1$, then it is straightforward to see $\mathbf{A}_c(1:m,:) = \mathbf{F}\left[\mathbf{A}_{c,1}, \mathbf{A}_{c,2}, \cdots, \mathbf{A}_{c,K}\right]$. Hence, $\mathbf{g}_{i,r}$ can be expressed as

$$\begin{aligned}
\mathbf{g}_{i,r} &= \mathbf{F}\left[\mathbf{A}_{c,1}, \mathbf{A}_{c,2}, \cdots, \mathbf{A}_{c,K}\right]\mathbf{\Phi}^{1-r}\mathbf{d}_i \\
&= \mathbf{B}_c\mathbf{\Phi}^{1-r}\mathbf{d}_i, \quad r = 1, 2, \cdots, L \qquad \text{(A.6)}
\end{aligned}$$

where $\mathbf{B}_c = \mathbf{F}\left[\mathbf{A}_{c,1}, \mathbf{A}_{c,2}, \cdots, \mathbf{A}_{c,K}\right]$.

A.3 Proof of $\mathbf{J}\mathbf{B}_c^{*} = \mathbf{B}_c\mathbf{\Phi}^{1-m}$

From the above justification, evidently $\mathbf{B}_c = \mathbf{A}_c(1:m,:)$ is a Vandermonde matrix. The property $\mathbf{J}\mathbf{B}_c^{*} = \mathbf{B}_c\mathbf{\Phi}^{1-m}$ is well-recognised in forward/backward spatial smoothing,

and easily verified by the structure of Vandermonde matrix. Let $z_{kP_k} = e^{j\frac{2\pi d}{\lambda}\sin\theta_{kP_k}}$, then

$$
\begin{aligned}
\mathbf{JB}_c^* &= \begin{bmatrix} & & 1 \\ & 1 & \\ 1 & & \end{bmatrix} \begin{bmatrix} 1 & \cdots & 1 & \cdots & 1 & \cdots & 1 \\ z_{11}^{-1} & \cdots & z_{1P_1}^{-1} & \cdots & z_{K1}^{-1} & \cdots & z_{KP_K}^{-1} \\ \vdots & & & & & & \\ z_{11}^{1-m} & \cdots & z_{1P_1}^{1-m} & \cdots & z_{K1}^{1-m} & \cdots & z_{KP_K}^{1-m} \end{bmatrix} \\
&= \begin{bmatrix} z_{11}^{1-m} & \cdots & z_{1P_1}^{1-m} & \cdots & z_{K1}^{1-m} & \cdots & z_{KP_K}^{1-m} \\ \vdots & & & & & & \\ z_{11}^{-1} & \cdots & z_{1P_1}^{-1} & \cdots & z_{K1}^{-1} & \cdots & z_{KP_K}^{-1} \\ 1 & \cdots & 1 & \cdots & 1 & \cdots & 1 \end{bmatrix} \\
&= \begin{bmatrix} 1 & \cdots & 1 & \cdots & 1 & \cdots & 1 \\ \vdots & & & & & & \\ z_{11}^{m-2} & \cdots & z_{1P_1}^{m-2} & \cdots & z_{K1}^{m-2} & \cdots & z_{KP_K}^{m-2} \\ z_{11}^{m-1} & \cdots & z_{1P_1}^{m-1} & \cdots & z_{K1}^{m-1} & \cdots & z_{KP_K}^{m-1} \end{bmatrix} \begin{bmatrix} z_{11}^{1-m} & & & & & & \\ & \ddots & & & & & \\ & & z_{1P_1}^{1-m} & & & & \\ & & & \ddots & & & \\ & & & & z_{K1}^{1-m} & & \\ & & & & & \ddots & \\ & & & & & & z_{KP_K}^{1-m} \end{bmatrix} \\
&= \mathbf{B}_c \begin{bmatrix} z_{11} & & & & & & \\ & \ddots & & & & & \\ & & z_{1P_1} & & & & \\ & & & \ddots & & & \\ & & & & z_{K1} & & \\ & & & & & \ddots & \\ & & & & & & z_{KP_K} \end{bmatrix}^{1-m} \\
&= \mathbf{B}_c\mathbf{\Phi}^{1-m}
\end{aligned}
\tag{A.7}
$$

where $\mathbf{\Phi} = \mathrm{diag}\{z_{11}, \cdots, z_{1P_1}, \cdots, z_{K1}, \cdots, z_{KP_K}\}$.

A.4 Proof of (5.37)

One can readily find that

$$
\begin{aligned}
&\left[\boldsymbol{\Phi}^{1-L}\mathbf{d}_i, \boldsymbol{\Phi}^{2-L}\mathbf{d}_i, \cdots, \mathbf{d}_i\right] \\
&= \boldsymbol{\Phi}^{1-L}\left[\mathbf{d}_i, \boldsymbol{\Phi}\mathbf{d}_i, \cdots, \boldsymbol{\Phi}^{L-1}\mathbf{d}_i\right] \\
&= \boldsymbol{\Phi}^{1-L}\begin{bmatrix}
d_{11}^{(i)} & e^{j\frac{2\pi d}{\lambda}\sin\theta_{11}}d_{11}^{(i)} & \cdots & e^{j\frac{2\pi(L-1)d}{\lambda}\sin\theta_{11}}d_{11}^{(i)} \\
\vdots & \vdots & \cdots & \vdots \\
d_{1P_1}^{(i)} & e^{j\frac{2\pi d}{\lambda}\sin\theta_{1P_1}}d_{1P_1}^{(i)} & \cdots & e^{j\frac{2\pi(L-1)d}{\lambda}\sin\theta_{1P_1}}d_{1P_1}^{(i)} \\
\vdots & \vdots & \cdots & \vdots \\
d_{K1}^{(i)} & e^{j\frac{2\pi d}{\lambda}\sin\theta_{K1}}d_{K1}^{(i)} & \cdots & e^{j\frac{2\pi(L-1)d}{\lambda}\sin\theta_{K1}}d_{K1}^{(i)} \\
\vdots & \vdots & \cdots & \vdots \\
d_{KP_K}^{(i)} & e^{j\frac{2\pi d}{\lambda}\sin\theta_{KP_K}}d_{KP_K}^{(i)} & \cdots & e^{j\frac{2\pi(L-1)d}{\lambda}\sin\theta_{KP_K}}d_{KP_K}^{(i)}
\end{bmatrix} \\
&= \boldsymbol{\Phi}^{1-L}\begin{bmatrix}
d_{11}^{(i)} & & & & & & \\
& \ddots & & & & & \\
& & d_{1P_1}^{(i)} & & & & \\
& & & \ddots & & & \\
& & & & d_{K1}^{(i)} & & \\
& & & & & \ddots & \\
& & & & & & d_{KPK}^{(i)}
\end{bmatrix}\begin{bmatrix}
1 & e^{j\frac{2\pi d}{\lambda}\sin\theta_{11}} & \cdots & e^{j\frac{2\pi(L-1)d}{\lambda}\sin\theta_{11}} \\
\vdots & \vdots & \cdots & \vdots \\
1 & e^{j\frac{2\pi d}{\lambda}\sin\theta_{1P_1}} & \cdots & e^{j\frac{2\pi(L-1)d}{\lambda}\sin\theta_{1P_1}} \\
\vdots & \vdots & \cdots & \vdots \\
1 & e^{j\frac{2\pi d}{\lambda}\sin\theta_{K1}} & \cdots & e^{j\frac{2\pi(L-1)d}{\lambda}\sin\theta_{K1}} \\
\vdots & \vdots & \cdots & \vdots \\
1 & e^{j\frac{2\pi d}{\lambda}\sin\theta_{KP_K}} & \cdots & e^{j\frac{2\pi(L-1)d}{\lambda}\sin\theta_{KP_K}}
\end{bmatrix} \\
&= \mathrm{diag}\left\{e^{j\frac{2\pi(1-L)d}{\lambda}\sin\theta_{11}}d_{11}^{(i)}, \cdots, e^{j\frac{2\pi(1-L)d}{\lambda}\sin\theta_{1P_1}}d_{1P_1}^{(i)}, \cdots, e^{j\frac{2\pi(1-L)d}{\lambda}\sin\theta_{K1}}d_{K1}^{(i)}, \cdots,\right. \\
&\qquad \left. e^{j\frac{2\pi(1-L)d}{\lambda}\sin\theta_{KP_K}}d_{KP_K}^{(i)}\right\}\mathbf{A}_c^T\left(1:L, 1:N_c\right) \\
&= \mathbf{T}_i\mathbf{V} \qquad \text{(A.8)}
\end{aligned}
$$

where $\mathbf{T}_i = \mathrm{diag}\left\{e^{j\frac{2\pi(1-L)d}{\lambda}\sin\theta_{11}}d_{11}^{(i)}, \cdots, e^{j\frac{2\pi(1-L)d}{\lambda}\sin\theta_{1P_1}}d_{1P_1}^{(i)}, \cdots, e^{j\frac{2\pi(1-L)d}{\lambda}\sin\theta_{K1}}d_{K1}^{(i)}, \cdots, e^{j\frac{2\pi(1-L)d}{\lambda}\sin\theta_{KP_K}}d_{KP_K}^{(i)}\right\}$ and $\mathbf{V} = \mathbf{A}_c^T\left(1:L, 1:N_c\right)$.

By the similar principle, one also has

$$
\begin{aligned}
&\left[\boldsymbol{\Phi}^{1-m}\mathbf{d}_i^*, \boldsymbol{\Phi}^{2-m}\mathbf{d}_i^*, \cdots, \boldsymbol{\Phi}^{L-m}\mathbf{d}_i^*\right] \\
&= \boldsymbol{\Phi}^{1-m}\left[\mathbf{d}_i^*, \boldsymbol{\Phi}\mathbf{d}_i^*, \cdots, \boldsymbol{\Phi}^{L-1}\mathbf{d}_i^*\right]
\end{aligned}
$$

$$
\begin{aligned}
&= \mathbf{\Phi}^{1-L}\mathbf{\Phi}^{L-m}\text{diag}\left\{d_{11}^{(i)},\cdots,d_{1P1}^{(i)},\cdots,d_{K1}^{(i)},\cdots,d_{KP_K}^{(i)}\right\}^{*}\mathbf{A}_c^T\left(1:L,1:N_c\right)\\
&= \mathbf{T}_i\mathbf{\Phi}^{L-m}\text{diag}\left\{\frac{d_{11}^{*(i)}}{d_{11}^{(i)}},\cdots,\frac{d_{1P_1}^{*(i)}}{d_{1P_1}^{(i)}},\cdots,\frac{d_{K1}^{*(i)}}{d_{K1}^{(i)}},\cdots,\frac{d_{KP_K}^{*(i)}}{d_{KP_K}^{(i)}}\right\}\mathbf{A}_c^T\left(1:L,1:N_c\right)\\
&= \mathbf{T}_i\left\{e^{j\frac{2\pi(L-m)d}{\lambda}\sin\theta_{11}}\frac{d_{11}^{*(i)}}{d_{11}^{(i)}},\cdots,e^{j\frac{2\pi(L-m)d}{\lambda}\sin\theta_{1P_1}}\frac{d_{1P_1}^{*(i)}}{d_{1P_1}^{(i)}},\cdots,e^{j\frac{2\pi(L-m)d}{\lambda}\sin\theta_{K1}}\frac{d_{K1}^{*(i)}}{d_{K1}^{(i)}},\cdots,\right.\\
&\qquad\left.e^{j\frac{2\pi(L-m)d}{\lambda}\sin\theta_{KP_K}}\frac{d_{KP_K}^{*(i)}}{d_{KP_K}^{(i)}}\right\}\mathbf{A}_c^T\left(1:L,1:N_c\right)\\
&= \mathbf{T}_i\mathbf{H}\mathbf{V}
\end{aligned}
\tag{A.9}
$$

where $\mathbf{H} = \left\{e^{j\frac{2\pi(L-m)d}{\lambda}\sin\theta_{11}}\frac{d_{11}^{*(i)}}{d_{11}^{(i)}},\cdots,e^{j\frac{2\pi(L-m)d}{\lambda}\sin\theta_{1P_1}}\frac{d_{1P_1}^{*(i)}}{d_{1P_1}^{(i)}},\cdots,e^{j\frac{2\pi(L-m)d}{\lambda}\sin\theta_{K1}}\frac{d_{K1}^{*(i)}}{d_{K1}^{(i)}},\cdots,\right.$
$\left.e^{j\frac{2\pi(L-m)d}{\lambda}\sin\theta_{KP_K}}\frac{d_{KP_K}^{*(i)}}{d_{KP_K}^{(i)}}\right\}$.

Hence, equation (5.35) can be rewritten as

$$
\begin{aligned}
\mathbf{D}_i &= \frac{1}{L}\sum_{r=1}^{L}\left\{\mathbf{\Phi}^{1-r}\mathbf{d}_i\mathbf{d}_i^H\mathbf{\Phi}^{r-1}+\mathbf{\Phi}^{r-m}\mathbf{d}_i^*\mathbf{d}_i^T\mathbf{\Phi}^{m-r}\right\}\\
&= \frac{1}{L}\left[\mathbf{\Phi}^{1-L}\mathbf{d}_i,\mathbf{\Phi}^{2-L}\mathbf{d}_i,\cdots,\mathbf{d}_i,\mathbf{\Phi}^{1-m}\mathbf{d}_i^*,\mathbf{\Phi}^{2-m}\mathbf{d}_i^*,\cdots,\mathbf{\Phi}^{L-m}\mathbf{d}_i^*\right]\\
&\quad\times\left[\mathbf{\Phi}^{1-L}\mathbf{d}_i,\mathbf{\Phi}^{2-L}\mathbf{d}_i,\cdots,\mathbf{d}_i,\mathbf{\Phi}^{1-m}\mathbf{d}_i^*,\mathbf{\Phi}^{2-m}\mathbf{d}_i^*,\cdots,\mathbf{\Phi}^{L-m}\mathbf{d}_i^*\right]^H\\
&= \frac{1}{L}\left[\mathbf{T}_i\mathbf{V},\mathbf{T}_i\mathbf{H}\mathbf{V}\right]\left[\mathbf{T}_i\mathbf{V},\mathbf{T}_i\mathbf{H}\mathbf{V}\right]^H\\
&= \frac{1}{L}\mathbf{T}_i\left[\mathbf{V},\mathbf{H}\mathbf{V}\right]\left[\mathbf{V},\mathbf{H}\mathbf{V}\right]^H\mathbf{T}_i^H.
\end{aligned}
\tag{A.10}
$$

A.5 Analysis of the k-th Row of $\mathbf{D}_1 - \lambda\mathbf{I}$

Recalling $\mathbf{D}_1 = \text{diag}\left\{\frac{\overline{\mathbf{A}}(2,1)}{\overline{\mathbf{A}}(1,1)},\cdots,\frac{\overline{\mathbf{A}}(2,K)}{\overline{\mathbf{A}}(1,K)}\right\}$, it is obvious that

$$
\mathbf{D}_1-\lambda\mathbf{I} = \begin{bmatrix}
\frac{\overline{\mathbf{A}}(2,1)}{\overline{\mathbf{A}}(1,1)}-\lambda & & & & \\
& \ddots & & & \\
& & \frac{\overline{\mathbf{A}}(2,k)}{\overline{\mathbf{A}}(1,k)}-\lambda & & \\
& & & \ddots & \\
& & & & \frac{\overline{\mathbf{A}}(2,K)}{\overline{\mathbf{A}}(1,K)}-\lambda
\end{bmatrix}. \tag{A.11}
$$

Once $\lambda = \frac{\overline{\mathbf{A}}(2,k)}{\overline{\mathbf{A}}(1,k)}$, then

$$\mathbf{D}_1 - \lambda\mathbf{I} = \begin{bmatrix} \frac{\overline{\mathbf{A}}(2,1)}{\overline{\mathbf{A}}(1,1)} - \frac{\overline{\mathbf{A}}(2,k)}{\overline{\mathbf{A}}(1,k)} & & & \\ & \ddots & & \\ & & 0 & \\ & & & \ddots \\ & & & & \frac{\overline{\mathbf{A}}(2,K)}{\overline{\mathbf{A}}(1,K)} - \frac{\overline{\mathbf{A}}(2,k)}{\overline{\mathbf{A}}(1,k)} \end{bmatrix} \tag{A.12}$$

which evidently shows that the k-th row of $\mathbf{D}_1 - \lambda\mathbf{I}$ becomes zero.

Appendix B

Proof of Equations and Statements in Chapter 6

THIS appendix contains the details of intermediate steps for some equations and statements developed in Chapter 6.

B.1 Interpretation of G and Corresponding Examples

Kronecker product of two steering vectors for a ULA has redundant entries and the effective aperture is $2M-1$ elements where M is the number of physical sensors. In our case, $\mathbf{C}_{x1} = \text{cum}\left\{\mathbf{x}^*(t), \mathbf{x}^T(t), \mathbf{x}^*(t), \mathbf{x}^T(t)\right\}$, by the principle introduced in [37], the synthetic array manifold after the cumulant operation is $\mathbf{A}^* \circ \mathbf{A}^* = [\mathbf{a}^*(\theta_1) \otimes \mathbf{a}^*(\theta_1), \mathbf{a}^*(\theta_2) \otimes \mathbf{a}^*(\theta_2), \cdots, \mathbf{a}^*(\theta_N) \otimes \mathbf{a}^*(\theta_N)]$. Considering a three-element ULA, one has

$$\mathbf{a}^*(\theta_i) \otimes \mathbf{a}^*(\theta_i) = \left[1, z_i^{-1}, z_i^{-2}, z_i^{-1}, z_i^{-2}, z_i^{-3}, z_i^{-2}, z_i^{-3}, z_i^{-4}\right] \tag{B.1}$$

where $z_i = e^{j\frac{2\pi d}{\lambda}\sin\theta_i}$. Obviously the effective entries are $\left\{z_i^{-k}\right\}_{k=0}^{4}$, and the effective array aperture is 5 elements. Although Prof. Jeny M. Mendel and his colleagues did not propose explicit methods to remove the redundancy, it is not difficult to achieve. Here, we provide a possible solution to this issue while keeping the same maximum effective aperture. Note that $\left\{z_i^{-k}\right\}_{k=0}^{4}$ are located at the both ends of the vector $\mathbf{a}^*(\theta_i) \otimes \mathbf{a}^*(\theta_i)$, we define

$$\mathbf{G} = \begin{bmatrix} \mathbf{I}_M & \mathbf{0}_{M\times(M^2-M)} \\ \mathbf{0}_{(M-1)\times(M^2-M+1)} & \mathbf{I}_{M-1} \end{bmatrix}. \tag{B.2}$$

From the previously constructed $\mathbf{C}_{x1}$ and $\mathbf{C}_{x2}$, we can reduce the problem size by (6.8) and (6.9). Still taking the three-element ULA as an instance, one has

$$\mathbf{G}\mathbf{C}_{x1}\mathbf{G}^H = \begin{bmatrix} 1 & 0 & 0 & 0 & 0 & 0 & 0 & 0 & 0 \\ 0 & 1 & 0 & 0 & 0 & 0 & 0 & 0 & 0 \\ 0 & 0 & 1 & 0 & 0 & 0 & 0 & 0 & 0 \\ 0 & 0 & 0 & 0 & 0 & 0 & 0 & 1 & 0 \\ 0 & 0 & 0 & 0 & 0 & 0 & 0 & 0 & 1 \end{bmatrix} \begin{bmatrix} 1 & 1 & \cdots & 1 \\ z_1^{-1} & z_2^{-1} & \cdots & z_N^{-1} \\ z_1^{-2} & z_2^{-2} & \cdots & z_N^{-2} \\ z_1^{-1} & z_2^{-1} & \cdots & z_N^{-1} \\ z_1^{-2} & z_2^{-2} & \cdots & z_N^{-2} \\ z_1^{-3} & z_2^{-3} & \cdots & z_N^{-3} \\ z_1^{-2} & z_2^{-2} & \cdots & z_N^{-2} \\ z_1^{-3} & z_2^{-3} & \cdots & z_N^{-3} \\ z_1^{-4} & z_2^{-4} & \cdots & z_N^{-4} \end{bmatrix} \mathbf{C}_s$$

$$\times \begin{bmatrix} 1 & 1 & \cdots & 1 \\ z_1^{-1} & z_2^{-1} & \cdots & z_N^{-1} \\ z_1^{-2} & z_2^{-2} & \cdots & z_N^{-2} \\ z_1^{-1} & z_2^{-1} & \cdots & z_N^{-1} \\ z_1^{-2} & z_2^{-2} & \cdots & z_N^{-2} \\ z_1^{-3} & z_2^{-3} & \cdots & z_N^{-3} \\ z_1^{-2} & z_2^{-2} & \cdots & z_N^{-2} \\ z_1^{-3} & z_2^{-3} & \cdots & z_N^{-3} \\ z_1^{-4} & z_2^{-4} & \cdots & z_N^{-4} \end{bmatrix}^H \begin{bmatrix} 1 & 0 & 0 & 0 & 0 & 0 & 0 & 0 & 0 \\ 0 & 1 & 0 & 0 & 0 & 0 & 0 & 0 & 0 \\ 0 & 0 & 1 & 0 & 0 & 0 & 0 & 0 & 0 \\ 0 & 0 & 0 & 0 & 0 & 0 & 0 & 1 & 0 \\ 0 & 0 & 0 & 0 & 0 & 0 & 0 & 0 & 1 \end{bmatrix}^H$$

$$= \begin{bmatrix} 1 & 1 & \cdots & 1 \\ z_1^{-1} & z_2^{-1} & \cdots & z_N^{-1} \\ z_1^{-2} & z_2^{-2} & \cdots & z_N^{-2} \\ z_1^{-3} & z_2^{-3} & \cdots & z_N^{-3} \\ z_1^{-4} & z_2^{-4} & \cdots & z_N^{-4} \end{bmatrix} \mathbf{C}_s \begin{bmatrix} 1 & 1 & \cdots & 1 \\ z_1^{-1} & z_2^{-1} & \cdots & z_N^{-1} \\ z_1^{-2} & z_2^{-2} & \cdots & z_N^{-2} \\ z_1^{-3} & z_2^{-3} & \cdots & z_N^{-3} \\ z_1^{-4} & z_2^{-4} & \cdots & z_N^{-4} \end{bmatrix}^H . \tag{B.3}$$

The specified matrix manipulation for $\mathbf{G}\mathbf{C}_{x2}\mathbf{G}^H$ is the same as the above, so we omit here. It should be noted that the construction of $\mathbf{G}$ is not unique as $\left\{z_i^{-k}\right\}_{k=1}^{3}$ are also located in the middle of the vector $\mathbf{a}^*(\theta_i) \otimes \mathbf{a}^*(\theta_i)$. For example,

$$\mathbf{G} = \begin{bmatrix} 1 & 0 & 0 & 0 & 0 & 0 & 0 & 0 & 0 \\ 0 & 0 & 0 & 1 & 0 & 0 & 0 & 0 & 0 \\ 0 & 0 & 0 & 0 & 1 & 0 & 0 & 0 & 0 \\ 0 & 0 & 0 & 0 & 0 & 1 & 0 & 0 & 0 \\ 0 & 0 & 0 & 0 & 0 & 0 & 0 & 0 & 1 \end{bmatrix} \tag{B.4}$$

can also achieve the same result.

B.2 Interpretation of (6.51)

The vector $\boldsymbol{\eta}$ appears to contain more parameters, i.e., the product of the number of array elements and the number of snapshots, than the DOFs, resulting in unsolvable unknowns. However, it is known that the deterministic CRLB holds for overdetermined

estimation no matter whether the signals are uncorrelated or coherent [56], which implies that the signal waveform estimates $\mathbf{s}(t)$ exist for each snapshot. By this principle, one can solve the real symbols $\mathbf{s}_0(t)$ for each snapshot if the uncorrelated and coherent components can be dealt with separately as the estimation problem becomes overdetermined for uncorrelated or coherent snapshots only. To be specific, given $\boldsymbol{\theta}_u, \boldsymbol{\theta}_c, \boldsymbol{\phi}_u$, which are obtained by the proposed method, and $\boldsymbol{\alpha}$ estimated by the method in [165], by employing oblique projection $\mathbf{E}_{\mathbf{A}_u|\mathbf{A}_c} = \mathbf{A}_u \left(\mathbf{A}_u^H \mathbf{P}_{\mathbf{A}_c}^{\perp} \mathbf{A}_u\right)^{-1} \mathbf{A}_u^H \mathbf{P}_{\mathbf{A}_c}^{\perp}$ in Section 3.8.2, one can readily eliminate the coherent components from the observations and get the uncorrelated part as

$$\begin{aligned}\mathbf{x}_u(t) &= \mathbf{E}_{\mathbf{A}_u|\mathbf{A}_c}\mathbf{x}(t) = \mathbf{E}_{\mathbf{A}_u|\mathbf{A}_c}\left(\mathbf{A}_c\boldsymbol{\Gamma}\boldsymbol{\Psi}_c\mathbf{s}_{c,0}(t) + \mathbf{A}_u\boldsymbol{\Psi}_u\mathbf{s}_{u,0}(t) + \mathbf{n}(t)\right) \\ &= \mathbf{A}_u\boldsymbol{\Psi}_u\mathbf{s}_{u,0}(t) + \mathbf{E}_{\mathbf{A}_u|\mathbf{A}_c}\mathbf{n}(t) \\ &= \mathbf{A}_u\boldsymbol{\Psi}_u\mathbf{s}_{u,0}(t) + \mathbf{n}_u(t) \end{aligned} \tag{B.5}$$

where $\mathbf{n}_u(t) \triangleq \mathbf{E}_{\mathbf{A}_u|\mathbf{A}_c}\mathbf{n}(t)$.

To make the best of noncircularity, one can construct $\mathbf{x}_u^*(t) = \mathbf{A}_u^*\boldsymbol{\Psi}_u^*\mathbf{s}_{u,0}(t) + \mathbf{n}_u^*(t)$. Stacking $\mathbf{x}_u(t)$ and $\mathbf{x}_u^*(t)$ in column format, one has a $2M \times 1$ vector

$$\tilde{\mathbf{x}}_u(t) = \begin{bmatrix}\mathbf{x}_u(t) \\ \mathbf{x}_u^*(t)\end{bmatrix} = \begin{bmatrix}\mathbf{A}_u\boldsymbol{\Psi}_u \\ \mathbf{A}_u^*\boldsymbol{\Psi}_u^*\end{bmatrix}\mathbf{s}_{u,0}(t) + \begin{bmatrix}\mathbf{n}_u(t) \\ \mathbf{n}_u^*(t)\end{bmatrix} = \mathbf{B}_u\mathbf{s}_{u,0}(t) + \tilde{\mathbf{n}}_u(t) \tag{B.6}$$

where $\mathbf{B}_u \triangleq \begin{bmatrix}\mathbf{A}_u\boldsymbol{\Psi}_u \\ \mathbf{A}_u^*\boldsymbol{\Psi}_u^*\end{bmatrix}$ and $\tilde{\mathbf{n}}_u(t) \triangleq \begin{bmatrix}\mathbf{n}_u(t) \\ \mathbf{n}_u^*(t)\end{bmatrix}$.

Likewise, the coherent information can be obtained by removing the uncorrelated components from the received data in conjunction with oblique projection $\mathbf{E}_{\mathbf{A}_c|\mathbf{A}_u} = \mathbf{A}_c \left(\mathbf{A}_c^H \mathbf{P}_{\mathbf{A}_u}^{\perp} \mathbf{A}_c\right)^{-1} \mathbf{A}_c^H \mathbf{P}_{\mathbf{A}_u}^{\perp}$ as

$$\begin{aligned}\mathbf{x}_c(t) &= \mathbf{E}_{\mathbf{A}_c|\mathbf{A}_u}\mathbf{x}(t) = \mathbf{E}_{\mathbf{A}_c|\mathbf{A}_u}\left(\mathbf{A}_c\boldsymbol{\Gamma}\boldsymbol{\Psi}_c\mathbf{s}_{c,0}(t) + \mathbf{A}_u\boldsymbol{\Psi}_u\mathbf{s}_{u,0}(t) + \mathbf{n}(t)\right) \\ &= \mathbf{A}_c\boldsymbol{\Gamma}\boldsymbol{\Psi}_c\mathbf{s}_{c,0}(t) + \mathbf{E}_{\mathbf{A}_c|\mathbf{A}_u}\mathbf{n}(t) \\ &= \mathbf{B}_c\mathbf{s}_c(t) + \mathbf{n}_c(t) \end{aligned} \tag{B.7}$$

where $\mathbf{B}_c \triangleq \mathbf{A}_c\boldsymbol{\Gamma}, \mathbf{s}_c(t) \triangleq \boldsymbol{\Psi}_c\mathbf{s}_{c,0}(t)$, and $\mathbf{n}_c(t) \triangleq \mathbf{E}_{\mathbf{A}_c|\mathbf{A}_u}\mathbf{n}(t)$.

Then, the well-known least-squares solution for each real symbol can be determined as $\mathbf{s}_{u,0}(t) = \mathbf{B}_u^{+}\tilde{\mathbf{x}}_u(t) = \left(\mathbf{B}_u^H\mathbf{B}_u\right)^{-1}\mathbf{B}_u^H\tilde{\mathbf{x}}_u(t)$ and $\mathbf{s}_c(t) = \mathbf{B}_c^{+}\mathbf{x}_c(t) = \left(\mathbf{B}_c^H\mathbf{B}_c\right)^{-1}\mathbf{B}_c^H\mathbf{x}_c(t)$. In other words, by separating the uncorrelated observations from the coherent ones and dealing with the real symbols individually rather than solving them all at once, the unknown parameters included in $\boldsymbol{\eta}$ can be estimated. It should be emphasised that $\tilde{\mathbf{n}}_u(t) = \tilde{\mathbf{x}}_u(t) - \mathbf{B}_u\mathbf{s}_{u,0}(t)$ and $\mathbf{n}_c(t) = \mathbf{x}_c(t) - \mathbf{B}_c\mathbf{s}_c(t)$, so-called residuals or errors, are not the unknown parameters as they are not deterministic but normally characterised by mean and variance in the statistical sense. By the definition of noncircular signal, each signal snapshot can be split as one noncircularity phase and one real-valued symbol, i.e., $s_{k,c}(t) = e^{j\frac{\phi_k}{2}}s_{k,0}(t)$ where $s_{k,c}(t)$ is the k-th entry of $\mathbf{s}_c(t)$, and both unknowns, ϕ_k and $|s_{k,0}(t)|$, can be determined accordingly. It should be noted that for multiple observations $\{\mathbf{x}_c(t)\}_{t=1}^{L}$ one will get multiple signal snapshots estimates $\{\mathbf{s}_c(t)\}_{t=1}^{L}$ with the identical $\boldsymbol{\Psi}_c$. By this property, the signs of the real-valued symbol $\mathbf{s}_{c,0}(t)$ can be determined by adjusting the noncircularity phases, i.e., the estimates ϕ_k and $s_{k,0}(t)$ are finally obtained for each coherent noncircular signal at one time point.

In summary, the signal snapshots, i.e., noncircularity phases and real-valued symbols, can be estimated from the observations by our algorithm. Although the signal snapshots are not the parameters of interest in our study, it does not mean these nuisance unknowns cannot be dealt with. Due to the fact that the unknown parameters interact with and mutually influence each other, the signal snapshots cannot be excluded from the deterministic CRLBs.

B.3 Interpretation of (6.52)

The equation (6.52) is the so-called Slepian-Bangs formula. Indeed, Prof. Stoica and Prof. Nehorai did not show exactly the same expression in [56] but actually following its principle, and the formula does appear in Prof. Stoica's book [164] (see pp. 363, (B.3.25)). Because the Slepian-Bangs formula was first employed by Prof. Stoica and Prof. Nehorai for deterministic CRLB derivation, the following work always attributes this contribution to [56] like [91] by Prof. Gershman and his colleague, and this is why we cite [56] for (6.52). It should be noted that (B.3.25) in [164] is derived for the FIM

of single snapshot, whereas (6.52) in the thesis is for the multiple snapshots case. It is known that the joint probability density function (PDF) of multiple snapshots is the product of the PDF of each snapshot since all snapshots are independent to each other. As FIM stems from the logarithm of the joint PDF of multiple snapshots which converts multiplication to summation, (6.52) is naturally obtained from the sum of (B.3.25) over the number of snapshots.

B.4 Detailed Derivation of Some FIM Blocks

Derivatives with Respect to DOA:

$$\begin{aligned}
\mathbf{F}_{\theta_m\theta_n} &= \frac{2}{\sigma_n^2}\sum_{i=1}^{L}\mathrm{Re}\left\{\frac{\partial \mathbf{s}_0^H(i)\boldsymbol{\Psi}^H\mathbf{Y}^H\mathbf{A}^H}{\partial\theta_m}\frac{\partial \mathbf{A}\mathbf{Y}\boldsymbol{\Psi}\mathbf{s}_0(i)}{\partial\theta_n}\right\} \\
&= \frac{2}{\sigma_n^2}\sum_{i=1}^{L}\mathrm{Re}\left\{\mathbf{s}_0^H(i)\boldsymbol{\Psi}^H\mathbf{Y}^H\left(\dot{\mathbf{A}}\mathbf{e}_m\mathbf{e}_m^T\right)^H\left(\dot{\mathbf{A}}\mathbf{e}_n\mathbf{e}_n^T\right)\mathbf{Y}\boldsymbol{\Psi}\mathbf{s}_0(i)\right\} \\
&= \frac{2}{\sigma_n^2}\sum_{i=1}^{L}\mathrm{Re}\left\{\left(\mathbf{e}_m^T\dot{\mathbf{A}}^H\dot{\mathbf{A}}\mathbf{e}_n\right)\left(\mathbf{e}_n^T\mathbf{Y}\boldsymbol{\Psi}\mathbf{s}_0(i)\mathbf{s}_0^H(i)\boldsymbol{\Psi}^H\mathbf{Y}^H\mathbf{e}_m\right)\right\} \\
&= \frac{2L}{\sigma_n^2}\mathrm{Re}\left\{\left(\mathbf{e}_m^T\dot{\mathbf{A}}^H\dot{\mathbf{A}}\mathbf{e}_n\right)\left(\mathbf{e}_n^T\mathbf{Y}\boldsymbol{\Psi}\left(\frac{1}{L}\sum_{i=1}^{L}\mathbf{s}_0(i)\mathbf{s}_0^H(i)\right)\boldsymbol{\Psi}^H\mathbf{Y}^H\mathbf{e}_m\right)\right\} \\
&= \frac{2L}{\sigma_n^2}\mathrm{Re}\left\{\left(\mathbf{e}_m^T\dot{\mathbf{A}}^H\dot{\mathbf{A}}\mathbf{e}_n\right)\left(\mathbf{e}_n^T\mathbf{Y}\boldsymbol{\Psi}\hat{\mathbf{P}}\boldsymbol{\Psi}^H\mathbf{Y}^H\mathbf{e}_m\right)\right\}
\end{aligned} \tag{B.8}$$

where $\mathbf{e}_k$ is a vector of all zeros except the k-th entry being 1, and we have used the identity that $\mathbf{u}^H\mathbf{A}\mathbf{x}\mathbf{y}^H\mathbf{B}\mathbf{v} = \mathbf{y}^H\mathbf{B}\mathbf{v}\mathbf{u}^H\mathbf{A}\mathbf{x}$ holds for arbitrary vectors $\mathbf{u}\in\mathbb{C}^M, \mathbf{x}\in\mathbb{C}^N, \mathbf{y}\in\mathbb{C}^I, \mathbf{v}\in\mathbb{C}^J$, and matrices $\mathbf{A}\in\mathbb{C}^{M\times N}, \mathbf{B}\in\mathbb{C}^{I\times J}$.

Thereby we can obtain the FIM corresponding to $\boldsymbol{\theta}$ in matrix format as

$$\mathbf{F}_{\boldsymbol{\theta}\boldsymbol{\theta}} = \frac{2L}{\sigma_n^2}\mathrm{Re}\left\{\left(\dot{\mathbf{A}}^H\dot{\mathbf{A}}\right)\odot\left(\mathbf{Y}\boldsymbol{\Psi}\hat{\mathbf{P}}\boldsymbol{\Psi}^H\mathbf{Y}^H\right)^T\right\}. \tag{B.9}$$

In a similar manner, blocks $\mathbf{F}_{\mu\mu}, \mathbf{F}_{\nu\nu}$, and $\mathbf{F}_{\boldsymbol{\phi}\boldsymbol{\phi}}$ can be obtained.

Derivatives with Respect to Real-valued Symbols:

$$\mathbf{F}_{s_{0,m}(i)s_{0,n}(k)} = \frac{2}{\sigma_n^2}\sum_{l=1}^{L}\mathrm{Re}\left\{\frac{\partial \mathbf{s}_0^H(l)\boldsymbol{\Psi}^H\mathbf{Y}^H\mathbf{A}^H}{\partial s_{0,m}(i)}\frac{\partial \mathbf{A}\mathbf{Y}\boldsymbol{\Psi}\mathbf{s}_0(l)}{\partial s_{0,n}(k)}\right\}$$

$$= \frac{2}{\sigma_n^2}\mathrm{Re}\left\{\mathbf{e}_m^T\boldsymbol{\Psi}^H\boldsymbol{\Upsilon}^H\mathbf{A}^H\mathbf{A}\mathbf{Y}\boldsymbol{\Psi}\mathbf{e}_n\right\}\delta_{i,k}. \tag{B.10}$$

Then

$$\mathbf{F}_{\mathbf{s}_0(i)\mathbf{s}_0(k)} = \frac{2}{\sigma_n^2}\mathrm{Re}\left\{\boldsymbol{\Psi}^H\boldsymbol{\Upsilon}^H\mathbf{A}^H\mathbf{A}\mathbf{Y}\boldsymbol{\Psi}\right\}\delta_{i,k} \tag{B.11}$$

$$\mathbf{F}_{\mathbf{s}_0\mathbf{s}_0} = \mathrm{blkdiag}\left\{\mathbf{F}_{\mathbf{s}_0(1)\mathbf{s}_0(1)}, \mathbf{F}_{\mathbf{s}_0(2)\mathbf{s}_0(2)}, \cdots, \mathbf{F}_{\mathbf{s}_0(L)\mathbf{s}_0(L)}\right\}. \tag{B.12}$$

Derivatives with Respect to DOA–Real-valued Symbols Cross Terms:

$$\begin{aligned}\mathbf{F}_{\theta_m s_{0,n}(i)} &= \frac{2}{\sigma_n^2}\sum_{l=1}^{L}\mathrm{Re}\left\{\frac{\partial\mathbf{s}_0^H(l)\boldsymbol{\Psi}^H\boldsymbol{\Upsilon}^H\mathbf{A}^H}{\partial\theta_m}\frac{\partial\mathbf{A}\mathbf{Y}\boldsymbol{\Psi}\mathbf{s}_0(l)}{\partial s_{0,n}(i)}\right\}\\ &= \frac{2}{\sigma_n^2}\mathrm{Re}\left\{\mathbf{s}_0^H(i)\boldsymbol{\Psi}^H\boldsymbol{\Upsilon}^H\left(\dot{\mathbf{A}}\mathbf{e}_m\mathbf{e}_m^T\right)^H\mathbf{A}\mathbf{Y}\boldsymbol{\Psi}\mathbf{e}_n\right\}\\ &= \frac{2}{\sigma_n^2}\mathrm{Re}\left\{\mathbf{s}_0^H(i)\boldsymbol{\Psi}^H\boldsymbol{\Upsilon}^H\mathbf{e}_m\mathbf{e}_m^T\dot{\mathbf{A}}^H\mathbf{A}\mathbf{Y}\boldsymbol{\Psi}\mathbf{e}_n\right\}.\end{aligned} \tag{B.13}$$

Here, note that $\mathbf{s}_0^H(i)\boldsymbol{\Psi}^H\boldsymbol{\Upsilon}^H\mathbf{e}_m\mathbf{e}_m^T = \mathbf{e}_m^T\mathbf{Q}^H(i)$, one has

$$\mathbf{F}_{\theta_m s_{0,n}(i)} = \frac{2}{\sigma_n^2}\mathrm{Re}\left\{\mathbf{e}_m^T\mathbf{Q}^H(i)\dot{\mathbf{A}}^H\mathbf{A}\mathbf{Y}\boldsymbol{\Psi}\mathbf{e}_n\right\} \tag{B.14}$$

$$\mathbf{F}_{\boldsymbol{\theta}\mathbf{s}_0(i)} = \frac{2}{\sigma_n^2}\mathrm{Re}\left\{\mathbf{Q}^H(i)\dot{\mathbf{A}}^H\mathbf{A}\mathbf{Y}\boldsymbol{\Psi}\right\}. \tag{B.15}$$

By the same principle, one has

$$\begin{aligned}\mathbf{F}_{s_{0,m}(i)\theta_n} &= \frac{2}{\sigma_n^2}\mathrm{Re}\left\{\mathbf{e}_m^T\boldsymbol{\Psi}^H\boldsymbol{\Upsilon}^H\mathbf{A}^H\left(\dot{\mathbf{A}}\mathbf{e}_n\mathbf{e}_n^T\right)\mathbf{Y}\boldsymbol{\Psi}\mathbf{s}_0(i)\right\}\\ &= \frac{2}{\sigma_n^2}\mathrm{Re}\left\{\mathbf{e}_m^T\boldsymbol{\Psi}^H\boldsymbol{\Upsilon}^H\mathbf{A}^H\dot{\mathbf{A}}\mathbf{Q}(i)\mathbf{e}_n\right\}\end{aligned} \tag{B.16}$$

$$\mathbf{F}_{\mathbf{s}_0(i)\boldsymbol{\theta}} = \frac{2}{\sigma_n^2}\mathrm{Re}\left\{\boldsymbol{\Psi}^H\boldsymbol{\Upsilon}^H\mathbf{A}^H\dot{\mathbf{A}}\mathbf{Q}(i)\right\}. \tag{B.17}$$

Therefore,

$$\begin{aligned}\mathbf{F}_{\boldsymbol{\theta}\mathbf{s}_0} &= \mathbf{F}_{\mathbf{s}_0\boldsymbol{\theta}}^T\\ &= \left[\mathbf{F}_{\boldsymbol{\theta}\mathbf{s}_0(1)}, \mathbf{F}_{\boldsymbol{\theta}\mathbf{s}_0(2)}, \cdots, \mathbf{F}_{\boldsymbol{\theta}\mathbf{s}_0(L)}\right].\end{aligned} \tag{B.18}$$

Similarly, one can calculate blocks $\mathbf{F}_{\boldsymbol{\mu}\mathbf{s}_0(i)}, \mathbf{F}_{\boldsymbol{\mu}\mathbf{s}_0}, \mathbf{F}_{\boldsymbol{\nu}\mathbf{s}_0(i)}, \mathbf{F}_{\boldsymbol{\nu}\mathbf{s}_0}, \mathbf{F}_{\boldsymbol{\phi}\mathbf{s}_0(i)}$, and $\mathbf{F}_{\boldsymbol{\phi}\mathbf{s}_0}$.

Derivatives with Respect to DOA–Fading Coefficients Cross Terms:

$$\begin{aligned}
\mathbf{F}_{\theta_m\mu_n} &= \frac{2}{\sigma_n^2}\sum_{i=1}^{L}\mathrm{Re}\left\{\frac{\partial \mathbf{s}_0^H(i)\boldsymbol{\Psi}^H\boldsymbol{\Upsilon}^H\mathbf{A}^H}{\partial\theta_m}\frac{\partial\mathbf{A}\boldsymbol{\Upsilon}\boldsymbol{\Psi}\mathbf{s}_0(i)}{\partial\mu_n}\right\} \\
&= \frac{2}{\sigma_n^2}\sum_{i=1}^{L}\mathrm{Re}\left\{\mathbf{s}_0^H(i)\boldsymbol{\Psi}^H\boldsymbol{\Upsilon}^H\left(\dot{\mathbf{A}}\mathbf{e}_m\mathbf{e}_m^T\right)^H\mathbf{A}_c\left(\mathbf{e}_n\mathbf{e}_n^T\boldsymbol{\Pi}\right)\boldsymbol{\Psi}_c\mathbf{s}_{c,0}(i)\right\} \\
&= \frac{2}{\sigma_n^2}\sum_{i=1}^{L}\mathrm{Re}\left\{\mathbf{s}_0^H(i)\boldsymbol{\Psi}^H\boldsymbol{\Upsilon}^H\mathbf{e}_m\mathbf{e}_m^T\dot{\mathbf{A}}^H\mathbf{A}_c\mathbf{e}_n\mathbf{e}_n^T\boldsymbol{\Pi}\boldsymbol{\Psi}_c\mathbf{s}_{c,0}(i)\right\} \\
&= \frac{2L}{\sigma_n^2}\mathrm{Re}\left\{\left(\mathbf{e}_m^T\dot{\mathbf{A}}^H\mathbf{A}_c\mathbf{e}_n\right)\left(\mathbf{e}_n^T\boldsymbol{\Pi}\boldsymbol{\Psi}_c\hat{\mathbf{P}}_d\boldsymbol{\Psi}^H\boldsymbol{\Upsilon}^H\mathbf{e}_m\right)\right\} \qquad \text{(B.19)} \\
\mathbf{F}_{\boldsymbol{\theta\mu}} &= \frac{2L}{\sigma_n^2}\mathrm{Re}\left\{\left(\dot{\mathbf{A}}^H\mathbf{A}_c\right)\odot\left(\boldsymbol{\Pi}\boldsymbol{\Psi}_c\hat{\mathbf{P}}_d\boldsymbol{\Psi}^H\boldsymbol{\Upsilon}^H\right)^T\right\}. \qquad \text{(B.20)}
\end{aligned}$$

Following the similar procedures, one can arrive at

$$\begin{aligned}
\mathbf{F}_{\mu_m\theta_n} &= \frac{2}{\sigma_n^2}\sum_{i=1}^{L}\mathrm{Re}\left\{\mathbf{s}_{c,0}^H(i)\boldsymbol{\Psi}_c^H\left(\mathbf{e}_m\mathbf{e}_m^T\boldsymbol{\Pi}\right)^H\mathbf{A}_c^H\left(\dot{\mathbf{A}}\mathbf{e}_n\mathbf{e}_n^T\right)\boldsymbol{\Upsilon}\boldsymbol{\Psi}\mathbf{s}_0(i)\right\} \\
&= \frac{2L}{\sigma_n^2}\mathrm{Re}\left\{\left(\mathbf{e}_m^T\mathbf{A}_c^H\dot{\mathbf{A}}\mathbf{e}_n\right)\left(\mathbf{e}_n^T\boldsymbol{\Upsilon}\boldsymbol{\Psi}\hat{\mathbf{P}}_d^H\boldsymbol{\Psi}_c^H\boldsymbol{\Pi}^H\mathbf{e}_m\right)\right\} \qquad \text{(B.21)} \\
\mathbf{F}_{\boldsymbol{\mu\theta}} &= \frac{2L}{\sigma_n^2}\mathrm{Re}\left\{\left(\left(\dot{\mathbf{A}}^H\mathbf{A}_c\right)\odot\left(\boldsymbol{\Pi}\boldsymbol{\Psi}_c\hat{\mathbf{P}}_d\boldsymbol{\Psi}^H\boldsymbol{\Upsilon}^H\right)^T\right)^H\right\} \\
&= \mathbf{F}_{\boldsymbol{\theta\mu}}^T. \qquad \text{(B.22)}
\end{aligned}$$

The rest cross terms $\mathbf{F}_{\boldsymbol{\theta\nu}}, \mathbf{F}_{\boldsymbol{\theta\phi}}, \mathbf{F}_{\boldsymbol{\mu\nu}}, \mathbf{F}_{\boldsymbol{\mu\phi}}$, and $\mathbf{F}_{\boldsymbol{\nu\phi}}$ can be calculated in the same way.

Derivatives with Respect to Noise Power:

$$\begin{aligned}
\mathbf{F}_{\sigma_n^2\sigma_n^2} &= \sum_{i=1}^{L}\mathrm{tr}\left\{\left(\sigma_n^2\mathbf{I}_M\right)^{-1}\frac{\partial\sigma_n^2\mathbf{I}_M}{\partial\sigma_n^2}\left(\sigma_n^2\mathbf{I}_M\right)^{-1}\frac{\partial\sigma_n^2\mathbf{I}_M}{\partial\sigma_n^2}\right\} \\
&= \sum_{i=1}^{L}\mathrm{tr}\left\{\sigma_n^{-2}\mathbf{I}_M\mathbf{I}_M\sigma_n^{-2}\mathbf{I}_M\mathbf{I}_M\right\} \\
&= \frac{ML}{\sigma_n^4}. \qquad \text{(B.23)}
\end{aligned}$$

All FIM cross terms involving both signal and noise parameters are identically zero.

Bibliography

[1] M. Shell, "How to use the IEEEtran LATEX class," *J. LATEX Class Files*, vol. 13, no. 9, pp. 1–27, Sep. 2014.

[2] Bureau International des Poids et Mesures. The international system of units (SI). [Online]. Available: http://www.bipm.org/utils/common/pdf/si_brochure_8_en.pdf [22 February 2015].

[3] H. L. Van Trees, *Detection Estimation and Modulation Theory, Part IV, Optimum Array Processing*. New York: John Wiley and Sons, 2002.

[4] M. I. Skolnik, *Introductioni to Radar Systems*. New York: McGraw-Hill, 1980.

[5] F. L. Chevalier, *Principles of Radar and Sonar Signal Processing*. Norwood, MA: Artech House, 2002.

[6] A. V. Oppenheim, *Applications of Digital Signal Processing*. Englewood Cliffs, New Jersey: Prentice-Hall, 1978.

[7] S. D. Blostein and H. Leib, "Multiple antenna systems: Role and impact in future wireless access," *IEEE Commun. Mag.*, vol. 41, no. 7, pp. 94–101, Jul. 2003.

[8] D. Tse and P. Viswanath, *Fundamentals of Wireless Communication*. Englewood Cliffs, New Jersey: Cambridge Univ. Press, 2005.

[9] M. Wang, A. Wang, A. Gorokhov, T. Kadus, and M. Dong, "Multi-antenna techniques for evolved 3G wireless communication networks: An overview," *J. Commun.*, vol. 4, no. 1, pp. 61–69, Jul. 2009.

[10] R. L. Fante and J. J. Vaccaro, "Wideband cancellation of interference in a GPS receive array," *IEEE Trans. Aerosp. Electron. Syst.*, vol. 36, no. 2, pp. 549–564, Apr. 2000.

[11] A. El-Rabbany, *Introduction to GPS—The Global Positioning System*, 2nd ed. Boston, MA: Artech House, 2006.

[12] E. D. Kaplan and C. J. Hegarty, Eds., *Understanding GPS: Principles and Applications*, 2nd ed. Boston, MA: Artech House, 2006.

[13] J. C. J. Benesty and Y. Huang, *Microphone Array Signal Processing*. Berlin, Germany: Springer-Verlag, 2008.

[14] M. Brandstein and D. Ward, Eds., *Microphone Arrays: Signal Processing Techniques and Applications*. Berlin, Germany: Springer-Verlag, 2001.

[15] J. C. Chen, K. Yao, and R. E. Hudson, "Source localization and beamforming," *IEEE Signal Process. Mag.*, vol. 19, no. 2, pp. 30–39, Mar. 2002.

[16] H. Sato, M. C. Fehler, and T. Maeda, *Seismic Wave Propagation and Scattering in the Heterogeneous Earth*, 2nd ed. Berlin Heidelberg: Springer-Verlag, 2012.

[17] A. L. Swindlehurst, "Time delay and spatial signature estimation using known asynchronous signals," *IEEE Trans. Signal Process.*, vol. 46, no. 2, pp. 449–462, Feb. 1998.

[18] A.-J. van der Veen, M. C. Vanderveen, and A. Paulraj, "Joint angle and delay estimation using shift-invariance techniques," *IEEE Trans. Signal Process.*, vol. 46, no. 2, pp. 405–418, Feb. 1998.

[19] O. Simeone, Y. Bar-Ness, and U. Spagnolini, "Pilot-based channel estimation for OFDM systems by tracking the delay-subspace," *IEEE Trans. Wireless Commun.*, vol. 3, no. 1, pp. 315–325, Jan. 2004.

[20] J. Liu, Z. Huang, and Y. Zhou, "Extended 2q-MUSIC algorithm for noncircular signals," *Signal Process.*, vol. 88, no. 6, pp. 1327–1339, Jun. 2008.

[21] J. E. Evans, J. R. Johnson, and D. F. Sun, "High resolution angular spectrum estimation techniques for terrain scattering analysis and angle of arrival estimation," in *Proc. 1st ASSP Workshop Spectral Estimation*, Hamilton, Ontario, Canada, 1981, pp. 134–139.

[22] T. J. Shan and T. Kailath, "Adaptive beamforming for coherent signals and interference," *IEEE Trans. Acoust., Speech, Signal Process.*, vol. 33, no. 3, pp. 527–536, Jun. 1985.

[23] T. J. Shan, M. Wax, and T. Kailath, "On spatial smoothing for direction-of-arrival estimation of coherent signals," *IEEE Trans. Acoust., Speech, Signal Process.*, vol. 33, no. 4, pp. 806–811, Aug. 1985.

[24] S. U. Pillai and B. H. Kwon, "Forward/backward spatial smoothing techniques for coherent signal identification," *IEEE Trans. Acoust., Speech, Signal Process.*, vol. 37, no. 1, pp. 8–15, Jan. 1989.

[25] A. Moghaddamjoo and T. C. Chang, "Signal enhancement of the spatial smoothing algorithm," *IEEE Trans. Signal Process.*, vol. 39, no. 8, pp. 1907–1911, Aug. 1991.

[26] J. Li, "Improved angular resolution for spatial smoothing techniques," *IEEE Trans. Signal Process.*, vol. 40, no. 12, pp. 3078–3081, Dec. 1992.

[27] D. A. Linebarger, R. D. DeGroat, and E. M. Dowling, "Efficient direction-finding methods employing forward/backward averaging," *IEEE Trans. Signal Process.*, vol. 42, no. 8, pp. 2136–2145, Aug. 1994.

[28] A. Z. Di, "Multiple source location—A matrix decomposition approach," *IEEE Trans. Acoust., Speech, Signal Process.*, vol. 33, no. 5, pp. 1086–1091, Oct. 1985.

[29] J. A. Cadzow, Y. S. Kim, and D. C. Shiue, "General direction-of-arrival estimation: A signal subspace approach," *IEEE Trans. Aerosp. Electron. Syst.*, vol. 25, no. 1, pp. 31–47, Jan. 1989.

[30] F. M. Han and X. D. Zhang, "An ESPRIT-like algorithm for coherent DOA estimation," *IEEE Antennas Wireless Propag. Lett.*, vol. 4, no. 1, pp. 443–446, 2005.

[31] B. Friedlander, "A sensitivity analysis of the MUSIC algorithm," *IEEE Trans. Acoust., Speech, Signal Process.*, vol. 38, no. 10, pp. 1740–1751, Oct. 1990.

[32] F. Li and R. J. Vaccaro, "Sensitivity analysis of DOA estimation algorithms to sensor errors," *IEEE Trans. Aerosp. Electron. Syst.*, vol. 28, no. 3, pp. 708–717, Jul. 1992.

[33] A. L. Swindlehurst and T. Kailath, "A performance analysis of subspaced-based methods in the presence of model errors, Part I: The MUSIC algorithm," *IEEE Trans. Signal Process.*, vol. 40, no. 7, pp. 1758–1773, Jul. 1992.

[34] A. Paulraj and T. Kailath, "Eigenstructure methods for direction of arrival estimation in the presence of unknown noise field," *IEEE Trans. Acoust., Speech, Signal Process.*, vol. 34, no. 1, pp. 13–20, Feb. 1986.

[35] M. Kaveh and A. Barabell, "The statistical performance of the MUSIC and the minimum-norm algorithms in resolving plane waves in noise," *IEEE Trans. Acoust., Speech, Signal Process.*, vol. 34, no. 2, pp. 331–341, Apr. 1986.

[36] B. Porat and B. Friedlander, "Direction finding algorithms based on higher order statistics," *IEEE Trans. Signal Process.*, vol. 39, no. 9, pp. 2016–2024, Sep. 1991.

[37] M. C. Dŏgan and J. M. Mendel, "Applications of cumulants to array processing—Part I: Aperture extension and array calibration," *IEEE Trans. Signal Process.*, vol. 43, no. 5, pp. 1200–1216, May 1995.

[38] E. Gönen and J. M. Mendel, "Applications of cumulants to array processing—Part III: Blind beamforming for coherent signals," *IEEE Trans. Signal Process.*, vol. 45, no. 9, pp. 2252–2264, Sep. 1997.

[39] E. Gönen, J. M. Mendel, and M. C. Dŏgan, "Applications of cumulants to array processing—Part IV: Direction finding in coherent signals case," *IEEE Trans. Signal Process.*, vol. 45, no. 9, pp. 2265–2276, Sep. 1997.

[40] N. Yuen and B. Friedlander, "DOA estimation in multipath: An approach using fourth-order cumulants," *IEEE Trans. Signal Process.*, vol. 45, no. 5, pp. 1253–1263, 1997.

[41] R. Rajagopal and P. R. Rao, "Generalized algorithm for DOA estimation in a passive sonar," *IEE Proc. F, Radar Signal Process.*, vol. 140, no. 1, pp. 12–20, Feb. 1993.

[42] J. S. Thompson, P. M. Grant, B. Mulgrew, and P. Rajagopal, "Generalized algorithm for DOA estimation in a passive sonar," *IEE Proc. F, Radar Signal Process.*, vol. 140, no. 5, pp. 339–340, Oct. 1993.

[43] C. Qi, Y. Wang, Y. Zhang, and Y. Han, "Spatial difference smoothing for DOA estimation of coherent signals," *IEEE Signal Process. Lett.*, vol. 12, no. 11, pp. 800–802, Nov. 2005.

[44] Z. Ye and X. Xu, "DOA estimation by exploiting the symmetric configuration of uniform linear array," *IEEE Trans. Antennas Propag.*, vol. 55, no. 12, pp. 3716–3720, Dec. 2007.

[45] Y. Zhang and Z. Ye, "Efficient method of DOA estimation for uncorrelated and coherent signals," *IEEE Antennas Wireless Propag. Lett.*, vol. 7, pp. 799–802, 2008.

[46] Z. Ye, Y. Zhang, X. Xu, and C. Liu, "Direction of arrival estimation for uncorrelated and coherent signals with uniform linear array," *IET Radar Sonar Navig.*, vol. 3, no. 4, pp. 144–154, Apr. 2009.

[47] F. Liu, J. Wang, C. Sun, and R. Du, "Spatial differencing method for DOA estimation under the coexistence of both uncorrelated and coherent signals," *IEEE Trans. Antennas Propag.*, vol. 60, no. 4, pp. 2052–2062, Apr. 2012.

[48] E. M. Al-Ardi, R. M. Shubair, and M. E. Al-Mualla, "Computationally efficient high resolution DOA estimation in multipath environment," *IEE Electron. Lett.*, vol. 40, no. 1, pp. 908–910, Jul. 2004.

[49] Z. Ye and Y. Zhang, "DOA estimation for non-Gaussian signals using fourth-order cumulants," *IET Microw. Antennas Propag.*, vol. 3, no. 7, pp. 1069–1078, Oct. 2009.

[50] Z. Ye, Y. Zhang, and C. Liu, "Direction-of-arrival estimation for uncorrelated and coherent signals with fewer sensors," *IET Microw. Antennas Propag.*, vol. 3, no. 3, pp. 473–482, Apr. 2009.

[51] L. C. Godara, "Beamforming in the presence of correlated arrivals using structured correlation matrix," *IEEE Trans. Acoust., Speech, Signal Process.*, vol. 38, no. 1, pp. 1–15, Jan. 1990.

[52] K. Takao and N. Kikuma, "An adaptive array utilizing an adaptive spatial averaging technique for multipath environments," *IEEE Trans. Antennas Propag.*, vol. 35, no. 12, pp. 1389–1396, Dec. 1987.

[53] Y. M. Chen, J. H. Lee, C. C. Yeh, and J. Mar, "Bearing estimation without calibration for randomly perturbed arrays," *IEEE Trans. Signal Process.*, vol. 39, no. 1, pp. 194–197, Jan. 1991.

[54] J. J. Fuchs, "Rectangular Pisarenko method applied to source localization," *IEEE Trans. Signal Process.*, vol. 44, no. 10, pp. 2377–2383, Oct. 1996.

[55] I. Ziskind and M. Wax, "Maximum likelihood localization of multiple sources by alternating projection," *IEEE Trans. Signal Process.*, vol. 36, no. 10, pp. 1553–1560, Oct. 1996.

[56] P. Stoica and A. Nehorai, "MUSIC, maximum likelihood, and Cramer-Rao bound," *IEEE Trans. Acoust., Speech, Signal Process.*, vol. 37, no. 5, pp. 720–741, May 1989.

[57] P. Stoica and K. C. Sharman, "Maximum likelihood methods for direction of arrival estimation," *IEEE Trans. Acoust., Speech, Signal Process.*, vol. 38, no. 7, pp. 1132–1143, Jul. 1990.

[58] M. I. Miller and D. R. Fuhrmann, "Maximum-likelihood narrow-band direction finding and the EM algorithm," *IEEE Trans. Acoust., Speech, Signal Process.*, vol. 38, no. 9, pp. 1560–1577, Sep. 1990.

[59] P. Stoica and A. Nehorai, "Performance study of conditional and unconditional direction-of-arrival estimation," *IEEE Trans. Acoust., Speech, Signal Process.*, vol. 38, no. 10, pp. 1783–1795, Oct. 1990.

[60] M. Wax, "Detection and localization of multiple sources in noise with unknown covariance," *IEEE Trans. Acoust., Speech, Signal Process.*, vol. 40, no. 1, pp. 245–249, Jan. 1992.

[61] B. Ottersten, M. Viberg, and T. Kailath, "Analysis of subspace fitting and ML techniques for parameter estimation from sensor array data," *IEEE Trans. Signal Process.*, vol. 40, no. 3, pp. 590–600, Mar. 1992.

[62] G. H. Golub and V. Pereyra, "The differentiation of pseudo-inverses and nonlinear least squares problems whose variables separate," *SIAM J. Numer. Anal.*, vol. 10, pp. 413–432, 1973.

[63] J. A. Cadzow, "Multiple source location—The signal subspace approach," *IEEE Trans. Acoust., Speech, Signal Process.*, vol. 38, no. 7, pp. 1110–1125, Jul. 1990.

[64] M. Viberg and A. L. Swindlehurst, "A Bayesian approach to auto-calibration for parametric array signal processing," *IEEE Trans. Signal Process.*, vol. 42, no. 12, pp. 3495–3507, Dec. 1994.

[65] S. K. Oh and C. K. Un, "Simple computational methods of the AP algorithm for maximum likelihood localization of multiple radiating sources," *IEEE Trans. Signal Process.*, vol. 40, no. 11, pp. 2848–2854, Nov. 1992.

[66] A. P. Dempster, N. M. Laird, and D. B. Rubin, "Maximum likelihood from incomplete data via the EM algorithm," *J. Roy. Statist. Soc.*, vol. 39, pp. 1–38, 1977.

[67] X. Meng and D. V. Dyk, "The EM algorithm—An old folk-song sung to a fast new tune," *J. Roy. Statist. Soc.*, vol. 59, pp. 511–567, 1997.

[68] N. Cadalli and O. Arikan, "Wideband maximum likelihood direction finding and signal parameter estimation by using treeructured EM algorithm," *IEEE Trans. Signal Process.*, vol. 47, no. 1, pp. 201–206, Jan. 1999.

[69] R. J. Kozick and B. M. Sadler, "Maximum-likelihood array processing in non-Gaussian noise with Gaussian mixtures," *IEEE Trans. Signal Process.*, vol. 48, no. 12, pp. 3520–3535, Dec. 2000.

[70] M. Viberg, B. Ottersten, and T. Kailath, "Detection and estimation in sensor arrays using weighted subspace fitting," *IEEE Trans. Signal Process.*, vol. 39, no. 11, pp. 2436–2449, 1991.

[71] J. Li, P. Stoica, and Z. S. Liu, "Comparative study of IQML and MODE direction-of-arrival estimators," *IEEE Trans. Signal Process.*, vol. 46, no. 1, pp. 149–160, Jan. 1998.

[72] M. Viberg and B. Ottersten, "Sensor array processing based on subspace fitting," *IEEE Trans. Signal Process.*, vol. 39, no. 5, pp. 1110–1121, May 1991.

[73] M. Viberg, B. Ottersten, and T. Kailath, "Detection and estimation in sensor arrays using weighted subspace fitting," *IEEE Trans. Signal Process.*, vol. 39, no. 11, pp. 2436–2449, Nov. 1991.

[74] B. Ottersten, M. Viberg, P. Stoica, and A. Nehorai, "Exact and large sample maximum likelihood techniques for parameter estimation and detection in array processing," in *Radar Array Processing*, S. Haykin, J. Litva, and T. J. Shepherd, Eds., Berlin, 1993, ch. 4.

[75] H. Wang and M. Kaveh, "Coherent signal-subspace processing for the detection and estimation of angles of arrival of multiple wide-band sources," *IEEE Trans. Acoust., Speech, Signal Process.*, vol. 33, no. 4, pp. 823–831, Aug. 1985.

[76] H. Wang and M. Kaveh, "On the performance of signal-subspace processing—Part II: Coherent wide-band systems," *IEEE Trans. Acoust., Speech, Signal Process.*, vol. 35, no. 11, pp. 1583–1591, Nov. 1987.

[77] J. Li and R. T. Compton Jr., "Angle and polarization estimation in a coherent signal environment," *IEEE Trans. Aerosp. Electron. Syst.*, vol. 29, no. 3, pp. 706–716, Jul. 1993.

[78] D. Rahamim, J. Tabrikian, and R. Shavit, "Source localization using vector sensor array in a multipath environment," *IEEE Trans. Signal Process.*, vol. 52, no. 11, pp. 3096–3103, Nov. 2004.

[79] C. P. Mathews and M. D. zoltowski, "Eigenstructure techniques for 2-D angle estimation with uniform circular arrays," *IEEE Trans. Signal Process.*, vol. 42, no. 9, pp. 2395–2407, Sep. 1994.

[80] A. J. Weiss and B. Friedlander, "Direction finding using spatial smoothing with interpolated arrays," *IEEE Trans. Aerosp. Electron. Syst.*, vol. 28, no. 2, pp. 574–587, Apr. 1992.

[81] A. J. Weiss, B. Friedlander, and P. Stoica, "Direction-of-arrival estimation using MODE with interpolated arrays," *IEEE Trans. Signal Process.*, vol. 43, no. 1, pp. 296–300, Jan. 1995.

[82] B. Friedlander and A. J. Weiss, "Direction finding using noise covariance modeling," *IEEE Trans. Signal Process.*, vol. 43, pp. 1557–1567, Jul. 1995.

[83] S. Haykin, *Advances in Spectrum Analysis and Array Processing*. Englewood Cliffs, NJ: Prentice-Hall, 1995, vol. II and III.

[84] J. LeCadre, "Parametric methods for spatial signal processing in the presence of unknown colored noise fields," *IEEE Trans. Acoust., Speech, Signal Process.*, vol. 37, no. 7, pp. 965–983, Jul. 1989.

[85] K. M. Wong, J. P. Reilly, Q. Wu, and S. Qiao, "Estimation of the directions of arrival of signals in unknown correlated noise, Part I: The MAP approach and its implementation," *IEEE Trans. Signal Process.*, vol. 40, no. 8, pp. 2007–2017, Aug. 1992.

[86] P. Stoica, M. Viberga, and B. Ottersten, "Instrumental variable approach to array processing in spatially correlated noise fields," *IEEE Trans. Signal Process.*, vol. 42, no. 1, pp. 121–133, Jan. 1994.

[87] H. Ye and R. D. DeGroat, "Maximum likelihood DOA estimation and asymptotic Cramér-Rao bounds for additive unknown colored noise," *IEEE Trans. Signal Process.*, vol. 43, no. 4, pp. 938–949, Apr. 1995.

[88] A. B. Gershman, A. L. Matveyev, and J. F. Böhme, "Maximum likelihood estimation of signal power in sensor array in the presence of unknown noise field," *IEE Proc. Radar, Sonar, Navig.*, vol. 142, no. 5, pp. 218–224, Oct. 1995.

[89] V. Nagesha and S. Kay, "Maximum likelihood estimation for array processing in colored noise," *IEEE Trans. Signal Process.*, vol. 44, no. 2, pp. 169–180, Feb. 1996.

[90] M. Viberg, P. Stoica, and B. Ottersten, "Maximum likelihood array processing in spatially correlated noise fields using parameterized signals," *IEEE Trans. Signal Process.*, vol. 45, no. 4, pp. 996–1004, Apr. 1997.

[91] M. Pesavento and A. B. Gershman, "Maximum-likelihood direction of arrival estimation in the presence of unknown nonuniform noise," *IEEE Trans. Signal Process.*, vol. 49, no. 7, pp. 1310–1324, Jul. 2001.

[92] C. E. Chen, F. Lorenzelli, and K. Yao, "Stochastic maximum likelihood DOA estimation in the presence of unknown nonuniform noise," *IEEE Trans. Signal Process.*, vol. 56, no. 7, pp. 3038–3044, Jul. 2008.

[93] B. Goransson and B. Ottersten, "Direction estimation in partially unknown noise fields," *IEEE Trans. Signal Process.*, vol. 47, no. 9, pp. 2375–2385, Sep. 1999.

[94] M. Agrawal and S. Prasad, "A modified likelihood function approach to DOA estimation in the presence of unknown spatially correlated Gaussian noise using a uniform linear array," *IEEE Trans. Signal Process.*, vol. 48, no. 10, pp. 2743–2749, Oct. 2000.

[95] S. A. Vorobyov, A. B. Gershman, and K. M. Wong, "Maximum likelihood direction-of-arrival estimation in unknown noise fields using sparse sensor arrays," *IEEE Trans. Signal Process.*, vol. 53, no. 1, pp. 34–43, Apr. 2005.

[96] A. Moghaddamjoo, "Transform-based covariance difference approach to the array with spatially nonstationary noise," *IEEE Trans. Signal Process.*, vol. 39, no. 1, pp. 219–221, Jan. 1991.

[97] Y. Wu, C. Hou, G. Liao, and Q. Guo, "Direction of arrival estimation in the presence of unknown nonuniform noise fields," *IEEE J. Ocean. Eng.*, vol. 31, no. 2, pp. 504–510, Apr. 2006.

[98] B. Liao, G. Liao, and J. Wen, "A method for DOA estimation in the presence of unknown nonuniform noise," *J. Electromagn. Waves Appl.*, vol. 22, no. 14-15, pp. 2113–2123, 2008.

[99] T. Li and A. Nehorai, "Maximum likelihood direction finding in spatially colored noise fields using sparse sensor arrays," *IEEE Trans. Signal Process.*, vol. 59, no. 3, pp. 1048–1062, Mar. 2011.

[100] P. Stoica, M. Agrawal, and P. Åhgren, "Array processing for signals with non-zero means in colored noise fields," *Digit. Signal Process.*, vol. 14, no. 4, pp. 296–311, Jul. 2004.

[101] J. K. Tugnait, "On time delay estimation with unknown spatially correlated gaussian noise using fourth-order cumulants and cross cumulants," *IEEE Trans. Signal Process.*, vol. 39, no. 6, pp. 1258–1267, Jun. 1991.

[102] J. K. Tugnait, "Time delay estimation with unknown spatially correlated gaussian noise," *IEEE Trans. Signal Process.*, vol. 41, no. 2, pp. 549–558, Feb. 1993.

[103] Y. H. Chen and Y. S. Lin, "Cumulant-based method for bearing estimation in the presence of non-Gaussian noise," *IEEE Trans. Antennas Propag.*, vol. 42, no. 4, pp. 548–552, Apr. 1994.

[104] J. F. Cardoso and E. Moulines, "Asymptotic performance analysis of direction-finding algorithms based on fourth-order cumulants," *IEEE Trans. Signal Process.*, vol. 43, no. 1, pp. 214–224, Jan. 1995.

[105] P. Chargé, Y. Wang, and J. Saillard, "A non-circular sources direction finding method using polynomial rooting," *Signal Process.*, vol. 81, no. 8, pp. 1765–1770, Aug. 2001.

[106] M. Haardt and F. Roemer, "Enhancements of unitary ESPRIT for noncircular sources," in *Proc. IEEE Int. Conf. Acoust., Speech, Signal Process. (ICASSP)*, vol. 2, Montreal, QC, Canada, May 2004, pp. 101–104.

[107] F. Roemer and M. Haardt, "Efficient 1-D and 2-D DOA estimation for noncircular sources with hexagonal shaped ESPAR arrays," in *Proc. IEEE Int. Conf. Acoust., Speech, Signal Process. (ICASSP)*, vol. 5, Toulouse, France, May 2006, pp. 881–884.

[108] H. Abeida and J. P. Delmas, "MUSIC-like estimation of direction of arrival for noncircular sources," *IEEE Trans. Signal Process.*, vol. 54, no. 7, pp. 2678–2690, Jul. 2006.

[109] Z. Liu, Z. Huang, Y. Zhou, and J. Liu, "Direction-of-arrival estimation of noncircular signals via sparse representation," *IEEE Trans. Aerosp. Electron. Syst.*, vol. 48, no. 3, pp. 2690–2698, Jul. 2012.

[110] J. P. Delmas and H. Abeida, "Stochastic Cramér-Rao bound for noncircular signals with application to DOA estimation," *IEEE Trans. Signal Process.*, vol. 52, no. 11, pp. 3192–3199, Nov. 2004.

[111] H. Abeida and J. P. Delmas, "Statistical performance of MUSIC-like algorithms in resolving non-circular sources," *IEEE Trans. Signal Process.*, vol. 56, no. 9, pp. 4317–4329, Sep. 2008.

[112] F. Roemer and M. Haardt, "Deterministic Cramér-Rao bounds for strict sense non-circular sources," in *Proc. ITG/IEEE Workshop Smart Antennas (WSA)*, Vienna, Austria, Feb. 2007.

[113] J. Steinwandt, F. Roemer, M. Haardt, and G. D. Galdo, "*R*-dimensional ESPRIT-type algorithms for strictly second-order non-circular sources and their performance analysis," *IEEE Trans. Signal Process.*, vol. 62, no. 18, pp. 4824–4838, Sep. 2014.

[114] F. Gao, A. Nallanathan, and Y. Wang, "Improved MUSIC under the coexistence of both circular and noncircular sources," *IEEE Trans. Signal Process.*, vol. 56, no. 7, pp. 3033–3038, Jul. 2008.

[115] P. Gounon, C. Adnet, and J. Galy, "Localization angulaire de signaux non circulaires," *Traitement du Signal*, vol. 15, no. 1, pp. 17–23, 1998.

[116] J. Galy, "Antenne adaptative: Du seconde ordre aux ordres supérieurs, applications aux signaux de télécommunications," Ph.D thesis, Toulouse, France, 1998.

[117] A. J. Barabell, "Improving the resolution performance of eigenstructure based direction finding algorithms," in *Proc. IEEE Int. Conf. Acoust., Speech, Signal Process. (ICASSP)*, vol. 8, Boston, MA, Apr. 1983, pp. 336–339.

[118] P. Chevalier, A. Ferreol, and L. Albera, "High resolution direction finding from higher order statistics: The 2q-MUSIC algorithm," *IEEE Trans. Signal Process.*, vol. 54, no. 8, pp. 2986–2997, Aug. 2006.

[119] D. P. Wipf, B. D. Rao, and S. Nagarajan, "Latent variable Bayesian models for promoting sparsity," *IEEE Trans. Inf. Theory*, vol. 57, no. 9, pp. 6236–6255, Sep. 2011.

[120] D. P. Wipf and B. D. Rao, "Sparse Bayesian learning for basis selection," *IEEE Trans. Signal Process.*, vol. 52, no. 8, pp. 2153–2164, Aug. 2004.

[121] J. Yin and T. Chen, "Direction-of-arrival estimation using a sparse representation of array covariance vectors," *IEEE Trans. Signal Process.*, vol. 59, no. 9, pp. 4489–4493, Sep. 2011.

[122] X. Xu, X. Wei, and Z. Ye, "DOA estimation based on sparse signal recovery utilizing weighted ℓ_1-norm penalty," *IEEE Signal Process. Lett.*, vol. 19, no. 3, pp. 155–158, Mar. 2012.

[123] H. Abeida and J. P. Delmas, "Gaussian Cramer-Rao bound for direction estimation of noncircular signals in unknown noise fields," *IEEE Trans. Signal Process.*, vol. 53, no. 12, pp. 4610–4618, Dec. 2005.

[124] S. Jha and T. Durrani, "Direction of arrival estimation using artificial neural networks," *IEEE Trans Syst. Man Cybern.*, vol. 21, no. 5, pp. 1192–1201, Sep. 1991.

[125] H. L. Southall, J. A. Simmers, and T. H. O'Donnell, "Direction finding in phased arrays with a neural network beamformer," *IEEE Trans. Antennas Propag.*, vol. 43, no. 12, pp. 1369–1374, Dec. 1995.

[126] C. W. Ma and C. C. Teng, "Fuzzy neural network method approach for 2-D direction finding in multipath environments," *IEE Proc. Radar, Sonar, Navig.*, vol. 146, no. 2, pp. 78–83, Apr. 1999.

[127] C. S. Shieh and C. T. Lin, "Direction of arrival estimation based on phase differences using neural fuzzy network," *IEEE Trans. Antennas Propag.*, vol. 48, no. 7, pp. 1115–1124, Jul. 2000.

[128] T. N. E. Greville, "Note on the weighted generalized inverse of the product of matrices," *SIAM Review*, vol. 8, no. 4, pp. 518–521, Oct. 1966.

[129] D. Cherney, T. Denton, R. Thomas, and A. Waldron, "Linear algebra," University of California, Davis, Aug. 2016. [Online]. Available: https://www.math.ucdavis.edu/~linear/linear-guest.pdf

[130] M. S. Bartlett, "Smoothing periodograms from time series with continuous spectra," *Nature*, vol. 161, pp. 686–687, 1948.

[131] J. Capon, "High-resolution frequency-wavenumber spectral analysis," in *Proc. IEEE*, vol. 57, no. 8, Aug. 1969, pp. 1408–1418.

[132] D. P. Bertsekas, A. Nedić, and A. E. Ozdaglar, *Convex Analysis and Optimization*. Nashua, NH, USA: Athena Scientific, 2003.

[133] R. O. Schmidt, "Multiple emitter location and signal parameter estimation," *IEEE Trans. Antennas Propag.*, vol. 34, no. 3, pp. 276–280, Mar. 1986.

[134] R. Roy and T. Kailath, "ESPRIT—Estimation of signal parameters via rotational invariance techniques," *IEEE Trans. Acoust., Speech, Signal Process.*, vol. 37, no. 7, pp. 984–995, Jul. 1989.

[135] M. Wax, "Detection and localization of multiple sources via the stochastic signals model," *IEEE Trans. Signal Process.*, vol. 39, no. 11, pp. 2450–2456, Nov. 1991.

[136] B. D. Rao and K. V. S. Hari, "Performance analysis of Root-MUSIC," *IEEE Trans. Acoust., Speech, Signal Process.*, vol. 37, no. 12, pp. 1939–1949, Dec. 1989.

[137] H. Krim, P. Forster, and J. G. Proakis, "Operator approach to performance analysis of root-MUSIC and root min-norm," *IEEE Trans. Signal Process.*, vol. 40, no. 7, pp. 1687–1696, Jul. 1992.

[138] M. Haardt and J. A. Nossek, "Unitary ESPRIT: How to obtain increased estimation accuracy with a reduced computational burden," *IEEE Trans. Signal Process.*, vol. 43, no. 5, pp. 1232–1242, May 1995.

[139] M. Wax and T. Kailath, "Detection of signals by information theoretic criteria," *IEEE Trans. Acoust., Speech, Signal Process.*, vol. 33, no. 2, pp. 387–392, Apr. 1985.

[140] H.-T. Wu, J.-F. Yang, and F.-K. Chen, "Source number estimators using transformed gerschgorin radii," *IEEE Trans. Signal Process.*, vol. 43, no. 6, pp. 1325–1333, Jun. 1995.

[141] J. H. Cozzens and M. J. Sousa, "Source enumeration in a correlated signal environment," *IEEE Trans. Signal Process.*, vol. 42, no. 2, pp. 304–317, Feb. 1994.

[142] G. Xu, R. H. Roy, and T. Kailath, "Detection of number of sources via exploitation of centro-symmetry property," *IEEE Trans. Signal Process.*, vol. 42, no. 1, pp. 102–112, Jan. 1994.

[143] C. W. Ma and C. C. Teng, "Detection of coherent signals using weighted subspace smoothing," *IEEE Trans. Antennas Propag.*, vol. 44, no. 2, pp. 179–187, Feb. 1996.

[144] M. Wax and I. Ziskind, "Detection of the number of coherent signals by the MDL principle," *IEEE Trans. Acoust., Speech, Signal Process.*, vol. 37, no. 8, pp. 1190–1196, Aug. 1989.

[145] X. Xu, Z. Ye, Y. Zhang, and C. Chang, "A deflation approach to direction of arrival estimation for symmetric uniform linear array," *IEEE Antennas Wireless Propag. Lett.*, vol. 5, no. 1, pp. 486–489, Dec. 2006.

[146] J. M. Mendel, "Tutorial on higher-order statistics (spectra) in signal processing and system theory: theoretical results and some applications," *Proc. IEEE*, vol. 79, no. 3, pp. 278–305, Mar. 1991.

[147] Y. C. Eldar, *Sampling Theory: Beyond Bandlimited Systems*. Cambridge, U.K.: Cambridge Univ. Press, 2015.

[148] Z. He, A. Cichocke, S. Xie, and K. Choi, "Detecting the number of clusters in n-way probabilistic clustering," *IEEE Trans. Pattern Anal. Mach. Intell.*, vol. 32, no. 11, pp. 2006–2021, Nov. 2010.

[149] N. Yilmazer, J. Koh, and T. K. Sarkar, "Utilization of a unitary transform for efficient computation in the matrix pencil method to find the direction of arrival," *IEEE Trans. Antennas Propag.*, vol. 54, no. 1, pp. 175–181, 2006.

[150] W. Du and R. L. Kirlin, "Improved spatial smoothing techniques for DOA estimation of coherent signals," *IEEE Trans. Signal Process.*, vol. 39, no. 5, pp. 1208–1210, May 1991.

[151] K.-C. Huarng and C.-C. Yeh, "A unitary transformation method for angle-of-arrival estimation," *IEEE Trans. Signal Process.*, vol. 39, no. 4, pp. 975–977, Apr. 1991.

[152] W.-K. Ma, T.-H. Hsieh, and C.-Y. Chi, "Direction-of-arrival estimation of quasistationary signals with less sensors than sources and unknown spatial noise covariance: A Khatri-Rao subspace approach," *IEEE Trans. Signal Process.*, vol. 58, no. 4, pp. 2168–2180, Apr. 2010.

[153] P. Pal and P. P. Vaidyanathan, "Nested arrays: A novel approach to array processing with enhanced degrees of freedom," *IEEE Trans. Signal Process.*, vol. 58, no. 8, pp. 4167–4181, Aug. 2010.

[154] H. Chen, C. Hou, Q. Wang, L. Huang, and W. Yan, "Cumulants-based Toeplitz matrices reconstruction method for 2-D coherent DOA estimation," *IEEE Sens. J.*, vol. 14, no. 8, pp. 2824–2832, Aug. 2014.

[155] A. N. Lemma, A.-J. van der Veen, and E. F. Deprettere, "Analysis of joint angle-frequency estimation using ESPRIT," *IEEE Trans. Signal Process.*, vol. 51, no. 5, pp. 1264–1283, May 2003.

[156] G. Xu and T. Kailath, "Direction-of-arrival estimation via exploitation of cyclostationarity—A combination of temporal and spatial processing," *IEEE Trans. Signal Process.*, vol. 40, no. 7, pp. 1775–1786, Jul. 1992.

[157] E. T. Jaynes, *Probability Theory: The Logic of Science*. Cambridge, U.K.: Cambridge Univ. Press, 2003.

[158] Y. Hua and T. K. Sarkar, "Matrix pencil method for estimation parameters of exponentially damped/undamped sinusoids in noise," *IEEE Trans. Acoust., Speech, Signal Process.*, vol. 38, no. 5, pp. 814–824, May 1990.

[159] G. W. Stewart and C. F. V. Loan, *Matrix Computations*, 3rd ed. Baltimore and London: The Johns Hopkins University Press, 1996.

[160] A. J. Weiss and B. Friedlander, "On the Cramér-Rao bound for direction finding of correlated sources," *IEEE Trans. Signal Process.*, vol. 41, pp. 495–499, Jan. 1993.

[161] M. Pesavento, A. B. Gershman, and K. M. Wong, "Direction finding in partly-calibrated sensor arrays composed of multiple subarrays," *IEEE Trans. Signal Process.*, vol. 50, no. 9, pp. 2103–2115, Sep. 2002.

[162] C. M. S. See and A. B. Gershman, "Direction-of-arrival estimation in partly calibrated subarray-based sensor arrays," *IEEE Trans. Signal Process.*, vol. 52, no. 2, pp. 329–338, Feb. 2004.

[163] R. Goossens and H. Rogier, "A hybrid UCA-RARE/Root-MUSIC approach for 2-D direction of arrival estimation in uniform circular arrays in the presence of mutual coupling," *IEEE Trans. Antennas Propag.*, vol. 55, no. 3, pp. 841–849, Mar. 2007.

[164] P. Stoica and R. Moses, *Spectral analysis of signals*. Upper Saddle River, New Jersey: Prentice Hall, 2005.

[165] Y. Zhang, Z. Ye, and C. Liu, "Estimation of fading coefficients in the presence of multipath propagation," *IEEE Trans. Antennas Propag.*, vol. 57, no. 7, pp. 2220–2224, Jul. 2009.